

Members of the dissertation committee:

Prof.dr. Patrick Cordier

Université Lille
France

Prof.dr. Alexander Deutsch

Westfälische Wilhelms-Universität Münster
Germany

Dr. Geoff Lloyd

University of Leeds
United Kingdom

Prof.dr. Wolf Uwe Reimold

Museum für Naturkunde Berlin
Germany

Prof.dr. Claudia Trepmann

Ludwig-Maximilians-Universität München
Germany

This research was funded by the Netherlands Organisation for Scientific Research (NWO).

Printing of this thesis was generously supported by the Stichting tot bevordering van de Electronenmicroscopie in Nederland (SEN).

Cover illustration: shock microstructures in quartz, imaged using different SEM techniques

ISBN 978-90-6266-325-5

USES 32

Copyright © 2013 Maartje Hamers

All rights reserved. No part of this publication may be reproduced in any form, by print or photo print, microfilm or any other means, without written permission by the publishers.

Identifying shock microstructures in quartz from terrestrial impacts

new scanning electron microscopy methods

Identificatie van schokmicrostructuren in kwarts gevormd door meteorietinslagen

nieuwe rasterelektronenmicroscopiemethoden

(met een samenvatting in het Nederlands)

PROEFSCHRIFT

ter verkrijging van de graad van doctor aan de Universiteit Utrecht
op gezag van de rector magnificus, prof. dr. G.J. van der Zwaan,
ingevolge het besluit van het college voor promoties
in het openbaar te verdedigen

op vrijdag 31 mei 2013 des middags te 2.30 uur

door

Maartje Francine Hamers

geboren op 5 december 1981 te Amsterdam

Promotor:

Prof.dr. M.R. Drury

Co-promotor:

Dr. G.M. Pennock

“Prav! Der Hemeldonderweder”

Professor Prlwytzkofsky

Contents

	Summary	9
	Samenvatting	11
	General introduction and outline	15
Chapter 1	A summary of shock effects in quartz	21
Chapter 2	Scanning electron microscope cathodoluminescence imaging of planar deformation features and tectonic deformation lamellae in quartz	39
Chapter 3	No evidence for shocked quartz at the Cretaceous-Palaeogene boundary in the Geulhemmerberg section, south-east Netherlands	61
Chapter 4	Distinction between amorphous and healed planar deformation features in shocked quartz using composite colour scanning electron microscope cathodoluminescence imaging	73
Chapter 5	Characterisation of shock microstructures in quartz by foreshatter electron imaging and electron backscatter diffraction	97
Chapter 6	Scanning electron microscope cathodoluminescence imaging of dislocations, subgrain boundaries and twin boundaries in quartz	119
Chapter 7	An integrated scanning electron microscopy approach for shocked quartz	133
Chapter 8	Afterthoughts – mechanical twinning and the formation of planar deformation features in quartz	153
Chapter 9	Main conclusions and suggestions for further research	169
	References	173
	Publications	185
	Curriculum Vitae	187
	Dankwoord	189

Summary

Impact cratering is a fundamental geological process, shaping and modifying planetary surfaces. Terrestrial impact craters and ejecta layers are widely studied as an analogue to craters and impact formations on other rocky planets, moons and asteroids, but also for their relevance to the geology of the Earth. Therefore, the correct identification of impact structures and ejecta layers on the Earth is essential, but recognition of the characteristic circular crater morphology is often hindered by erosion and deformational processes.

One of the most reliable impact indicators is the presence of shock metamorphosed minerals in target rocks and in material ejected out of the crater. Many minerals can show these shock effects, but for many reasons quartz is the most widely studied. A wide variety of shock effects form in quartz, at different peak shock pressures, but in particular the presence of planar deformation features (PDFs - originally amorphous microlamellae or twin structures) is universally accepted as the most reliable form of impact evidence.

In a light microscope, however, distinction between PDFs and other, non-shock related planar or sub-planar microstructures in quartz is not always possible. To prove the shock origin of planar microstructures in quartz, time-consuming, difficult and expensive transmission electron microscopy (TEM) analysis of the sub-micrometer scale defect structure of the lamellae is often required. Scanning electron microscopy (SEM) techniques, on the other hand, are relatively easy and quick. Major advances in SEM techniques over the last decades have made it possible to do analyses in the SEM that could previously only be carried out using TEM. Therefore, the aim of the research presented in this thesis is to develop SEM methods that can be used for reliably identifying and characterising shock microstructures in quartz, in particular PDFs, as an alternative and as an addition to existing TEM techniques. The SEM techniques employed here include cathodoluminescence (CL) and foreshattered electron (FSE) imaging and electron backscatter diffraction (EBSD) mapping. A direct, often one to one comparison of sample areas that were studied in the SEM with focussed ion beam prepared TEM foils provides a direct correlation of the information provided by the SEM techniques to the microstructures analysed using TEM.

Cathodoluminescence imaging in the SEM (SEM-CL) clearly shows the presence of PDFs in quartz. Both greyscale and composite colour SEM-CL images can be used as a basis for distinguishing PDFs from tectonic deformation lamellae. Composite colour SEM-CL images show the presence of different types of PDFs: non-luminescent PDFs are amorphous, while healed PDFs and (mechanical) basal Brazil twins are red luminescent, with a dominant emission peak at 650 nm, related to the non-bridging oxygen hole centre defect in quartz. Analysis of unshocked quartz (tectonically deformed grains and as-grown single crystals) shows that also

Dauphiné twin boundaries, subgrain boundaries, growth Brazil twins and some dislocations are red luminescent in SEM-CL images. The red CL emission is probably related to preferential beam damage at defects and fluid inclusions in healed PDFs, at twin and subgrain boundaries and at some dislocations. Composite colour SEM-CL images can furthermore indicate the presence of potential high pressure phases in shocked quartz grains, which can be confirmed by other techniques.

FSE imaging and EBSD mapping are closely related techniques that record information about the crystallographic structure and orientation of minerals. These methods are very sensitive to small changes and can give an indication of the structural state of PDFs (amorphous vs. healed). A very useful aspect of FSE images and EBSD maps is that they provide detailed information on the structure and orientation of the host grain. Microcrystallinity and the presence of Dauphiné twins are easily detected using these techniques.

Combined SEM and TEM observations on shocked quartz grains show combinations of microstructures that can be related to different stages of healing in grains shocked to moderate and high pressure and suggest that mechanical twinning in the low shock pressure regime may play a more important role in PDF development than previously assumed.

The combination of CL, FSE and EBSD techniques and more standard applications in the SEM, such as backscattered and secondary electron imaging, provides a powerful and easy to use, non-destructive integrated approach for studying shock microstructures in quartz. Direct correlation with light microscopy is possible, because standard petrographic thin sections can be studied in both the light microscope and the SEM. The combined SEM techniques described in this thesis bridge the gap between highly detailed TEM analysis and general observations in light microscopy that are relevant for larger sample volumes. For the identification and general characterisation of shock microstructures in quartz, SEM analysis is sufficient. This conclusion is a major step forward for terrestrial impact research and will contribute to the reliable identification of proposed impact structures and ejecta layers.

Samenvatting

Het ontstaan van inslagkraters is een fundamenteel geologisch proces en geeft vorm aan de oppervlakte van planeten. Inslagkraters en ejectalagen op aarde worden veel onderzocht als analoog voor kraters op andere terrestrische planeten, manen en asteroiden, maar ook om hun relevantie voor de geologie op aarde. De correcte identificatie van inslagstructuren en ejectalagen op aarde is daarom essentieel, maar door erosie en deformatie is de karakteristieke cirkelvormige morfologie van inslagkraters vaak moeilijk te herkennen.

Eén van de betrouwbaarste inslagindicatoren is de aanwezigheid van schok-gemetamorfoseerde mineralen in kratergesteenten en in uitgeworpen materiaal uit de krater. Veel mineralen laten schokeffecten zien, maar om verschillende redenen wordt kwarts het meest bestudeerd. Specifieke schokeffecten in kwarts ontstaan bij verschillende piekdrukwaarden, maar vooral de aanwezigheid van planaire deformatiestructuren (PDFs – oorspronkelijk amorfe lamellen) is algemeen geaccepteerd als bewijs voor een meteorietinslag.

In een lichtmicroscop is het echter niet altijd mogelijk onderscheid te maken tussen PDFs en andere, niet door schok gevormde planaire of subplanaire microstructuren in kwarts. Als bewijs voor de schokoorsprong van microlamellen in kwarts zijn vaak tijdrovende, moeilijke en kostbare transmissie elektronenmicroscopie (TEM)-observaties nodig van de sub-micrometer defectstructuur van de lamellen. Rasterelektronenmicroscopie (SEM)-methoden daarentegen zijn relatief snel en eenvoudig. De enorme vooruitgang in SEM-technieken in de afgelopen decennia heeft het mogelijk gemaakt om analyses uit te voeren in de SEM die vroeger alleen mogelijk waren in de TEM. Het doel van het onderzoek in dit proefschrift is daarom om SEM-methoden te ontwikkelen voor de betrouwbare identificatie van schokmicrostructuren in kwarts, met name PDFs, als alternatief voor en uitbreiding van de bestaande TEM-technieken. De SEM-technieken die hier gebruikt worden zijn cathodoluminescentie (CL) en forescattered electron (FSE) afbeeldingen en electron backscatter diffraction (EBSD). De preparatie van TEM-secties met een focussed ion beam in eerder in de SEM bestudeerde gebieden van monsters maakt directe correlatie mogelijk van informatie verkregen via SEM en de microstructuren geobserveerd in de TEM.

PDFs in kwarts zijn duidelijk zichtbaar in SEM-CL afbeeldingen. Zowel zwart-witte als samengestelde kleuraanbeelden vormen een goede basis voor het onderscheiden van PDFs en tektonische deformatielamellen. In samengestelde SEM-CL kleuraanbeelden kunnen verschillende typen PDFs onderscheiden worden: niet-luminescente PDFs zijn amorf, terwijl gerekristalliseerde PDFs en (mechanische) Brazil-type tweelingen rood luminescent zijn, met een dominante emissiepiek rond 650 nm gerelateerd aan het non-bridging oxygen hole centre defect in kwarts. Analyse van niet-geschokte kwarts (tektonisch gedeformeerde korrels en

ongedeformeerde kristallen) laat zien dat ook Dauphiné tweelinggrenzen, subkorrelgrenzen, gegroeide Brazil-type tweelingen en sommige dislocaties rood luminescent zijn in SEM-CL afbeeldingen. Samengestelde kleuren SEM-CL afbeeldingen kunnen bovendien een indicatie geven dat hogedrukfasen aanwezig zijn in geschokte kwartskorrels, wat bevestigd kan worden met andere technieken.

FSE en EBSD-afbeeldingen zijn nauw verwante technieken, waarmee informatie verzameld kan worden over de kristalstructuur en –oriëntatie van mineralen. Deze methoden zijn erg gevoelig voor kleine veranderingen en kunnen een indicatie geven van de structurele staat van PDFs (amorf of gerekristalliseerd). Een erg bruikbaar aspect van FSE- en EBSD-afbeeldingen is dat ze gedetailleerde informatie verschaffen over de structuur en oriëntatie van de korrel waarin de PDFs zich bevinden. Microkristalliniteit en de aanwezigheid van Dauphiné tweelingen kunnen eenvoudig gedetecteerd worden met deze technieken.

Gecombineerde SEM- en TEM-observaties van geschokte kwartskorrels laten combinaties van microstructuren zien, die gerelateerd kunnen worden aan verschillende stadia van rekristallisatie in korrels die geschokt zijn onder gematigde en hoge druk, en suggereren dat de vorming van mechanische tweelingen in het lage drukregime belangrijker zijn voor het ontstaan van PDFs dan tot nu toe werd aangenomen.

De combinatie van CL-, FSE- en EBSD-technieken en standaardapplicaties in SEM, zoals teruggestrooide en secundaire elektronenafbeeldingen, vormt een krachtige en eenvoudig toepasbare, niet-destructieve integrale aanpak voor het bestuderen van schokmicrostructuren in kwarts. Directe correlatie met lichtmicroscopie is mogelijk, omdat standaard petrografische dunne doorsneden zowel in de lichtmicroscopie als de SEM bestudeerd kunnen worden. De gecombineerde SEM-technieken die beschreven worden in dit proefschrift overbruggen de kloof tussen zeer gedetailleerde TEM-analyse en algemene observaties aan grotere monsters in de lichtmicroscopie. Voor de identificatie en algemene karakterisering van schokmicrostructuren in kwarts voldoet SEM-analyse. Deze conclusie is een belangrijke vooruitgang in terrestrisch inslagonderzoek en zal bijdragen aan de betrouwbare identificatie van mogelijke inslagstructuren en ejectalagen.

General introduction and outline

Impact and shock metamorphism

Impact craters are one of the most prominent and eye-catching features on the surfaces of all terrestrial planets, asteroids and rocky moons in our solar system. Impact cratering is an important surface-shaping process and is responsible for inter-planetary transfer of material. Impact processes and the resulting craters are therefore of great interest to the planetary sciences, but are also very relevant in the study of our own planet. A huge impact is likely to have been responsible for the formation of the Moon (Canup, 2004), much of the water in our oceans might have been brought here by comets and asteroids (Hartogh et al., 2011), early bacterial life forms have possibly reached our planet travelling on an asteroid (e.g. Meyer et al., 2011 and references therein) and a major impact has probably destroyed almost all life on Earth on at least one occasion (Alvarez et al., 1980; Smit and Hertogen, 1980). Terrestrial impact craters are therefore studied for their relevance to the Earth's history, but also as an analogue to craters on other planetary bodies.

Although the existence of meteorites has been accepted since the early nineteenth century, it remained unthinkable that extraterrestrial bodies could be responsible for catastrophic events on the Earth. In the early twentieth century, meteorite impacts were proposed to have formed the Barringer crater in Arizona (USA) (Barringer, 1906) and the Ries crater in southern Germany (Werner, 1904, cited in Shoemaker and Chao, 1961), but these structures were generally believed to be of volcanic origin. Only in the 1960s, in parallel with the development of space exploration programmes, was the existence of terrestrial impact craters seriously considered. Unequivocal shock effects were discovered (Chao et al., 1960; Shoemaker and Chao, 1961) and both Barringer and Ries were accepted as impact craters. Since then, more and more impact structures and ejecta layers have been recognised on Earth. As of January 2013, 183 confirmed impact structures are listed in the Earth Impact Database. Especially since the Cretaceous-Palaeogene (K-Pg) boundary mass extinction was confidently linked to a major meteorite impact (Alvarez et al., 1980; Smit and Hertogen, 1980) and the subsequent discovery of the associated crater near Chicxulub, Mexico (Hildebrand et al., 1991), impact research has received a growing amount of both scientific and public attention. Following the K-Pg impact hypothesis, an extraterrestrial event has also been proposed as the cause of the end-Permian mass extinction (Basu et al., 2003; Becker et al., 2004; Retallack et al., 1998) and some preliminary impact evidence has been found near the Triassic-Jurassic boundary (Badjukov et al., 1987; Bice et al., 1992; Olsen et al., 2002; Simms, 2003). Although the end-Triassic extinction is now generally believed to have been caused by extensive volcanism (e.g. Deenen et al., 2010) and conclusive evidence for an

end-Permian impact has not been found to this day, the catastrophic effects of large meteorite impacts remain a fascinating subject to many scientists.

For effective impact research, the correct identification of craters, impact related rocks and ejecta layers is crucial. On Earth, where impact structures suffer the effects of weathering and erosion, this is not always easy. If a crater is not covered and protected by newly formed sediments soon after the impact event, any topographical expression slowly vanishes with time. Only recent craters can be recognised by their typical circular morphology, but older or deformed impact structures can be hard to distinguish from volcanic or tectonically formed (semi-)circular structures. Other characteristic features of impact events (so-called ‘impact indicators’) are therefore required for a reliable identification of craters and related rocks.

One of the most reliable forms of impact evidence is the presence of shock metamorphosed minerals. The extreme pressure and temperature conditions during an impact event last only for seconds, but can induce microscopic changes in the minerals in the target rocks (shock metamorphism). Because the impact conditions and the timescale of the process are so vastly different from normal conditions and timescales of crustal deformation, shock metamorphic effects are distinctively different from tectonic microstructures and are therefore diagnostic for impact. Microscopic shock effects can occur in, for example, feldspars, quartz, olivine and biotite. Of these, quartz is the most widely used mineral, because it is one of the main constituents of the Earth’s crust. Furthermore, quartz is resistant to weathering and therefore stable over considerable and geologically significant periods of time. For these reasons, both natural and experimentally produced shock effects in quartz have been studied extensively since the early days of impact research (e.g. Alexopoulos et al., 1988; Carter, 1965; Engelhardt and Bertsch, 1969; French and Short, 1968; Goltrant et al., 1992; Gratz et al., 1996; Gratz et al., 1992; Grieve et al., 1996; Kieffer, 1971; Langenhorst, 1994; Langenhorst and Deutsch, 1994; Müller, 1969; Robertson, 1975; Stöffler, 1972; Stöffler and Langenhorst, 1994).

A wide range of shock effects occur in quartz, including planar fractures (PFs), mosaicism, mechanical twinning, planar deformation features (PDFs), high pressure polymorphs of quartz and amorphous phases. These effects occur at different peak shock pressures, so apart from demonstrating the impact origin of a proposed structure, they can provide information on the shock conditions. The wide variety of pressure dependent shock effects in quartz is another reason why it is the most studied mineral exhibiting shock deformation. Especially PDFs are an important fingerprint of shock. PDFs are thin, planar microstructures that usually occur in multiple, differently oriented sets per grain. Their orientation is crystallographically determined and pressure dependent and serves as one of the most important, experimentally calibrated, shock barometers. PDFs are universally acknowledged as the most reliable microscopic terrestrial impact indicator.

Aims and outline of this thesis

Although PDFs in quartz can be quickly identified in a standard petrographic microscope, using light microscopy it can be difficult to distinguish PDFs from tectonically formed (sub-)planar microstructures in quartz, such as tectonic deformation lamellae or healed fractures. This has led to heated scientific discussions in the past and has resulted in a number of misidentifications and

controversies over proposed impact structures or ejecta layers (e.g. Vrána, 1987 vs. Cordier et al., 1994; Surenian, 1988 vs. Leroux and Doukhan, 1993; Ernstson and Fiebag, 1992 vs. Langenhorst et al., 1996; Becker et al., 2004 vs. Glikson 2004; Retallack et al., 1998 vs. Langenhorst et al., 2005). The most reliable method to unequivocally determine the shock origin of planar microstructures in quartz is transmission electron microscopy (TEM) analysis of the sub-micrometer scale defect structure of the lamellae. However, TEM analysis is difficult, very time consuming and expensive. Only very small sample volumes can be studied in a TEM, on the order of tens of micrometers wide and 100 to 200 nm in thickness, making it challenging to obtain results that are representative for larger samples. Furthermore, TEM sample preparation is destructive and TEM facilities are not readily available to many research groups.

Over the past decades, there have been major advances in scanning electron microscopy (SEM) techniques and their application to the structural analysis of rocks and minerals. Modern SEM instruments allow microstructural analysis at high spatial resolution. With the development of techniques like electron backscatter diffraction (EBSD) and cathodoluminescence spectroscopy and colour imaging and improvements in spatial resolution, SEM can often be used for applications that, in the past, could only be achieved using TEM. Some earlier studies on the identification of PDFs in quartz using the SEM were promising. These early applications include secondary electron (SE) imaging of etched PDFs (Gratz et al., 1996) and greyscale cathodoluminescence imaging (Boggs et al., 2001). Use of the SEM has several advantages over TEM analysis. In the SEM, much larger samples can be studied than in TEM. Standard sized petrographic thin sections are easily handled, allowing a direct correlation with light microscopy and bridging the gap between the light microscopy and TEM scales (see figure I), and SEM techniques are non-destructive. Furthermore, most SEM techniques are relatively quick and easy to apply to a larger sample set.

The research presented in the following chapters aims to develop SEM methods that can be used to reliably identify and characterise shocked quartz, in particular PDFs, as an alternative and as an addition to existing TEM techniques. The newly applied SEM techniques provide an extra basis for the reliable identification of newly discovered or disputed terrestrial impact structures and ejecta layers.

Chapter 1 provides an overview of the microscopic shock effects that can occur in quartz and how these microstructures are related to the conditions prevailing during an impact. PDFs are discussed in more detail, providing a basis for the discussions in the following chapters.

Chapter 2 aims to identify PDFs in scanning electron microscope cathodoluminescence (SEM-CL) images and to define criteria for the reliable distinction of PDFs and tectonic deformation lamellae in both greyscale and composite colour SEM-CL images.

In **chapter 3** a case study is presented to test the SEM-CL imaging methods developed in chapter 1. Potentially shocked quartz grains from the Cretaceous-Palaeogene (K-Pg) boundary section in the Geulhemmerberg in Limburg, the Netherlands, are studied in SEM-CL images. The presence of shocked quartz in the Geulhemmerberg section would confirm the hypothesis that the hiatus at the boundary is negligible and that the section represents a rare expanded shallow marine record of the latest Cretaceous and early Palaeogene. The microstructures in the Geulhemmerberg quartz are compared to PDFs in quartz grains from K-Pg boundary sites in Italy and the USA.

Chapter 4 builds on the results obtained in chapter 2 in a more detailed technical analysis of the CL emission of PDFs in quartz. The relationship between the CL behaviour of PDFs and their defect structure is specified with the help of TEM analyses of samples prepared with a focused ion beam (FIB). The FIB preparation method allows precise localisation of the TEM foil and provides a direct correlation between CL emission in the SEM and the microstructures observed in the TEM. Spectroscopic measurements quantify the CL emission of red luminescent PDFs.

In **chapter 5** the potential and limitations of forescatter electron (FSE) imaging and electron backscattered diffraction (EBSD) mapping to identify and characterise PDFs in quartz are explored. We discuss the presence and origin of shock-related Dauphiné twins. Furthermore, we discuss the distinction between PDFs and tectonic deformation lamellae using FSE and EBSD techniques.

Chapter 6 is an excursion outside the field of impact metamorphism and deals with SEM-CL imaging of dislocations, subgrain boundaries and twin boundaries in quartz. Most of these microstructures, which are closely related to shock deformation, but also relevant in other fields of geology, cannot be observed directly in a light microscope. Composite colour and red filtered SEM-CL imaging allows a fast analysis of the distribution and geometry of these microstructures over relatively large sample areas and is applied to as-grown single quartz crystals and a tectonically deformed quartzite. EBSD and TEM analysis of the samples confirm the nature of the microstructures that are visualised in CL images.

Chapter 7 combines the methods developed in chapters 2-6 and describes an integrated SEM approach to the study of shocked quartz, allowing non-destructive study of thin sections that can also be studied using light microscopy. A general characterisation of PDFs in quartz, obtained using combined CL and FSE imaging and EBSD mapping, is compared to TEM analysis of the sub-micrometer scale defect structure of the same samples. The combined SEM and TEM observations show groups of shocked quartz grains with different microstructures, which are interpreted as a healing trend in grains that have been shocked to moderate or high pressures.

Chapter 8 is a preliminary exploration of the role of mechanical twinning in shocked quartz and its potential relation to PDF formation. A quartzite sample that has been shocked experimentally to 8 GPa is studied using SEM-CL imaging and TEM analysis, in order to study the microstructures forming in the low shock pressure range in more detail.

Chapter 9 summarises the main conclusions of this thesis and provides suggestions for further research.

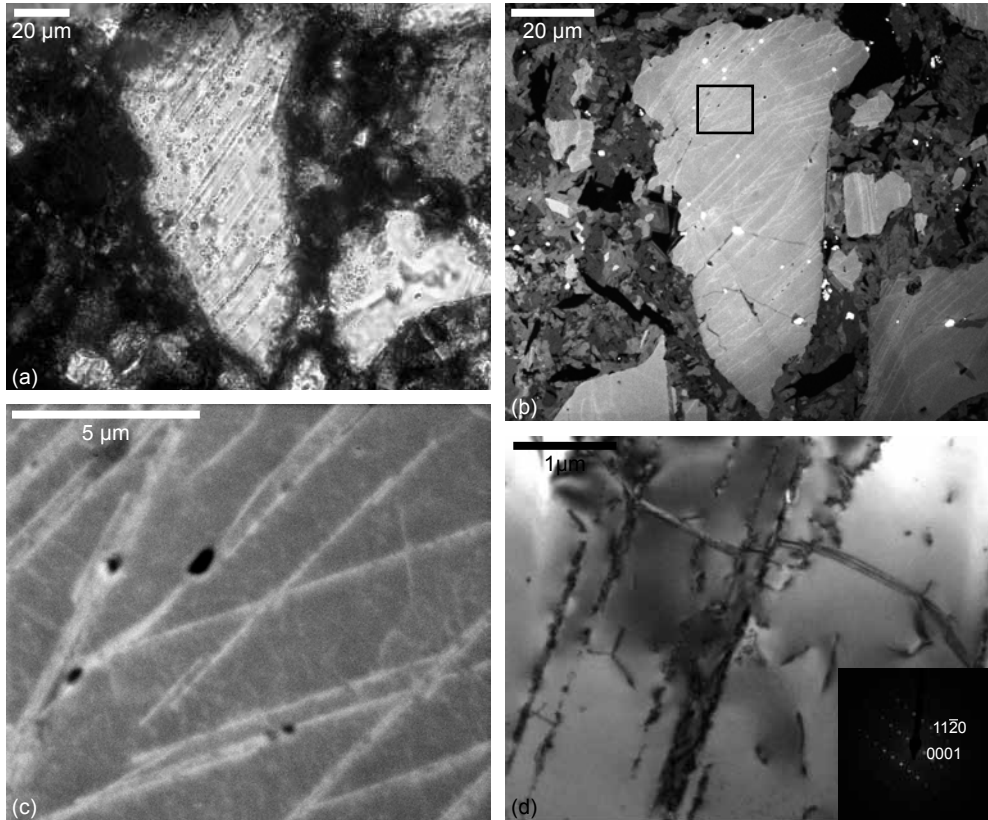
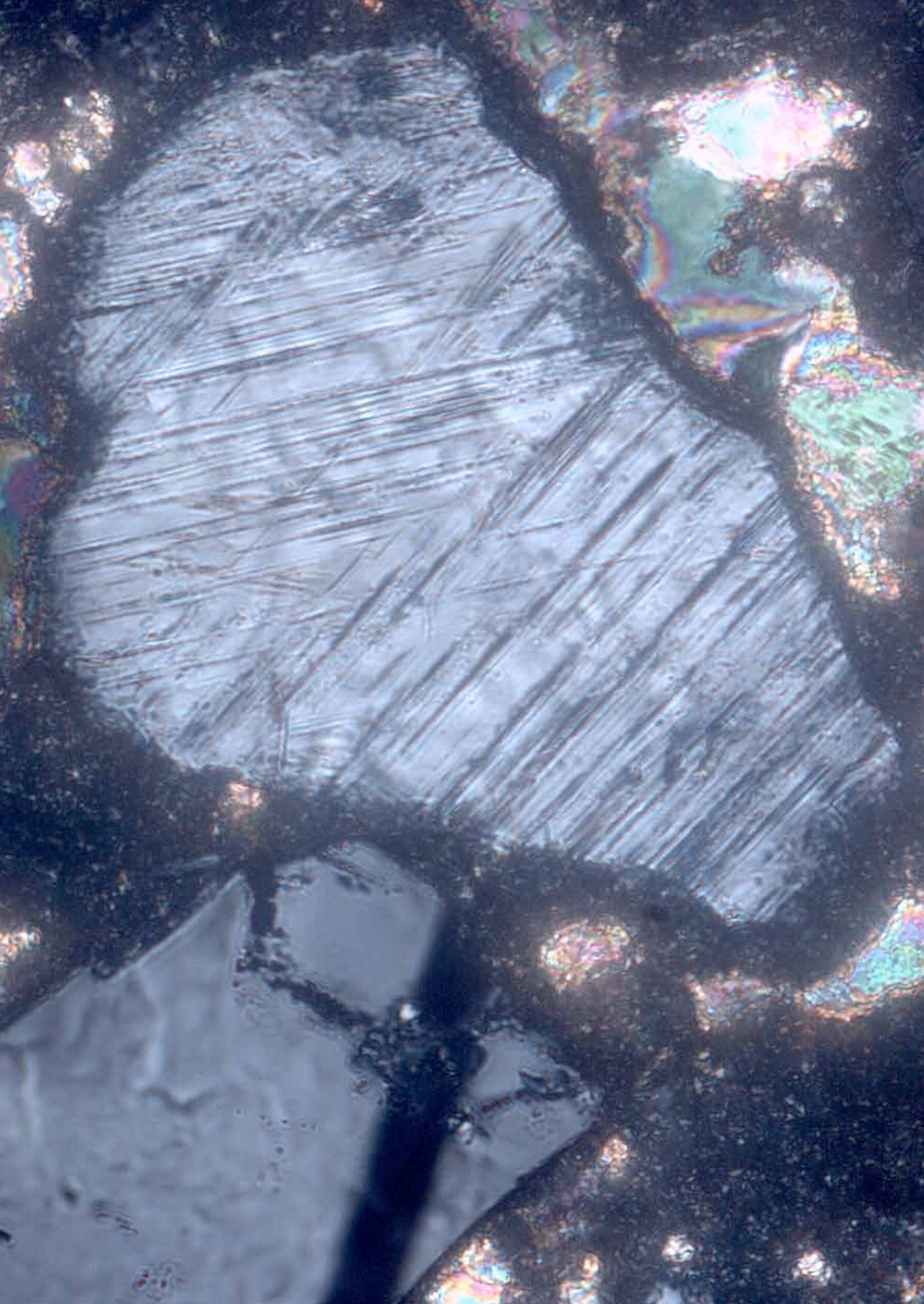


Figure I Illustration of the different scales of observation of light microscopy and TEM, and the bridging scale of SEM. **a** Light micrograph of a shocked quartz grain from the Rochechouart impact structure (~201 Ma), France, with one set of PDFs, decorated with fluid inclusions. **b** Cathodoluminescence image recorded in the SEM (SEM-CL), showing the same grain as in **a**. Note the second set of PDFs that is revealed in the SEM image. Black rectangle shows the location of the image shown in **c**. **c** Higher magnification SEM-CL image of an area in the grain shown in **b**, showing PDFs in two orientations and some fluid inclusions. **d** TEM bright field image of another grain from Rochechouart, showing PDFs (oriented NNE-SSW) and a Dauphiné twin boundary (WNW-ESE). The scale of this image, which has a relatively low magnification for TEM, is comparable to the scale of the image in **c**, which has a relatively high magnification for SEM.



Chapter 1

A summary of shock effects in quartz

A shock wave resulting from the impact of an extraterrestrial body on the Earth's surface can cause a wide range of diagnostic shock effects in quartz, which can provide information on shock conditions. At low pressures, between ~5 and 30 GPa, brittle effects and the onset of phase transformations result in the formation of planar fractures (PFs), mechanical twins, mosaicism and planar deformation features (PDFs). At higher pressures, between 30 and 50 GPa, phase transformations dominate and diaplectic glass and high pressure polymorphs are produced. At pressures >50 GPa, quartz melts and forms lechatelierite and above ~100 GPa vaporisation occurs.

Most of these effects are diagnostic for shock, but PDFs are the most widely used microstructure to identify potential impact structures and ejecta layers. Because other, non-shock related planar microstructures in quartz can be misidentified as PDFs, it is important to carefully study their defect structure and the presence of other indicative shock effects that can confirm a potential shock origin.

1.1 Introduction

Since the early years of impact research in the 1960s, shock metamorphism in crustal minerals has been a very important line of evidence for the shock origin of proposed impact structures or ejecta layers. Shock metamorphosed minerals in target rocks or in material ejected from a crater record microscopic changes that develop as a result of the unique conditions induced by an impact. The extreme pressure and temperature conditions occurring on a very short timescale are far removed from the equilibrium conditions that are associated with most geological processes. Impacts are catastrophic events, associated with typical pressure ranges from a few to several hundred GPa and temperatures up to a few thousand degrees Celsius on a timescale of nanoseconds to seconds. For comparison, the pressure and temperature in the Earth's inner core are about 330 GPa and 5500°C and crustal deformation and metamorphic conditions are normally in the range of 0-10 GPa and 100-1000°C. Because the impact conditions and the timescale on which impact processes occur are so vastly different from normal conditions and timescales of crustal deformation, shock metamorphic effects are distinctively different from tectonic microstructures and are therefore diagnostic for impact. The disequilibrium conditions during impact leave very little time for standard mineral reactions and metamorphic processes. Instead, a typical mix of brittle and plastic deformation and the combination of various low and high pressure polymorphs and amorphous phases is normally observed in shocked minerals.

Microscopic shock effects can occur in a variety of minerals, such as feldspars, quartz, olivine, calcite and biotite. Of these, quartz is the most extensively studied mineral. Quartz is one of the main constituents of the Earth's crust and therefore widely spread, it is stable over geological time scales and it is a mineral in which very specific, diagnostic shock microstructures develop. Furthermore, because a wide range of microscopic shock effects can occur that are indicative for different shock pressures, shock microstructures in quartz serve as a shock pressure barometer, which has been calibrated experimentally. Shocked quartz is therefore used both to prove the impact origin of a structure or stratigraphic level and to obtain detailed information about the scale and pressure conditions of the impact event. For these reasons, both natural and experimentally produced shock effects in quartz have been studied extensively since the early days of impact research (e.g. Alexopoulos et al., 1988; Carter, 1965; Engelhardt and Bertsch, 1969; French and Short, 1968; Goltrant et al., 1992; Gratz et al., 1996; Gratz et al., 1992; Grieve et al., 1996; Kieffer, 1971; Langenhorst, 1994; Langenhorst and Deutsch, 1994; Müller, 1969; Robertson, 1975; Stöffler, 1972; Stöffler and Langenhorst, 1994). Shock metamorphosed minerals are found in the crater floor, in displaced rocks and breccias within the crater and in the ejected material that is deposited outside of the crater, which can have a global distribution in the case of large impacts. Especially when only an ejecta layer is found, but not the associated crater, or in case of a heavily eroded or deformed crater, shocked quartz can be the only available unequivocal proof for the shock origin of an impact layer or structure.

The most widely studied shock microstructures in quartz are planar deformation features (PDFs) (figure 1.1). PDFs are thin, planar microstructures that usually occur in multiple, differently oriented sets per grain and they are universally acknowledged as the most reliable microscopic terrestrial impact indicator. Although PDFs can be observed in thin sections in a light microscope, they show some similarity to non-shock related tectonically formed (sub-) planar microstructures in quartz, such as tectonic deformation lamellae and healed fractures. Tectonic deformation lamellae in particular are frequently misidentified as PDFs (see figure 1.2).

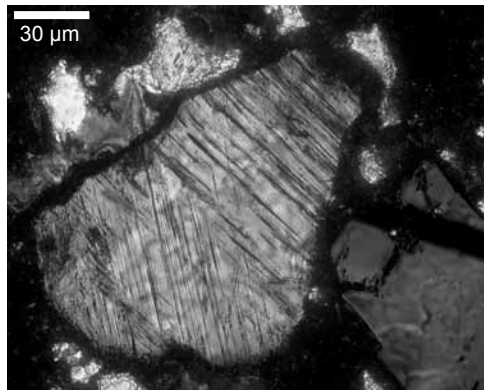


Figure 1.1 Light micrograph of a typical shocked quartz grain with multiple sets of PDFs from the Ries crater (~14.8 Ma), Germany.

The most reliable technique to unequivocally identify PDFs in quartz is transmission electron microscopy (TEM) analysis, but this is difficult, time-consuming and only small sample volumes can be studied in a TEM. A gap exists between light microscopy, in which PDFs are easily observed and large sample sets can be studied, but shock proof is unreliable, and the TEM, in which the defect structure can be studied in detail and the shock origin of the microstructures can be unequivocally determined, but only in very limited sample volumes.

In the following sections, background on impact conditions and a review of shock effects in quartz will be provided. The emphasis is on planar deformation features (PDFs), which are the most widely studied microscopic shock effect in quartz and are the main object of study in this thesis. More detailed and complete reviews exist in the literature, of which the most important are Stöfler and Langenhorst (1994) and Grieve et al. (1996). For more recent comprehensive reviews of terrestrial impact cratering and shock metamorphism see French (1998), French and Koeberl (2010), the special issue on impact of Elements (Jourdan and Reimold, 2012) and Osinski and Pierazzo (2013).

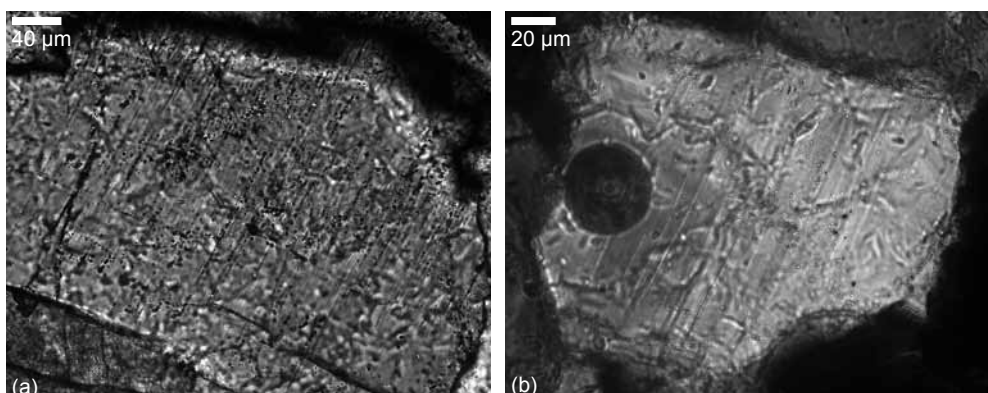


Figure 1.2 Light micrographs of quartz grains with **a** PDFs (basal Brazil twins), decorated with fluid inclusions, from the Vredefort impact structure (~2 Ga), South-Africa; **b** tectonic deformation lamellae from the Flinders Ranges, Australia.

1.2 Shock waves and impact conditions

The extreme conditions required for natural shock metamorphism on the Earth's surface can only be generated by hypervelocity impacts. Shock metamorphic effects occur when a mineral suffers shock pressures above their Hugoniot elastic limit (HEL, the yield strength of a mineral under shock). In quartz, the HEL is between 5 and 8 GPa (Stöffler, 1972; Stöffler and Langenhorst, 1994). Upon impact, a shock wave spreads out radially from the point of impact, propagating at supersonic velocity and compressing the target material. The shock front is followed by a rarefaction or release wave, which travels faster than the shock front and will at some point overtake it, causing a decrease of the peak pressure and broadening of the shock transition with increasing propagation distance (Stöffler, 1972). All shock states (pressure, temperature and volume states) that can be reached in a particular material by shock waves of various intensities are described by the Hugoniot curve (figure 1.3). The Rayleigh line shows the ratio of change in pressure and change in volume ($-\Delta P/\Delta V$) between the starting state and the final shocked state of the target material at the Hugoniot curve. The release wave adiabatically returns the compressed material to ambient conditions. Because the compressional work done by the shock wave is irreversible, excess heat is generated during the shock process, resulting in a high post-shock temperature, which increases with increasing shock pressure.

The Hugoniot curve of minerals exhibiting a HEL has a discontinuity related to the transition from elastic to plastic deformation. In these materials, multiple wave structures may form. This is illustrated in figure 1.3 for an ideal material showing a HEL: for a range of peak shock pressures, between the HEL and the point where the Rayleigh line cuts the Hugoniot curve, a two-wave

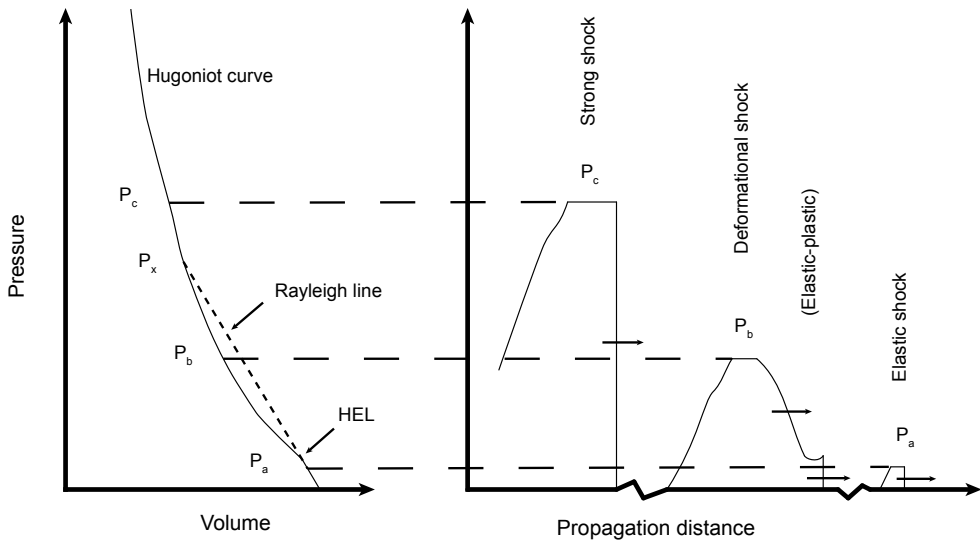


Figure 1.3 The left panel shows an idealised Hugoniot curve for a material with an elastic limit. On the right an illustration is shown of the pressure-time (or propagation distance) profiles of shock waves with three different peak shock pressures (P_a , P_b and P_c) and their relation to points on the Hugoniot curve. Double wave profiles occur for peak shock pressures between the HEL and P_x , which are the two points connected by the Rayleigh line in the left panel (after Stöffler and Langenhorst (1994)).

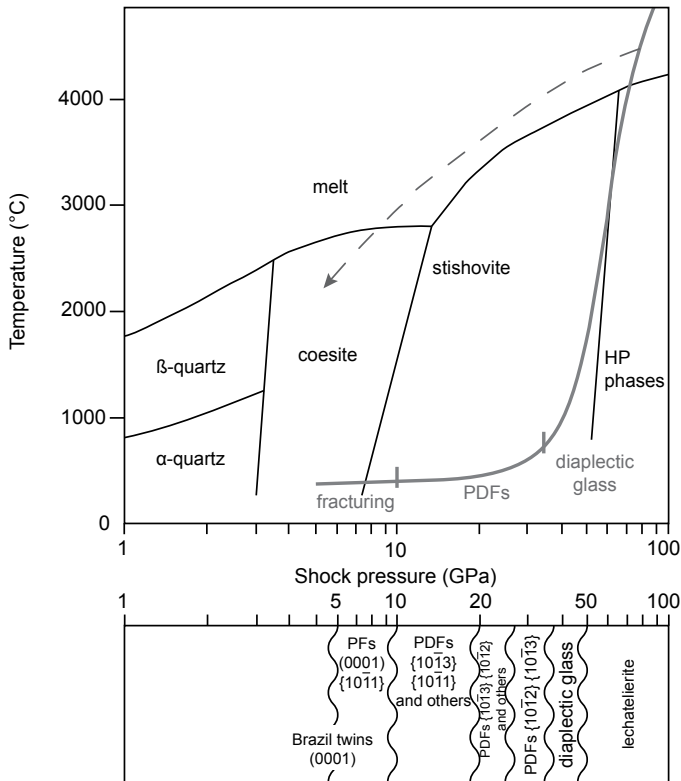


Figure 1.4 The simplified Hugoniot curve of quartz with a possible release curve, with the most important shock effects indicated, projected on the equilibrium phase diagram of SiO_2 (after Langenhorst and Deutsch (2012) and Grieve et al. (1996)).

structure exists (Stöffler, 1972; Stöffler and Langenhorst, 1994). In minerals like quartz, that, in addition to a HEL, show transitions to denser polymorphs at high pressure, also the phase transformation(s) may induce multiple wave structures. In this case, the Hugoniot curve is characterised by three regimes: elastic, plastic and transformational. Ideally, the shock wave in a material exhibiting a HEL and a phase transition may therefore split into a three-wave structure: an elastic precursor, a plastic and a transformational wave. In reality, multiple wave fronts are not as ideal as those in figure 1.3, but are influenced by time and strain rate effects related to various material properties, especially in multi-component and porous rocks (Stöffler, 1972).

The complicated form of the ideal shock wave caused by the mechanical properties of quartz can explain the wide variety of shock effects that are found in quartz. The Hugoniot curve and experimental results have been used to predict which phases will form upon release of the shock wave (Stöffler and Langenhorst, 1994 and references therein). Quartz shocked to a point on the elastic part of Hugoniot curve (below the HEL) will be released to α - or β -quartz. When a shock state between the onset and completion of the phase transformation (the mixed phase regime) is reached, a mix will be found between low pressure forms of quartz and higher pressure polymorphs or amorphised SiO_2 . In the highest pressure regime the compressed quartz

is released as a quenched melt. A projection of the quartz Hugoniot curve on the equilibrium phase diagram of SiO_2 is shown in figure 1.4. In real impacts, whether natural or experimental, the shock pressure conditions may be further complicated by reflections and reverberations due to inhomogeneities in the target material.

1.3 Shock effects in quartz

A wide range of shock effects occur in quartz, including planar fractures (PFs), mosaicism, mechanical twinning, planar deformation features (PDFs), high pressure polymorphs of quartz and amorphous phases. Until recently, studies of these features have mostly been focused on crystalline, non-porous rocks. In more porous sedimentary rocks, the effects are complicated by the collapse of pore space and heterogeneous distribution of the shock wave energy. Although roughly the same effects are observed in crystalline and porous rocks, the onset pressures for various effects can differ. Shock and post-shock temperatures in porous rocks are generally much higher and very heterogeneous, resulting in more melt production and localised shock effects (Kieffer, 1971; Kieffer et al., 1976; Osinski, 2007). The effects of target rock porosity and pore fluid content on the cratering process and on shock effects are now being studied in more detail using shock experiments and numerical modelling (e.g. Buhl et al., 2013; Ebert et al., 2013; Güldemeister et al., 2013; Kenkmann et al., 2011; Kowitz et al., 2013).

For reference throughout this section, the crystal structure of α -quartz with the orientation of the c- and a-axes is shown in figure 1.5a and some important crystal faces are indicated in figure 1.5b. Table 1.1 summarises the crystallographic differences between low and high pressure crystalline forms of SiO_2 (quartz, coesite and stishovite). Figure 1.6 and table 1.2 indicate the main PDF orientations.

1.3.1 Planar microstructures

1.3.1.1 Planar fractures

Planar fractures (PFs) are thin (3-10 μm), regular, parallel planar microfractures with a typical spacing of about 20-30 μm (French and Koeberl, 2010). PFs are a low shock feature, forming at peak shock pressures below ~ 10 GPa (French and Koeberl, 2010; Grieve et al., 1996; Langenhorst and Deutsch, 2012), and develop parallel to rational crystallographic planes with low Miller indices. Usually these are (0001) and $\{10\bar{1}1\}$ (Stöffler and Langenhorst, 1994), but also $\{11\bar{2}2\}$ and $\{51\bar{6}1\}$ have been observed (Trepmann and Spray, 2005). Normally PFs are open features, but they can be filled with secondary minerals. When they are not open, PFs may be difficult to distinguish from PDFs using light microscopy. Similar to PDFs, PFs can occur in multiple sets (usually 2-3) in one grain (French et al., 2004; French and Koeberl, 2010), but they do not cross grain boundaries or cracks that were present prior to the shock event. PFs are very similar in appearance to cleavage, so they can only reliably serve as a diagnostic impact indicator when they occur associated with PDFs (French et al., 2004; French and Koeberl, 2010).

1.3.1.2 Planar deformation features

Planar deformation features (PDFs) are very thin (< 1 μm), straight, amorphous lamellae (figure 1.1) that form in quartz as a result of a shock wave passing through the mineral. They are the most unambiguous impact indicator in quartz and therefore represent the most essential proof

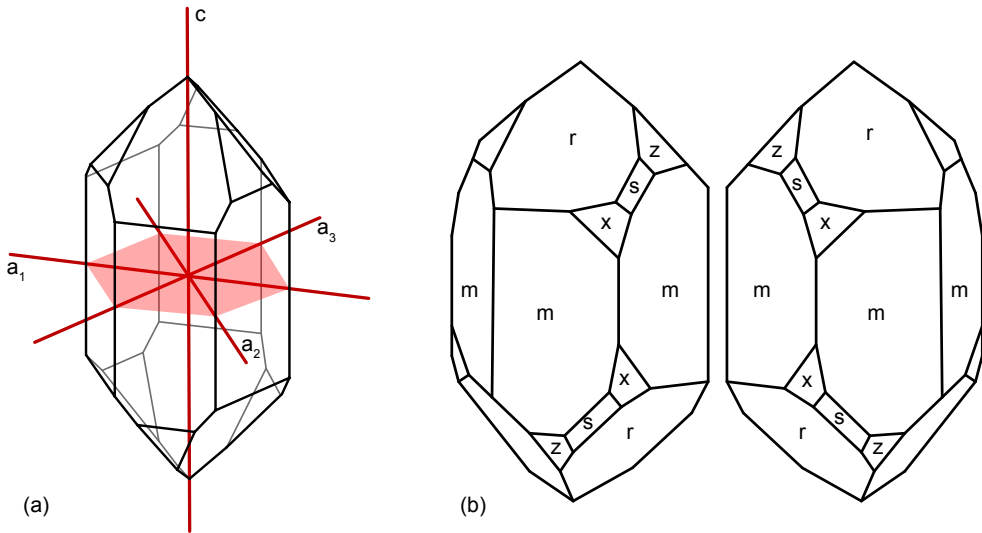


Figure 1.5 Illustrations of the crystal structure of quartz, with indicated in **a** the location of the *c*- and *a*-axes, and in **b** some of the main crystal faces.

for the shock origin of potential impact structures or ejecta layers. PDFs will be discussed in more detail in section 1.4.

1.3.2 Amorphous quartz: diaplectic glass

At relatively high pressures, but with post-shock temperatures below the melting point (>30–50 GPa), quartz is transformed to a short-range order (amorphous) phase, called diaplectic glass, without melting (French et al., 2004; Grieve et al., 1996; Stöffler and Langenhorst, 1994). Diaplectic quartz glass has a higher density and refractive index than synthetic silica glass (fused at low pressure and high temperature), but lower than crystalline quartz (Langenhorst, 1994; Langenhorst and Deutsch, 1994). It inherits the morphology of the original quartz grains (such as fractures and grain boundaries) and shows no flow structures or vesicles.

Diaplectic glass is generally thought to form by direct transformation of crystalline quartz into the short-range order amorphous phase during shock compression and subsequent pressure release (French and Koeberl, 2010; Grieve et al., 1996; Stöffler and Grieve, 2007; Stöffler and Langenhorst, 1994). Langenhorst (1994) proposed a model in which an increasing amount of amorphous PDFs in a grain leads to shock melting of the whole grain under high pressure, because of local high temperatures within the PDFs. The grain in high-pressure melt state is then quenched to diaplectic glass during pressure release, but before complete decompression (see also section 1.4.1.3 on PDF formation). However, Stähle et al. (2008) observed areas of diaplectic glass in grains that also contain PDFs, with in between the PDFs stishovite and a high-density amorphous silica phase. They suggest that the nature of the transition between areas of diaplectic glass and areas with PDFs, stishovite and amorphous silica implies that diaplectic glass forms from the breakdown of PDFs, stishovite and the high-density amorphous phase, under

the influence of post-shock residual heat. This interpretation implies that diaplectic glass is in fact a secondary feature.

1.3.3 High-pressure phases: coesite and stishovite

Table 1.1 and figure 1.4 show the stability fields and main characteristics of low and high pressure forms of crystalline SiO_2 that are relevant in terrestrial impact structures. Two high-pressure polymorphs of SiO_2 , coesite and stishovite, can form at high shock levels (Chao et al., 1961; Chao et al., 1962; Chao et al., 1960). These forms of SiO_2 are normally only stable under mantle conditions. Both polymorphs occur as tiny crystallites ($< 1 \mu\text{m}$) or fine-grained polycrystalline aggregates in diaplectic glass or in shock pseudotachylite veins and high-pressure melt pockets (Grieve et al., 1996; Langenhorst and Deutsch, 2012; Stähle et al., 2008; Stöffler and Langenhorst, 1994) and rarely within PDFs (Stähle et al., 2008).

Pressure ranges for shock formation of stishovite and coesite in non-porous rocks were originally estimated at 12-45 GPa and 30-60 GPa respectively, implying that during an impact event stishovite forms at lower pressures than coesite, in contrast to under equilibrium conditions, when stishovite forms at higher pressure than coesite (Grieve et al., 1996; Stöffler and Langenhorst, 1994). More recently however, it has been suggested that coesite occurs in rocks that have suffered peak shock pressures in the 30-60 GPa range, but that it crystallises from a high pressure melt during pressure release, when the release path passes through the coesite stability field (3-10 GPa, e.g. the path shown in figure 1.4) (Langenhorst and Deutsch, 2012; Stähle et al., 2008).

Stishovite, on the other hand, is thought to form during shock compression, although there is some discussion about the exact mechanism of the transformation. It is likely that both solid-state transformation and crystallisation from silica melt occur, depending on the circumstances (Langenhorst and Deutsch, 2012; Stähle et al., 2008; Tschauer et al., 2006). Although theory predicts that a solid-state transformation of quartz to stishovite (or a stishovite-like six-fold coordinated amorphous phase) occurs under shock loading (e.g. Luo et al., 2003), shock experiments usually only produce crystalline quartz and amorphous silica phases, with only traces of stishovite observed in some experiments. Therefore, either stishovite does form during shock compression, but reverts to amorphous or lower pressure phases upon release, or under shock conditions quartz transforms to a dense amorphous phase, with or without additional stishovite present (Stähle et al., 2008). Tschauer et al. (2006), based on studies of the crystalline state of silica that was recovered from shock experiments, proposed that stishovite forms under shock loading by a solid state transformation, with post-shock heating inducing a slightly disordered to amorphous state. The small amounts of stishovite that are observed in shock experiments would therefore represent a locally different release path, rather than inhomogeneous shock conditions.

Langenhorst (1994) and Langenhorst and Deutsch (2012) consider a model including solid-state transformation implausible, as such a transformation requires atomic diffusion and rearrangement of the crystal structure. On the short timescale of natural impacts and especially shock experiments, there is simply insufficient time for these processes to occur. Instead, both coesite and stishovite crystallise from melt that formed at 'hot spots', where temperatures are locally high enough to melt quartz during shock compression. In support of this scenario, Langenhorst and Deutsch (2012) mention the absence of lattice defects that are known to form during solid-state transformation and the presence of rotation twins (a growth defect) in impact-

related coesite. This might be well-established for coesite, but Stähle et al. (2008), suggested that the transformation from low-pressure tetrahedral four-fold Si coordination (quartz) to high-pressure, collapsed octahedral six-fold Si coordination (stishovite) is not necessarily limited by diffusion, but can be a continuous process. They pointed out that Stolper and Ahrens (1987) suggested that the transformation of tetrahedral to octahedral Si coordination in amorphous silica with increasing pressure can be achieved by a continuous distortion of the tetrahedral framework (Stähle et al., 2008).

From the literature it seems, therefore, most likely that coesite crystallises from a high pressure melt during pressure release, but that stishovite can form both by solid-state transformation and by crystallisation under high pressure. In samples from the Ries crater in Germany, Stähle et al. (2008) found evidence for the formation of stishovite from both solid-state transformation (in parts of grains in between PDFs, associated with an amorphous silica phase) and from crystallisation from high-pressure melt (in pseudotachylite veins, where temperatures are locally increased due to friction, and in PDFs adjacent to a pseudotachylite vein, probably in melt resulting from conductive heating). According to Stähle et al. (2008) the pressure ranges for these two formation mechanisms of stishovite differ; crystallisation from melt occurs under relatively low pressure (<30 GPa) and locally increased temperatures, while solid-state transformation needs higher pressures of 30-45 GPa.

Coesite can form at equilibrium under high static pressure (about 3-9 GPa) and therefore can be present in non-impact related rocks from great depth (Chopin, 1984; French and Koeberl, 2010; Smith, 1984). Recently, stishovite has been observed in non-impact rocks, as a nanocrystalline phase within minute inclusions in 'superdeep' diamonds (Wirth et al., 2007) and there is evidence for post-stishovite phases in ultra-high-pressure rocks (Liu et al., 2007). However, when found in near-surface rocks and in a context free from ultra-high-pressure rocks, the presence of coesite and especially stishovite is very reliable as impact evidence.

Table 1.1 Low and high pressure crystalline forms of SiO₂ (modified from Stöffler and Langenhorst, 1994)

	α-Quartz	β-quartz	Coesite	Stishovite
Equilibrium pressure range	0-3 GPa	0-3 GPa	3-10 GPa	>10 GPa
Shock pressure range	0-35(?) GPa	0-35(?) GPa	30-60 GPa (Stöffler and Langenhorst, 1994) 3-10 G Pa (Stähle et al., 2008)	12-45 GPa
Crystal symmetry	trigonal	hexagonal	monoclinic	tetragonal
Space group	P3 ₁ 21	P6 ₂ 22	C2/c	P4 ₂ /mnm
Unit cell dimensions (Å)	a = 4.913 c = 5.405	a = 5.01 c = 5.47	a = 7.23 b = 12.52 c = 7.23, β = 120°	a = 4.18 c = 2.665
Si coordination number	4 (tetrahedral)		4 (tetrahedral)	6 (octahedral)
density (g/cm³)	2.65 (α) 2.53 (β)		2.93	4.30

1.3.4 Melt: lechatelierite

At pressures >50 GPa the post-shock temperature exceeds the melting temperature of quartz. Upon pressure release, melt forms and is quenched to glass with vesicles and flow structures (lechatelierite) (Stöffler and Langenhorst, 1994). Lechatelierite is normally not present in quartz-bearing non-porous rocks, even if they are highly shocked, because its formation requires peak shock pressures above the point at which whole-rock melting occurs. In whole-rock melt, however, it can be present as inclusions or schlieren. In porous rocks on the other hand, lechatelierite is very common and occurs together with less highly shocked crystalline quartz or coesite. This is a result of the large local pressure and temperature differences that are present in shocked inhomogeneous rocks (Grieve et al., 1996; Kieffer et al., 1976; Stöffler and Langenhorst, 1994).

1.3.5 Mosaicism

Mosaicism is a phenomenon observed in some shocked quartz grains, with or without PDFs. In the light microscope it is manifested as highly irregular ‘mottled’ extinction under crossed polarisers (French and Koeberl, 2010; Grieve et al., 1996; Leroux and Doukhan, 1996; Stöffler and Langenhorst, 1994). Grains with a mosaic structure consist of submicroscopic crystalline domains (200 nm – 3 µm) that are slightly misoriented (up to ~20°) with respect to each other. In general, domain size decreases and misorientation increases with increasing peak shock pressure (Grieve et al., 1996; Stöffler and Langenhorst, 1994 and references therein; Trepmann, 2008), but no quantitative relation has been established. Mosaicism is detected in X-ray diffraction and in TEM diffraction patterns by elongation of the diffraction spots (asterism), which also allows for measurement of the degree of misorientation of the domains. TEM images show the size and shape of individual domains (e.g. Leroux and Doukhan, 1996; Trepmann, 2008).

Stöffler and Langenhorst (1994) classify mosaicism as a relatively low shock phenomenon, starting to occur at 10 GPa and increasing in intensity until ~35 GPa. In shock experiments, mosaicism identified in with light microscopy is observed in isolated grains from ~10 GPa and becomes pervasive between 10 and 20 GPa (Huffman et al., 1993; Huffman and Reimold, 1996; Reimold and Hörz, 1986a, b). Mosaicism is often observed in combination with PDFs in the same grain and is thought to represent a plastic response of quartz shocked at or above the Hugoniot elastic limit, distorting the lattice into misoriented microdomains (Huffman et al., 1993; Huffman and Reimold, 1996; Stöffler and Langenhorst, 1994). More recently mosaicism has been interpreted as the result of two intersecting sets of closely spaced PDFs, dividing the grain into small, slightly misoriented, crystalline domains surrounded by (initially) amorphous material in the PDFs (Leroux and Doukhan, 1996; Trepmann, 2008). Subsequent recrystallisation of the amorphous PDFs induces dislocations, which can evolve into low-angle (sub)grain boundaries and might enhance the misorientation between the domains (Trepmann, 2008). Since a high density and close spacing of PDFs indicate relatively high shock pressures (Ferrière et al., 2008; Langenhorst, 1994; Stöffler and Langenhorst, 1994), this model would imply that mosaicism is a high shock pressure phenomenon (most likely ~30-35 GPa, just before the onset of diaplectic glass formation).

1.3.6 Dauphiné twins

Recently, Dauphiné twins have received some interest in relation to shock effects in quartz (Chen et al., 2011; Trepmann and Spray, 2005; Wenk et al., 2011; Wenk et al., 2005). Dauphiné twins are a type of twin in quartz that can be described as a 180° (or apparent 60°) rotation around the c-axis. Dauphiné twins form by cooling down β -quartz through the inversion point (573°C at ambient pressure) to α -quartz, or by the local application of high stress at room temperature or higher (Frondel, 1945). Although Dauphiné twins can form as a result of stress, no permanent strain results from their formation. However, Dauphiné twinning reduces the stiffness of quartz crystals, i.e. it increases their compliance and makes them more easily deformable (Menegon et al., 2011; Tullis, 1970; Tullis and Tullis, 1972; Wenk et al., 2006). The nature of Dauphiné twins in shocked quartz grains is not completely understood, as there is some evidence for both formation mechanisms.

At the Charlevoix impact structure, Trepmann and Spray (2005) studied the occurrence of Dauphiné twins closely associated with PDFs. They observed twins with boundaries parallel to PDFs and PDFs crossing Dauphiné twin boundaries (thereby changing the PDF orientation from positive into negative forms and vice versa). Usually PDFs with orientations that correspond to both positive and negative orientations within a grain do not occur (Grieve et al., 1996; Langenhorst and Deutsch, 1994; Trepmann and Spray, 2005). Trepmann and Spray (2005) propose that Dauphiné twinning in the Charlevoix samples mainly occurred as a result of the reversion to α -quartz during cooling of quartz that was in the β -state due to pre-impact high temperature and shock heating to temperatures above the α - β transition. Furthermore, they concluded that twinning occurred after PDF development, in order to account for the occurrence of both positive and negative PDF orientations occurring in the same grain, which is normally not observed in α -quartz. The number of grains with PDFs parallel to both positive and negative rhombs (i.e. grains with Dauphiné twins) in this study increased with increasing shock pressure.

However, Wenk et al. (2011; 2005) found Dauphiné twins in shocked quartz samples from the Vredefort crater (South-Africa) and concluded that they formed due to stresses during the impact. They proposed that the direction of the compressive shock wave can be inferred from the preferred orientation of r and z planes in quartz crystals, as Dauphiné twinning causes the positive rhombs $\{r\}$ to align perpendicular to the direction of compressive stress.

Gratz et al. (1992), in an experimental study, noted that Dauphiné twins occur both in quartz grains that have only been in the α -stability field, but also in grains that were preheated to temperatures above the α - β transition and for which the entire experiment was conducted above the α - β transition temperature. They conclude that shock-related Dauphiné twins must be generated during cooling. However, in the grains that have only been in the α -stability field, the twins must be mechanical.

From these studies it seems likely that both stress-induced Dauphiné twins and twins formed during cooling can be present in shocked quartz grains, closely associated with PDFs.

1.3.7 Other effects

1.3.7.1 Bulk physical properties

Some easily observed changes in bulk physical properties of quartz occur as a result of shock damage. The refractive index decreases with increasing shock pressure from $n_o=1.5442$ and $n_e=1.5533$ to about 1.468 in diaplectic glass. Related to the refractive index, shocked quartz shows decreased birefringence, changing from 0.0091 in unshocked quartz to about zero in diaplectic glass. Also density decreases with increasing shock pressure, from 2.65 g/cm³ in unshocked quartz to 2.28 g/cm³ in diaplectic glass (Grieve et al., 1996; Stöffler and Langenhorst, 1994). However, the changes in these properties are only useful as shock pressure indicators in samples that have not experienced post-shock alteration and recrystallisation.

1.3.7.2 Feather features

Only very recently so-called feather features (French et al., 2004; Poelchau and Kenkmann, 2011) have been proposed as a potential shock indicator in quartz, occurring at low shock pressure (probably ~7-10 GPa). Feather features are a combination of PFs and PDF-like lamellae, with closely spaced lamellae branching off from one side of, or developing at an angle to, a planar fracture. Together, the PF and the lamellae form a feather-shaped structure. Orientations of both the PF and the lamellae are crystallographically determined, mostly parallel to c (0001), r/z $\{10\bar{1}1\}$ and ξ $\{11\bar{2}2\}$. The most frequent orientations of rhombohedral PDFs, ω $\{10\bar{1}2\}$ and π $\{10\bar{1}3\}$, are rare in the lamellae in feather features. The lamellae are always shorter than the PF, closely spaced (2-10 μm) and are straight to slightly curved (Poelchau and Kenkmann, 2011). The lamellae have been interpreted as incipient PDFs (e.g. French et al., 2004), but Poelchau and Kenkmann (2011) propose that, based on several characteristics of feather features and the relation between their orientation and stress direction, the lamellae are more likely to be a specific type of shear-related, crystallographically controlled fracture. Future studies of the small scale defect structures will have to determine their structure and formation mechanism.

1.3.7.3 Ballen silica

Ballen silica is a peculiar texture in silica that has only been observed in natural impact rocks and has therefore been proposed as an additional impact indicator (Ferrière et al., 2010; Ferrière et al., 2009a). Ballen silica occurs as rounded or elongate clasts (~10-200 μm), which internally consist of small spherical domains (~1-5 μm) that cut off each other. This appearance has been described as a grape-like texture (Ferrière et al., 2010). Ballen silica can be α -quartz or α -cristobalite, or a mixture of both and occurs within diaplectic glass, as inclusions in lechatelierite or as individual clasts in impact melt rock or suevite. Tiny coesite inclusions have been observed in α -cristobalite from the Bosumtwi crater in Ghana (Ferrière et al., 2009a). Several types of α -quartz ballen and α -cristobalite ballen have been distinguished (see Ferrière et al. (2010; 2009a) for a detailed description). The structure is interpreted as the result of a back-transformation from β -quartz or β -cristobalite to α -quartz. The β -quartz and/or β -cristobalite is thought to crystallise from diaplectic glass and lechatelierite at high temperature (~1100-1700°C) and transforms into α -quartz and/or α -cristobalite with time (Ferrière et al., 2009a). It seems likely that these high temperatures can occur in the post-shock stage after the high pressure that is required to form diaplectic glass (>30-50 GPa) and lechatelierite (>50 GPa).

1.4 Planar deformation features in quartz

Planar deformation features (PDFs) are planar microstructures that form in quartz as a result of a shock wave passing through the mineral. They are the most unambiguous impact indicator in quartz and therefore represent the most essential proof for the shock origin of potential impact structures or ejecta layers (e.g. Alexopoulos et al., 1988; Engelhardt and Bertsch, 1969; French and Koeberl, 2010; papers in French and Short, 1968; Grieve et al., 1996; Stöffler and Langenhorst, 1994). Furthermore, because their orientation is crystallographically determined and depends on peak shock pressure, they serve as an excellent shock barometer that is well-calibrated experimentally (Ferrière et al., 2009b; Grieve et al., 1996).

1.4.1 The nature of PDFs

1.4.1.1 Basal Brazil twins

In quartz affected by low shock pressures, very narrow mechanical Brazil twins occur parallel to the basal plane (0001) (Goltrant et al., 1991; Goltrant et al., 1992; Leroux and Doukhan, 1996; Leroux et al., 1994; Trepmann, 2008; Trepmann and Spray, 2006). A Brazil twin represents a change of hand across the twin boundary and can be mechanical in origin or form during growth of the crystal. No change in lattice symmetry results from the formation of Brazil twins. Mechanical basal Brazil twins are produced by high shear stress (~ 2 GPa) on the basal plane (McLaren et al., 1967) and are therefore thought to result from high shear stresses accompanying the shock wave (Goltrant et al., 1992; Trepmann, 2008). In nature, Brazil twins in this orientation have only been observed in quartz from impact rocks and they are considered as diagnostic impact evidence. Similar to planar fractures, basal Brazil twins are a low shock feature, developing at shock pressures < 10 GPa. Unless they are decorated by fluid inclusions, basal Brazil twins are generally not visible in the optical microscope (Grieve et al., 1996). Basal Brazil twins in shocked quartz are usually referred to as (basal) PDFs, although their microstructure is different to that of rhombohedral PDFs, which are originally amorphous lamellae.

1.4.1.2 Rhombohedral PDFs

Planar deformation features that are not basal Brazil twins consist of thin ($< 1 \mu\text{m}$), parallel, closely spaced (typically $< 2 \mu\text{m}$ apart) amorphous lamellae parallel to specific crystallographic planes. Because the most frequently observed orientations are the rhombohedral planes $\{10\bar{1}n\}$, these non-basal PDFs are often collectively referred to as ‘rhombohedral’ PDFs, even though not all forms are parallel to the rhombohedral planes. Usually multiple sets develop in the same grain: typically there are 2-10 sets. Although PDFs are generally described as strictly straight and planar, some bending or slight curvature has been reported (Engelhardt and Bertsch, 1969; Stöffler and Langenhorst, 1994; Trepmann and Spray, 2005). PDFs can be penetrative through a whole grain or be concentrated in parts of a grain, but they do not cross grain boundaries, faults or planar fractures that were present before PDF formation.

Structurally, PDFs consist of planes of amorphous silica. This amorphous phase is not melt glass, but a high-pressure amorphous silica phase. In experiments, Langenhorst (1994) observed that at low peak shock pressures (< 25 GPa) PDFs occur mainly in single sets and are extremely narrow (~ 30 nm), but around 25 GPa thickness increases to > 200 nm, multiple sets appear and PDFs can become slightly curved and show thickness variations along their length.

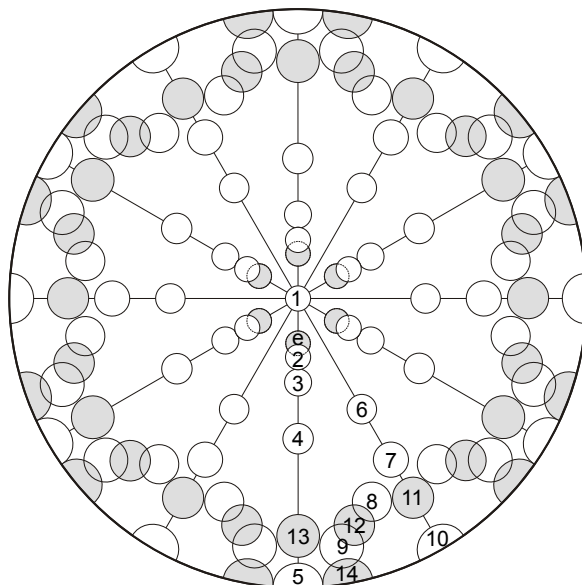


Figure 1.6 Stereographic projection (lower hemisphere equal area) of the orientations of poles to PDFs relative to the c-axis (modified from Ferrière et al. (2009b)). Numbers are explained in table 1.2.

Table 1.2 Typical PDF orientations in quartz (modified from Ferrière et al. 2009)

Nr.	Symbol	Miller-Bravais indices {hkil}	Polar angle(°)*	Azimuthal angle (°)	Nr. of symmetrically equivalent planes
1	c	{0001}	0	-	1
2	ω, ω'	{10 $\bar{1}$ 3}	22.95	30	3
3	π, π'	{10 $\bar{1}$ 2}	32.42	30	3
4	r, z	{10 $\bar{1}$ 1}	51.79	30	3
5	m	{10 $\bar{1}$ 0}	90	30	3
6	ξ	{11 $\bar{2}$ 2}	47.73	60	3
7	s	{11 $\bar{2}$ 1}	65.56	60	3
8	-	{21 $\bar{3}$ 1}	73.71	50	6
9	x	{51 $\bar{6}$ 1}	82.07	40	6
10	a	{11 $\bar{2}$ 0}	90	60	3
11	-	{22 $\bar{4}$ 1}	77.20	60	3
12	-	{31 $\bar{4}$ 1}	77.91	45	6
13	t	{40 $\bar{4}$ 1}	78.87	30	3
14	k	{51 $\bar{6}$ 0}	90	40	6
e	-	{10 $\bar{1}$ 4}	17.62	30	3

*Angle between the pole to the PDF plane and the c-axis

One of the most widely used characteristics of PDFs is their pressure dependent crystallographic orientation. The most frequently observed orientations (see also figure 1.6 and table 1.2) are c (0001) (basal Brazil twins, see section 1.4.1.1), ω $\{10\bar{1}2\}$ and π $\{10\bar{1}3\}$, but also r/z $\{10\bar{1}1\}$, m $\{10\bar{1}0\}$, ξ $\{11\bar{2}2\}$, s $\{11\bar{2}1\}$, $\{21\bar{3}1\}$ and x $\{51\bar{6}1\}$ occur, as well as some other orientations (Ferrière et al., 2009b; Stöffler and Langenhorst, 1994). In α -quartz, correlative positive and negative forms (such as $\{10\bar{1}3\}$ and $\{011\bar{3}\}$) do not occur in the same grain and the negative form $\{01\bar{2}1\}$ only occurs in the same grain with the positive rhombohedra $\{10\bar{1}3\}$ and $\{10\bar{1}1\}$, but not with their negative forms (Langenhorst and Deutsch, 1994; Stöffler and Langenhorst, 1994; Trepmann and Spray, 2005). At low shock pressures, only basal Brazil twins occur, followed by mainly $\{10\bar{1}3\}$ and $\{10\bar{1}1\}$ orientations from ~ 10 GPa. From ~ 20 GPa, also $\{10\bar{1}2\}$ orientations start to occur and become increasingly dominant at higher pressure. Between ~ 25 GPa and the onset of diaplectic glass formation at ~ 35 GPa, only $\{10\bar{1}3\}$ and $\{10\bar{1}2\}$ are formed (see also the lower panel in figure 1.4). Other orientations are mostly accessory and occur only between ~ 10 and 25 GPa (Grieve et al., 1996). The crystallographic orientation of PDFs can be measured in the TEM on small samples, and more conveniently using a light microscope with a universal stage (see Ferrière et al. (2009b) for a review of the method). Although the universal stage allows the collection of large datasets, the method is limited by the optical properties of quartz: only the c -axis orientation can be measured, but not the a -axes. Therefore, PDF planes can be indexed, but indexing of the orientations only shows that the PDF orientations are consistent with particular crystal orientations. The actual orientations cannot be directly measured using this technique. Furthermore, a single PDF orientation cannot be indexed unequivocally. Electron backscattered diffraction (EBSD) measurements in a scanning electron microscope (SEM) are capable of determining the full crystallographic orientation of quartz grains and can be combined with universal stage data to obtain more reliable and complete orientation measurements (e.g. Trepmann, 2008; Trepmann and Spray, 2005).

1.4.1.3 Formation of PDFs

The very local collapse of the crystal structure and amorphisation along specific planes is different from the deformational behaviour of quartz under tectonic stress, when dislocations play an important role in the accommodation of strain. Goltrant et al. (1992) suggested that the local amorphisation can be explained by elastic instabilities in the shear modulus of specific planes in quartz at high pressure. His calculations of the elastic stiffness coefficients of certain planes indicate that around 10 GPa, instabilities occur in planes close to the main PDF orientations (i.e. these planes are weaker at these high pressures and therefore more likely to accommodate deformation locally by collapse of the crystal structure). The shock front separates an uncompressed (unshocked) zone in the crystal from a compressed zone behind the shock front. The misfit between the compressed and uncompressed crystal lattices is compensated by local collapse of the lattice, resulting in solid-state transformation to amorphous SiO_2 . This happens preferentially in the weaker planes at shock pressures above ~ 10 GPa, with the shock front driving growth and expansion of the amorphous nuclei into straight and narrow lamellae. Under compression, the amorphous phase is denser than crystalline quartz and has a predominantly six-fold Si coordination, but upon pressure release and decompression the amorphous phase transforms into a lower density configuration (Langenhorst, 1994).

The solid-state transformation model by Goltrant et al. (1992) was expanded with a temperature component by Langenhorst (1994), who observed a marked increase in PDF thickness and the number of PDFs present in shock experiments above 25 GPa. This is explained by the

shock and post-shock temperature. Four shock pressure and temperature states are discussed in Langenhorst's model, which can each explain different shock structures in quartz, ranging from thin amorphous PDFs at low shock intensity to lechatelierite at very high shock intensity. At low shock pressure, both shock and post-shock temperature stay below the melting temperature of quartz. Thin PDFs are formed in the shock front by the solid-state mechanism proposed by Goltrant et al. (1992). At higher shock pressure (>25 GPa), the shock temperature in the PDFs exceeds the quartz melting temperature, but the post-shock temperature stays below the melting temperature. Because of the different thermodynamic properties of amorphous and crystalline quartz, the temperature can be higher in the high density amorphous phase in the PDFs than in the crystalline quartz. Furthermore, amorphous material generally melts at lower temperature than crystalline material. Therefore, in this second situation, the amorphous thin PDFs are superheated and melt a small portion of the adjacent crystalline quartz ('shock melting'), with subsequent quenching of the structure before complete decompression. This results in the thicker PDFs observed above 25 GPa. The third and fourth shock states explain the formation of diaplectic glass and lechatelierite. If the shock pressure is even higher (>35 GPa) than in the second scenario, the shock temperature exceeds the quartz melting temperature during the compression phase, but also during decompression. This might result in shock melting of the complete grain, which is quenched before complete decompression and becomes diaplectic glass. In the highest shock stage (>50 GPa), both the shock and post-shock temperature exceed the melting temperature and a fluidised melt glass (lechatelierite) is produced. This extended model by Langenhorst (1994) explains the presence of different amorphous phases in various proportions at various shock pressures and is the most widely accepted formation model for PDFs and amorphous phases in shocked quartz.

1.4.1.4 Healed PDFs

It is well known that PDFs can heal under influence of post-shock high temperatures and metamorphic events (Goltrant et al., 1992; Leroux and Doukhan, 1996; Trepmann and Spray, 2006). The amorphous SiO₂ in the PDFs recrystallises, aided by the presence of water that easily penetrates the deformed and broken impact rocks. Healed PDFs consist of planes with a high density of dislocations and fluid inclusions on the TEM scale (Goltrant et al., 1992; Leroux and Doukhan, 1996; Trepmann and Spray, 2006) and can be observed in light microscopy as traces of fluid inclusions (Grieve et al., 1996; Stöffler and Langenhorst, 1994). Because the inclusions lie in the originally amorphous PDF plane, the crystallographic orientations of healed PDFs can be determined with a universal stage (Ferrière et al., 2009b; Grieve et al., 1996). Basal Brazil twins can only be recognised in a light microscope after secondary decoration with fluid inclusions.

1.4.2 Potential misidentification of PDFs

Although with some practice PDFs are quickly identified in a light microscope, for an inexperienced observer the distinction between PDFs and other (sub-)planar microstructures in quartz might not always be straightforward (compare, for example, figures 1.2a and b). Especially in grains with lamellae in only one or two different orientations, or when a limited number of isolated grains are available for study, a reliable demonstration of the shock origin of the microstructures may be difficult. Despite the vast amount of research on shocked quartz that has been published since the 1960s, misidentifications of planar microstructures in quartz as PDFs frequently leads to controversies over proposed impact structures or ejecta layers (e.g.

Vrána, 1987 vs. Cordier et al., 1994; Surenian, 1988 vs. Leroux and Doukhan, 1993; Ernstson and Fiebag, 1992 vs. Langenhorst et al., 1996; Becker et al., 2004 vs. Glikson 2004; Retallack et al., 1998 vs. Langenhorst et al., 2005).

Tectonic deformation lamellae (also called Böhm lamellae or metamorphic deformation lamellae, figure 1.2b) are most frequently misidentified as PDFs. Tectonic deformation lamellae are planar or slightly curved features that form in quartz during slow tectonic processes, usually in single sets. Rarely two or three orientations are observed in one grain (Drury, 1993). In naturally deformed quartz, they consist of very narrow, elongated subgrains or domains with a small misorientation, and like PDFs they can be decorated with fluid inclusions. A range of microstructures and orientations are associated with deformation lamellae in experimentally deformed quartz (e.g. Blenkinsop and Drury, 1988; Drury, 1993; McLaren et al., 1970; Twiss, 1974; White, 1973). Tectonic deformation lamellae often have a sub-basal orientation and might therefore most readily be confused with decorated basal Brazil twins. However, tectonic deformation lamellae are the result of a completely different process and have a fundamentally different microstructure (e.g. Drury, 1993; McLaren et al., 1970).

A relatively easy, but laborious method to prove the shock origin of planar microstructures in quartz is the collection of crystallographic orientation measurements in a light microscope with a universal stage (Ferrière et al., 2009b; Grieve et al., 1996). However, as was mentioned above, the technique has its limitations, due to the optical symmetry of quartz, which inhibits determination of the orientation of the a-axes. This limitation can be eliminated by a combination of EBSD and universal stage data (Trepmann, 2008; Trepmann and Spray, 2005). Gratz et al. (1996) described a method to distinguish between PDFs and tectonic deformation lamellae in the SEM after etching with hydrofluoric acid. The amorphous phase in unaltered PDFs is etched out by the acid, while tectonic deformation lamellae are unetched. This method is relatively straightforward for amorphous PDFs, but healed PDFs are not attacked by the acid to the same extent as the amorphous planes. The most reliable proof for the presence of PDFs is obtained by TEM analysis of the sub-micrometer scale defect structure of the lamellae. Also crystallographic orientation can be determined in TEM, but because of the small sample volumes that can be studied, no statistically significant data can be obtained and the observations are only valid for a limited sample volume.

1.5 Concluding remarks

A wide range of microscopic shock effects occurs in quartz, which have been studied in great detail over the last 50 years in both natural and experimentally shocked material. Shocked quartz, in particular PDFs, can provide a lot of information about shock conditions and the presence of PDFs is often one of the main arguments in the proposal of newly discovered impact craters or ejecta layers. However, it can be difficult to unequivocally identify PDFs without TEM observations, especially when a limited number of grains are available, such as in the case of dubious ejecta layers. Therefore, a thorough study of the microstructure and crystallographic orientations of planar features in quartz and a search for other impact indicators are required before they can serve as a reliable shock indicator.



Chapter 2

Scanning electron microscope cathodoluminescence imaging of planar deformation features and tectonic deformation lamellae in quartz

M.F. Hamers and M.R. Drury

Planar deformation features (PDFs) in quartz are essential proof for the correct identification of meteorite impact structures and related ejecta layers, but can be confused with tectonic deformation lamellae. The only completely reliable method to demonstrate the shock origin of suspected (sub-) planar microstructures, transmission electron microscope (TEM) observations, is costly and time consuming. We have used a cathodoluminescence (CL) detector attached to a scanning electron microscope (SEM) to image both PDFs and tectonic deformation lamellae in quartz, in order to demonstrate the potential of a simple method to identify PDFs and define characteristics that allow their distinction from tectonic deformation lamellae. In both limited wavelength greyscale and composite colour SEM-CL images, PDFs are easily identified. They are straight, narrow, well-defined features, while tectonic deformation lamellae are thicker, slightly curved, and there is often no clear boundary between lamella and host quartz. Composite colour images reveal two types of CL behaviour in PDFs: either they emit a red to infrared CL signal, or they are non-luminescent. The colour of the CL signal emitted by tectonic deformation lamellae ranges from blue to red. For comparison, we imaged several shocked quartz grains also at cryogenic temperature. In most cases the PDF characteristics in cryo-CL images do not differ significantly from those in images recorded at room temperature. We conclude that SEM-CL imaging, especially when colour composites are used, provides a promising, practical, low-cost and non-destructive method to distinguish between PDFs and tectonic lamellae, even when the simplest CL techniques available are used.

2.1 Introduction

Shock metamorphism in terrestrial minerals is diagnostic of meteorite impacts. The presence of shock-metamorphosed quartz in particular is essential for the correct identification of impact craters and distal ejecta layers. Because quartz displays a wide arrange of shock features and is one of the most abundant and most stable minerals in the Earth's crust, shock metamorphism in quartz has been extensively studied in both natural and experimental settings (e.g. Engelhardt et al., 1969; Goltrant et al., 1992; Gratz et al., 1992; Grieve et al., 1996; Kieffer et al., 1976; Langenhorst, 1994; Langenhorst et al., 1994; Leroux et al., 1994; Stöffler et al., 1994; Trepmann et al., 2005; Trepmann, 2008). Shock features in quartz comprise mosaicism, planar fractures (PFs), planar deformation features (PDFs) or shock lamellae, high pressure polymorphs (coesite and stishovite), diaplectic glass and lechatelierite. Recently, feather features (French et al., 2004; Poelchau and Kenkmann, 2011) and ballen silica (Ferrière et al. 2009; 2010) have been proposed as additional shock indicators. PDFs are the most widely studied and most easily recognized shock features that form in quartz. They can be recognized as multiple sets of thin, very closely spaced ($<2\ \mu\text{m}$) sets of planar features that develop parallel to rational low index crystallographic planes, of which the most frequent orientations are (0001), $\{10\bar{1}3\}$ and $\{10\bar{1}2\}$ (e.g. Grieve et al., 1996). PDFs can be subdivided into non-decorated (fresh) and decorated (annealed) types. Fresh PDFs are thin, amorphous lamellae, while older structures are annealed or recrystallized and can usually only be recognized as traces of microscopic fluid inclusions. PDFs parallel to (0001) are not amorphous lamellae, but mechanical Brazil twins (Goltrant et al., 1992) and unless they are annealed and decorated, they cannot be resolved in the optical microscope. Often multiple (max. 18) sets of PDFs develop in a single quartz grain, with the number of sets per grain increasing as a function of shock pressure. PDFs are usually penetrative through a whole grain, but do not cut across grain boundaries, fractures or planar fractures, unless these form at a later stage than the PDFs. A thorough review of shock metamorphic effects in quartz is given in Stöffler and Langenhorst (1994) and Grieve et al. (1996).

Because PDFs are such important features of impact evidence, their correct identification is crucial. However, using a standard petrographic microscope it can be difficult to distinguish between PDFs and non shock-related planar microstructures in quartz. On several occasions lamellar microstructures in quartz have been identified as PDFs, but have subsequently been disproved to be shock-related, or they remain controversial (e.g. Vrána 1987 vs. Cordier et al. 1994; Surenian 1988 vs. Leroux and Doukhan 1993; Ernstson et al., 1992 vs. Langenhorst et al., 1996; Becker et al., 2004 vs. Glikson 2004; Retallack et al., 1998 vs. Langenhorst et al., 2005). Tectonic deformation lamellae in particular are often confused with PDFs, even though these two types of microstructure are fundamentally different in character. Tectonic deformation lamellae are more or less planar features that form in quartz grains as a result of comparatively slow, tectonic processes. When decorated with fluid inclusions, they are also known as Böhm lamellae (Böhm, 1882; Christie and Raleigh, 1959). Similar to PDFs, tectonic deformation lamellae are restricted to single grains and do not cross grain boundaries or fractures that formed before the lamellae. Tectonic deformation lamellae are often recognized in transmission electron microscopy (TEM) as slight misorientations in the crystal lattice; elongated, extremely narrow subgrains; arrays of fluid inclusions; subgrain walls, and zones of different dislocation density (Drury, 1993; Vernooij et al., 2005; White, 1973). Usually a maximum of two sets develops, in a sub-basal orientation (Drury, 1993). Although recently the term 'Metamorphic Deformation Lamellae' was used in a review paper by French and Koeberl (2010), we will retain the term

‘tectonic deformation lamellae’, which is more widely used in the literature. In general, tectonic lamellae are thicker, more widely spaced, and more curved than PDFs, but the two types of structure can be remarkably similar in appearance in a light microscope (figure 2.1; see also for example Officer and Carter, 1991; Lyons et al., 1993; figure 2c in Vernooij and Langenhorst (2005), or figure 29 and 30 in French and Koeberl (2010)). As a result of their apparent similarity, TEM observations of the microstructures are required to convincingly demonstrate the shock origin of lamellar microstructures in quartz (Cordier et al., 1995; Leroux et al., 1994; Vernooij

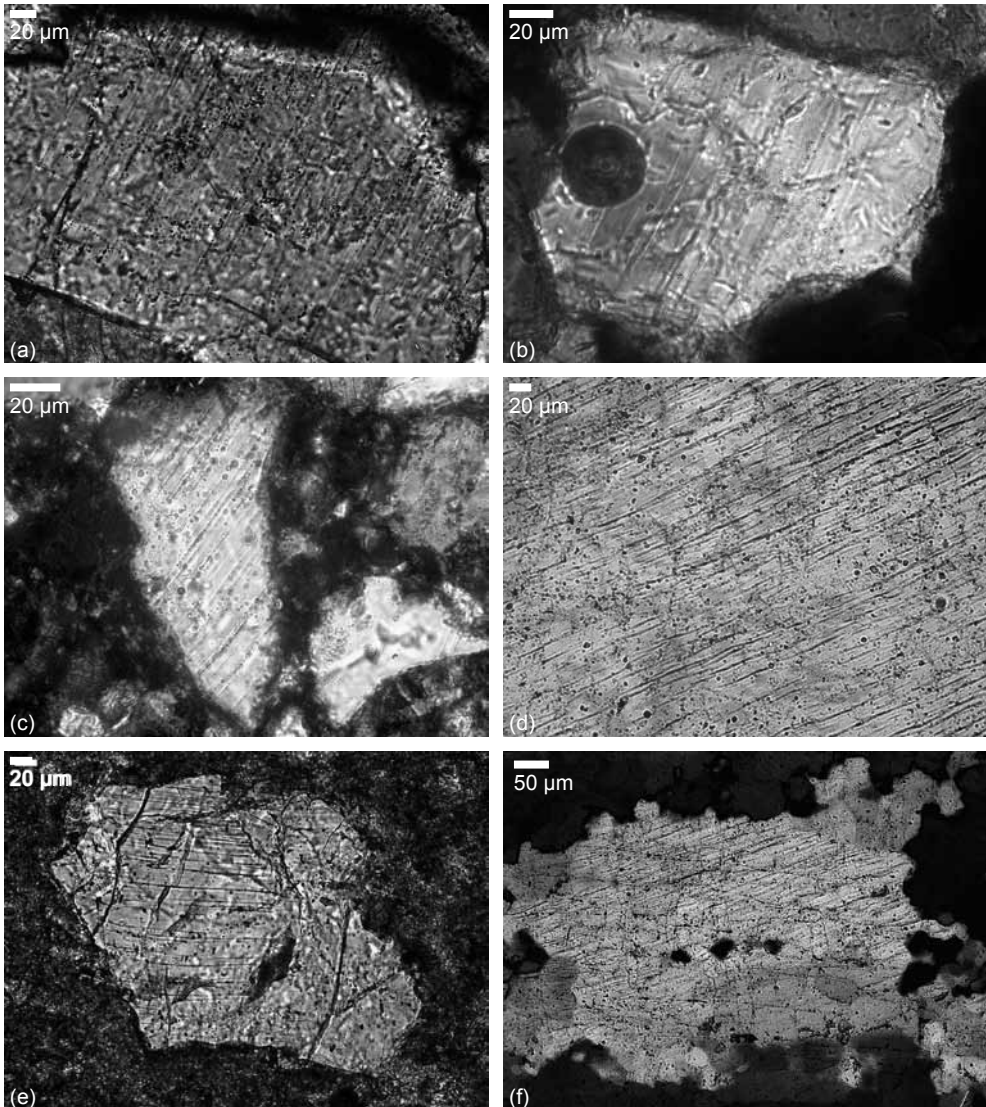


Figure 2.1 Light microscopic images of PDFs in grains from **a** Vredefort, **b, c** Rochechouart, and of tectonic deformation lamellae from **d** Flinders Ranges, Australia, **e, f** the Belgian Ardennes. Especially the PDFs from Vredefort (**a**) and tectonic deformation lamellae from Flinders Ranges (**d**) look similar on first inspection. **a, b, d** and **f** are taken with cross-polarized light; **c** and **e** with plane-polarized light.

Table 2.1 Sample locations and properties

Sample	Location	Rock type	Lat/lon (WGS84)	Nr. of grains			PDF luminescence	Grain luminescence
				PanaCL	Centaurus	Cryo		
OTT-1	Ries (Germany), Orting	Suevite	48°52'32.07"N/ 10°47'42.37"E	1	3	-	Non-luminescent	Red
OTT-2	Ries (Germany), Orting	Suevite	48°52'32.07"N/ 10°47'42.37"E	3	16	6	Red/non-luminescent	Blue/red to blue
RI-37	Ries (Germany), Aumühle	Granite fragment (loose block, probably from suevite)	48°58'16.84"N/ 10°37'43.95"E	3	6	-	Red	Blue
RI-43	Ries (Germany), Polsingen	Gneiss fragment from impact melt rock	48°55'4.61"N/ 10°42'19.36"E	3	2	-	Non-luminescent	Red
RI-47	Ries (Germany), Polsingen	Granite fragment with quartz vein from impact melt rock	48°55'4.61"N/ 10°42'19.36"E	2	5	-	Non-luminescent/ red	Red/blue
MRO-3	Rochechouart (France), Montoume	Impact melt rock	45°46'31.94"N/ 0°46'30.01"E	4	-	-	Red	Reddish brown or blue
MRO-4	Rochechouart (France), Montoume	Impact melt rock	45°46'31.94"N/ 0°46'30.01"E	3	-	-	Non-luminescent/ red	Red/reddish brown or blue
MRO-5	Rochechouart (France), Montoume	Impact melt rock	45°46'31.94"N/ 0°46'30.01"E	9	-	-	Non-luminescent/ red	Red/reddish brown or blue
RO-2	Rochechouart (France), Rochechouart	Lithic breccia		6	23	-	Red	Blue
P2	Popigai (Russia)	Impact melt rock	71°45'31.00"N/110°15'10.00"E	4	1	4	Non-luminescent/ red	Red/blue
E3	Vredefort (South Africa)	Granulite (Inlandsee Leucogranofels)	26°58'15.24"S/ 27°23'18.96"E	3	1	-	Red	Blue

H4	Vredefort (South Africa)	Granulite (Inlandsee Leucogramofels)	26°58'15.24"S/ 27°23'18.96"E	6	-	-	Red	Blue
VTM12C	Vredefort (South Africa)	Granite gneiss	For location see Fig. 1 of Cloete et al. 1999 (same location as sample VTM1.1)	4	-	-	Red	Blue
SARB-03	Flinders Ranges (Australia), south of Wälpena Pound	ABC quartzite	31°39'14.81"S/138°35'15.11"E	2	9	-	-	Blue to purple with red rims/ red
SAPP-02	Flinders Ranges (Australia), south of Pichi Pichi Railway Bridge	Quartzite	32°26'7.29"S/137°58'37.41"E	10	-	-	-	Blue to purple with red rims/ red
B14	High Ardennes Slate Belt (Belgium)	Quartz vein	49°47'54.92"N/ 5°13'11.16"E	5	-	-	-	Red
HV07A	High Ardennes Slate Belt (Belgium)	Quartz vein	49°47'54.92"N/ 5°13'11.16"E	3	-	-	-	Red
HV07B	High Ardennes Slate Belt (Belgium)	Quartz vein	49°47'54.92"N/ 5°13'11.16"E	3	-	-	-	Red
CV4	Bayas Fault Zone, Cantabria (Spain)	Quartzite	(Blenkinsop and Drury 1988, Drury 1993)	4	-	-	-	Blue with red rims/ red

et al., 2005). However, TEM analysis can only be done on very small sample volumes, is time consuming and costly, and TEM facilities are not easily accessible to many research groups. Scanning electron microscopy (SEM) observations, on the other hand, are quick and nowadays many groups have access to an SEM instrument. Observations can be done on relatively large specimens and standard polished thin sections can be handled without difficulties. This is a great advantage, since it enables direct comparison to light microscopy. For example, the same thin section could be used to obtain statistically significant universal stage orientation data, in order to estimate shock pressures. Using a TEM, the same type of measurements can only be made on a few grains. Therefore, reliable SEM methods to identify PDFs in quartz would form a welcome addition to TEM observations. Furthermore, SEM techniques are non-destructive, which is a great advantage in the study of shocked minerals.

Gratz et al. (1996) already showed that etching techniques and secondary electron (SE) imaging provide an unambiguous criterion for distinction of PDFs and tectonic deformation lamellae: amorphous PDFs etch out when treated with HF acid; tectonic deformation lamellae, in contrast, do not exhibit such well-developed etching patterns (Wegner and Christie 1983). Cathodoluminescence (CL) imaging, both in light microscopy and in an SEM, is a technique that has been used to image shocked quartz grains in general (Ramseyer et al., 1992; Trepmann et al. 2005) and PDFs in quartz in particular (Boggs et al., 2001; Cavosie et al., 2010; Gucsik et al., 2003; Seyedolali et al., 1997), but no comparison of PDFs with tectonic deformation lamellae has been made. Seyedolali et al. (1997) used CL to determine the provenance of quartz grains from different settings, including impact sites and stratigraphic impact layers. They found that PDFs can be imaged using a CL detector attached to an SEM, although Gucsik et al. (2003) did not report PDFs in SEM-CL images of experimentally shocked quartzites. Cavosie et al. (2010) imaged shocked quartz grains from the Vredefort crater, showing that also basal (Brazil twin type) PDFs can be observed with SEM-CL. Boggs et al. (2001) used SEM-CL methods to show that in CL images, PDFs can be distinguished from healed tectonic microfractures, but this is the only tectonic structure they looked at and they did not consider tectonic deformation lamellae. We used SEM-CL imaging techniques, both greyscale (limited wavelength) and composite colour, to study known examples of PDFs and of tectonic deformation lamellae in quartz, in order to define characteristics that can be used to identify PDFs and distinguish them from other, non-shock related lamellar microstructures. In this paper, we primarily aim to provide an easy, low-cost method to reliably distinguish between PDFs and tectonic deformation lamellae and not to explain the CL behaviour of the structures in detail, but some possible interpretations of the CL emission of PDFs will be discussed.

2.2 Samples and methods

2.2.1 Samples and imaging techniques

Two SEM systems, each equipped with a CL detector, were used to record CL images in this study. Both systems are located at the Electron Microscopy Laboratory at Utrecht University in the Netherlands. The first system is a Philips XL30S FEG SEM equipped with a Centaurus CL detector (K.E. Developments Ltd, Cambridge, UK), which has a wavelength detection range of 300-650 nm with a peak at 420 nm and is thus most sensitive to blue to violet light. In addition the samples were studied in an FEI Nova Nanolab 600 SEM with Gatan PanaCL

detector (Gatan UK, Oxford, UK). The PanaCL detector is more or less panchromatic and has a detection range of 185-850 nm. Three colour filters (red, green and blue) can be fitted to the Gatan detector for recording colour filtered images. The red filter primarily transmits light in the range 595-850 nm, the green filter in the range 495-575 nm, and the blue filter in the range 185-510 nm. Both unfiltered and filtered images were recorded; the filtered images were subsequently

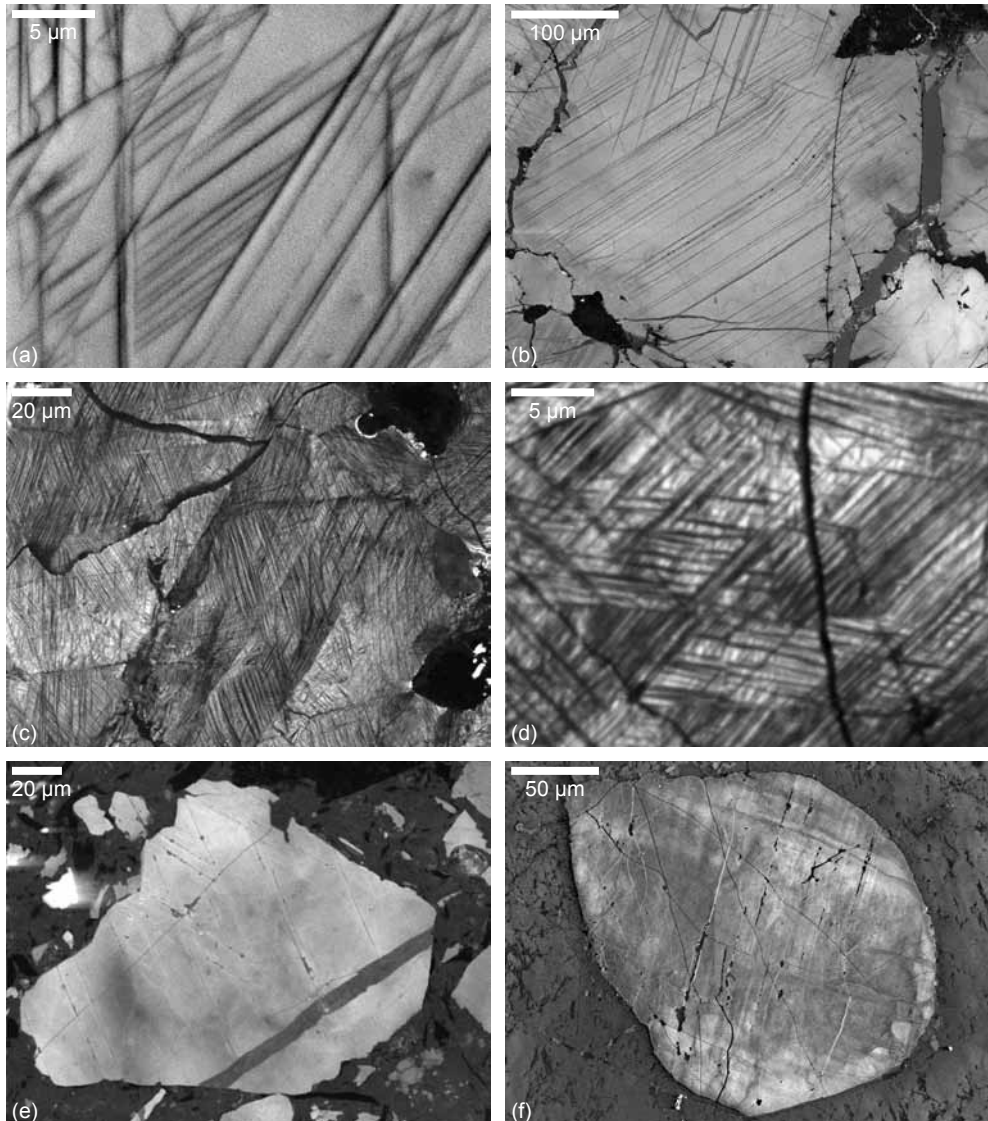


Figure 2.2 Limited wavelength CL images of PDFs from the Ries (a-d), Rochechouart (e) and Vredefort (f) impact structures. PDFs are visible in the Ries and Rochechouart samples, but in the Vredefort sample they can only be recognized from the traces of holes or fluid inclusions. The semi-linear features in the top of the Vredefort grain (f), running NW-SE, are not PDFs and are not visible in the light microscope.

combined into composite RGB colour images in Adobe Photoshop, by including them in the red, green and blue channels of a new image file. Because red, green and blue channels were optimized individually in order to obtain the maximum amount of information from the image, colour information in the images is non-quantitative. The instruments were operated at an acceleration voltage of 5-10 kV and with a beam current of 1.6-6.3 nA, at room temperature. For comparison, ten shocked quartz grains were also imaged at cryogenic temperatures, between -140°C and -170°C, using a liquid nitrogen cooled cryostage in the Nova Nanolab 600 SEM with colour filtered CL. In addition to the CL images, secondary electron and, for most grains, light microscopic images were recorded. All samples are standard polished thin sections, which were carbon coated to prevent charging.

Greyscale (limited wavelength) CL images were recorded, using the Centaur CL detector, for fifty-seven shocked quartz grains in eight samples from well-known impact structures that have been extensively studied (Ries, Rochechouart, Popigai and Vredefort) and for nine grains in one sample containing tectonic deformation lamellae from the Flinders Ranges, Australia. For colour CL, using the Gatan PanaCL detector, fifty-one quartz grains containing PDFs were studied in thirteen different samples from the same impact structures. Six grains from the Ries crater and four grains from the Popigai crater were also imaged at temperatures between -140°C and -170 °C. Furthermore, twenty-seven grains with tectonic deformation lamellae were studied in six samples from three locations (Flinders Ranges, Australia; the Belgian Ardennes and Cantabria, Spain). These numbers are summarized in table 1.1. In several cases the same grains were studied with the two different SEM-CL systems for comparison.

Although the Flinders Ranges in the Adelaide Fold Belt, from which the Australian deformation lamellae samples were taken, is within the range of the ejecta layer of the Late Neoproterozoic Acraman impact structure (Williams et al., 2005), we are quite certain that the samples do not come from this impact layer. The samples were taken from massive quartzite layers such as the ABC quartzite, while the impact ejecta are found in the Bunyerroo mudstone formation.

2.2.2 Cathodoluminescence background

When an electron beam hits a sample in an SEM, several types of beam-sample interaction can occur. One result is that electrons can be excited to a higher energy level. When excited electrons fall back to their original state, either directly or via a trap (in the form of a lattice defect, impurity, or vacancy), photons can be emitted with energies in the infrared, visible or ultraviolet wavelength ranges. This photon emission is the basis of cathodoluminescence. The wavelength (and thus the colour) and intensity of the emitted photons vary depending on the mineral composition of the sample (intrinsic luminescence) and on the number and nature of defects and impurities in the material (extrinsic luminescence). Quartz can exhibit several different CL colours, ranging from bright blue to red, brown or nearly non-luminescent. Several studies have attempted to use CL colour and intensity as a provenance tool, (e.g. Zinkernagel, 1978; Seyedolali et al., 1997; Boggs et al., 2002; Bernet and Bassett, 2005), but there is too much overlap in the colour ranges to make this a reliable quantitative method (Boggs et al., 2002). Furthermore, the crystallographic orientation of quartz grains can have a significant effect on CL colour (Walderhaug and Rykkje, 2000). In general, volcanic quartz has blue CL colour, while plutonic, metamorphic and hydrothermal quartz CL colours range from blue to red (Marshall, 1988; Boggs et al., 2002).

The CL emission of quartz depends on many factors, such as the degree of ordering in the crystal lattice; vacant lattice sites; trace amounts of activators such as Fe^{3+} , Al^{3+} , H^+ , Li^+ , Na^+ , K^+ , and Ti^{4+} ; water content; or damage resulting from radiation, strain, or shock (Marshall, 1988; Ramseyer and Mullis, 1990; Perny et al., 1992). Recently, many studies have focused on the causes of CL intensity differences in quartz (Rusk and Reed, 2002; Landtwing and Pettke, 2005; Rusk et al., 2006) and of specific emission bands in the CL spectra of quartz and other forms of SiO_2 (Ramseyer and Mullis, 1990; Perny et al., 1992; Stevens Kalceff and Phillips, 1995; Stevens

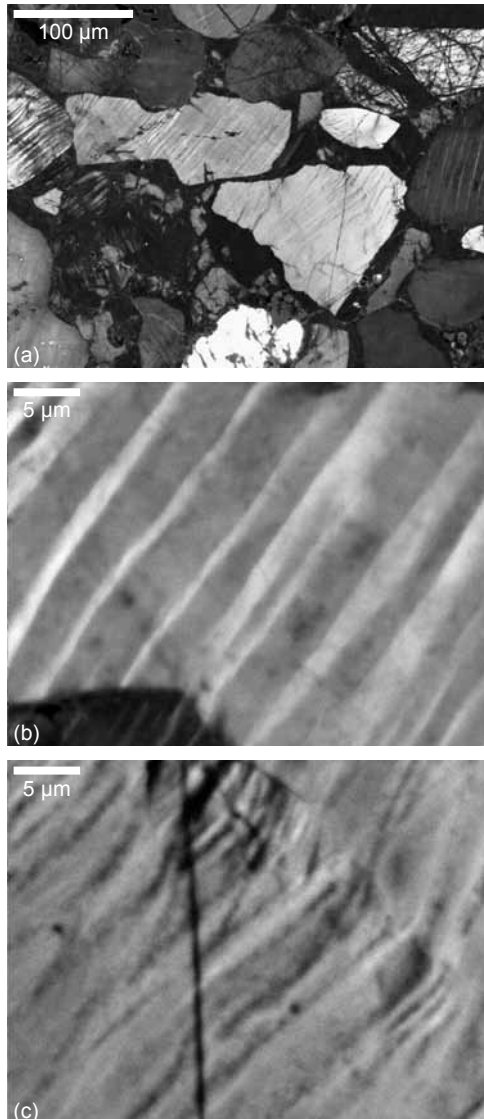


Figure 2.3 **a** Limited wavelength CL images of tectonic deformation lamellae from the Flinders Ranges. **b** Close-up of the grain above and left of the centre in **a**. **c** Close-up of the grain below and right of the centre in **a**.

Kalceff et al., 2000; Götze et al., 2001; Trukhin et al., 2003, 2004; Götze and Kempe, 2008; Stevens Kalceff, 2009). Common emission bands are around 340 nm (Al and Li impurities), 420 nm (intrinsic emission) and 620-650 nm (non-bridging oxygen hole centre, NBOHC) (Stevens Kalceff and Phillips, 1995; Stevens Kalceff et al., 2000; Götze et al., 2001), but many more are described in the literature. The relative intensities of the dominant emission bands in the visible light range (380-700 nm) determine the CL colour that is perceived by the eye (Götze et al., 2001).

Shocked quartz is generally blue luminescent, with an additional emission band at 630-650 nm (Ramseyer et al., 1992; Ramseyer and Mullis, 2000; Trepmann et al., 2005; Götze, 2009; Okumura, 2009; Kayama et al., 2010), although the 630-650 nm band was not observed in experimentally shocked quartzite (Gucsik et al., 2003).

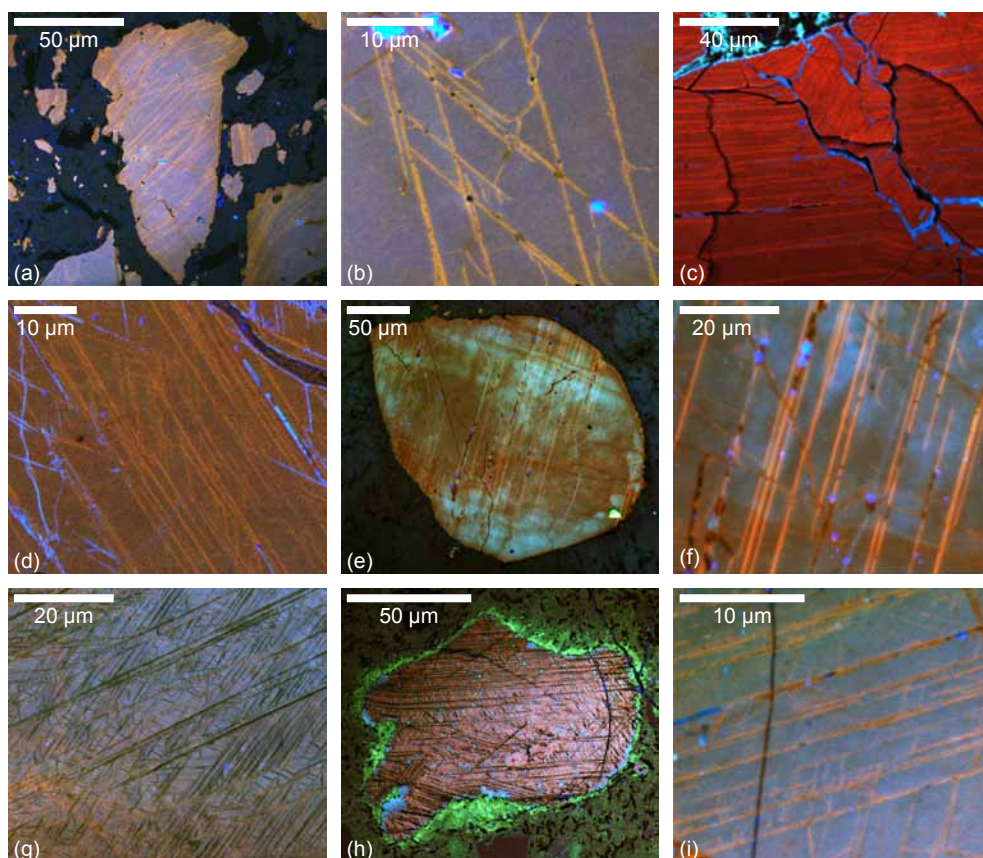


Figure 2.4 Composite colour CL images of PDFs from **a** Rochechouart – same grain as in figure 2.1b. **b** Rochechouart – higher magnification image of the grain in figure 2.2e. **c** Rochechouart – higher magnification image of the grain in figure 2.1c. **d** Rochechouart. **e** Vredefort – same grain as in figure 2.2f. **f** Vredefort – higher magnification of the grain in figures 2.4e and 2.2f. **g** Ries. **h** Popigai. **i** Popigai. In all samples, including those from Vredefort, PDFs are clearly visible as either red or non-luminescent linear features. Bright blue-luminescent spots are caused by remains of aluminium oxide polishing grains.

2.3 Results

2.3.1 Greyscale cathodoluminescence

In the limited wavelength greyscale SEM-CL images (figure 2.2), PDFs appear as well-defined, narrow darker lines that are non-luminescent, in contrast to the host quartz grains, which are lighter in the CL images. Usually the PDFs are straight and of constant thickness (figures 2.2a, b, and e), but in some grains they appear slightly curved and show slight thickness variations (figures 2.2c and d). In all of these grains, multiple sets of PDFs are present (at least three, often four or more) and they are very closely and regularly spaced, thicker, and with slightly wavy edges. PDFs from different impact structures show the same CL characteristics; only in the Vredefort samples (figure 2.2f) no clear PDFs are visible in the greyscale images.

Tectonic deformation lamellae in greyscale SEM-CL images (figure 2.3) can be either more luminescent than the host quartz grain or non-luminescent. Generally, the lamellae are slightly wavy features with a varying thickness; they are thicker and much less well-defined than the PDFs in figure 2.2.

2.3.2 Composite colour cathodoluminescence

In terms of shape and thickness, PDFs in the composite colour SEM-CL images (figure 2.4) are identical to the limited wavelength images (figure 2.2). However, it is evident that the PDFs are usually luminescent and emit mainly red light (figures 2.4a-f and i), which differs from the CL information in the greyscale images shown in figure 2.2. This is true for most PDFs, including the Vredefort samples (figures 2.4e and f), and in host quartz grains, which have different CL colours, ranging from red and brown to purple and blue. The red emission of the PDFs becomes brighter with increasing scanning time and after repeated scanning with the electron beam, making them more easily discernible. Only in highly shocked grains with multiple sets of closely spaced PDFs are the lamellae non-luminescent (figures 2.4g and h). This is the case in the grains that show more, thicker, less straight and more sets of PDFs in limited wavelength images. Figure 2.4g shows that also partly red, partly non-luminescent PDFs occur (bottom right, SW-NE trending set). Red luminescent PDFs usually occur in violet to blue-luminescent host quartz (figures 2.4a, b, e, f, and i), although in Rochechouart grains also reddish-brown host quartz is observed (figures 2.4c and d). Non-luminescent PDFs most often occur in red luminescent host quartz (figure 2.4h), but in some cases the host quartz shows both red and blue luminescent parts (figure 2.4g).

Composite colour images of tectonic deformation lamellae (figure 2.5) are very similar to the limited wavelength images shown in figure 2.4, but differ very much from the colour images of PDFs. Although shape and thickness alone is clearly sufficient to distinguish between tectonic deformation lamellae and PDFs, the CL colour information further emphasizes the different appearance of the two microstructures. While PDFs are consistently red or non-luminescent, tectonic deformation lamellae show a range of colours from blue to red. It is not always clear where host quartz and tectonic lamella begin or end, or even which part of the grain should be defined as 'grain' or 'lamella'. Due to their variable CL emission and the vague boundaries between lamellae and host quartz, in both greyscale and colour CL images, it is very difficult to accurately define and measure the spacing and thickness of tectonic deformation lamellae. PDFs

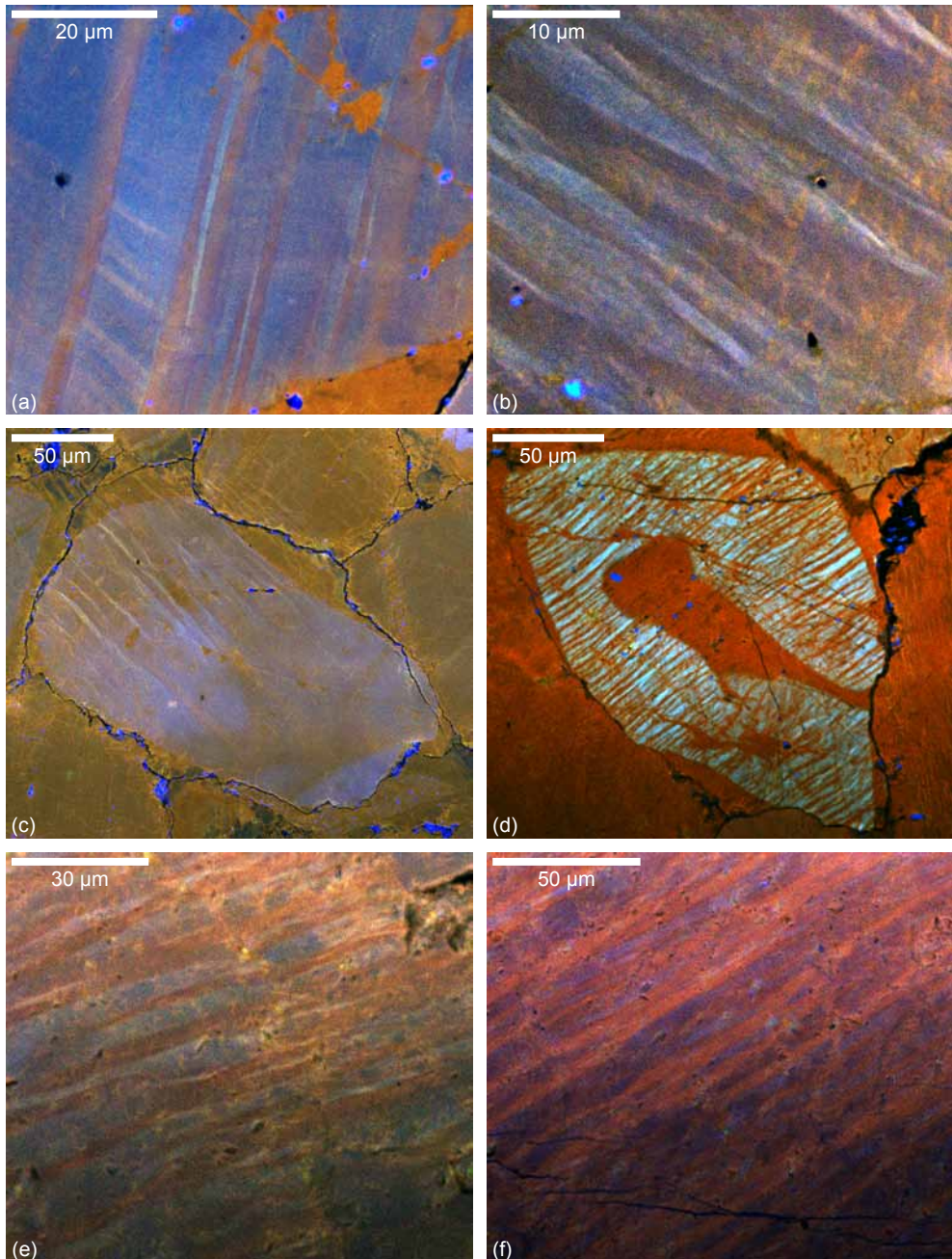


Figure 2.5 Composite colour CL images of tectonic deformation lamellae from **a-c** Flinders Ranges (same grain as in figure 2.1d), **d** Cantabria, **e, f** the Ardennes. Bright blue-luminescent spots are caused by remains of aluminium oxide polishing grains.

on the other hand have sharp boundaries, and a clear distinction can be made between PDF and host quartz, making accurate measurements of their (apparent) spacing and thickness possible.

Table 2.2 summarizes the characteristics of both PDFs and tectonic deformation lamellae in CL images.

2.3.3 Secondary electron imaging

Secondary Electron (SE) images of two tectonically deformed and six shocked quartz grains are shown in figure 2.6. Tectonic deformation lamellae (figures 2.6a and b) are barely detectable in SE images. In some grains they show up as more or less linear, but relatively broad (compared to decorated PDFs), traces of fluid inclusions (figure 2.6b, through the centre from top left to bottom right). PDFs are only visible in SE images when they are decorated; these PDFs show up as strictly linear traces of tiny holes or fluid inclusions (figure 2.6d). It is clear from figure 2.6c that undecorated PDFs cannot be recognized in SE images (compare figure 2.6c to figure 2.4d, where the same grain shows multiple sets of PDFs in the colour CL image that are invisible in the SE image). In some grains where many sets of closely spaced PDFs are present, the PDFs are not decorated by small holes, but are partly open features (as in figure 2.6e). It seems that these partly open PDFs are always of the non-luminescent type, while both ‘normal’ decorated and undecorated PDFs are red luminescent (in between the fluid inclusions, in the case of decorated PDFs). The non-luminescence occurs not only in the open parts of these PDFs, where there is no material to produce a CL signal, but also in the rest of the lamellae (compare figures 2.4g and 2.6e). Therefore there is a genuine lack of CL signal in these PDFs.

2.3.4 Cryogenic composite colour cathodoluminescence

Figure 2.7 shows composite colour images of the same grains, recorded at room temperature and at -140°C or -170°C . Using the liquid nitrogen-cooled cryostage, the intensity of the CL emission strongly increases, especially in the blue and green colour ranges. In most cases the overall colour characteristics of the shocked quartz grains remain the same: red luminescent and non-luminescent PDFs occur, although the CL colour of the host quartz often changes slightly at cryogenic temperature. However, in some grains that contain the non-luminescent type of PDFs at room temperature, red luminescent PDFs appear at cryogenic temperatures that are not visible at room temperature (compare figure 2.4h with figures 2.7f and 2.7i).

For many grains the image quality is better at room temperature than at cryogenic temperatures. As a result of the extreme increase in intensity of the blue emission, there is less detail in the cryo-CL images (compare figures 2.7g and h, or figures 2.4h and 2.7f).

2.4 Discussion

2.4.1 Distinction between planar deformation features and tectonic deformation lamellae

The most important characteristics of PDFs and deformation lamellae are summarized in tables 1.1 and 1.2. Our results show that CL imaging is a very promising method to distinguish between

shock and tectonic deformation lamellae, even on a visual basis alone. In cases where only one or two sets of lamellar microstructures are present, which could lead to misidentification in a light microscope, the CL characteristics of the structures clearly show whether they are PDFs or tectonic deformation lamellae (figures 2.2-2.5): PDFs are thin, straight lines that are dark in greyscale CL images and red or non-luminescent in composite colour CL images, while tectonic deformation lamellae are less well-defined, thicker and slightly wavy, with varying thickness and can show varying CL colours in composite colour images.

The physical basis of the difference in CL emission between shocked and tectonically deformed grains is unclear and requires further research into the relationship between the CL emission and the nature of the different microstructures. However, even without knowing the exact cause of the CL signal, SEM-CL imaging appears to be a useful technique to distinguish between tectonic and shock lamellae and to identify PDFs in quartz.

Spacing and (apparent) thickness of planar microstructures in quartz have been mentioned as characteristic features to distinguish between tectonic and shock lamellae (French et al., 2010; Grieve et al., 1996; Stöffler et al., 1994), but are in practice not often used quantitatively. In general, tectonic deformation lamellae are thicker, more widely spaced and usually slightly curved, whereas PDFs are extremely thin, closely spaced and straight (Alexopoulos et al., 1988; Lyons et al., 1993). However, these are not definitive criteria; a range of different types of tectonic deformation lamellae has been recognized (Christie and Raleigh, 1959; Christie et al., 1974; Drury, 1993; Vernooij et al., 2005; White, 1973). For both PDFs and tectonic deformation lamellae there are many cases in which spacing, thickness and straightness deviate from the 'standard' values. Even in a relatively small sample set such as ours, these characteristics show considerable variation, which is obvious from figure 2.2 to 2.5. Whereas the PDF spacing depends on the impact pressure, the spacing of tectonic deformation lamellae depends on stress level (Koch et al., 1981). Tectonic lamellae may occur that are as closely spaced as PDFs (see for example the tectonic lamellae in figures 2.5d, e, and f). Furthermore, spacing and thickness measurements will depend on the imaging method used; in SEM-CL images, for example, more and thinner individual lamellae can be recognized than in light microscopic images, and thus the results of spacing and thickness measurements could differ if the size and spacing of the PDFs are below the spatial resolution for the imaging method used. The spatial resolution of a standard light microscope is theoretically limited to ~200-400 nm (Nesse, 2004), but is worse in practice. It is known from TEM measurements that many PDFs and some types of tectonic deformation lamellae are thinner than this limit (Langenhorst, 1994; McLaren et al., 1970; Stöffler et al., 1994), and some of these lamellae, therefore, will not be detected in a light microscope. As already mentioned in section 2.3.2, it is questionable whether it is at all possible to perform reliable measurements of spacing and thickness on tectonic deformation lamellae. Tectonic deformation lamellae are not as clearly defined as PDFs. In CL images it is not always evident which part of the grain is lamella and which part is host quartz (see for example figures 2.3c and 2.5b, c, and e). McLaren et al. (1970) also pointed out that in a light microscope, tectonic deformation lamellae are most easily observed when the microscope is focused on the upper surface of the thin section, and that when the lamellae are exactly in focus (which would be required for accurate thickness measurements) they are almost invisible. Thus measurements on tectonic deformation lamellae are difficult and unreliable.

The presence of multiple, differently oriented sets of (indexed) planar features in a quartz grain of course remains a good indicator for shock, but in cases where light microscopy shows only

one or two sets of lamellae, and when it is not immediately obvious whether these are shock or tectonic lamellae, CL imaging can distinguish between the two. In addition to the shape criteria described above, CL images often show more sets of PDFs than can be observed in light microscopy. This is readily seen when comparing for example figures 2.1c and 2.4c, or figures 2.1b and 2.4a, which show the same grain in a light microscopic and colour CL image respectively.

Filtered, colour and cryo-CL imaging and CL spectroscopy can all provide extra information on the nature of planar microstructures in quartz. However, unfiltered greyscale CL images will in many cases be sufficient to distinguish PDFs from tectonic deformation lamellae and show features that are unclear in light microscopy.

All our shocked samples are from impact structures in predominantly crystalline, non-porous target rocks. Because of the porosity of sedimentary target rocks, the shock wave energy is distributed much more heterogeneously than in crystalline targets. As a result, shock effects representative of different shock stages in the classification for non-porous rock types can occur together in porous rocks (Grieve et al., 1996). However, the same types of shock effects occur and there is essentially no structural difference between PDFs in quartz grains from crystalline (non-porous) or from sedimentary (porous) target rocks (Kieffer, 1971; Kieffer et al., 1976). We therefore do not expect that the CL characteristics from PDFs in quartz from sedimentary rocks differ so much from those in crystalline rocks, that the distinction between PDFs and tectonic deformation lamellae becomes impossible. Future research is needed to show how the extra heat production involved in impacts into porous rocks might affect the CL emission of (parts of) shocked quartz grains.

2.4.2 Cathodoluminescence characteristics of planar deformation features in quartz

2.4.2.1 Cryo-cathodoluminescence

In contrast to many other minerals, such as feldspars, calcite or zircons, quartz does not exhibit high intensity CL emission at room temperature. At temperatures below -80 to -100°C the CL emission of quartz shows a dramatic increase in intensity by factors of 100 to 1000 (Marshall, 1988), so in order to get the highest intensity signal, CL work is often carried out at low temperature. In our low temperature comparison, the intensity of the CL emission strongly increased, as expected, especially in the blue and green range. However, the overall results at

Table 2.2 Cathodoluminescence characteristics of planar deformation features and tectonic deformation lamellae

	Planar deformation features	Tectonic deformation lamellae
CL colour	Red/non	Red/blue
Number of sets	(Usually) multiple	Usually one, rarely two
'Sharpness'	Very well defined	Hard to distinguish lamellae from host quartz
Thickness	(Usually) thin	(Usually) much thicker
Spacing	Variable, but usually closely spaced	Closely spaced
Straightness	Straight	Slightly curved, sub-planar

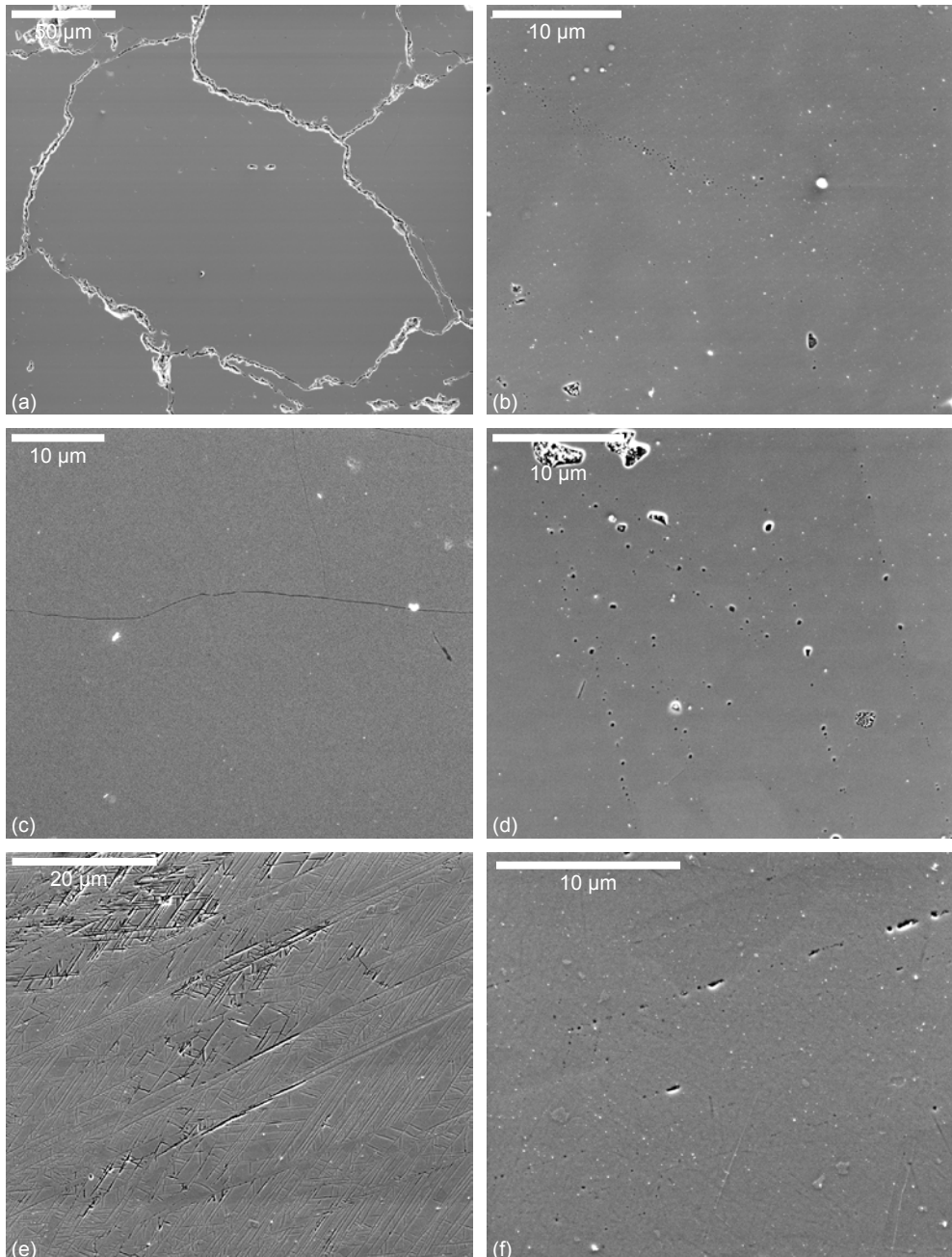


Figure 2.6 Secondary electron images of **a** Tectonic deformation lamellae from Flinders Ranges – same grain as in figure 2.5c. **b** Tectonic deformation lamellae from Flinders Ranges – same grain as in figure 2.5b. **c** Undecorated PDFs from Rochechouart – same grain as in figures 2.1c and 2.4c. Note that the PDFs in this grain can be seen in both light microscopic and CL images, but are invisible in this SE image. **d** Decorated PDFs from Rochechouart – same grain as in figures 2.2e and 2.4b. **e** PDFs from Ries – same grain as figure 2.4f. Black linear features in this image are open PDFs; other contrast

cryogenic temperatures were the same as those found at room temperature: both red- and non-luminescent PDFs are present and in most cases also the CL colour of the host quartz does not change significantly. These results show that, although cryo-CL does give a higher intensity CL emission, cryo is not required to image shocked quartz grains and identify PDFs. On the contrary, as Boggs et al. (2001) already observed, the quality of the CL images is often better at room temperature than at cryogenic temperatures. Although cryo-CL can often provide extra information, even the simplest method of SEM-CL imaging, at room temperature, produces high quality images that are sufficient to identify PDFs in quartz and distinguish them from tectonic deformation lamellae.

2.4.2.2 Cathodoluminescence of shocked quartz

Boggs et al. (2001) reported that PDFs can be imaged with SEM-CL methods and concluded that PDFs are visible in CL images because they are non-luminescent, in contrast to the host quartz grain. Our results show that the latter is not the case; in fact, most PDFs do emit light, mostly in the red to infrared wavelength range (595-850 nm, red filter). PDFs often appear non-luminescent in (panchromatic) CL images, because the intensity of the (usually) blue light emitted by the surrounding quartz is often so much higher than the intensity of the signal coming from the material in the PDFs. In the case of Boggs et al. (2001) the apparent non-luminescence of the PDFs might also be a result of the CL detector they use, which has a detection range of ~185-700 nm and detects (part of) the ultraviolet and the complete blue wavelength range, but does not detect all of the red range (620-750 nm), and none of the infrared wavelengths. The PDFs could appear non-luminescent because of the low intensity CL signal emitted by the PDFs and the limited range of the detector, although this would depend on the specific wavelength of the CL emission of the PDFs. In the images recorded with our blue-sensitive limited wavelength CL detector, PDFs are dark because they emit red light, which is not detected and therefore the structures appear to be non-luminescent. Several studies have shown that shocked quartz is usually blue luminescent, with an additional emission band at 630-650 nm (Ramseyer et al., 1992; Ramseyer and Mullis, 2000; Trepmann et al., 2005; Götte, 2009; Okumura, 2009; Kayama et al., 2010). The red luminescent PDFs observed in our samples could (partly) be the source of this band.

The two types of CL behaviour observed in PDFs (red to infrared or non-luminescent) are possibly related to shock intensity. Non-luminescence of PDFs only occurs in grains with multiple sets of closely and regularly spaced, thicker PDFs (figures 2.4g and h), which indicate high shock pressure (Ferrière et al., 2008; Grieve et al., 1996). Okumura et al. (2009) found that shocked quartz grains from the Ries crater show the usual emission bands with maxima around 385 nm (violet) and around 650 nm (red). The 650 nm band is observed independent of shock pressure, whereas the 385 nm band disappears in more highly shocked grains. This seems to be in line with the observation that non-luminescent PDFs usually occur in highly shocked, red luminescent quartz grains. Red CL emission of PDFs is seen in grains with a lower number of sets of PDFs, which should be more widely and less regularly spaced and are, therefore, interpreted as the result of lower shock pressure.

is probably the result of some slight orientation contrast detected. **f** PDFs from Popigai – same grain as in figure 2.4g. Some PDFs are decorated, but most are not (note that they can be recognized in the CL image in figure 2.4g).

Most of the PDFs from the Vredefort impact structure occur in single sets and are of the basal, Brazil twin type (Carter, 1965; Grieve et al., 1990; Leroux et al., 1994). In our Vredefort samples, we observed only grains with one set of PDFs, so it is likely that most of these are basal PDFs. It is striking that the characteristic red CL emission is observed in features that have a fundamentally different structure: in PDFs that are considered amorphous (Ries) as well as in basal, Brazil twin type PDFs (Vredefort) and decorated PDFs (Rochechouart, Popigai). An explanation for this is not apparent from the CL images alone and will require further research into the exact nature of the defects, composition or water content variations that might cause the typical red CL signal of PDFs.

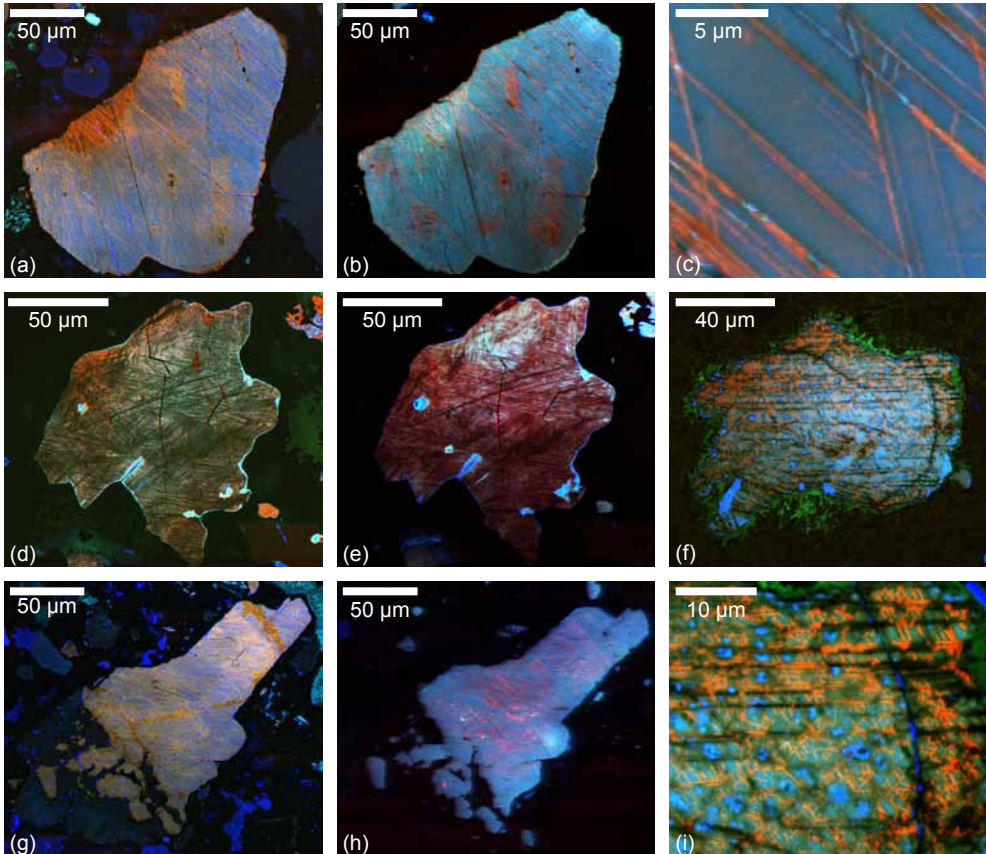


Figure 2.7 Composite colour CL images recorded at room temperature (RT) and at cryogenic temperatures. **a** Shocked quartz grain from the Ries crater, showing red luminescent PDFs, RT. Red patches are beam damage from earlier scanning. Same grain as in figure 2.2a. **b** Same grain as in a, -140°C. **c** Higher magnification of the grain in a and b, -140°C. Small irregularities in the PDFs are a relic of slight charging of the sample. **d** Shocked quartz grain from the Ries crater, showing non-luminescent PDFs, RT. **e** Same grain as in d, -170°C. **f** Shocked quartz grain from the Popigai crater, same grain as in figure 2.4h, -170°C. At RT, this grain contains non-luminescent PDFs and the host quartz is red luminescent. At -170°C also red luminescent PDFs appear and the host quartz shows more blue CL. **g** Shocked quartz grain from the Ries crater, showing red luminescent PDFs, RT. **h** Same grain as in g, -170°C. **i** Higher magnification image of the grain in f, -170°C. Bright blue spots in these images are remains of polishing grains.

2.4.2.3 Possible causes of the cathodoluminescence behaviour of planar deformation features and difference between red- and non-luminescent PDFs

Several causes of red CL emission in quartz are mentioned in the literature. High water content or low Ti/Fe ratio can result in a red CL emission (Marshall, 1988). Substitutional incorporation of Fe^{3+} into the quartz lattice probably gives rise to an emission band around 705 nm (red to infra-red) (Götze et al., 2001). Fitting et al. (2001) observed a red peak (around 650 nm) in the CL spectrum of SiO_2 glass, indicating that also amorphous SiO_2 is capable of producing red CL (although of course CL colour cannot prove anything on crystal structure). The most important red CL peak is the common 620-650 nm emission band in quartz. It consists of two overlapping components at 620 nm and at 650 nm and can be caused by an oxygen vacancy or a non-bridging oxygen hole centre (NBOHC, $\equiv\text{Si}-\text{O}^\cdot$, a dangling oxygen bond) (Stevens Kalceff and Phillips, 1995; Stevens Kalceff et al., 2000; Götze et al., 2001). Different precursors for the NBOHC have been proposed that influence the band position. Among these precursors are hydrogen and sodium impurities, hydroxyl groups ($\equiv\text{Si}-\text{OH}$) (620 nm), peroxy linkages ($\equiv\text{Si}-\text{O}-\text{O}-\text{Si}\equiv$) (650 nm), and strained silicon-oxygen bonds ($\text{Si}-\text{O}$) (650 nm) (Stevens Kalceff and Phillips, 1995; Götze et al., 2001).

The 650 nm emission increases during electron bombardment (Götze et al., 2001), which is an indication that this might be the emission of the red luminescent PDFs, since they become brighter after repeated scanning with the electron beam. Furthermore, this emission band is commonly observed in shocked quartz grains (Ramseyer et al., 1992; Ramseyer and Mullis, 2000; Trepmann et al., 2005; Götze, 2009; Okumura, 2009; Kayama et al., 2010). Götze (2009) attributed the presence of a 630-650 nm emission band in shocked quartz from the Siljan and Araguainha craters to thermal breaking of OH groups, which are incorporated in the quartz. However, according to Stevens Kalceff et al. (2000), the emission related to the NBOHC with OH precursor is at 620 nm and attenuates quickly under electron irradiation at room temperature. This does not fit our observation that the intensity of the emission in red luminescent PDFs increases after repeated scanning.

Also high water content or hydrogen impurities in the PDFs could explain the red luminescence, because H_2O is much more soluble in the amorphous material within PDFs than in the adjacent crystalline quartz (Grieve et al., 1996). The occurrence of basal PDFs decorated with tiny fluid inclusions illustrates that also along Brazil twin boundaries water content might be locally increased, giving rise to the same CL behaviour for the two different types of PDF.

A final explanation for the red luminescence of PDFs might be strained silicon-oxygen bonds. It is possible that strained Si-O bonds are present in the SiO_2 within PDFs (or were present before annealing), where the crystal structure is disordered or (partly) destroyed by the shock wave. These strained bonds could form the precursors for NBOHCs. Also basal, Brazil twin PDFs might contain strained silicon-oxygen bonds as a result of the high differential stresses that form these structures during the shock event. Although no bonds need to be broken to form this type of twin, there will be some strain at the twin boundary (McLaren 1970).

Of course the above interpretations remain rather speculative and measurements of CL spectra of the emission from the PDFs could provide valuable extra information for the interpretation of the PDF characteristics in CL images.

The difference in CL emission between the red- and non-luminescent PDFs could be caused by structural differences of the material within the PDFs, as a result of increasing shock

pressure and temperature. As mentioned in section 2.4.2.2, the occurrence of multiple sets of non-luminescent PDFs per grain, their close and regular spacing, thickness and slightly wavy boundaries all indicate formation under high shock pressures (Langenhorst, 1994; Ferrière et al., 2008). According to the model presented by Langenhorst (1994), the transformation of crystalline quartz to diaplectic quartz glass is a process in which the number of dense, amorphous PDFs increases with increasing shock pressure and temperature, until the whole grain consists of diaplectic glass, with fluidal glass (lechatelierite) only occurring when the residual (post-shock) temperature is sufficiently high. Three phases occur during this process: 1) when both shock and post-shock temperatures are below the melting point of quartz, extremely narrow, straight PDFs, consisting of a superheated, dense, amorphous phase, form by solid-state transformation, to compensate for crystal lattice incompatibilities at the shock wave propagation front; 2) at higher shock pressure the shock temperature increases to just above the quartz melting temperature and the PDFs are at a sufficiently high temperature to melt a small region of the adjacent crystalline quartz, resulting in thicker PDFs with more wavy boundaries; 3) when, at even higher shock pressure, the shock temperature is significantly higher than the quartz melting temperature, the crystalline regions between the PDFs melt completely and the whole grain transforms into diaplectic quartz, which is quenched before complete decompression.

In this model, the red luminescent (rhombohedral) PDFs could form during the first stage, when no melt is formed, but an amorphous phase in which the quartz lattice is disordered, but retains some of its structure. The CL emission centres that form during this stage must either survive post-shock annealing, or be a secondary feature, because the red luminescent PDFs are also observed in altered impact structures, such as the Rochechouart structure. During the second stage, the thicker, non-luminescent PDFs form, filled with quartz melt or diaplectic glass, because of the higher temperature associated with higher shock pressure. The complete destruction of the quartz crystal structure might result in non-luminescence of the material within the PDFs.

2.5 Conclusions

Both greyscale (limited wavelength) and composite colour SEM-CL images provide strong criteria for distinction between planar deformation features and tectonic deformation lamellae in quartz, based on shape, thickness variability and straightness, with in addition different CL colour signatures when colour CL images are recorded. Colour imaging is the most reliable technique, since it shows that PDFs occur as two main types: either red- or non-luminescent, while tectonic deformation lamellae show varying CL colours, ranging from blue to red. When colour CL facilities are unavailable, greyscale CL images are, depending on the detection range of the CL detector, in most cases sufficient to distinguish shock from tectonic lamellae. Although the causes of the CL behaviour of PDFs remain uncertain, SEM-CL imaging provides a promising qualitative method to identify PDFs in quartz and to distinguish them from tectonic deformation lamellae.

Acknowledgements – We thank Roald Tagle for providing the Popigai samples, Rodger Hart for the Vredefort samples and Hervé van Baelen and Manuel Sintubin for the Ardennes samples. Pim van Wamel is thanked for field support at the Ries crater; Philippe Lambert for a great excursion around the Rochechouart crater. Matthijs de Winter provided invaluable support for the SEM work. Gill Pennock is gratefully acknowledged for her help and comments. Constructive reviews by Martin Schmieder and Arnold Gucsik, as well as comments from the editor, Gordon Osinski, have significantly improved the manuscript.



Chapter 3

No evidence for shocked quartz at the Cretaceous-Palaeogene boundary in the Geulhemmerberg section, south-east Netherlands

M.F. Hamers, M.R. Drury and J. Smit

The Cretaceous-Palaeogene (K-Pg) boundary section in the Geulhemmerberg caves, south-east Netherlands, might be one of the most complete and continuous shallow marine K-Pg sections known. The globally observed impact ejecta layer at the boundary is missing, indicating a hiatus at the boundary, but traces of elevated iridium content and the presence of organic biomarkers near the boundary suggest that the hiatus is limited. Material from the impact layer may be preserved in burrows extending from the boundary into the latest Cretaceous sediments. To check this hypothesis, burrows extending from the K-Pg boundary level in this section were checked for shocked quartz by light microscopy and scanning electron microscope-cathodoluminescence (SEM-CL) imaging. If the hiatus at the boundary is indeed negligible, remains of the Chicxulub ejecta layer that is found worldwide at this level should be present, such as shocked quartz grains. However, no planar deformation features in quartz were found, but instead all planar or sub-planar microstructures were tectonic deformation lamellae or healed microfractures. Therefore the continuity of the section cannot be confirmed. The successful application of SEM-CL imaging confirms the potential of this technique for the study of shocked quartz.

3.1 Introduction

An ejecta layer containing impact material from the Chicxulub crater in Mexico has been recognised at the Cretaceous-Palaeogene (K-Pg) boundary (66 Ma) worldwide and is often used to identify the exact level of the K-Pg boundary. The impact layer contains impact spherules, Ni-rich spinel, high iridium (Ir) content, nanodiamonds and shocked minerals such as quartz, feldspars and zircon (Alvarez et al., 1980; Bohor et al., 1987; Carlisle and Braman, 1991; Morgan et al., 2006; Smit and Hertogen, 1980; Smit and Kyte, 1984). Of these, shocked quartz grains are the most abundant and easily detected feature, which is furthermore resistant to post-deposition alteration. Shocked quartz grains display one or (usually) more sets of planar deformation features (PDFs), which are diagnostic for meteorite impact and straightforward to detect in a standard petrographic microscope (Grieve et al., 1996; Stöffler and Langenhorst, 1994). However, other (sub-)planar microstructures in quartz are frequently misidentified as PDFs, especially tectonic deformation lamellae (sometimes mentioned as Böhm lamellae or metamorphic deformation lamellae) (Ernstson and Fiebag, 1992; Ernstson et al., 1985; Langenhorst and Deutsch, 1996; Langenhorst et al., 2005; Retallack et al., 1998). Reliable distinction between the two types of microstructure can be difficult in a light microscope and transmission electron microscope (TEM) observations are often required to prove the shock origin of planar microstructures in quartz (Grieve et al., 1996; Stöffler and Langenhorst, 1994). Recently, scanning electron microscopy (SEM) cathodoluminescence (CL) techniques were proposed as an easy and quick alternative method to identify PDFs in quartz and distinguish them from non-shock related (sub-)planar microstructures (chapter 2; Boggs et al., 2001). In this study, we used SEM-CL imaging to check the presence of shocked quartz grains at the Geulhemmerberg K-Pg boundary in the Netherlands.

3.1.1 The Geulhemmerberg Cretaceous-Palaeogene boundary section

The Geulhemmerberg K-Pg boundary section, exposed in manmade caves in the Geulhemmerberg in Limburg, the Netherlands, has been described in detail in a special issue of Netherlands Journal of Geosciences (*Geologie en Mijnbouw*) in 1996 (Brinkhuis and Smit, 1996a). The section is located in the southern part of the Netherlands in the Maastrichtian type area and can be correlated to nearby deposits in the Curfs quarry (figure 3.1). The Geulhemmerberg K-Pg boundary sediments (figure 3.2) were deposited in a shallow marine environment and the section is characterised by a succession of shallow water calcarenites in the top Maastrichtian deposits (unit IVf-6). The K-Pg boundary level is represented by an undulating hardground (the Berg and Terblijt Horizon), from which burrows extend into the underlying calcarenites. This conspicuous hardground is only found in this form in the Geulhemmerberg section; it changes laterally into the flat, burrowed surface that is recognised in the Curfs quarry. Above the hardground, storm and backwash deposits are found in the basal Danian (earliest Palaeogene), which was deposited in a marginal setting above wave base, with intercalated clay layers up to 15 cm thick (unit IVf-7) (Roep and Smit, 1996; Smit and Brinkhuis, 1996) (figure 3.2).

Like most other known K-Pg boundary sections that were deposited in a marginal setting, the Geulhemmerberg section contains a hiatus at the boundary. However, unlike in other sections, the time span contained in the hiatus in the Geulhemmerberg section is believed to be negligible (less than a hundred years) for various reasons, summarised by Smit and Brinkhuis (1996). Integrated sedimentological, geochemical, biostratigraphic and isotope studies point to

an early Danian age of the strata immediately above the Berg and Terblijt Horizon, with the earliest Danian missing (Smit and Brinkhuis, 1996). However, C17 \rightarrow KP boundary biomarkers (a cyclopropyl fatty acid that is present in the K-Pg boundary clay in other sections) were found in burrows extending from the hardground (Yamamoto et al., 1996). Neither an impact layer nor a clear Ir anomaly have been found at the boundary, but the Ir/Th and Cr/Th ratios, which are elevated in the global ejecta layer, directly below the boundary in the uppermost Maastrichtian are slightly elevated, which could be the result of downward diffusion or transport from a once-present ejecta deposit (Smit and Rocchia, 1996).

If the interpretation of a very short to negligible hiatus is correct, the Geulhemmerberg K-Pg boundary section represents a very rare expanded earliest Palaeogene succession and could provide detailed information about the events immediately after the mass extinction. The

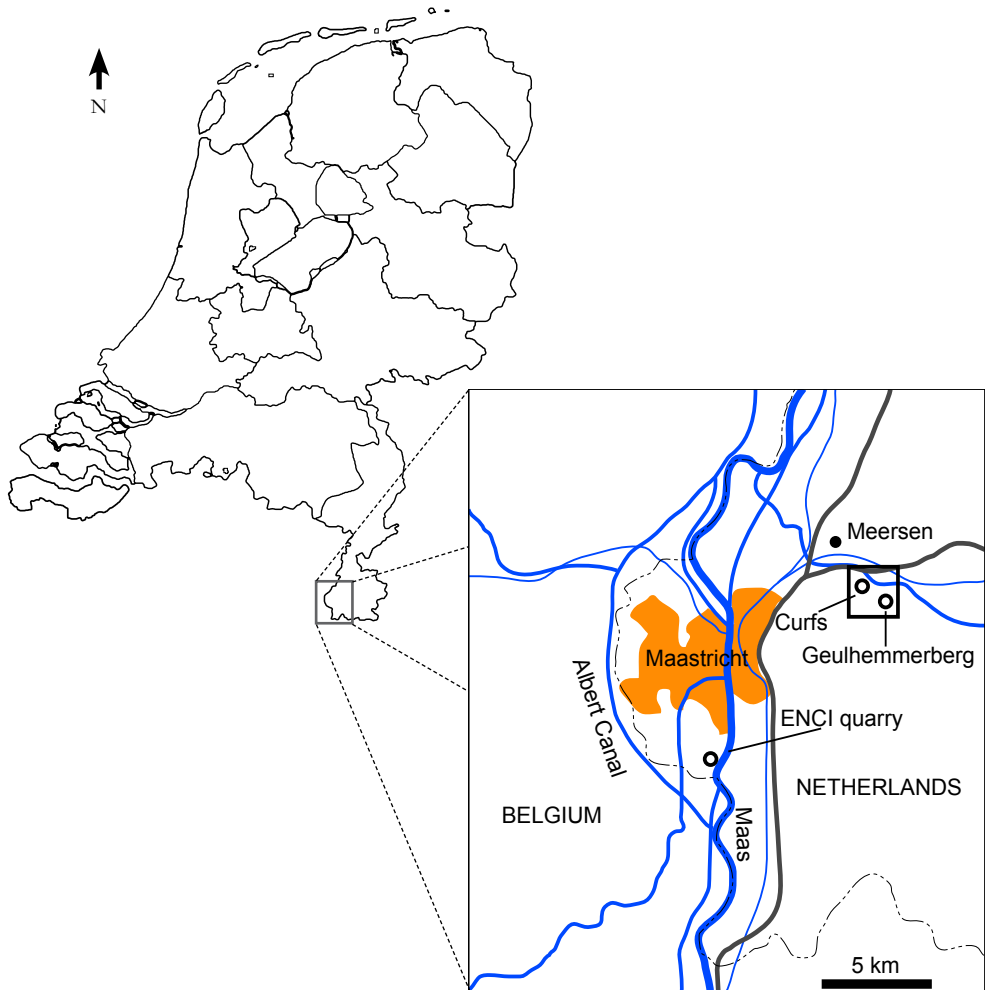


Figure 3.1 Location of the Geulhemmerberg caves (modified after figure 1 in Brinkhuis and Smit (1996b)).

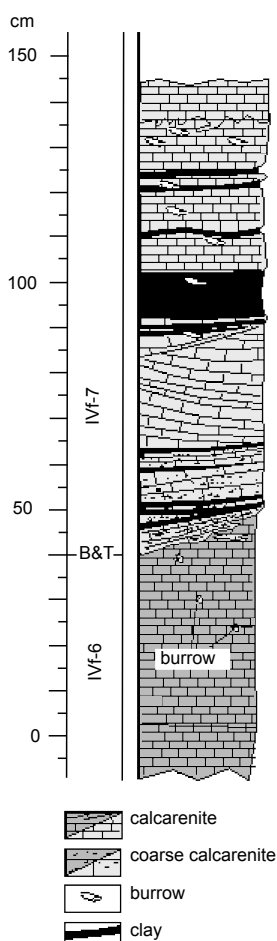


Figure 3.2 Simplified lithostratigraphic column of the Geulhemmerberg K-Pg boundary section (modified after figure 4 in Brinkhuis and Smit (1996b)). B&T indicates the K-Pg boundary level (Berg and Terblijt Horizon).

2.66 g/cm³. Fractions 2 and 3 were embedded in epoxy (Epotek 301) in 0.5 inch diameter moulds and polished using a standard polishing procedure. Although quartz has a density of 2.65 g/cm³, shocked quartz can have a lower density (Langenhorst and Deutsch, 1994). Therefore, both fractions 2 ($d = 2.63 \text{ g/cm}^3$) and 3 ($d = 2.65 \text{ g/cm}^3$) were studied.

17 samples, each containing hundreds of quartz grains, from the Geulhemmerberg were studied in a standard petrographic microscope. In total, 182 grains containing (sub-)planar microstructures were found, 130 of which were subsequently imaged using the SEM-CL techniques described in chapter 2. Two SEM systems with CL detector were used, both located

presence of clay layers at and just above the boundary in such a marginal setting is unique. With the presence of potential boundary markers in the sediments and burrows directly below the boundary (elevated Ir concentration, C17 biomarkers), one might also expect shocked quartz grains to be found here. In order to test the hypothesis that the hiatus at the Geulhemmerberg K-Pg boundary is negligible, we checked for the presence of shocked quartz grains in burrows extending from the Berg en Terblijt Horizon (K-Pg boundary) using light microscopy and SEM-CL imaging. Shocked quartz grains from the K-Pg boundary in the Quagliotti (Italy) and Madrid Railroad (USA) sections were studied for comparison. Furthermore, this study serves as a practical test of the SEM-CL imaging technique as a quick and easy method to confirm the presence of PDFs and distinguish them from other, non-shock related, (sub-)planar microstructures in quartz, such as tectonic deformation lamellae and healed fractures.

3.2 Samples and methods

Two sample sets were collected at the Geulhemmerberg K-Pg boundary: the first in 1996 (Brinkhuis and Smit, 1996a) and the second on May 12th, 2009 on the same site. Material was collected from burrows extending directly from the KP boundary clay layer.

Bulk samples were crushed if necessary, treated with HCl to remove all CaCO₃ and sieved to retain only the fraction with a grain size of 20-250 μm. Quartz grains were separated out of the bulk samples at the Mineral Separation Laboratory at the Free University of Amsterdam, using a Loc50 centrifuge with diodomethane heavy liquid. For each sample three separations were done, with liquids of a density (d) of 2.66, 2.64 and 2.62 g/cm³, resulting in four density fractions: 1) $d \leq 2.62 \text{ g/cm}^3$, 2) $2.62 \text{ g/cm}^3 < d < 2.64 \text{ g/cm}^3$, 3) $2.64 \text{ g/cm}^3 \leq d < 2.66 \text{ g/cm}^3$, and 4) $d \geq$

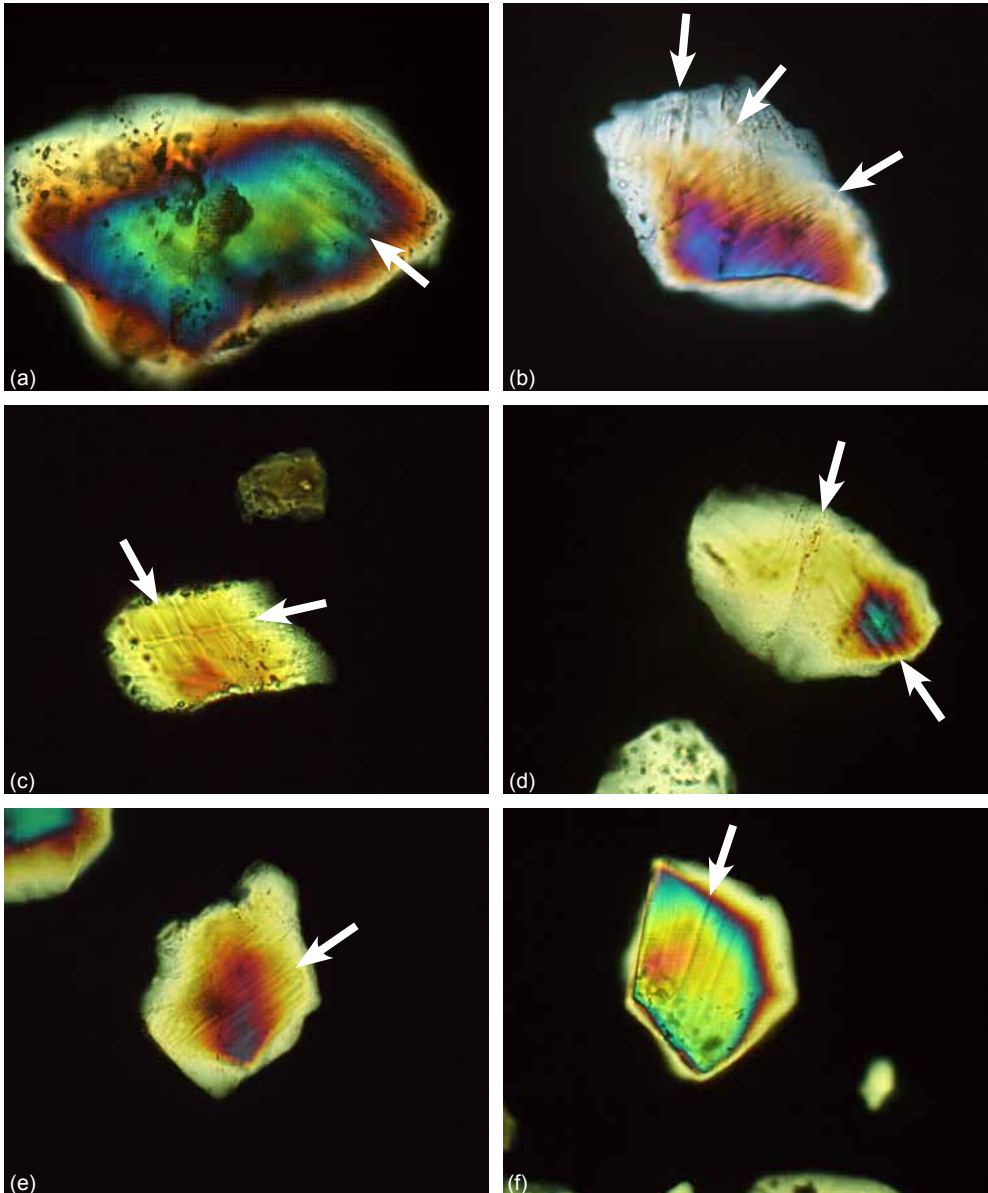


Figure 3.3 Light micrographs (crossed polars) of grains with (sub-)planar microstructures (white arrows) in quartz grains from burrows extending from the K-Pg boundary in the Geulhemmerberg section. Grains are between ~ 50 and $\sim 100 \mu\text{m}$ in size. Images courtesy of Jurian Scholten.

at the Electron Microscopy Utrecht lab (EMU) at Utrecht University. The first is a Philips XL30S FEG-SEM with a KE Developments Centaurus CL detector attached, which has a wavelength detection range of 300-650 nm with a peak at 420 nm and is thus more sensitive to blue to violet light. The second system is an FEI Nova Nanolab 600 SEM with Gatan PanaCL detector, which is more or less panchromatic and has a detection range of 185-850 nm. Three colour filters (red, green and blue) can be fitted to the detector to record wavelength filtered images. The red filter primarily transmits light in the range 595-850 nm, the green filter in the range 495-575 nm, and the blue filter in the range 185-510 nm. Both unfiltered and filtered images were recorded; the filtered images were subsequently combined into composite RGB colour images. Because red, green and blue channels were optimised individually in order to obtain the maximum amount of information from the image, colour information in the images is non-quantitative. The instruments were operated at an acceleration voltage of 5-10 kV and with a beam current of 1.6-6.3 nA, at room temperature. Before SEM imaging, samples were carbon coated to prevent charging.

Of the 130 grains from the Geulhemmerberg section studied using SEM-CL, greyscale images were recorded of 68 and composite colour images of 62. Furthermore, for comparison, 32 shocked quartz grains from K-Pg boundary sites in Italy (Quagliotti quarry, ~10 km east of Ancona, Umbria (Montanari and Koeberl, 2000)) and the USA (Madrid Railroad outcrops, ~20 km west of Trinidad, Colorado (Izett, 1990)), where the ejecta layer is present, were imaged using composite colour SEM-CL, of which three grains were also studied in greyscale SEM-CL images.

3.3 Results

3.3.1 Geulhemmerberg quartz grains

(Sub-)planar microstructures in quartz were observed in 182 grains using light microscopy. Examples are shown in figure 3.3. Lamellae are indicated with white arrows. Most grains contain a single set, but rarely two or even three sets seem to be present (e.g. figures 3.3b, c and d). Only rarely lamellae were observed that were decorated with fluid inclusions (e.g. the NNE-SSW oriented lamellae in figure 3.3d).

Examples of SEM-CL images of quartz grains with lamellae are shown in figure 3.4. Two types of sub-planar microstructures can be distinguished in the SEM-CL images of these grains. Most striking are the non-luminescent, sharply defined, irregular semi-linear features in figures 3.4c and e (indicated by black arrows). Most of these non-luminescent features are not strictly straight and different orientations can occur in one grain. The most frequently observed type of lamellae is shown in figures 3.4a, b, d and e (indicated by white arrows). They are wide (often several μm in width), slightly curved features of varying thickness that can be either darker or lighter than the surrounding quartz in greyscale CL images (figures 3.4e and f), and range in colour from red to blue in composite colour CL images (figures 3.4 a, b and c). The two types of lamellae can occur together in one grain (see figure 3.4e).

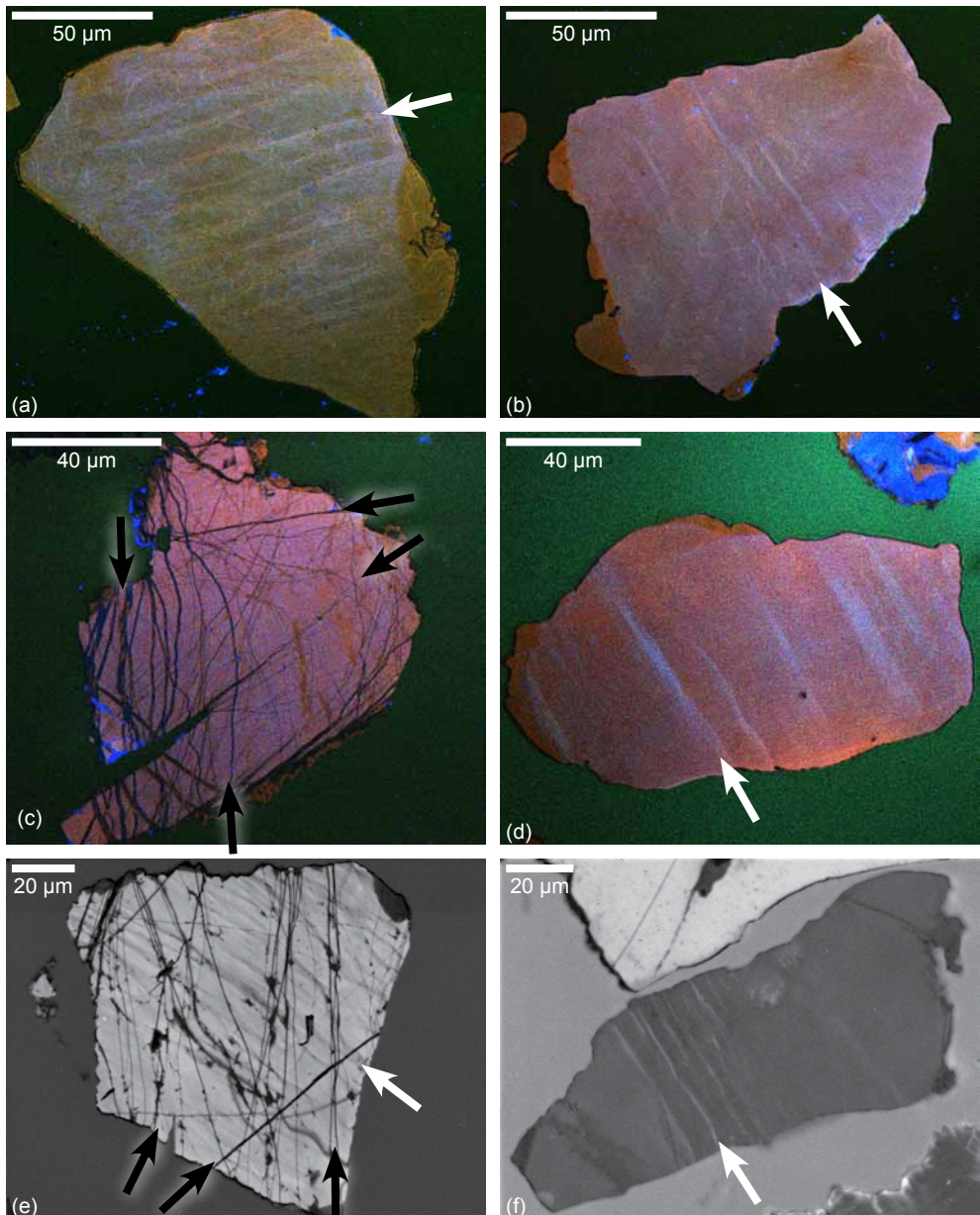


Figure 3.4 SEM-CL images of quartz grains from burrows extending from the Geulhemmerberg K-Pg boundary. **a-d** Composite colour SEM-CL images. **e-f** grayscale SEM-CL images. Two different types of microstructure are indicated by black and white arrows.

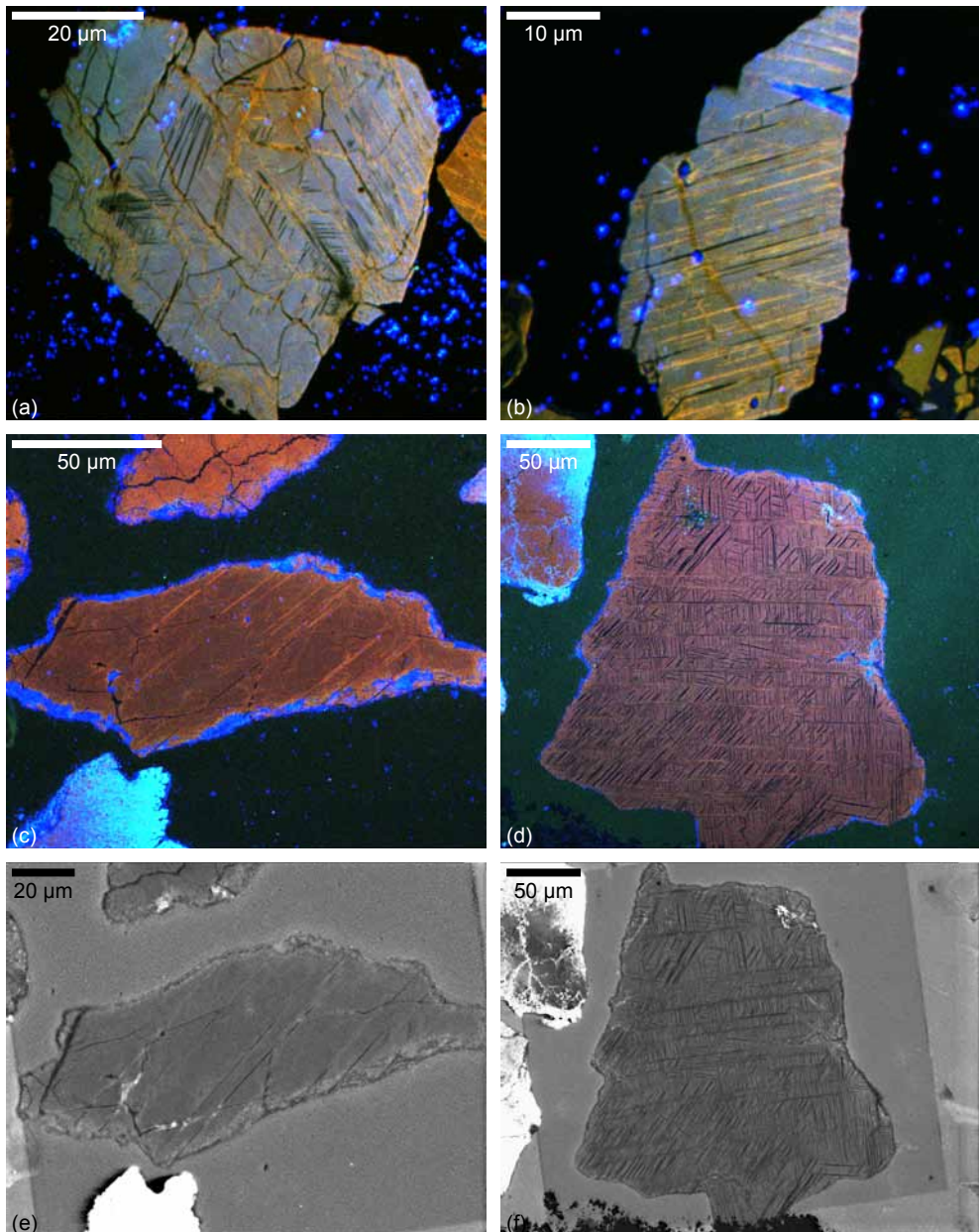


Figure 3.5 SEM-CL images of shocked quartz grains from the K-Pg boundary layers at the Quagliotti section (Italy) and Madrid Railroad section (USA). **a-b** Composite colour SEM-CL images of grains from the Quagliotti section in Italy. **c-d** Composite colour SEM-CL images of grains from the Madrid Railroad section, USA. **e-f** Greyscale SEM-CL images of the same two grains as in c and d. Bright blue spots (especially clear in 5a and 5b) are remains of polishing material on the sample surface.

3.3.2 Shocked quartz from other K-Pg boundaries

Figure 3.5 shows examples of SEM-CL images of shocked quartz grains with PDFs from the impact layer at K-Pg boundary sites in Italy (figures 3.5a and b) and the USA (figures 3.5c-f). The PDFs are thin ($< 1 \mu\text{m}$) and strictly planar, show no thickness variations and are red or non-luminescent. Some dark (parts of) PDFs are actually open or etched out instead of non-luminescent, but this distinction can only be made in secondary electron (SE) images showing surface topography. Especially in grains with multiple sets, the PDFs are closely spaced (1-2 μm). In greyscale CL images not all PDFs are clearly visible (figure 3.5e), but most are non-luminescent (figure 3.5f) or apparently non-luminescent. Apparent non-luminescence in greyscale CL images of features that are red in colour CL images can occur because the detector used for the greyscale images is relatively insensitive to red light. Usually multiple sets of PDFs are observed in one grain, but also single sets occur (e.g. figures 3.5c and d).

3.4 Discussion

In light microscopy, identification of the lamellar microstructures in quartz grains from the Geulhemmerberg K-Pg boundary section either as PDFs or tectonic deformation lamellae is not straightforward. The observed lamellae are not sharply defined and usually not penetrative through a whole grain, which would suggest they are tectonic deformation lamellae. On the other hand, two, or arguably even three, orientations were observed in single grains, which would suggest a shock origin of the lamellae. However, when comparing the SEM-CL images of the lamellar features in figure 3.4 to the PDFs in the grains in figure 3.5, it is clear that the microstructures in Geulhemmerberg quartz do not have the same characteristics as the PDFs in shocked quartz grains from Italy and the USA. The PDFs in figure 3.5 are straight and very thin, occur in multiple, closely spaced sets, and are either red or non-luminescent. These are clear characteristics of PDFs as described in chapter 2. The lamellae in the grains from the Geulhemmerberg, on the other hand, show mostly characteristics of tectonic deformation lamellae, also described in chapter 2: the lamellae are slightly curved, relatively wide features without clearly defined boundaries (figures 3.4a, b, d and f). CL colours range from red to blue and no more than two sets are observed in one grain. The non-luminescent irregular features (figures 3.4c and e) are healed fractures, which were described by Boggs et al. (2001), and are even more readily distinguished from PDFs in CL images by the highly irregular shape, thickness and spacing of the fractures.

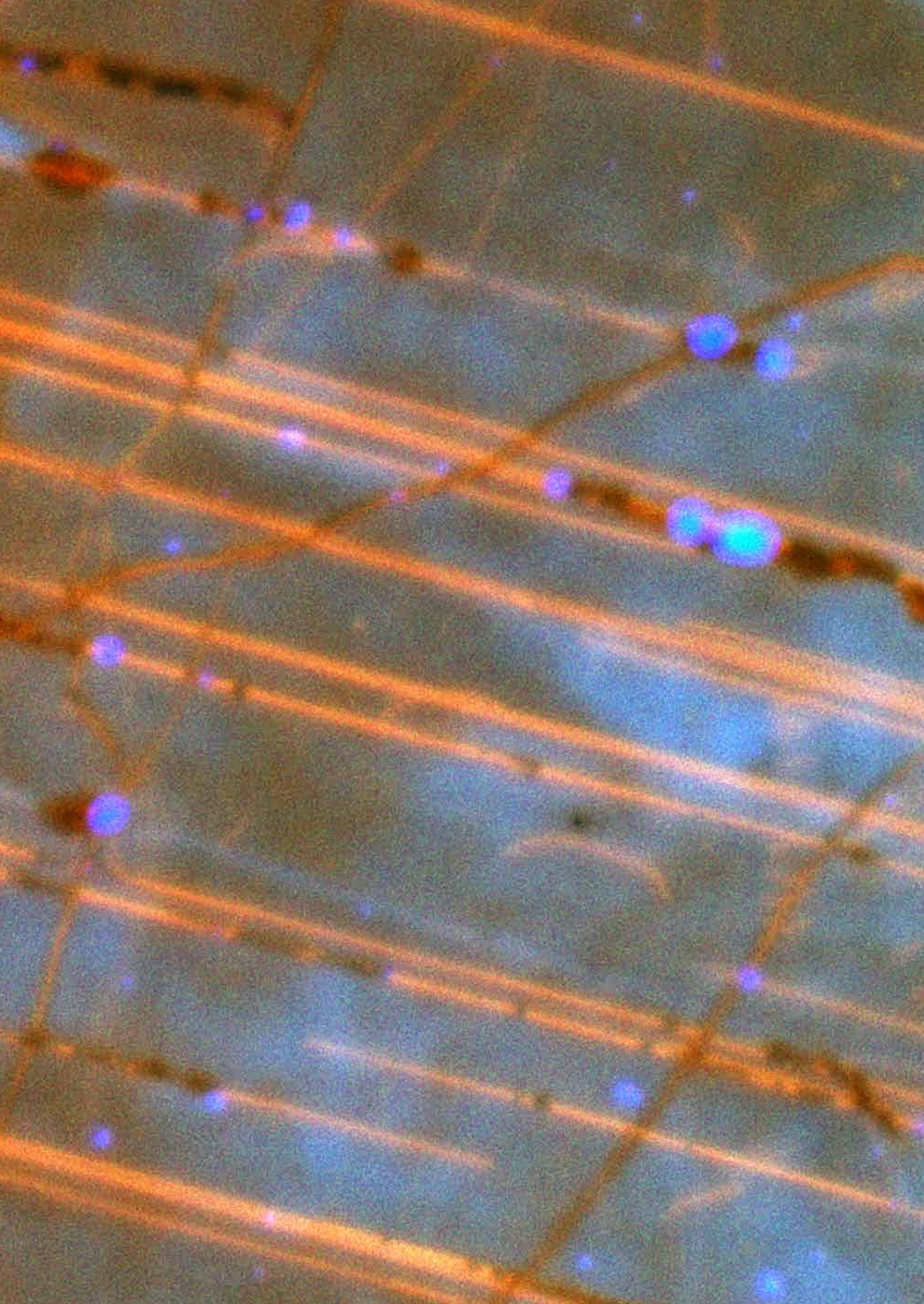
Clearly, the sub-planar microstructures that are observed in the optical microscope in quartz grains from the Geulhemmerberg K-Pg section are not PDFs, but tectonic deformation lamellae and healed fractures, which are not shock-related. Therefore, no new evidence for the presence of the characteristic ejecta layer at the K-Pg boundary level could be found in the Geulhemmerberg section and no more evidence is available for the short duration of the hiatus at the boundary than was reported in earlier studies. It remains probable, but not certain, that the Geulhemmerberg section represents a rare expanded record of the latest Cretaceous and early Palaeogene. However, our results confirm the conclusion of chapter 2, that SEM-CL images form a reliable basis for the distinction of PDFs and non-shock related (sub-)planar microstructures in quartz. The technique can be applied to separated and embedded quartz grains, but also to standard polished thin sections or rock slabs. SEM-CL imaging can therefore

be used to check the impact origin of both potential geological structures and stratigraphic levels.

3.5 Conclusions

Although using light microscopy (sub-)planar microstructures were observed in quartz grains from the Geulhemmerberg K-Pg boundary layer, no PDFs could be identified in SEM-CL images. Only tectonic deformation lamellae and healed fractures are present in the grains that were studied. We therefore conclude that no shocked quartz is present at or near the K-Pg boundary in the Geulhemmerberg section. The hypothesis that the hiatus at the boundary in this section is insignificant and that the section is therefore close to complete cannot be confirmed. The successful application of SEM-CL imaging techniques in this study confirms the potential of this method to prove or disprove the presence of PDFs in quartz.

Acknowledgements – Roel van Elsas is gratefully acknowledged for his separation work and help at the Mineral Separation Laboratory at the VU Amsterdam, Jurian Scholten for the light microscopic images of the Geulhemmerberg quartz grains and Sandro Montanari for his help and guidance while sampling the K-Pg boundary in Italy.



Chapter 4

Distinction between amorphous and healed planar deformation features in shocked quartz using composite colour scanning electron microscope cathodoluminescence imaging

M.F. Hamers, G.M. Pennock, M. Herwegh and M.R. Drury

Planar deformation features (PDFs) in quartz are one of the most reliable and most widely used forms of impact evidence. Recently it was demonstrated that PDFs can be identified in scanning electron microscope cathodoluminescence (SEM-CL) images and that not all PDFs show the same CL behaviour: there are non-luminescent and red luminescent PDFs. This study aims to explain the origin of the different CL emissions in PDFs in more detail. Focused ion beam (FIB) prepared thin foils were prepared of specific sample locations selected in composite colour SEM-CL images and were analysed in a transmission electron microscope (TEM). The FIB preparation technique allowed a direct, often one to one correlation between the CL images and the defect structure observed in TEM. This correlation shows that composite colour SEM-CL imaging of PDFs in quartz can be used to distinguish between amorphous PDFs on the one hand and healed PDFs and basal Brazil twins on the other hand: non-luminescent PDFs are amorphous, while healed PDFs (planes of high dislocation density) and basal Brazil twins are red luminescent, with a dominant emission peak at 650 nm. We suggest that the red luminescence is the result of preferential beam damage along dislocations, fluid inclusions and twin boundaries. Furthermore, a high pressure phase (possibly stishovite) in PDFs can be detected in colour SEM-CL images by its blue luminescence.

4.1 Introduction

The presence of planar deformation features (PDFs) in quartz is one of the most reliable forms of evidence for the impact origin of suspected geological structures or stratigraphic layers. PDFs are planar microstructures that form in quartz and other minerals (e.g. feldspar) as a result of a shock wave passing through the rocks (e.g. Engelhardt and Bertsch, 1969; papers in French and Short, 1968; Grieve et al., 1996; Stöffler and Langenhorst, 1994). Because PDFs are so widely used as impact evidence, their correct identification is crucial. The standard petrographic microscope is not the preferred instrument to confirm the shock origin of planar microstructures in quartz, because PDFs and non-impact related (sub-) planar microstructures, such as healed fractures or tectonic deformation lamellae, can look very similar in light microscopy. Transmission electron microscopy (TEM) observations on the fine scale microstructure of the suspect lamellae are often necessary to distinguish between shock and non-shock related structures (e.g. French and Koeberl, 2010; Grieve et al., 1996; Stöffler and Langenhorst, 1994). However, Boggs et al. (2001) and our study in chapter 2 showed that in addition to TEM, cathodoluminescence (CL) imaging in the scanning electron microscope (SEM) is a reliable method to distinguish between shock-related and tectonically formed planar microstructures in quartz. Composite colour SEM-CL imaging shows two main types of CL behaviour in PDFs: red luminescence and non-luminescence (chapter 2). In order to identify the relationship between CL emission and the microstructure of PDFs in quartz, we performed TEM analysis on both red and non-luminescent PDFs. To enable a direct, often one to one comparison of PDFs in CL and TEM and to control the exact location of the TEM samples, the TEM sections were prepared using a focused ion beam (FIB). In addition, CL spectroscopy of red luminescent PDFs provides an indication of the defects that are responsible for the CL emission. The comparison of the CL results with known TEM techniques, with the addition of CL spectroscopy, determines the source of the CL emission and helps to validate the SEM-CL method to identify and characterise PDFs in quartz.

4.1.1 Planar deformation features in quartz

PDFs consist of thin ($<1 \mu\text{m}$), parallel, closely spaced (typically $<2 \mu\text{m}$ apart) lamellae. Usually multiple sets of PDFs develop in the same grain, typically 2-10 sets are observed (Engelhardt and Bertsch, 1969; French and Koeberl, 2010; Grieve et al., 1996; Stöffler and Langenhorst, 1994). Although PDFs are generally described as strictly straight and planar, some bending or slight curvature has been reported (Engelhardt and Bertsch, 1969; Stöffler and Langenhorst, 1994; Trepmann and Spray, 2005). PDFs can be penetrative through a whole grain or be concentrated in parts of a grain, but do not cross grain boundaries, cracks, faults or fractures that were present before PDF formation.

PDFs have a crystallographically determined orientation, mostly parallel to low-index rational planes (most frequently observed are c (0001), ω $\{10\bar{1}2\}$ and π $\{10\bar{1}3\}$) (Ferrière et al., 2009; Stöffler and Langenhorst, 1994). Unaltered PDFs are thin lamellae of amorphous silica, formed under high pressure during shock compression. Basal PDFs, parallel to c (0001), are not amorphous, but consist of mechanical Brazil twins. In shock experiments on quartz, Langenhorst (1994) observed that at low peak shock pressures ($<25 \text{ GPa}$) rhombohedral PDFs are extremely narrow ($\sim 30 \text{ nm}$), but around 25 GPa thickness increases to $>200 \text{ nm}$ and PDFs can become slightly curved and show thickness variations along their length.

During post-shock high temperature or metamorphic events, amorphous PDFs can easily recrystallise. Healed PDFs are recognised in TEM as planes with a very high dislocation density and in light microscopy they are often seen as traces of fluid inclusions along the original PDF plane, of which the crystallographic orientation can still be measured in the universal stage (e.g. Ferrière et al., 2009). Because amorphous PDFs only occur in relatively fresh, unaltered impact material, it is useful to be able to easily detect the presence of amorphous PDFs in shocked quartz: their presence can give a very preliminary indication of (source) crater age. At present, amorphous PDFs can only be detected using TEM analysis.

4.1.2 Cathodoluminescence background

When a material is scanned by the electron beam in the SEM, one effect of the interaction between beam and sample is that electrons in the sample are excited to a higher band level by the incoming energy of the electron beam. When the excited electrons fall back to their original energy state, photons are emitted. This phenomenon is known as cathodoluminescence. The wavelength spectrum and intensity of photon emission depend on the material and crystallographic defects (intrinsic emission) and on the presence of trace elements or fluids in the sample (extrinsic emission). The CL emission of quartz depends on many factors such as the degree of ordering in the crystal lattice; vacant lattice sites; trace amounts of activators such as Fe^{3+} , Al^{3+} , H^+ , Li^+ , Na^+ , K^+ , and Ti^{4+} ; water content; or damage resulting from radiation, strain, or shock (Marshall, 1988; Perny et al., 1992; Ramseyer and Mullis, 1990). Common emission bands in crystalline α -quartz are around 340 nm (Al and Li impurities), 420 nm (intrinsic emission) and 620-650 nm (non-bridging oxygen hole centre, NBOHC, $\text{O}_3\equiv\text{Si}-\text{O}\cdot$, an oxygen atom with an unpaired electron, i.e. a dangling oxygen bond, that is bonded to a silicon atom attached to three other oxygen atoms) (Götze et al., 2001; Stevens Kalceff, 2009; Stevens Kalceff and Phillips, 1995a; Stevens Kalceff et al., 2000), but many more emission bands are described in the literature. The relative intensities of the dominant emission bands in the visible light range (380-700 nm, blue to red) determine the CL colour that is perceived by the eye (Götze et al., 2001).

Shocked quartz is generally blue luminescent, with an additional emission band at 630-650 nm (Götze, 2009; Ramseyer et al., 1992; Ramseyer and Mullis, 2000; Trepmann et al., 2005). Boggs et al. (2001) first demonstrated the potential of SEM-CL to image PDFs in quartz and concluded that PDFs are non-luminescent in (greyscale) SEM-CL images. Chapter 2, however, showed that in composite colour SEM-CL images, PDFs can have different CL characteristics. Some are indeed non-luminescent, but many in fact are red-luminescent and also 'intermediate' cases were observed, with both red and non-luminescent (parts of) PDFs in the same grain.

4.2 Materials and methods

The quartz grains described in this study are mostly naturally shocked and come from different impact structures (El'gygytgyn, Ries, Popigai, Rochechouart and Vredefort). In addition to the shocked quartz samples studied in chapter 2, SEM-CL images were recorded of a granitic sample from the Vredefort structure in South Africa, a suevite sample from the El'gygytgyn crater in Russia, an experimentally shocked (23.5 GPa) Hospital Hill quartzite and an experimentally shocked (24 GPa) single crystal. The experimentally shocked samples were previously studied and described by Reimold and Hörz (1986a, b) (Hospital Hill quartzite) and Fritz et al. (2011)

(single crystal). In total, twelve TEM foils were studied. Table 4.1 lists the new samples and the TEM foils, with their locations, main characteristics and the observed microstructures.

SEM-CL images were recorded in an FEI Nova Nanolab 600 dual beam SEM with focused ion beam and a panchromatic Gatan PanaCL detector (Gatan UK, Oxford, UK) at the Electron Microscopy Utrecht lab (EMU), the Netherlands, using acceleration voltages of 5-10 kV and beam currents of 1.6-8.4 nA. Red (595-850 nm), green (495-575 nm) and blue (185-510 nm) filters in the CL detector were used to record colour filtered images, which were combined into an RGB colour composite image. Ten grains (six from Ries, four from Popigai) were previously imaged using composite colour SEM-CL at -170°C (liquid nitrogen temperature, LNT), using a liquid nitrogen-cooled cryostage (see chapter 2), but are now studied in more detail. TEM foils with a thickness of ~100-200 nm were also prepared in this instrument, with the focused ion beam, using a standard in situ lift-out procedure (Wirth, 2004, 2009), an acceleration voltage of 30 kV and beam currents ranging from 20 nA down to 0.3-0.5 nA for the final polishing steps. The FIB-SEM preparation of the TEM foils provides a direct, often one to one correspondence of PDFs in TEM and SEM-CL images.

TEM analysis was carried out on an FEI Tecnai 20 FEG instrument, also at EMU, operated at 200 kV, with double tilt holder. Bright field (BF) TEM imaging was used to show the microstructure in the samples, while diffuse dark field (DDF) TEM images show the presence of amorphous material. For diffuse dark field imaging, the objective aperture is moved away from any diffraction spots, to a position that intercepts the diffuse scattering from amorphous parts of the sample. Alternatively the electron beam can be tilted to move the diffraction pattern to the appropriate position for DDF imaging. The latter technique gives a higher spatial resolution at high magnification. Both techniques were applied in this study. In the resulting DDF image, amorphous areas are bright, while crystalline material is dark (Williams and Carter, 2009).

CL spectroscopic measurements were performed on a polished thin section of one sample (a granite fragment from the Ries crater with red luminescent PDFs) on a Zeiss EVO 50 instrument with Gatan MonoCL 3 system, at the Institute of Geological Sciences in Bern, Switzerland. Spectra were recorded with a PIXIS 100 CCD camera (Princeton Instruments). Grating of the spectroscopic system was set to 300 lines/mm with a slit size of 2 mm. Spectra were recorded in a 600 nm range and with a central wavelength of 500 nm, resulting in simultaneous measurement of the 200-800 nm spectra. Acceleration voltages of 5-8 kV were used, with beam currents of 1.4-3 nA. PDFs are too narrow to measure directly by spot measurements, because the interaction volume of the electron beam with the quartz is too large to only sample the PDF. Inevitably some of the surrounding quartz is sampled by the beam, especially if the PDF is oriented at an angle $<90^\circ$ to the sample surface. To overcome this problem, spectra were measured from areas with a high density of PDFs and areas in the same grain without PDFs. The ratio of the intensity of the main peaks between PDFs and host grain was then determined. Measurements were done in areas of the sample that had not been scanned by the electron beam before, with a measurement time of 30 seconds. Because only peak ratios were considered and not absolute values, no correction for detector response was carried out. The CCD has nearly constant detector efficiency for the visible light wavelength range.

Table 4.1 Sample locations and properties

sample	Location	lat/lon (WGS84)	Rock type	TEM section	CL emission of PDFs	PDF microstructure in TEM	Grain microstructure in TEM
RI-37	Ries (Germany), Auhmühle	48°58'16.84"N/ 10°37'43.95"E	granite fragment (loose block, probably from suevite)	RI-37_01	red	dislocations	single crystal, some dislocations
RI-37-1	Ries (Germany), Auhmühle	48°58'16.84"N/ 10°37'43.95"E	granite fragment (loose block, probably from suevite)	RI-37-1_71	red	dislocations	single crystal, some dislocations
OTT-2	Ries (Germany), Otting	48°52'32.07"N/ 10°47'42.37"E	suevite	OTT-2_17 OTT-2_22	no/red no	mixed amorphous	single crystal (micro?)crystalline
MRO-5-1	Rochechouart (France), Montoume	45°46'31.94"N/ 0°46'30.01"E	Impact melt rock	MRO-5-1_02 MRO-5-1_05 MRO-5-1_05A	red red red	dislocations dislocations dislocations	single crystal, some dislocations mosaic mosaic
55	Vreddefort (South-Africa)	W of Parys, exact location unknown	Granite gneiss	55_03_1 55_03_2 55_07 55_07A	red red red red	Brazil twins Brazil twins Brazil twins Brazil twins	single crystal, some dislocations single crystal, some dislocations single crystal, some dislocations
1270	experimental		quartzite, experimentally shocked, 23.5 GPa (see also Reimold and Hörz, 1986a, b)	1270_01	no	amorphous	(micro?)crystalline
24	experimental		quartz single crystal (see Fritz et al. 2011)	-	no/blue	-	-
320.27	El'gygytgyn	67°30'N/ 17°05'E	Suevite (probably reworked, see Reimold et al. 2012)	-	no/red	-	-

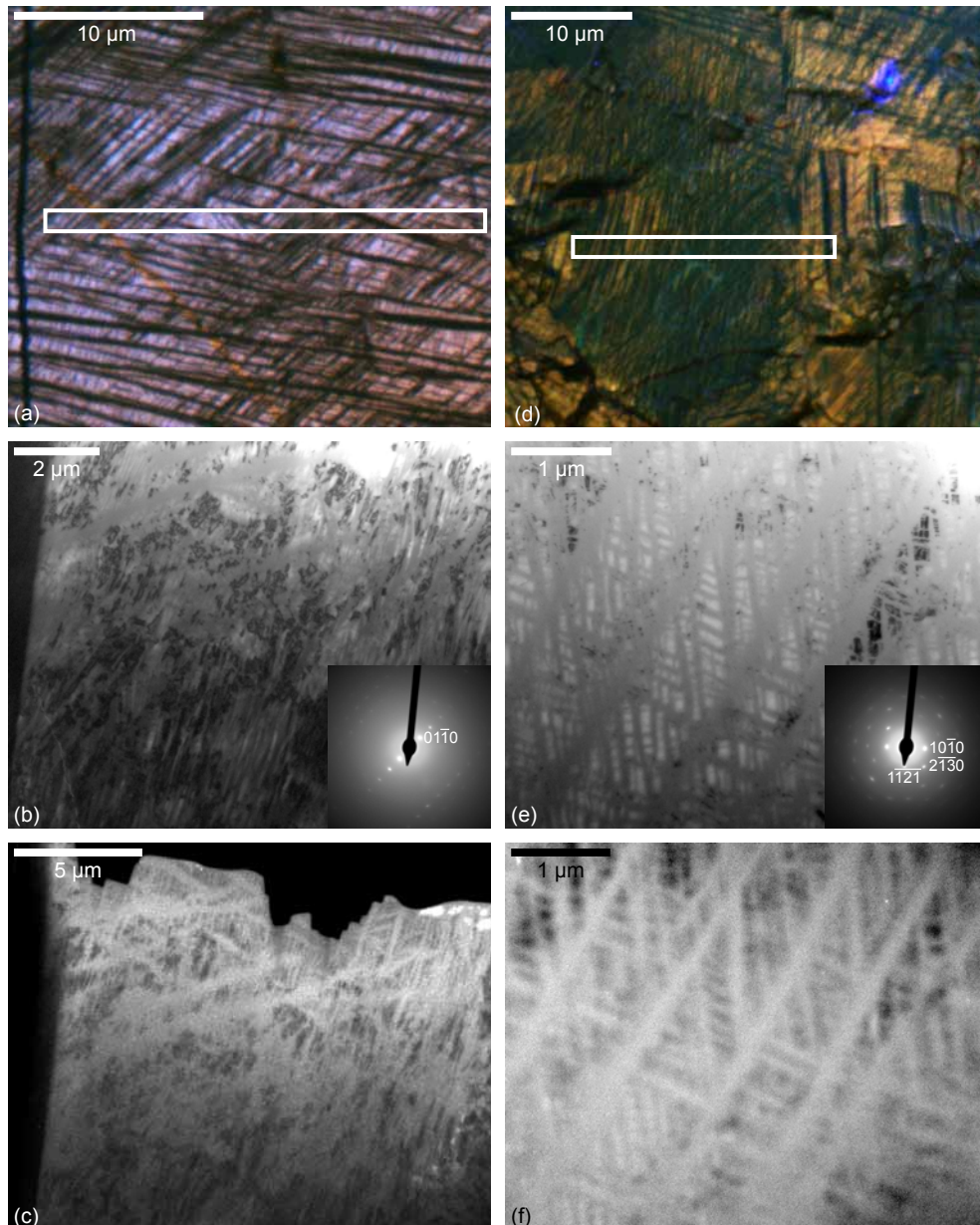


Figure 4.1 Non-luminescent PDFs in a suevite from the Ries crater (a, b, c) and experimentally shocked Hospital Hill quartzite (d, e, f). **a** Composite colour CL image showing non-luminescent PDFs. The white rectangle shows the location of the TEM foil. **b** Bright field TEM image of part of the foil. Medium grey PDFs are amorphous; in between diffracting (crystalline) material is present. Inset: SADP of PDFs and surrounding material. Bright diffuse scattering disk shows the presence of amorphous material. Slight streaking of diffraction spots indicates the presence of small misorientations in the crystalline material, possibly a microcrystalline grain structure. **c** Diffuse dark field image of the same grain, showing the presence of amorphous (bright) material in the PDFs. **d** Composite colour CL image showing non-luminescent PDFs. The white rectangle shows the location

4.3 Results

4.3.1 Non-luminescent PDFs

Figure 4.1 shows CL (a and d) and TEM (b, c, e and f) images of two grains with non-luminescent PDFs, in a suevite from the Ries crater in Germany and in a quartzite experimentally shocked to 23.5 GPa. In bright field TEM images (figures 4.1b and e), the PDFs are always a uniform grey, irrespective of tilt angle. In corresponding diffuse dark field images of the same area (figures 4.1c and f) PDFs are brighter than the surrounding material. Both bright field and diffuse dark field characteristics of non-luminescent PDFs therefore indicate that they are amorphous. This is confirmed by the presence of diffuse scattering intensity in the diffraction patterns (insets in figures 4.1b and e).

The quartz in between the PDFs is diffracting and therefore crystalline. Slight streaking of the (outer) diffraction spots (insets in figures 4.1b and e) points to a small misorientation between the crystalline domains. Dislocations and other defects were not observed in the crystalline quartz.

4.3.2 Red luminescent PDFs

Red luminescent PDFs can be either healed structures (figures 4.2 and 4.3) or basal Brazil twins (figure 4.4).

Figures 4.2a, b and c (Rochechouart) show that the red luminescent PDFs in this sample are planes of high dislocation density or arrays of dislocations, similar to what has been observed in healed PDFs in earlier studies (e.g. Goltrant et al., 1991; Trepmann and Spray, 2006). In grains like the one shown in figures 4.2a, b and c, with few sets and a relatively low density of PDFs, the crystalline host quartz is a single crystal and not microcrystalline; there are no misorientations in the grain (no streaking of diffraction spots occurs, see inset in figure 4.2b). Apart from in the PDF planes, only a few dislocations are present in the grain. In figures 4.2b and c, a Dauphiné twin boundary can be traced from the upper right corner along a PDF, then crosses to another PDF and again follows the PDF orientation. In rare cases, such as the grain from the Ries crater in figure 4.2d, SEM-CL images show that red luminescent PDFs consist of small sub-lamellae (black arrow in figure 4.2d) in a configuration similar to the dislocation arrays observed in TEM.

In a grain from the Vredefort Dome, red luminescent PDFs (figure 4.3a) consist of basal Brazil twins (shown edge on in bright field TEM in figure 4.3b and tilted in figure 4.3c). Some dislocations are present in this grain and parts of the Brazil twin boundaries are decorated with dislocations. However, there are also segments of the twin boundaries that are free of dislocations. It therefore appears that the red CL emission comes from the twin boundaries themselves and not (only) from dislocations, as opposed to the red luminescent PDFs shown in figure 4.2.

of the TEM foil. **e** Bright field TEM image of part of the foil. Medium grey PDFs are amorphous; in between diffracting (crystalline) material is present. Inset: SADP of PDFs and surrounding material. Bright diffuse scattering disk shows the presence of amorphous material. Slight streaking of diffraction spots indicates the presence of small misorientations in the crystalline material, possibly a microcrystalline grain structure. **f** Diffuse dark field image of the same grain, showing the presence of amorphous (bright) material in the PDFs.

4.3.3 Red and non-luminescent PDFs

Besides the red and non-luminescent end members of CL behaviour that PDFs exhibit in SEM-CL, an intermediate type occurs: grains with both red and non-luminescent PDFs, and PDFs that have both red and non-luminescent parts (see also chapter 2). SEM-CL and TEM images of this type of grain are shown in figure 4.4. This grain contains both amorphous PDFs (showing up light in the diffuse dark field image in figure 4.4b) and PDFs that are planes of high defect density (figure 4.4c). Again, also the presence of bright diffuse scattering intensity in the diffraction pattern indicates the presence of amorphous material in the grain.

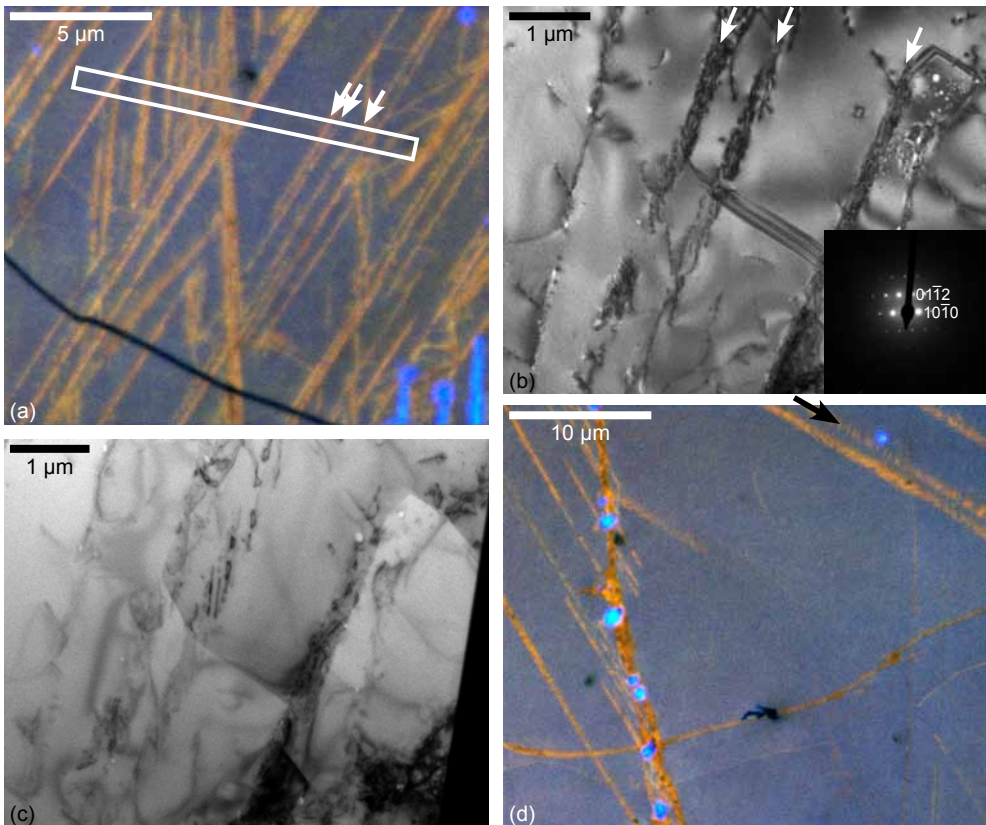


Figure 4.2 Red luminescent PDFs in an impact melt rock from Rochechouart (a, b, c) and a granite fragment from Ries (d). **a** Composite colour CL image showing at least three sets of red luminescent PDFs. The white rectangle shows the location of the TEM foil. The three white arrows indicate the three PDFs that are visible in the TEM image shown in b. **b** Bright field TEM image showing that the PDFs consist of arrays of dislocations. Dauphiné twins are also present, with boundaries partly following the orientation of PDFs. No streaking of diffraction spots occurs (inset), showing the single crystal nature of this grain. The three white arrows indicate the same three PDFs that are indicated in a. **c** Bright field TEM image of the same area as in b, tilted to show the Dauphiné twins more clearly. **d** Composite colour image showing red luminescent PDFs. In the upper right corner are three lamellae consisting of sub-lamellae that could be arrays of dislocations. This is particularly clear in the central lamella (black arrow).

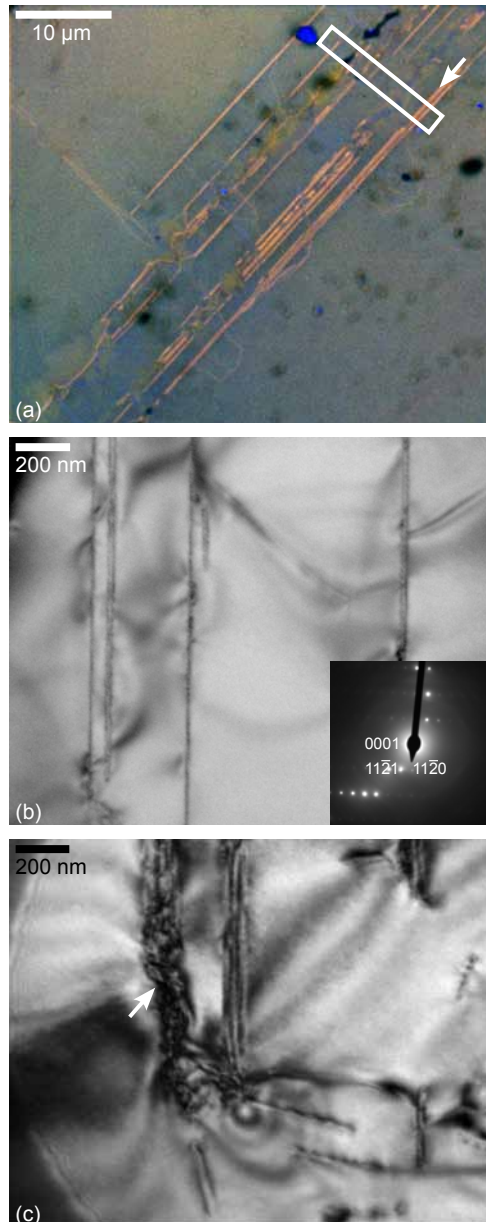


Figure 4.3 Red luminescent Brazil twins (Vredefort). **a** Composite colour CL image showing one set of red luminescent PDFs. The white rectangle shows the location of the TEM foil. The white arrow shows the group of twin boundaries that are shown in the TEM image in **b**. **b** Bright field TEM image showing that the PDFs are basal Brazil twins, oriented edge-on. The SADP (inset) shows the Brazil twins are parallel to the basal plane. **c** Bright field TEM image showing the Brazil twins in a tilted position. Parts of the twin plane are decorated by dislocations (white arrow).

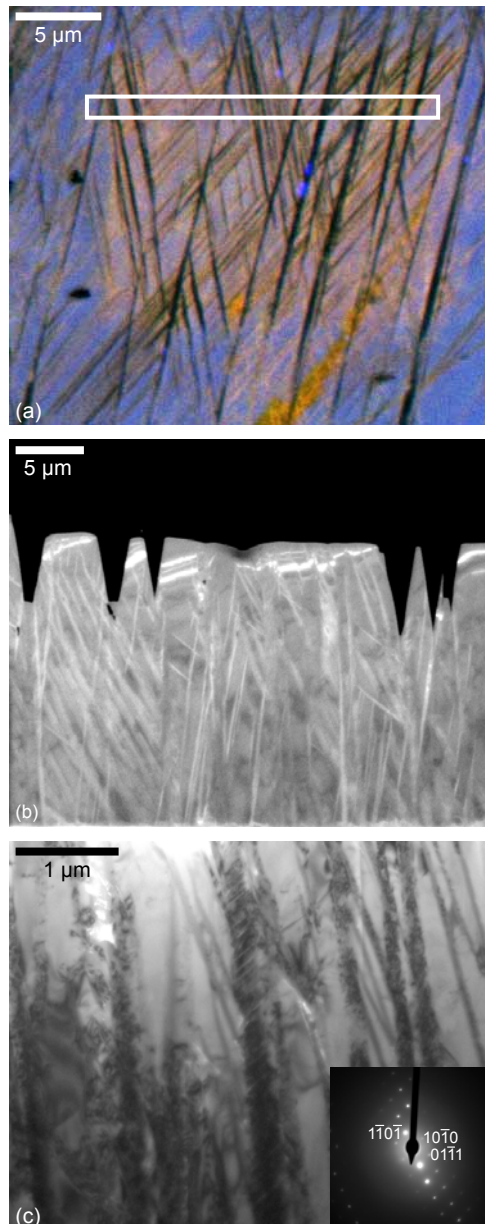


Figure 4.4 Red and non-luminescent PDFs (Ries, suevite). **a** Composite colour CL image showing both red and non-luminescent PDFs. The white rectangle shows the location of the TEM foil. The lighter pinkish square in the centre is radiation damage from previous scanning with the electron beam. **b** Diffuse dark field image of the same grain, showing the presence of amorphous (bright) material in some of the PDFs. **c** Bright field TEM image showing both amorphous PDFs and PDFs that are planes of high defect density. No streaking of diffraction spots occurs (inset), indicating that the grain is a single crystal. The PDF in the centre (oriented N-S) consists of defects and tiny sub-lamellae or dislocations.

4.3.4 CL spectra of red luminescent PDFs

CL spectra were measured in the SEM in five grains with red luminescent PDFs in a granite fragment from the Ries crater (figure 4.5). The main peaks in the spectra in both PDF and host quartz are at 410 nm and 650 nm, which are commonly occurring peaks in quartz; the 410-420 nm peak is an intrinsic emission of quartz and the 650 nm peak is usually related to a non-bridging oxygen hole centre (NBOHC) (Götze et al., 2001; Stevens Kalceff and Phillips, 1995a).

The results indicate that the CL spectra of red luminescent PDFs have a stronger 650 nm peak than the surrounding quartz. After a measurement time of 30 seconds, the intensity ratio of the 650 nm and 410 nm peaks is higher in the PDFs than in the host quartz (figure 4.5d). This is observed in all studied grains: on average, with a measurement time of 30 seconds the 650/410 nm peak ratio is 1.7 for PDFs versus 1.3 for the host quartz (figure 4.6); that is, the 650/410 nm peak ratio is 24% higher in PDFs.

The intensity of the red 650 nm peak in quartz increases with increasing irradiation time in the SEM, while the blue 410 nm peak slightly decreases. The intensity increase of the 650 nm emission is quicker in the PDFs than in the host quartz and therefore PDFs are red in CL images. This was also noted in chapter 2, in which we observed that the red luminescent PDFs become brighter in composite colour CL images after scanning the same area several times. This effect can furthermore be observed in figures 4.5a (first scan) and 4.5b (after several scans): the (panchromatic) CL emission from PDFs is lower than that of the host quartz in the first scan, but brighter in PDFs than in the rest of the grain after several slow scans. The effect can be shown with point measurement times around 30 seconds, but when longer measurements are taken, the difference between PDFs and host quartz decreases and eventually disappears.

Unfortunately no peak ratios could be determined for samples with basal Brazil twins (Vredefort), because no areas could be found with a high enough twin density for reliable measurements.

4.3.5 Changes in CL emission after prolonged exposure to the electron beam

Figure 4.7 illustrates the effect that irradiation with the electron beam has on the CL emission of quartz. In figures 4.7a and b, red squares clearly indicate areas that have been scanned previously at higher magnification. Prolonged exposure to the electron beam strongly increases the red CL emission of the whole area that was scanned previously. In figure 4.7b, the central red square is made up of red spots that show where spot measurements were taken for an electron backscattered diffraction (EBSD) map recorded before scanning this CL image. Figure 4.7c is a higher magnification scan of the red square on the right in figure 4.7b. In the centre of figure 4.7c another EBSD map was recorded using point measurements. The CL emission of the PDFs, which are mostly red luminescent in the rest of the image, has disappeared in the area that has suffered long exposure to the beam during point mapping: the PDFs have become non-luminescent. This effect is also observed in figure 4.7a in a small rectangular area in the top right of the image, indicated by the black arrow. Quenching of the CL emission was not observed as a result of scanning images (not even after repeated slow scanning). Only in sample areas on which the beam was stationary for a relatively long time (~ 0.2 s on each point in this case, whereas in scanned images, the dwell time was four orders of magnitude lower, typically 30-60

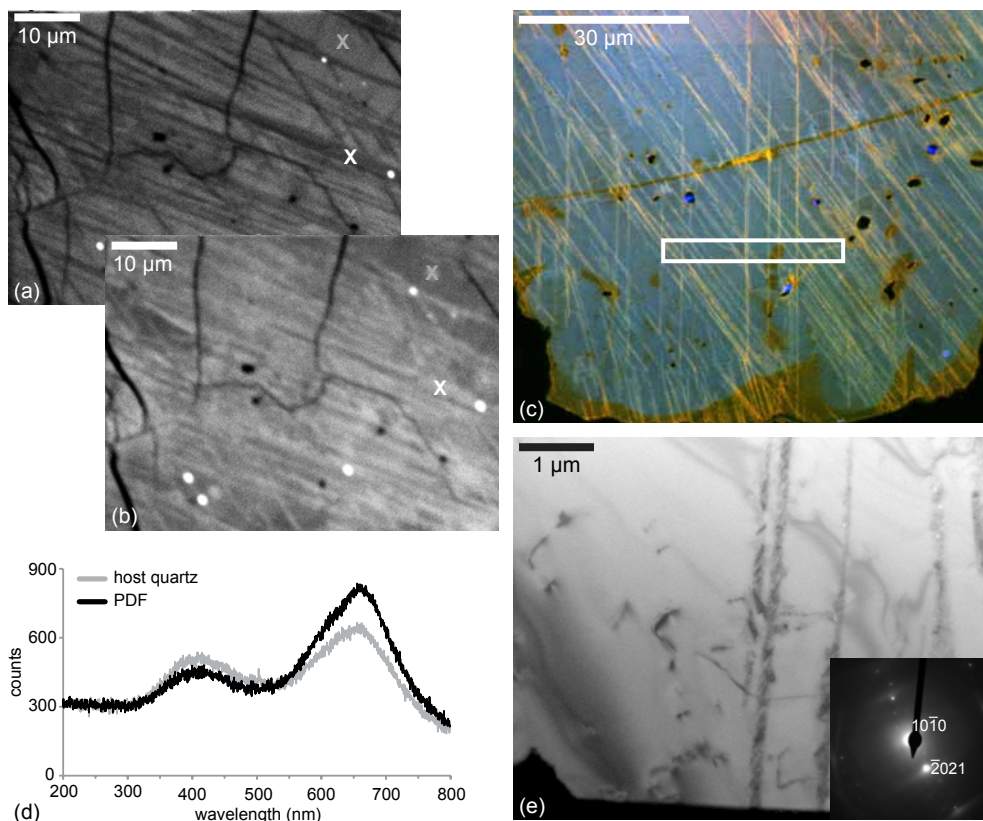


Figure 4.5 CL spectroscopic measurements of red luminescent PDFs in a granite fragment from Ries. **a** Panchromatic CL image showing multiple sets of PDFs, first scan. **b** Same area as in **a**, after repeated scanning with the electron beam, showing the increased intensity of the CL emission from the PDFs. **c** Composite colour CL image of a different grain from the same thin section showing multiple sets of red luminescent PDFs. The white rectangle shows the location of the TEM foil shown in **e**. **d** CL spectra of an area with a high density of PDFs (black line; white cross in **a**) and host quartz (grey line; grey cross in **a**). The 650 nm peak is higher in the PDFs than in the host quartz. **e** Bright field TEM image of the grain shown in **d**, showing that the red luminescent PDFs consist of arrays of dislocations.

μs per pixel) and using higher voltages and beam currents (20 kV and 2.4 nA) than that used for CL imaging was the CL emission quenched.

4.3.6 Cryo SEM-CL

Figure 4.8 shows three grains with, at room temperature, non-luminescent (figure 4.8a) or red and non-luminescent (figures 4.8c and e) PDFs. At LNT the PDFs in the grain shown in figures 4.8a and b and some (parts of) PDFs in figures 4.8c, d, e and f remain non-luminescent, but other PDFs in the grains in figures 4.8c, d, e and f, that were non- or very weakly red luminescent at room temperature, become bright red luminescent. A comparison of the CL images to secondary electron (SE) images with surface topography related information (not shown) of the same sample areas ensured that the indicated non-luminescent parts of PDFs were not porous.

Figures 4.8d and f show that in the same grain, both non-luminescent and bright red PDFs at LNT can occur. No grains were observed with exclusively bright red PDFs at LNT, but the LNT images data set is limited. In total, ten grains were imaged at LNT (see table 2.1 in chapter 2). Two grains were observed with exclusively non-luminescent PDFs at both room temperature and LNT (both in a suevite from the Ries crater) and two grains with parts of PDFs that are non-luminescent at room temperature, but bright red luminescent at LNT (both in an impact melt rock from Popigai).

Although the colours in composite colour SEM-CL images are not quantitative, within the same image colours can be compared qualitatively. For example, emissions produced by the same defect centre should have the same colour within one image, but the colour can differ slightly between different images. In the cryo-CL images, the bright red luminescent parts of PDFs seem to have a slightly different colour compared to PDFs that are also red luminescent at room temperature. The bright red LNT emission appears to be more towards the red end of the spectrum (i.e. slightly longer wavelengths) compared to the more orange-red of PDFs that are

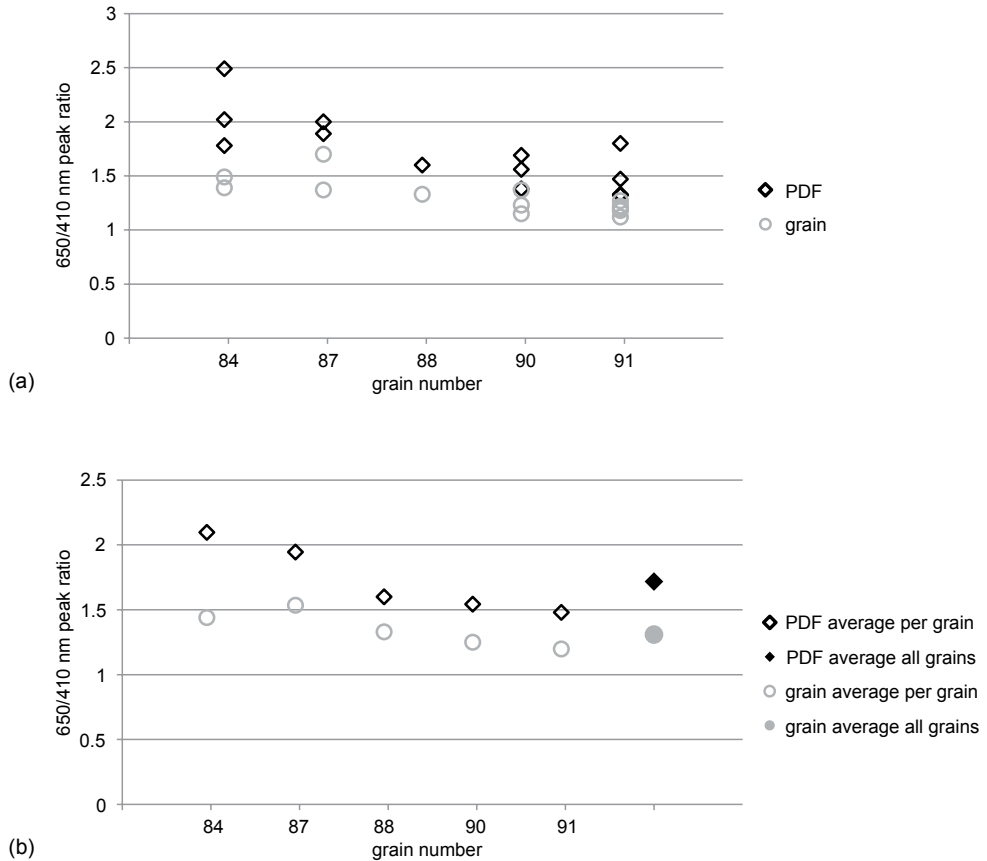


Figure 4.6 Plots of the 650/410 nm peak ratios show that the 650 peak is stronger in PDFs than in the host quartz. **a** 650/410 nm peak ratios of PDFs and host quartz; all measurements shown per grain. **b** Average 650/410 nm peak ratios of PDFs and host quartz shown per grain and as an average of all measurements.

also luminescent at room temperature. CL spectrometry measurements at LNT might be able to quantify the apparent wavelength difference between the two types of ‘red’, but unfortunately this was not possible on our systems.

4.3.7 PDFs filled with a blue luminescent phase

Figure 4.9 shows BSE, SE and composite colour SEM-CL images of a grain that was shocked experimentally to 24 GPa. EDX measurements of different parts of the grain (one spectrum is shown in figure 4.9b) indicate only SiO_2 , so the BSE image (figure 4.9a), shows only density contrast, but no phase contrast. Most of the PDFs are darker (less dense) than the surrounding

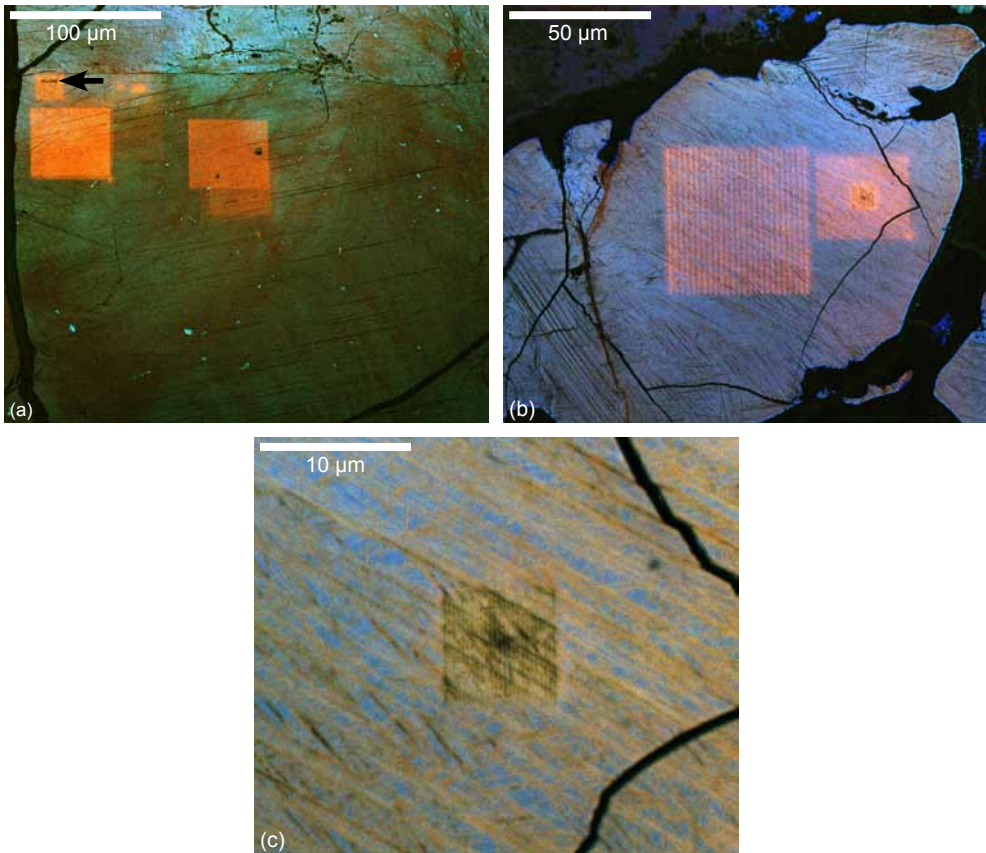


Figure 4.7 Composite colour images of grains in a granite fragment from the Ries crater. **a** Low magnification image showing red squares where higher magnification images have been scanned before at a slow scanning rate. A small rectangle has become completely non-luminescent after intense spot irradiation due to point measurements for an EBSD map (top left, black arrow). **b** Low magnification image showing red squares where higher magnification images have been scanned before at a slow scanning rate (right) and where an EBSD map was recorded using point measurements (centre). **c** Higher magnification image of the red square on the right in **b**. The square in the centre shows changes in CL emission of the part of the sample where point measurements have been taken for EBSD mapping. The PDFs in the square, which are mostly red in the rest of the image, have become non-luminescent.

quartz, as is commonly observed in BSE images of shocked quartz grains (Ebert et al., 2013; Stähle et al., 2008), because PDFs are filled with amorphous SiO_2 that is less dense than crystalline quartz. However, some PDFs in figure 4.9a are filled with a bright (denser) phase. An EDX spectrum measured in one of the bright PDFs (figure 4.9b) indicates that the bright phase has the same composition as the host quartz (SiO_2).

Figures 4.9c and d respectively show an SE and composite colour SEM-CL image of the same grain as is shown in figure 4.9a. Unfortunately, due to an extra polish that was applied to the sample between the SE/CL imaging and the BSE imaging, an exact correlation of the PDFs between BSE and SE/CL is not possible, because a small layer (a few microns) of the sample surface was removed. However, the PDFs in the SE image show the same characteristics as in the BSE image: some (parts of) PDFs are filled with a brighter phase. Using acceleration voltages above ~ 5 kV, also SE images can show some density or phase contrast, mainly because backscattered electrons excite some secondary electrons on their trajectories out of the surface layer (e.g. Reimer and Hawkes, 1998). Although the density component in the SE contrast is not as strong as in BSE images, it is observed in the grain in figure 4.9. The density contrast might be enhanced by our use of an Everhart-Thornley detector (Everhart and Thornley, 1960), which inevitably detects some backscattered electrons in addition to the secondary electrons. Furthermore, the higher density phase could be more resistant to polishing and therefore induce slight topography on the sample surface, enhancing the visibility of the brighter phase in the SE image even more.

When comparing the SE image to the composite colour SEM-CL image in figure 4.9d, the brighter SE regions clearly show blue luminescence, in contrast to the majority of PDFs which are non-luminescent.

4.4 Discussion

4.4.1 Cathodoluminescence of PDFs

The one to one correlation of FIB prepared TEM sections to composite colour SEM-CL images of PDFs in quartz clearly shows the relation between CL emission and microstructure of PDFs: non-luminescent PDFs are amorphous, while healed PDFs (consisting of planes of high defect density) and basal Brazil twins emit a red CL signal. A dominant peak at 650 nm was measured in the CL emission of healed PDFs of the Ries crater.

4.4.1.1 Red luminescent PDFs

From figure 4.2 it is clear that the red luminescence of healed PDFs is related to the high dislocation density in the PDF plane. The dominant emission peak in red luminescent PDFs is at 650 nm (figures 4.5 and 4.6), which is related to the NBOHC (Götze et al., 2001; Stevens Kalceff and Phillips, 1995a; Stevens Kalceff et al., 2000). The NBOHC defect ($\text{O}_3 \equiv \text{Si-O}\bullet$) can be induced under electron irradiation by the dissociation of a (strained) Si-O bond (beam damage) by radiolysis. Radiolysis is a process in which atoms are displaced by inelastic interactions of the electron beam with the sample and occurs in quartz at beam energies above ~ 5 kV (Stevens Kalceff, 2009; Stevens Kalceff et al., 2000). The 650 nm CL emission associated with dissociation of a Si-O bond increases with increasing scanning time and then stabilizes (Götze

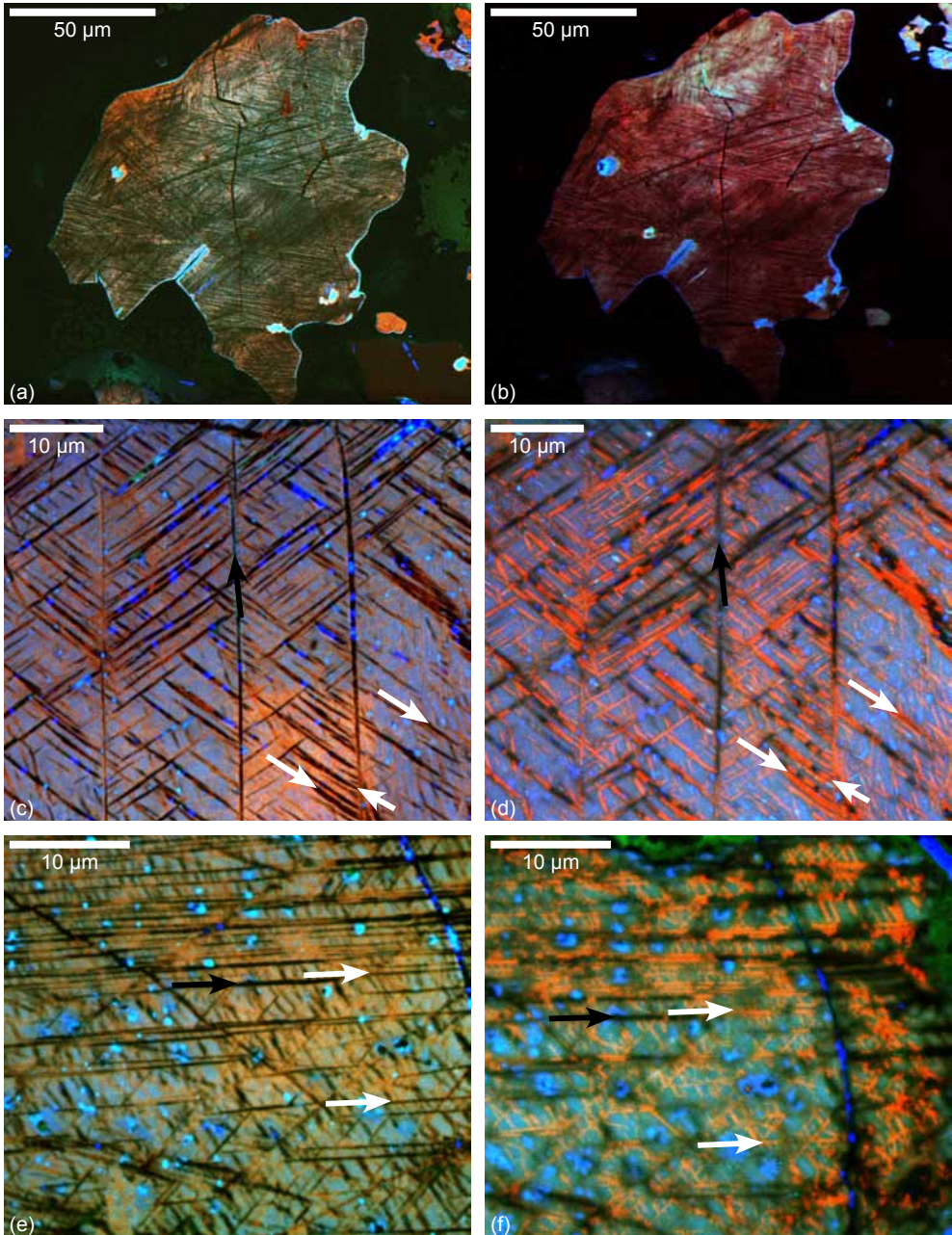
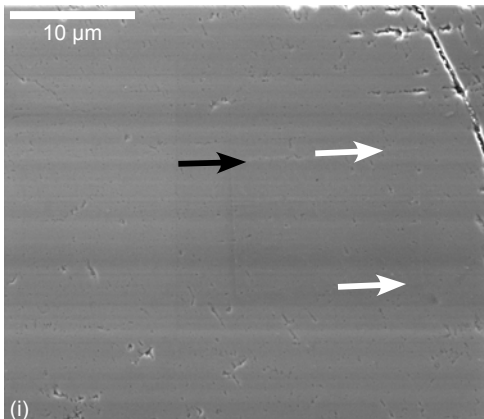
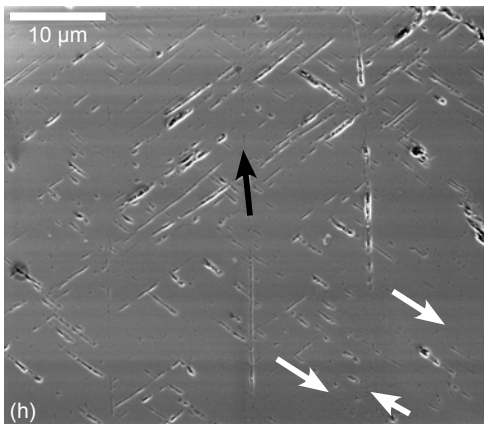
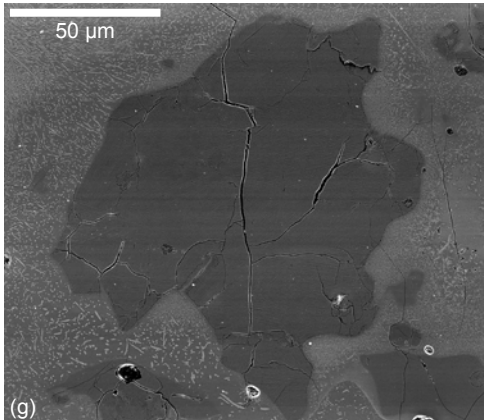


Figure 4.8 Composite colour SEM-CL images recorded at room temperature (left) and LNT (right) in a suevite from the Ries crater (a, b) and an impact melt rock from Popigai (c-f). **a** Non-luminescent PDFs at room temperature. **b** The non-luminescent PDFs shown in a are also non-luminescent at -170°C . **c** Red and non-luminescent (parts of) PDFs at room temperature. **d** Some of the non-luminescent PDFs shown in c are still non-luminescent at -170°C (centre, black arrows), but others become bright red luminescent (white arrows). **e** Red and non-luminescent (parts of) PDFs at room temperature. **f** Some of the non-luminescent PDFs shown in e are still but others become bright red



luminescent (white arrows). **g, h, i** Equivalent SE images of the CL images shown in **a, c** and **e**, showing that the non-luminescence is not due to pores or open PDFs.

et al., 2001; Stevens Kalceff et al., 2000). Two other precursors for the NBOHC are known, but the CL emission associated with these is quickly quenched (Götze et al., 2001; Stevens Kalceff, 2009): $O_3\equiv Si-O-H$, where electron irradiation breaks an O-H bond, and $O_3\equiv Si-O-M$, where M is an alkali ion and electron irradiation dissociates the O-M bond. Furthermore, peroxy linkages (Si-O-O-Si) are often mentioned as a precursor defect for the NBOHC (Götze et al., 2001; Stevens Kalceff and Phillips, 1995a; Stevens Kalceff et al., 2000). The CL emission of the red luminescent, healed PDFs shows an increase with increasing irradiation time (see figure 4.7 and chapter 2). This suggests that the NBOHC, induced by Si-O bond dissociation by radiolytic beam damage processes, is the main source for the red CL emission. Production of NBOHC defects and red CL emission is a standard observed process in quartz and also takes place in undamaged crystalline quartz (e.g. Götze et al., 2001; Stevens Kalceff, 2009; Stevens Kalceff and Phillips, 1995a) – as can also be observed in figure 4.7, where previously scanned areas show a strong red CL emission. However, PDFs are quicker to show effects of irradiation damage than the surrounding quartz, and therefore show an increasingly bright red luminescence. In TEM, localised electron beam damage, mainly by radiolytic processes, at dislocations, fluid inclusions and twin boundaries is a commonly observed phenomenon and continued beam damage finally results in complete (local) amorphisation (Carter and Kohlstedt, 1981; Cherns et al., 1980; Comer, 1972; McLaren et al., 1970). The combination of the red CL emission at 650 nm with initially strongly increasing intensity, the high dislocation density along healed PDFs in TEM, and the known phenomenon of localised beam damage in TEM at defects strongly suggest that preferential electron beam damage at dislocations produces NBOHC defects by

breaking of Si-O bonds, forming the source of the red luminescence in healed PDFs. In rare cases, even individual dislocations within the healed PDFs can be detected in SEM-CL images, as is shown by the PDFs in the upper right corner of figure 4.2d. These PDFs consist of arrays of tiny red luminescent ‘sub-lamellae’ that look similar to the arrays of dislocations observed in healed PDFs in TEM (e.g. figures 4.2b and c, and figures in Goltrant et al. (1991) and Trepmann and Spray (2006)). However, the presence of OH bonds may also play a role in the production of NBOHC defects and the related red CL emission. Healed PDFs are thought to form by water-assisted recrystallisation of the initially amorphous PDFs under high post-shock temperatures or metamorphic events (Grieve et al., 1996), so obviously water must be present in the healed PDFs. This is supported by the fluid inclusions that usually decorate healed PDFs. Since OH groups may preferentially bond to non-bridging atoms in dislocation cores bonds (e.g. Heggie, 1992; Trepied and Doukhan, 1978), it is very likely that a relatively high concentration of OH groups are present in healed PDFs and (at least initially) contributes to the red luminescence.

Brazil twins are also red luminescent in SEM-CL images (figure 4.3). If dislocations are present along the twin plane, they could be a source of the red luminescence, but more likely the red CL emission comes also from the twin plane itself, because the dislocation density in the Brazil twin plane is usually much lower than in healed PDFs and large parts of the twin plane are free of dislocations (figure 4.3). Furthermore, McLaren and Phakey (1965) observed very quick preferential damage along Brazil twin boundaries in amethyst in TEM, similar to the damage occurring at dislocations. The necessary precursors for the NBOHC may be strained bonds in the locally distorted tetrahedral structure in the twin boundary, or OH groups, peroxy linkages or impurities that might be concentrated at the twin boundary.

4.4.1.2 Non-luminescent PDFs

In the amorphous material in non-luminescent PDFs, such as the grain from the Ries crater and the experimentally shocked grain in figure 4.1, the structure is apparently so damaged and disordered that no CL emission is possible. Due to the extreme pressures and temperatures involved in impact processes, the crystal structure in PDFs formed at high pressure could be completely destroyed, preventing any photon emission under electron bombardment. Boggs et al. (2001) assumed that a non-crystalline material does not contain electron traps since a band structure is lacking, but the 650 nm CL emission is a commonly observed peak in fused (low pressure, high temperature produced) silica glass (Fitting et al., 2001; Stevens Kalceff et al., 2000). However, figure 4.7 shows that prolonged intense electron irradiation, with the beam in spot mode, first induces an increase in red CL emission, but finally results in non-luminescence. This suggests that ongoing beam damage eliminates all luminescence centres. Since damage processes in TEM and SEM are largely the same and beam damage in TEM finally results in local amorphisation, it is likely that the same happens in SEM and that the localised amorphisation is observed as localised quenching of CL emission.

An alternative explanation for the non-luminescence of amorphous PDFs might be variations in trace element concentrations, for example iron content. Although interstitial Fe³⁺ in (crystalline) quartz is mentioned as the source of a red luminescence peak around 700-750 nm (Götze, 2009; Stevens Kalceff, 2009), it has also been suggested that the presence of iron can quench other CL emissions (Haddad et al., 2006). Chemical analysis of experimentally shocked quartz grains suggests that grains with a high density of PDFs contain an increased amount of metals from the iron meteorite projectile that was involved (Ebert et al., 2013). If meteoritic iron, or iron

from another source, is in some way distributed preferentially into the PDFs, it could quench the luminescence. In this context it would be interesting in a future study to map the trace element distribution of shocked quartz grains with non-luminescent amorphous PDFs.

The breaking of Si-O bonds due to electron irradiation is in fact very local amorphisation in the direct vicinity of the defect. Because defects in SiO_2 disturb the short range order, the defect structure and most luminescence centres in crystalline and amorphous SiO_2 are similar (Sigel and Marrone, 1981; Stevens Kalceff and Phillips, 1995a). It has even been suggested that the NBOHC and most other defects in quartz are associated with locally amorphous parts of the crystal structure (Stevens Kalceff, 2009). Furthermore, as mentioned earlier, the 650 nm peak is a commonly observed CL emission in fused SiO_2 glass (Fitting et al., 2001; Stevens Kalceff et al., 2000). It is therefore theoretically possible that some amorphous PDFs are red luminescent. However, red luminescent amorphous PDFs were not observed in our samples. Apparently, the

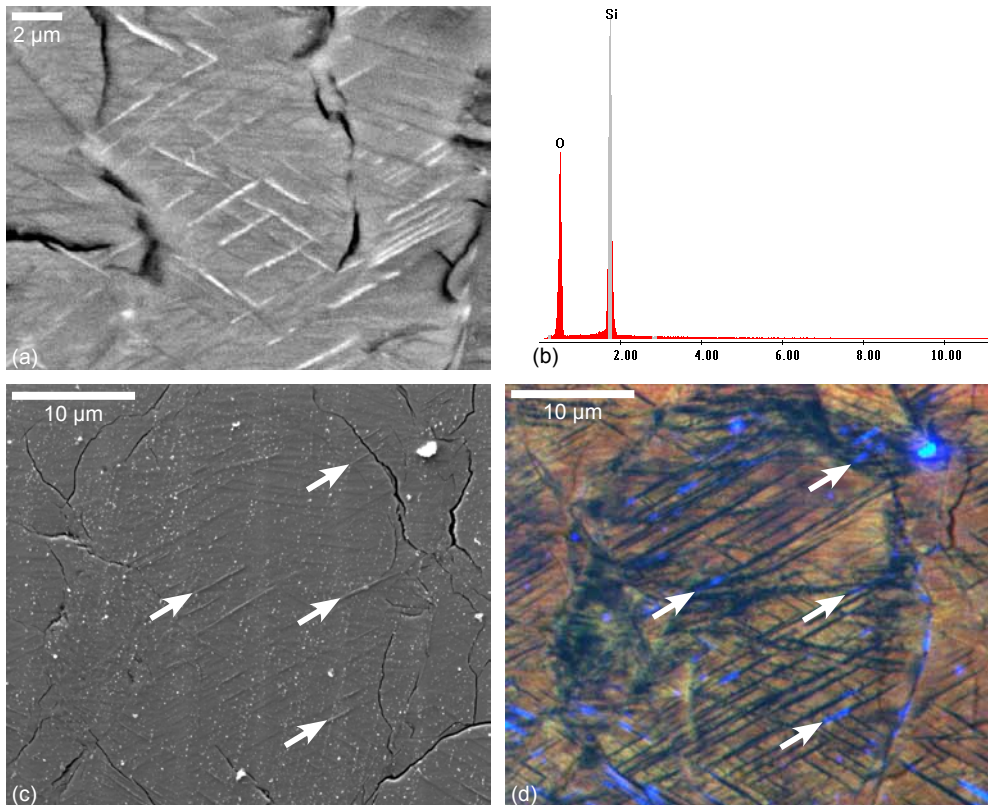


Figure 4.9 Experimentally shocked single crystal quartz. **a** BSE image, clearly showing that some PDFs are filled with a denser (brighter) phase. **b** The EDX spectrum from the brighter phase shows that it has SiO_2 composition. **c** SE image of the same grain as in **a** (lower magnification), showing some density contrast as well as topography. White arrows indicate some clear examples of PDFs that are filled with a denser (brighter) phase. The bright areas do not correspond exactly with those in the BSE image in **c**, because the grain has been polished in between imaging **c/d** and **a**, but the geometry of the denser phase is the same. **d** Composite colour SEM-CL image of the same area as shown in **c**. White arrows indicate the same PDFs filled with a denser phase as in **c**, that are brighter in the SE image. The denser phase shows blue luminescence.

structure or trace element composition of amorphous PDFs is not the same as that of most types of fused silica glass. It is worth noting, as was already reported in chapter 2, that only highly shocked grains were observed with exclusively non-luminescent PDFs. In these grains, the PDFs are always thick and slightly wavy and irregularly shaped: the characteristics of PDFs formed at high shock pressures > 25 GPa (Langenhorst, 1994). Grains with fewer sets of PDFs, more widely spaced and thin and straight (i.e. the characteristics of PDFs in grains of a lower shock stage), and only non-luminescent, were not observed. Even in relatively recent structures, such as the 3.6 Ma El'gygytgyn crater (not shown), grains with characteristics of lower shock pressure (thin, straight PDFs that are more widely spaced) and with only non-luminescent PDFs were not observed. The most probable explanation for the apparent lack of moderately shocked quartz grains with exclusively non-luminescent PDFs is that, even in relatively recent impact structures, a significant proportion of the amorphous material has recrystallised and many (parts of) PDFs are healed. Under similar temperature conditions, thinner PDFs, formed at lower shock pressures, will likely heal more easily than wider PDFs, which formed at much higher shock pressures.

Some other explanations for the lack of moderately shocked grains with non-luminescent PDFs might be considered: A) amorphous PDFs in grains shocked to lower pressures are too narrow to be detected as non-luminescent in CL images, but instead defects or damage zones along the PDFs give rise to a red luminescent signal; B) unaltered PDFs at lower shock stages are not (completely) amorphous; C) lower shock amorphous PDFs contain amorphous material with a different structure, that is red instead of non-luminescent – in this case these PDFs would be indistinguishable from healed ones in CL images. Scenario A is unlikely, as thin and straight, but non-luminescent and amorphous PDFs were observed in the grain in figure 4.4. No direct evidence for scenarios B or C can be found in our data, but from the literature and our results it is clear that different CL behaviour can be observed in amorphous SiO₂. TEM and SEM-CL observations on very recent or, preferably, experimentally shocked quartz should be able to solve this issue.

4.4.2 Cryo CL

In chapter 2 we concluded that the main CL characteristics of PDFs are not different at room temperature or LNT, but more detailed analysis of non-luminescent PDFs in CL images recorded at different temperatures does in fact reveal a difference. In cryo SEM-CL images recorded at -170°C (figure 4.7) two types of CL behaviour in non-luminescent PDFs are observed: those that are non-luminescent at both room temperature and LNT, and those that are non- to weakly red luminescent at room temperature, but bright red luminescent at LNT. This is very different behaviour from the red emission observed in healed PDFs and basal Brazil twins at room temperature, so the bright red emission at LNT cannot be produced by the same defect (NBOHC with probably the Si-O bond precursor). Furthermore, the NBOHC is induced by radiolysis, which is somewhat reduced by decreasing the temperature (Martin et al., 1996). The red luminescence reported here, however, is very strong at -170°C, stronger than the emission from (parts of) PDFs that are red also at room temperature, and the bright red luminescence is very weak to invisible at room temperature. Iron impurities in the quartz lattice are thought to induce a peak at ~705 nm (Götze et al., 2001; Kempe et al., 1999). The slightly longer wavelength of the Fe related emission would fit with the apparent colour difference between red luminescence at LNT and at room temperature, but the 705 nm peak was reported

from spectroscopy measurements at room temperature. Alternatively it might be hypothesised that parts of the amorphous PDFs contain differently coordinated silica than the low pressure tetragonal configuration (four-fold silica coordination). Since PDFs are thought to form through high pressure amorphisation, possibly with some subsequent melting, and quenching of the amorphous phase still under high pressure (Goltrant et al., 1992; Langenhorst and Deutsch, 1994), it is possible that parts of the amorphous material contain four-fold coordinated silica, while other parts are still in the high pressure six-fold coordination. This might result in differences in the available defect centres for CL emission. However, a denser high pressure phase can be expected to show contrast in high-contrast SE images, similar to the high density phase in figure 4.9, but this is not observed in the bright red luminescent phase. Furthermore, although the effects of Si coordination on CL emission are not well-studied, figure 4.9 shows that PDFs filled with a higher density phase can be blue luminescent. This high density phase is likely to be either a high pressure polymorph of SiO_2 or a high pressure amorphous phase (see also section 4.4.3), in which Si atoms have a predominantly six-fold coordination.

A third hypothesis to explain the bright red emission might be that the hydrogen content of the amorphous PDFs plays a role in the production of the bright red luminescence, since amorphous SiO_2 can contain more water than crystalline quartz. Radiolysis of hydroxyl groups in quartz produces a NBOHC and atomic hydrogen ($\text{O}_3\equiv\text{Si}-\text{OH} \rightarrow \text{O}_3\equiv\text{Si}-\text{O}\cdot + \text{H}^0$) (Griscom, 1985; Stevens Kalceff and Phillips, 1995b). At temperatures below $\sim -173^\circ\text{C}$ ($<100\text{ K}$), the interstitial atomic H is immobile and only at temperatures exceeding -143°C (130 K), thermal diffusion and dimerisation take place to form H_2 , which diffuses away rapidly at temperatures above $\sim -100^\circ\text{C}$ (170 K) (Stevens Kalceff and Phillips, 1995b). The formation of the NBOHC in this process might contribute to the bright red luminescence observed at -170°C , but it is probably not enough to account for the complete signal. Furthermore, there is no reason why, if a high concentration hydroxyl groups is present in the bright red luminescent amorphous PDFs, radiolytic dissociation of the OH groups would not take place at room temperature and show a (quickly decreasing) red luminescence. Also, a NBOHC contribution to the low temperature red emission does not explain the apparent colour difference observed in red PDFs at LNT and PDFs that are also red at room temperature. The effect of interstitial (neutral) atomic H at LNT on the CL emission of quartz is unknown.

The current dataset of grains imaged at LNT with non-luminescent PDFs at room temperature that show this bright red luminescence at LNT is too limited to fully explain the bright red CL emission in some PDFs that are non-luminescent at room temperature. Furthermore, spectroscopic measurements would be required to fully characterise the emission and determine the defect centres responsible for the red colour.

4.4.3 Blue luminescent high pressure phase

In the experimentally shocked quartz grain in figure 4.9, PDFs were observed filled with a phase that is bright in BSE images and blue luminescent in CL images. Because the phase is brighter than the host quartz in BSE images, it must have a higher density, but EDX spectra show that the bright phase and the host grain are both composed of SiO_2 . Therefore the phase can be interpreted as a high-pressure SiO_2 phase. Two high-pressure polymorphs of quartz are frequently observed in impact environments: coesite and stishovite (e.g. Stähle et al., 2008; Stöffler and Langenhorst, 1994). Stishovite is estimated to occur in quartz shocked to pressures

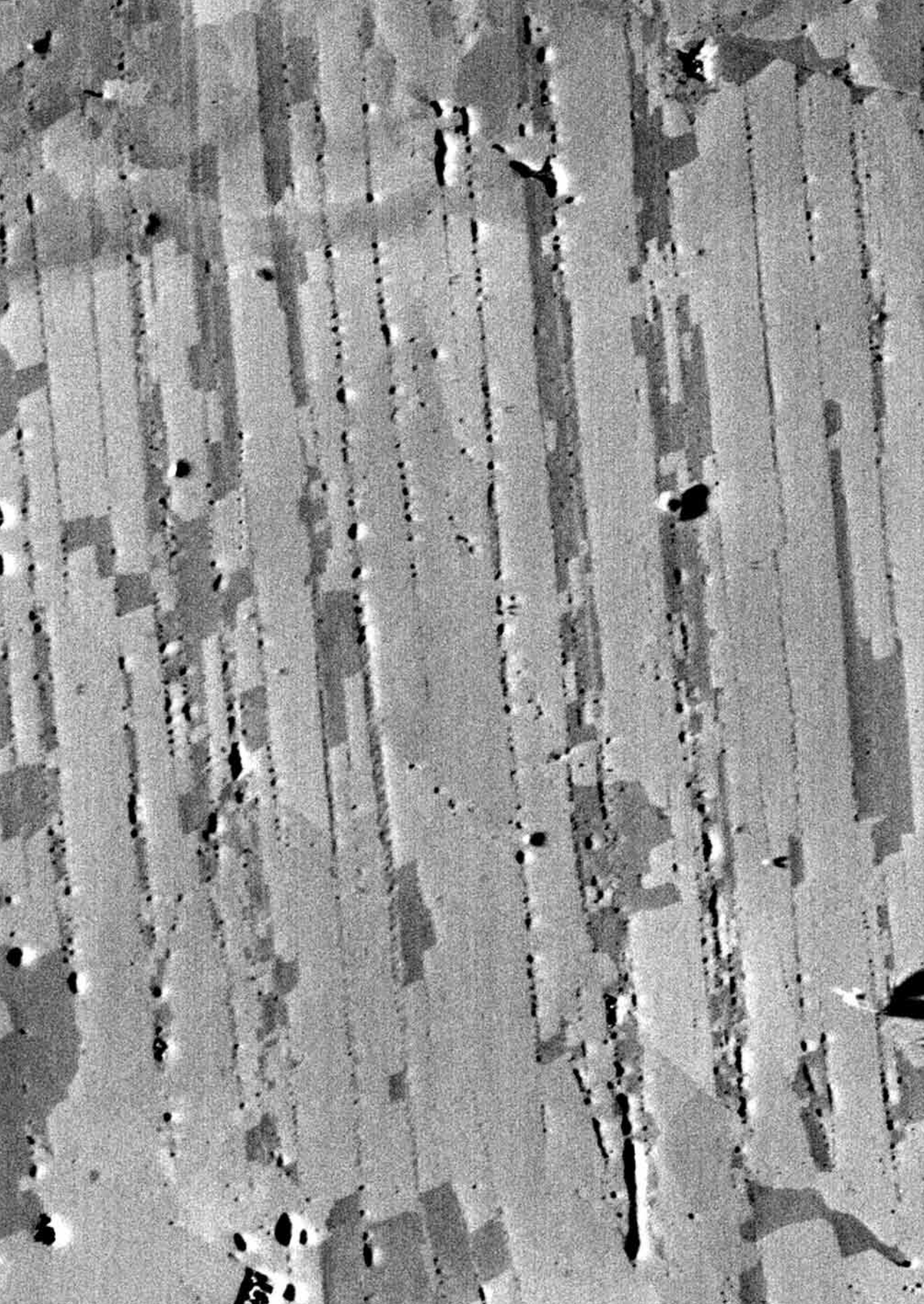
between ~12 and 45 GPa, while coesite only appears at pressures above ~30 GPa (Stöffler and Langenhorst, 1994). The grain in figure 4.9 was shocked to 24 GPa, which is in the pressure range in which stishovite can form. Furthermore, the high density phase has the same geometry and appearance as the stishovite-filled PDFs shown by Stähle et al. (2008) in their figure 2. The blue CL also fits with stishovite: Fitting et al. (2001) showed that the CL emission of stishovite from Barringer Crater (Arizona, USA) at room temperature has a broad band that is a combination of peaks around 420, 460 and 500 nm. Trukhin et al. (2003) also observed a blue luminescence band in stishovite. Because of the shock pressure, geometry and CL emission colour, the high-pressure phase observed in the grain in figure 4.9 can be interpreted as stishovite. Alternatively, as it is unknown whether this high density phase is crystalline or not, it could be a high pressure amorphous form of SiO_2 .

Composite colour SEM-CL imaging can therefore, like BSE images, be used as an indication for the presence of high pressure phases, possibly stishovite, in shocked quartz. However, care should be taken with a definitive interpretation, because remains of polishing material or dust particles on the sample surface can also be blue luminescent (see the bright blue spots present in most colour CL images in this paper and figure 2.4 in chapter 2), as might possible secondary minerals in altered rocks. Chemical analysis of the composition of the phase and TEM or EBSD observations, providing information on crystal structure, are required to confirm the nature of a potential high pressure form of SiO_2 .

4.5 Conclusions

The combination of colour SEM-CL imaging and TEM analysis of shocked quartz grains confirms the great potential of colour SEM-CL imaging as a method to identify PDFs in quartz, but also illustrates the complexities that are involved in interpreting CL emissions, especially in images. A very useful result of this study for crater research is that colour SEM-CL imaging can distinguish between fresh (amorphous) and healed PDFs or basal Brazil twins: non-luminescent PDFs are amorphous, while healed PDFs and basal Brazil twins are red luminescent. TEM and CL spectrometry confirm that the dominant peak in the emission from red luminescent PDFs is around 650 nm, related to the NBOHC, and is most likely the result of preferential beam damage at dislocations and twin boundaries. A high pressure phase, possibly stishovite, can be detected in colour SEM-CL images as blue luminescent parts of PDFs. Although not all details of the CL emission of PDFs can be explained at this time, SEM-CL imaging is a great method to visualise subtle differences in shock microstructures in quartz. For more quantitative information, additional analysis can be done on the same samples using other techniques, such as TEM, EBSD or light microscopy with universal stage for crystallographic orientations of grains or PDFs, and EDX mapping or CL spectroscopy for defect and trace element distributions.

Acknowledgements – Uwe Reimold and Jörg Fritz are thanked for kindly providing the experimentally shocked samples, Uwe Reimold and Uli Raschke for the El'gygytgyn sample, Roald Tagle for the Popigai samples and Rodger Hart for the Vredefort samples. Pim van Wamel has been of great help during sampling at the Ries crater, and Philippe Lambert at Rochechouart.



Chapter 5

Characterisation of shock microstructures in quartz by foreshatter electron imaging and electron backscatter diffraction

M.F. Hamers, G.M. Pennock, L. Palasse and M.R. Drury

Shocked quartz grains are crucial evidence for meteorite impact craters or ejecta layers, but the presence of shock microstructures can often only be confirmed reliably by expensive and time-consuming transmission electron microscopy. In this paper, electron backscatter diffraction (EBSD) mapping and foreshatter electron (FSE) imaging are assessed as a method to identify planar deformation features (PDFs) in quartz and characterise the structure of the host quartz grain, and to distinguish between PDFs and tectonically formed (sub-)planar microstructures. Our results show that FSE images and pattern quality maps can be used to identify PDFs and give an indication of their structural state (amorphous or healed). FSE imaging and EBSD mapping allow a quick and easy characterisation of grain structure: mosaicism is detected in FSE images and Dauphiné twins can be imaged with FSE and confirmed with EBSD measurements. Composite colour FSE images show the presence of Dauphiné twins even more clearly. The hypothesis that shock-induced mechanical Dauphiné twins play a role in PDF formation is discussed. We conclude that EBSD techniques and FSE imaging are a valuable addition to the study of shocked quartz.

5.1 Introduction

Meteorite impacts have played an important role throughout the Earth's history. They were an important surface-shaping process in the early history of the Earth and a major impact has caused a mass extinction on at least one occasion, at the Cretaceous-Palaeogene boundary (e.g. Alvarez et al., 1980; Smit and Hertogen, 1980). It is therefore important that geological structures and stratigraphic layers that are suspected of having an impact origin can be identified correctly. One of the most reliable and widely used forms of impact evidence is the presence of planar deformation features (PDFs) in quartz (e.g. Engelhardt and Bertsch, 1969; French and Koeberl, 2010; French and Short, 1968; Grieve et al., 1996; Stöffler and Langenhorst, 1994). PDFs are planar microstructures with a crystallographically determined orientation, which can only form as a result of an impact-induced shock wave passing through the rocks. These microstructures are universally accepted as definitive impact evidence. However, in light microscopy PDFs in quartz often resemble non-impact related (sub-)planar microstructures, such as healed fractures or tectonic deformation lamellae (sometimes called Böhme lamellae or metamorphic deformation lamellae). For a reliable interpretation of potential impact structures or layers the correct identification of PDFs is crucial. The only accepted reliable technique, transmission electron microscopy (TEM) analysis, is expensive, very time-consuming, and only appropriate to study tiny samples (some tens of micrometers in width and length). Furthermore, TEM sample preparation destroys the area of interest. Additional or alternative methods that are easier, quicker and can be applied to larger samples would be very useful. The scanning electron microscope (SEM) could be a suitable instrument, because most detectors used in modern SEMs have a very high spatial resolution, standard sized petrographic thin sections or polished rock slabs can be easily analysed and SEM techniques are non-destructive.

Recently, cathodoluminescence imaging in a scanning electron microscope (SEM-CL) was proposed as an additional method to identify and characterise PDFs in quartz (chapters 2 and 4; Boggs et al., 2001). Composite colour SEM-CL can discriminate between amorphous and healed PDFs: non-luminescent PDFs are amorphous, while healed PDFs (arrays of dislocations) have a red CL emission with a dominant peak at a wavelength of 650 nm (chapter 4). However, CL images do not provide information on the microstructure of the host quartz grain itself, or the crystallographic orientation of PDFs. Again, TEM is the designated technique to show whether a grain is a relatively undamaged single crystal, or, for example, has a mosaic structure. PDF orientations can be measured in TEM or a light microscope with a universal stage (Ferrière et al., 2009; Stöffler and Langenhorst, 1994), although in light microscopy only the c-axis orientation of the grain can be determined and not the complete crystallographic orientation including the a-axes. Electron backscatter diffraction (EBSD) and foreshatter electron (FSE) imaging are SEM techniques that can provide details on crystal structure and crystallinity of a material (e.g. Day, 1993; Lloyd, 1987; Prior et al., 1999; Prior et al., 1996). EBSD measurements (e.g. Adams et al., 1993; Dingley and Randle, 1992) can be used to determine crystallographic orientations and estimate PDF orientations. These methods could form a useful addition to existing SEM and TEM techniques used to study shocked quartz. In this paper, we evaluate the use and limitations of FSE imaging and EBSD mapping as methods to identify and characterise shocked quartz grains, by applying these methods to samples that have previously been studied by SEM-CL and TEM (chapters 2 and 4). Furthermore we assess how the techniques can be used to distinguish between PDFs and tectonic deformation lamellae.

5.1.1 Shock metamorphism in quartz

5.1.1.1 Planar deformation features

Planar deformation features consist of thin ($<1 \mu\text{m}$), parallel, closely spaced (typically $<2 \mu\text{m}$ apart) lamellae. Usually multiple PDF sets develop in the same grain; typically 2-10 are observed (Engelhardt and Bertsch, 1969). Although PDFs are generally described as strictly straight and planar, some bending or slight curvature has been reported (Engelhardt and Bertsch, 1969; Stöffler and Langenhorst, 1994; Trepmann and Spray, 2005). PDFs can be penetrative through a whole grain or be concentrated in parts of a grain, but do not cross grain boundaries, cracks, or planar fractures that were present before PDF formation.

PDFs have crystallographically determined orientations and are mostly parallel to low-index rational planes (most frequently observed are c (0001), ω $\{10\bar{1}2\}$ and π $\{10\bar{1}3\}$) (Ferrière et al., 2009; Stöffler and Langenhorst, 1994). Unaltered PDFs are lamellae of amorphous silica, formed under high pressure during shock. PDFs parallel to c (0001) are not amorphous, but consist of mechanical Brazil twins. As a result of post-shock high temperature or metamorphic events, amorphous PDFs heal and recrystallise easily. Healed lamellae are recognised in TEM images as planes with a very high dislocation density. In a light microscope, they can often still be recognised as planes of fluid inclusions with the same orientation as the originally amorphous PDFs, and their crystallographic orientations can be measured in the universal stage (e.g. Ferrière et al., 2009). Healed PDFs can also be imaged using SEM-CL (chapters 2 and 4).

5.1.1.2 Mosaicism

Mosaicism is a characteristic microstructure observed in some shocked quartz grains. In light microscopy mosaicism appears as an irregular ‘mottled’ extinction (Leroux and Doukhan, 1996; Stöffler and Langenhorst, 1994). TEM shows the presence of small (micrometer scale) slightly misoriented crystalline domains. Although no quantitative relationship has been established, it has been noted that misorientation increases and domain size decreases with increasing shock pressure (Stöffler and Langenhorst, 1994 and references therein). Leroux and Doukhan (1996) interpreted the mosaic structure as the result of shattering of a crystal, but Trepmann (2008) proposed that mosaicism could be caused by recrystallisation of a high density of closely spaced, crosscutting PDFs that bound slightly misoriented crystalline domains.

5.1.1.3 Dauphiné twins

Dauphiné twins are a common type of twin in quartz. Geometrically, host and twin are related by a 180° (or apparent 60°) rotation around the c -axis. Since the c -axis is the optical symmetry axis in quartz, Dauphiné twins cannot be distinguished in a light microscope in thin sections, but can only be observed in TEM and in FSE images and EBSD maps. The orientations of c - or a -axes are not affected by twinning, but it reverses positive (e.g. $\{10\bar{1}1\}$) and negative (e.g. $\{01\bar{1}1\}$) rhombs. Dauphiné twins can be produced in three different ways (Fron del, 1945): 1) by cooling β -quartz to temperatures below the inversion point (573°C) to α -quartz; 2) by rapidly cooling down (quenching) α -quartz from roughly the range 550 - 200°C ; 3) by the local application of high stresses at room temperature or higher. Although resulting from stress, no significant permanent strain results from mechanical Dauphiné twinning. However, mechanical Dauphiné twinning does reduce the stiffness of quartz crystals, i.e. twinning increases their compliance and facilitates deformation (Lloyd, 2004; Menegon et al., 2011; Tullis, 1970; Tullis and Tullis, 1972).

It is well known that Dauphiné twins are often present in shocked quartz grains, in close connection to PDFs (e.g. Chen et al., 2011; Goltrant et al., 1991; Trepmann and Spray, 2005; Wenk et al., 2011; Wenk et al., 2005). To account for the presence of Dauphiné twins in shocked quartz, both cooling down through the β - α transition and as a result of stresses during the impact have been proposed as formation mechanisms. Trepmann and Spray (2005) studied Dauphiné twins associated with PDFs in shocked quartz from the Charlevoix impact structure in Canada. They proposed that the twins occur mainly as a result of a reversion to α -quartz during cooling of quartz that was in the β state due to a pre-impact high temperature and shock heating to above the α - β transition temperature. Wenk et al. (2005), on the other hand, found Dauphiné twins in shocked quartz samples from the Vredefort crater (South-Africa) and conclude that they formed due to high stresses occurring during the impact. Trepmann and Spray (2005) furthermore concluded that the number of grains with PDFs parallel to both positive and negative rhombs (i.e. grains with Dauphiné twins) increases with increasing shock pressure.

5.2 Methods and samples

5.2.1 Technical background

Only a brief summary of the techniques used in this paper is given here. A thorough review of FSE imaging and EBSD and their use in the study of geological materials can be found in Prior et al. (1999; 1996).

5.2.1.1 Forescatter electron imaging

Forescatter electron (FSE) imaging, also known as orientation contrast (OC) imaging, is a method that uses electron channelling effects to image changes in crystal orientation or structure (e.g. Day, 1993; Lloyd, 1987; Prior et al., 1999; Prior et al., 1996). Although this technique is commonly referred to as orientation contrast imaging, in this paper we prefer use of the more neutral term forescatter electron imaging, because contrast can be produced by variations in crystallinity and by variations in crystal orientation.

FSE imaging is related to backscatter electron (BSE) imaging. The total BSE signal usually consists of compositional variations (z -contrast, arising from differences in atomic number) and of crystallographic variations. The proportion of the two components varies with scattering angle: low angle scattering is less dependent on the atomic number. Under normal scanning conditions (i.e. a flat-lying sample with the electron beam incident normal to the sample surface), electrons scattered at a high angle are detected (backscattered electrons). In this setup the proportion of the signal resulting from compositional variations is at least an order of magnitude higher than the proportion resulting from crystallographic differences and therefore the contrast mostly reflects compositional differences. However, when the sample is tilted so the surface is inclined to the incident beam and a different detector geometry is used, electrons scattered at a low angle are detected (forescattered electrons), reflecting a strong crystallographic component. Prior et al. (1996) found that electrons scattered by 60° or more give an image dominated by crystallographic contrast.

Two channelling effects occur when a sample interacts with the electron beam. Some incident electrons are channelled into the sample, to depths from which they cannot escape ('channelling

in"). A change in orientation or crystallinity will affect the number of electrons that channel in, and therefore induce a variation in the FSE signal. The second effect is that some backscattered electrons leaving the sample are diffracted by the crystal lattice, giving rise to variations in the FSE signal ("channelling out") (Day, 1993; Prior et al., 1999; Prior et al., 1996). It is likely that the channelling out (diffraction) effect is the main source of the contrast FSE images (Day, 1993; Prior et al., 1996). We suggest that little or no change in contrast will occur in an amorphous phase (i.e. amorphous material will be the same shade of grey in one image), because without an ordered crystal structure, no channelling out effects can occur. The intensity of the signal is then determined mainly by composition and density of the material and the detector geometry. Because FSE contrast is not quantitative and contrast and brightness are often adjusted for individual images, changes in grey level of amorphous material can be apparent between different images.

Contrast in FSE images is not quantitative, but orientation changes $<0.5^\circ$ can be detected (Lloyd, 1994). The spatial resolution of FSE images depends on the imaging resolution (i.e. the pixel density of the image) and is very high. Our imaging results indicate that features of $<0.1 \mu\text{m}$ can be seen in high quality images. One FSE image never shows all of the orientation variation within a grain, but several images recorded at different imaging conditions (acceleration voltage, beam current, sample tilt, working distance or detector distance) or from differently located detectors are required for recording a maximum amount of information (Day, 1993; Day and Quedstedt, 1999). When three detectors are used, three different greyscale signals are collected, which can be displayed in one image after colour-coding each signal with red, green or blue (RGB). The resulting RGB colour-coded image shows the same type of information as greyscale images. However, the colour-coded FSE image contains much more information in one image, because more colours exist than shades of grey. The chance of two differently oriented or structured neighbouring areas accidentally being assigned the same colour is therefore much smaller than in a monochrome image. Technically, in digital images there are 255 different grey scales, while in a colour-coded image there are $255 \times 255 \times 255 = 16.5$ million different colours. Of course adjacent grey or colour numbers are very hard, if not impossible, to discern by the human eye on a computer screen, let alone in print, but these numbers give an idea of the much larger amount of information that can be contained in a colour-coded FSE image. Furthermore, using three (for the colour-coded images) instead of two detectors (for the greyscale images) increases the signal to noise ratio, as three detectors record three different signals instead of two, but the same background noise. Therefore, the signal to noise ratio is increased when more detectors are used and more information is recorded in the image (Day, 1993).

Acceleration voltage, beam current, working distance, detector distance and sample tilt are all parameters that influence an FSE image. These parameters can be adjusted to optimize the contrast to obtain the highest amount of information in one image. Alternatively, conditions can be changed between images in order to collect several images of the same sample area using different imaging conditions and even combine them into one image. Topography effects should be taken into account when interpreting FSE images, because this can have a strong effect and often complicates interpretation of the FSE contrast.

5.2.1.2 Electron backscatter diffraction

Electron backscatter diffraction (EBSD) mapping (Adams et al., 1993) has become widely used in texture and structural analysis of geological materials (e.g. Prior et al., 1999; Schwartz et al.,

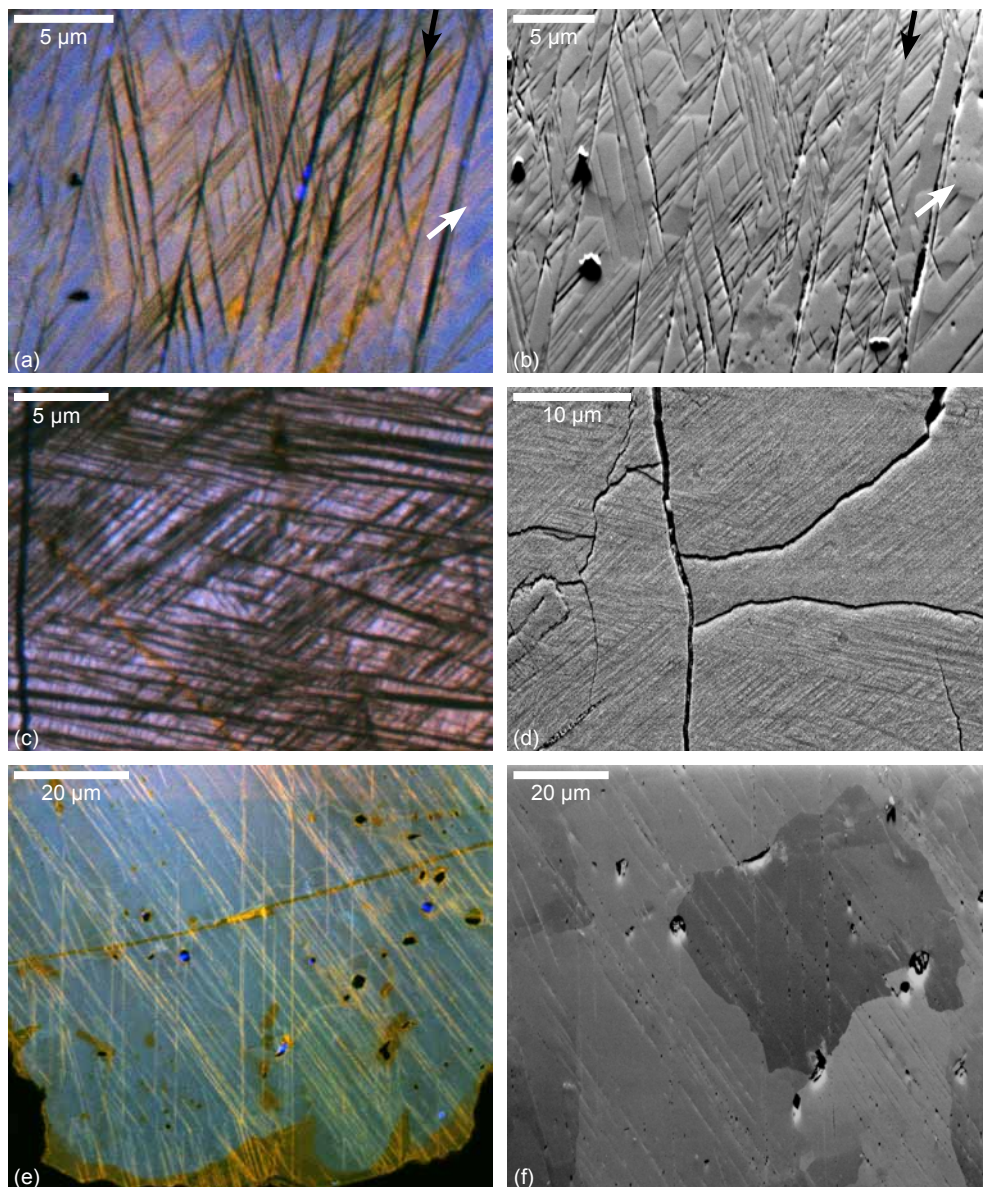


Figure 5.1 FSE images of shocked quartz grains from the Ries crater (right) and corresponding composite colour SEM-CL images (left). **a, b** Grain with both amorphous (non-luminescent) PDFs (black arrows) and healed (red luminescent) PDFs (white arrows). Amorphous PDFs have the same grey level in the whole FSE image, while healed PDFs are mostly invisible. **c, d** Grain with amorphous (non-luminescent) PDFs, which have the same grey level in the whole FSE image. **e, f** Grain with healed (red luminescent) PDFs that are mostly lighter than the surrounding quartz, or invisible. Lighter and darker domains in the grain are not Dauphiné twins, but probably subgrains.

2000). The technique uses point by point measurements to map the crystallographic orientation distribution of a sample. For most geological materials, the spatial resolution in EBSD mapped images is lower than in FSE images (see below), but EBSD enables quantitative orientation measurements and the detection of misorientations, twins or (sub)grain boundaries. Because the sample is tilted with respect to the electron beam, the spatial resolution of EBSD measurements is higher in the direction parallel to the tilt axis than in the direction perpendicular to it. Minimum separation distances to be able to distinguish two EBSD patterns are 20-30 nm in the direction parallel to the tilt axis and ~ 100 nm for the perpendicular direction, for Al grains in a field-emission gun SEM (Humphreys et al., 1999). When mapping metals, step sizes < 0.02 μm can be used (Schwarzer et al., 2009), but for geological materials, which are usually non-conducting, charging and drift problems often limit the minimum step size to ~ 0.2 μm (Prior et al., 1999; this study). The angular resolution of EBSD measurements depends on many factors, and resolutions $< 0.5^\circ$ can be achieved in high quality data sets (Field et al., 2012; Humphreys et al., 2001; Pennock et al., 2006; Pennock et al., 2002).

Pattern quality (PQ) maps show the quality of the EBSP at each data point (Wright and Nowell, 2006), where dark represents a weak or low quality pattern and light a strong or high quality pattern. Low quality EBSPs can result from, for example, high defect density, a disordered crystal structure, or amorphous material.

5.2.2 Methods

Samples were first polished down to 1 μm finish using standard polishing procedures with Al_2O_3 . Subsequently a chemical mechanical polish was applied using 50 nm colloidal silica (Syton) (Fynn and Powell, 1979) for 20-60 minutes, to remove surface strain induced by previous mechanical polishing and thereby improve the quality of EBSD patterns and FSE images. However, polishing differences between (amorphous) PDFs and host grain invariably leave some topography. A thin layer of carbon coating was applied to the samples to reduce charging and drift problems.

EBSD mapping and FSE imaging were done on two SEMs located at the Electron Microscopy Centre Utrecht (EMU) at Utrecht University in the Netherlands: a Philips XL30 SFEG SEM and an FEI Nova Nanolab 600, both with a Nordlys CCD EBSD camera, with two FSE detectors attached in the lower corners of the camera. On both systems Oxford Instruments HKL Technology Channel 5 software was used to collect the data.

For FSE imaging acceleration voltages between 15-22 kV were used, with a beam current of ~ 2.4 nA and an aperture size of 50 μm . Working distances were between 10 and 20 mm with a sample tilt of 68° to 70° . Contrast and brightness were adjusted for each image. Greyscale images were recorded on both SEM systems in Utrecht by automatically combining the signals from the two FSE detectors. We also show examples of colour-coded FSE images to illustrate the potential of this type of image for the study of shocked quartz. Colour-coded FSE images were recorded on a Carl Zeiss SUPRA 55 VP SEM, operated at high vacuum, with Bruker e-FlashHR+ (High Resolution EBSD camera) and ARGUSTM imaging system (BSE and FSE detectors), using CrystAlign software, at Bruker Nano GmbH, Berlin. This system uses three FSE detectors, mounted at the lower edge of the phosphor screen, which are controlled separately. The signal acquired by the three detectors is displayed using the RGB code as colour-coded images. In a separate experiment, a colour-coded FSE image was constructed from three greyscale images recorded with the FEI Nova Nanolab 600 at EMU. This colour-coded image is a combination

of images recorded with different working distances (WD) and sample tilts (red channel: WD 9.5 mm, tilt 68°; green channel: WD 15 mm, tilt 68°; blue channel: WD 15 mm, tilt 70°).

For EBSD orientation and pattern quality mapping the same kV, beam current and working distance settings were used, with a sample tilt of 70°. Typical step size for mapping was 0.2–0.5 μm . A Hough transform setting of 90 was used, with 9 bands detected and 4x4 binning. Maps of grains with PDFs were not processed, to avoid introducing artefacts in amorphous areas that could not be indexed. In order to improve the angular resolution of the data on tectonic deformation lamellae, maps of these grains were processed in the HKL Channel 5 software by extrapolating single pixels with very different orientations to neighbouring pixels and replacing non-indexed points with one of its four to six nearest neighbours. Remaining zero solutions were copied manually from one of the nearest neighbouring pixels. An orientation averaging filter (size 3x3, smoothing angle 5°) and artefact filter (critical angle 1°) were applied once (Humphreys et al., 2001).

5.2.3 Samples

49 shocked quartz grains were studied in rocks from different well-known and extensively studied impact structures in a different age range, so that both amorphous and healed PDFs are present in the samples: Vredefort (South-Africa, 2 Ga (Kamo et al., 1996), three grains), Rochechouart (France, 201 Ma (Schmieder et al., 2010), sixteen grains), Popigai (Russia, 35.7 Ma (Bottomley et al., 1997), six grains) and Ries (Germany, 14.3 Ma (Buchner et al., 2003), twenty four grains). Because the grains have been studied before using SEM-CL (chapter 2) and some also using TEM (chapter 4), the microstructural characteristics of the PDFs (amorphous vs. healed) were known. Four grains from the Ries and two grains from the Popigai crater were imaged using colour FSE. Colour images of three samples (two from the Ries crater, four grains; one from Popigai, two grains) were recorded with the Bruker system in Berlin (using three FSE detectors ascribed to the red, green and blue channels). One colour FSE image of a grain in the Popigai sample was constructed from three greyscale images with different sample tilts and working distances (see method section). Two grains from tectonically deformed grains from the Flinders Ranges in Australia were studied to compare PDFs and tectonic deformation lamellae in greyscale FSE images and EBSD maps.

5.3 Results

5.3.1 PDFs

5.3.1.1 PDFs in FSE images

Many PDFs show contrast in FSE images. Figures 5.1 and 5.2 show that the contrast in healed and amorphous PDFs has a different character. The grains in figure 5.1 were previously studied using SEM-CL and TEM (chapter 4). In chapter 4 we showed that the non-luminescent PDFs in these grains are amorphous, while the red luminescent PDFs are healed. Amorphous PDFs (figure 5.1b (black arrow) and d and 5.3a) are clearly visible and have the same grey level within the same image. Between different images the grey level can vary due to individual brightness and contrast adjustments. Some PDFs are open and therefore black in FSE images (parts of the NNE-SSW oriented set in figure 5.1b), or are decorated by tiny holes or fluid inclusions (e. g.

the N-S oriented set in figure 5.1f). Open (parts of) PDFs could indicate original porosity, but are more likely the result of differential polishing effects between crystalline and amorphous material. In contrast to the constant grey level of amorphous PDFs within one image, healed PDFs show more complex FSE contrast. Healed PDFs can be lighter or darker than the host quartz, or invisible, depending on the sample tilt and the orientations of PDF and host quartz (figures 5.1b (white arrow) and f and 5.2). Different parts of one PDF can have different grey levels in parts of a grain with slightly different orientations (see the PDFs indicated with black arrows in figure 5.2a). However, the majority of healed PDFs are invisible in FSE images (see for example figure 5.2c or 5.4b). No FSE contrast was observed from basal Brazil twins in quartz grains from the Vredefort structure.

To image PDFs with FSE, the image quality must be very high. Apart from a good polish and a clean surface, good FSE contrast requires a very thin carbon coat, slow scanning rates and a relatively high magnification. These conditions are often hard to obtain without charging and drift problems. Topography effects and beam damage can sometimes make it difficult to

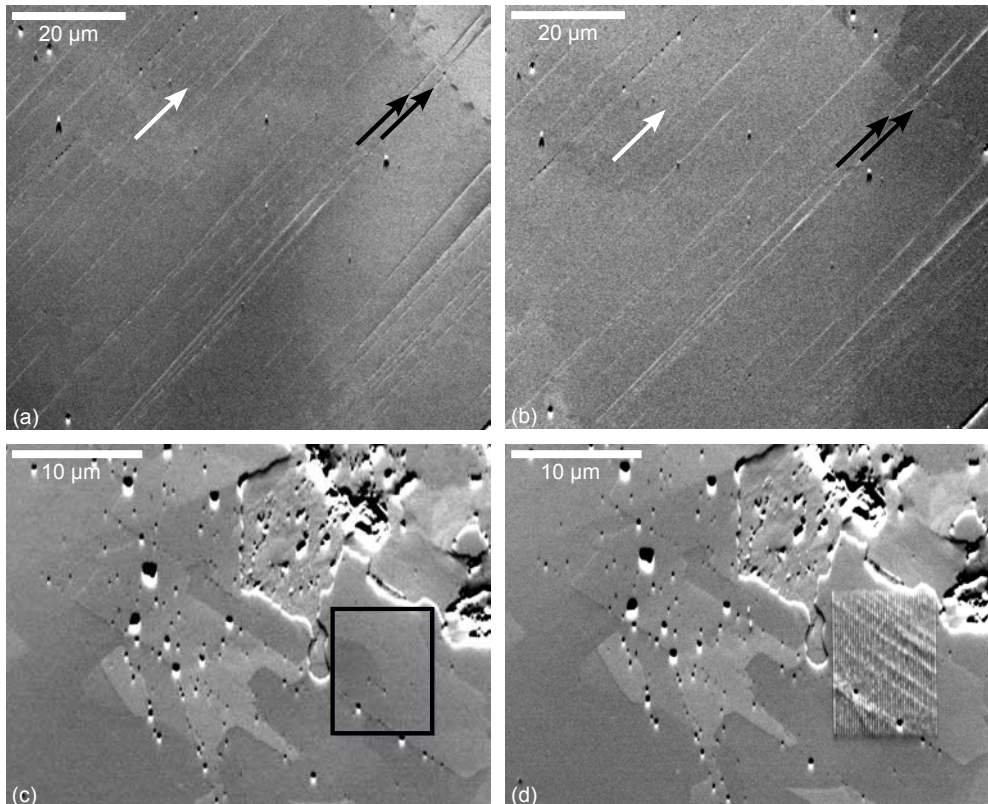


Figure 5.2 a, b Two FSE images of healed PDFs in a grain from the Ries crater, showing the same sample area at a slightly different tilt: 67° (a) and 68° (b). Image b was recorded before image a, so the brightness of the PDFs in image b is not a beam damage or charging effect. **c** FSE image of a grain from Rochechouart. Black box indicates the location where an EBSD map was recorded (not shown). PDFs are not visible. **d** FSE image of the same area as in c, but after recording the EBSD map. PDFs are now visible as brighter (damaged) regions in the square of the EBSD mapped area.

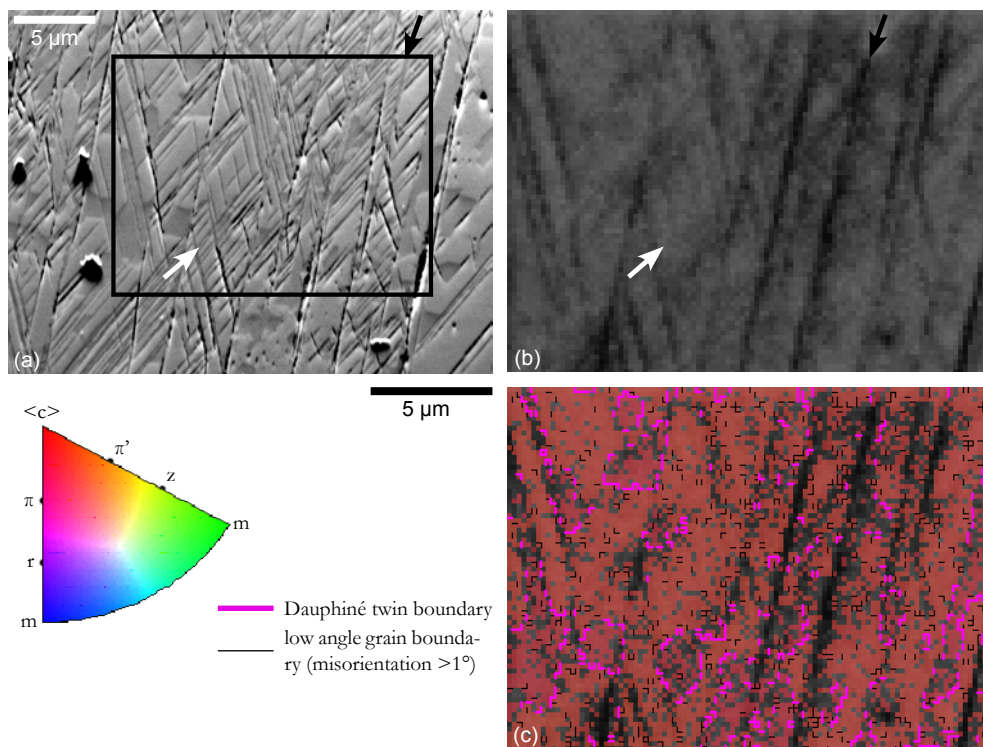


Figure 5.3 **a** FSE image of a grain from the Ries crater with both healed and amorphous PDFs (also shown in 2a and 2b). **b** Pattern quality map (step size 0.2 μm) of the black boxed area in a. Amorphous PDFs can be recognised as dark lines against the lighter background of the crystalline grain. A clear example is indicated by the black arrow in a and b. **c** Pattern quality + inverse pole figure map (step size 0.2 μm) of the same area, showing which crystallographic direction at each point is parallel to the x-direction of the map. Pink lines indicate Dauphiné twin boundaries. The 5 μm scale bar is for b and c.

interpret FSE images and characterise PDFs, as pores and differential polishing create surface irregularities, which can cast shadows on the image. When the FSE contrast is weak, it can be difficult to distinguish between FSE and topography contrast. In particular for amorphous PDFs topography effects can be relevant, because differential polishing effects can grind or etch out part the amorphous material. Furthermore, beam damage can influence the contrast after scanning an area several times or after acquiring EBSD data by point measurements. This is illustrated by figures 5.2c and d, which show a quartz grain from the Rochechouart impact structure with healed PDFs. The PDFs are invisible in the FSE image recorded before EBSD mapping (black box in figure 5.2c, EBSD map not shown), but bright lines show the location of beam-damaged healed PDFs where an EBSD map was recorded (figure 5.2d). The damage effect from a beam in spot mode is much stronger than that from scanning of sample areas for imaging, but the effect has to be kept in mind when interpreting FSE images of PDFs that have been scanned more than once at the slow rate required for high quality imaging. On the other hand, the effect can be useful to show the presence of PDFs that are at first invisible in FSE images.

5.3.1.2 PDFs in pattern quality maps

In pattern quality maps, providing the PDFs are wide enough to be resolved, amorphous PDFs are visible as dark lines in a lighter matrix (figures 5.3a and b, black arrow): the amorphous material gives no EBSD patterns, or weaker patterns than the host quartz. However, narrower amorphous PDFs are often not individually resolved in pattern quality maps (figures 5.3a and b, white arrow). Healed PDFs (figure 5.4) and basal Brazil twins (not shown) are generally not visible in pattern quality maps, except in rare cases where a large number of fluid inclusions or defects are present along the PDF.

5.3.2 Mosaicism

Mosaicism in shocked quartz grains can be detected in FSE images (figure 5.5a) as (sub) micrometer scale blocky domains with different shades of grey. Often no individual PDFs are visible in FSE images in mosaic grains, but usually a directional trend is present in the domain boundaries parallel to PDFs which are observed in CL images (figure 5.5b), or decorated PDFs are present. EBSD patterns from these grains are often too weak to index for orientation maps, or give a very low percentage of indexed measurements, hence the mosaic structure cannot be mapped. Pattern quality maps (figure 5.5d) can, in some grains, show the presence of PDFs as darker lines in a light matrix, but often not much contrast is seen in the maps, because the patterns from the whole grain are also very weak.

5.3.3 Dauphiné twins

Dauphiné twins are present in most of the studied grains (see figures 5.3 and 5.4), except in highly shocked grains with a very high density of crosscutting sets of PDFs, such as the grain shown in figure 5.1c and d. The twins can be recognized in FSE images as domains with a different grey level. EBSD maps show that these domains share the same c-axis, but rotated by 180° (or apparently 60°): a clear indication of Dauphiné twins. The twins are often parallel to and bound by PDFs, but not in all cases. Although Dauphiné twins can be very clearly visible in greyscale FSE images, it is not possible to distinguish the twins from other orientation differences, such as subgrains, without the help of orientation measurements or EBSD maps. Small differences in orientation can result in strong contrast, and vice versa, and therefore it can be hard to differentiate between contrast produced by different features within a grain. However, colour coding of the signals detected by three different FSE detectors highlights a single crystallographic orientation. Although quantification of the twin orientation with EBSD is still required for a definitive identification, Dauphiné twins are singled out much more easily from composite colour FSE images (figure 5.6). This is illustrated in figure 5.6a to d. Dauphiné twins in the same (part of a) grain have the same colour, which is very different from that of subgrains or other slight contrast changes (Dauphiné twins are blue and lime green in figures 5.6b and d respectively). Figures 5.6e and f illustrate that colour FSE images can also be composed manually of three images of the same area, but recorded under slightly different conditions. However, the contrast from a dedicated colour FSE system is much better.

Many pattern quality maps show the Dauphiné twins (a clear example can be found in figure 5.4c), where one of the twin orientations is brighter than the other: the quality of the EBSD patterns from one twin orientation is higher than from the other twin orientation. Because pattern quality is a measure of the band contrast in EBSD patterns, differences in the occurrence

or intensity of bands between the twin orientations can result in different intensities in the PQ map. Alternatively, differences between the EBSD patterns of the two twin parts might be partly explained by the higher diffraction intensity displayed by the positive r rhombs in quartz with respect to the equivalent negative z rhomb (Fron del, 1962; Wenk et al., 2011), which could result in contrast differences between different twin orientations.

5.3.4 Tectonic deformation lamellae

PDFs and tectonic deformation lamellae are easily distinguished in both FSE images and EBSD maps (figure 5.7). In FSE images PDFs are well-defined, narrow, straight features, while tectonic

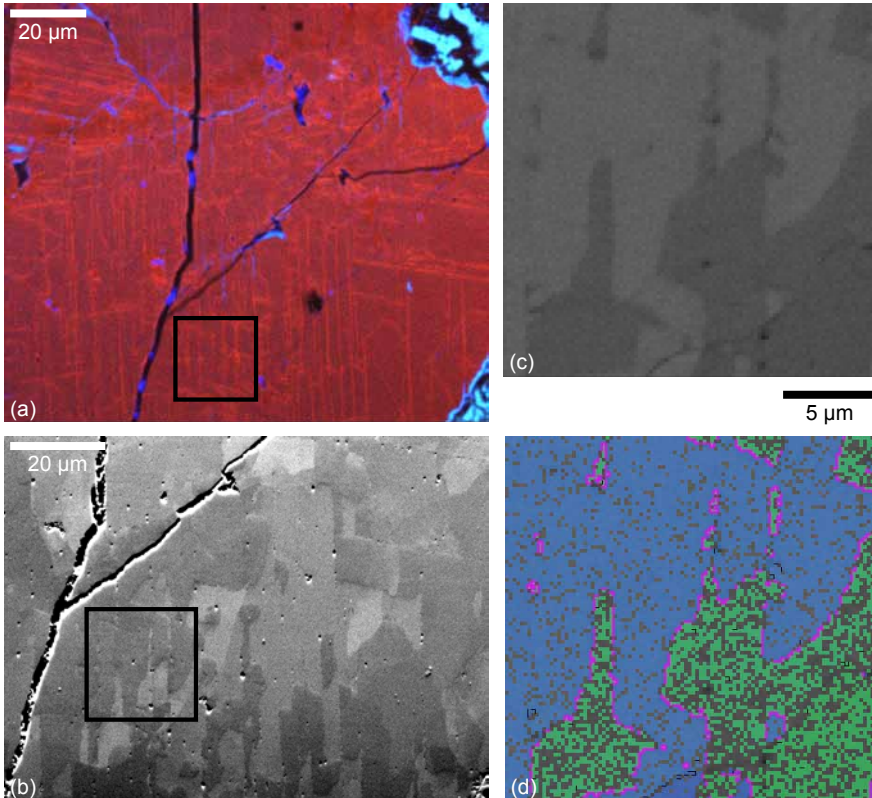
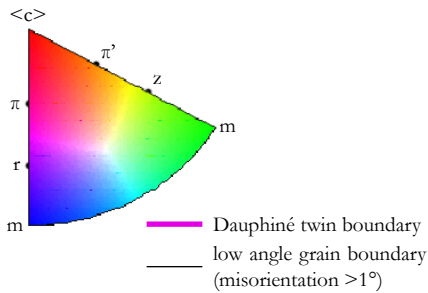


Figure 5.4 **a** CL image of a grain from the Rochechouart crater with healed (red luminescent) PDFs. **b** FSE image of the same area. **c** Pattern quality map (step size 0.2 μm) of the black boxed area in **a** and **b**. PDFs are not visible. **d** Pattern quality + inverse pole figure map (step size 0.2 μm) of the same area, showing which crystallographic direction at each point is parallel to the x -direction of the map. Pink lines indicate Dauphiné twin boundaries. The black 5 μm scale bar is for **c** and **d**.



deformation lamellae are hardly visible. When tectonic lamellae are decorated (figure 5.7b), a broad trace of fluid inclusions can be recognised in the FSE image, much broader than in the case of decorated PDFs. Undecorated lamellae (figure 5.7f) are often not visible at all in FSE images, but can in some cases be recognised as elongated, curvilinear domains with a slightly different orientation than the rest of the grain (figure 5.7i, arrows). This orientation difference is very small and hard to detect in EBSD orientation maps (figures 5.7d and h). In pattern quality maps (figures 5.7c and g), tectonic deformation lamellae are generally not expressed by darker pixels, because they are crystalline and therefore do not give weaker EBSPs. Occasionally, the trail of voids or fluid inclusions associated with some lamellae give weaker patterns and this is just visible in pattern quality maps (figure 5.7c).

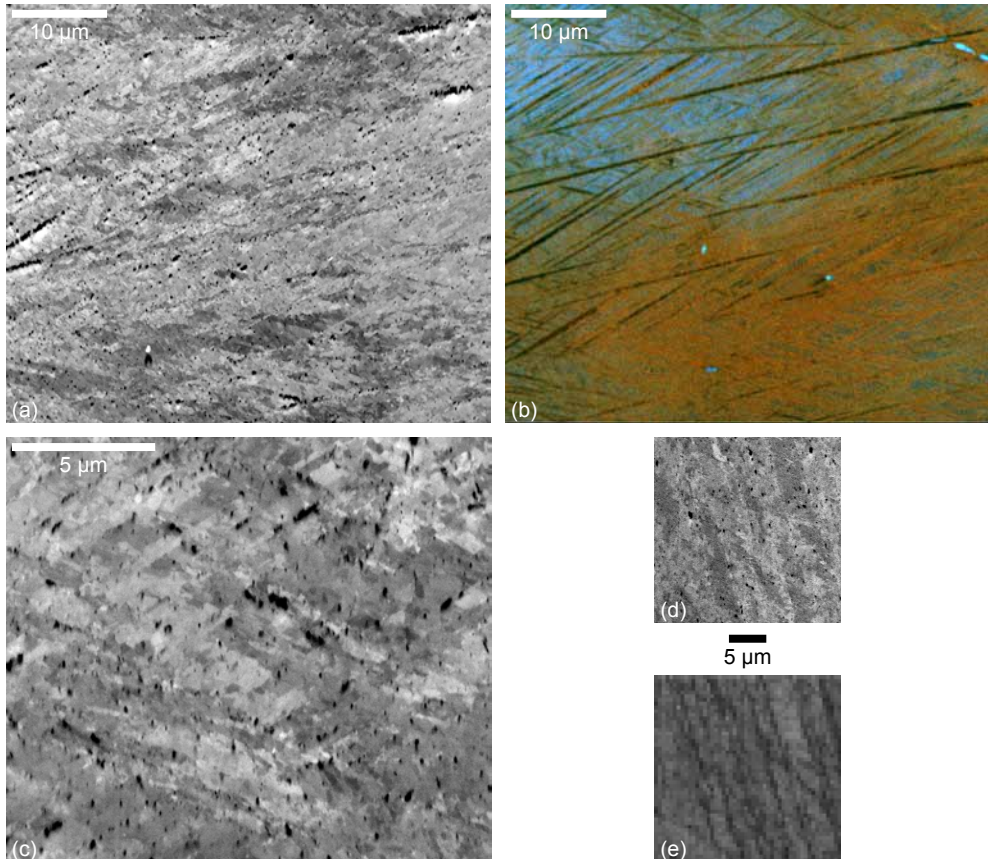


Figure 5.5 **a** FSE images of a grain from the Ries crater, showing submicrometer blocky domains of different greyscale. **b** Composite colour SEM-CL image of the same area as in **a**, showing a high density of crosscutting PDFs, both red and non-luminescent. **c** Higher magnification FSE image of part of **a**. **d** FSE image of a similar grain in the same thin section, showing microdomains, but also a clearer trend of PDFs. **e** Pattern quality map of the area shown in **d**. PDFs can be recognised as dark lines in a lighter matrix. The black 5 µm scale bar is for **c** and **d**.

5.4 Discussion

5.4.1 PDFs

5.4.1.1 PDFs in FSE images

Amorphous PDFs always show contrast in FSE images, due to the different crystal structure of the material within PDFs and host quartz (amorphous vs. crystalline), which is detected in the forescatter detector and displayed as a different shade of grey in PDFs and host quartz. As amorphous PDFs lack a regular crystal lattice, channelling of the electron beam does not occur and amorphous PDFs are predominantly darker than the surrounding matrix (see figures 5.1b and d). In a single greyscale FSE image, amorphous PDFs have a uniform, distinctive grey level. However, it should be noted that in greyscale FSE images, it is not impossible that, by coincidence, amorphous PDFs have the same grey level as a crystalline part of a grain. In composite colour FSE images, constructed using multiple detectors or images recorded under different diffracting conditions, amorphous PDFs should also appear grey: in RGB colour images, each channel should capture a similar BSE signal intensity from an amorphous area. The slight spatial difference between each detector might create small differences in intensity of the collected signal. Providing the brightness and contrast settings are the same for each channel, combining all three signals with the same intensity should result in grey to white areas in the RGB image, assuming that topography effects are insignificant. However, we were unable to obtain colour-coded FSE images of amorphous PDFs, because the few grains containing clearly amorphous PDFs had already been sectioned for TEM and could not be imaged using colour-coded FSE.

The reason why some healed PDFs can be seen in FSE images is less straightforward. Healed PDFs are very thin planes of high dislocation density that are probably too thin to be imaged directly using the forescatter detector. Topography effects should be minimal in healed PDFs, as they are planes of high defect density and not thin layers of material with a different structure and density. The most likely explanation for the observation of these features in some images is that the lamellae exhibit a diffraction-like behaviour, comparable to that observed using TEM: when diffraction conditions are favourable, the healed PDFs show a different contrast than the surrounding quartz. If the conditions are not good for diffraction, the PDFs are invisible (see also figure 5.2). This scenario explains the fact that the grey level of healed PDFs can vary and they can be darker or lighter than the host quartz, or invisible, depending on the imaging conditions, while amorphous PDFs seem to always have the same grey level throughout an image (although the grey can differ between images due to individual brightness and contrast adjustments). Additionally, preferential beam damage effects along healed PDFs have been observed (figure 5.2d), which can be a factor in the contrast shown by healed PDFs. For both amorphous and healed PDFs, any surface irregularities that are present can induce topography effects in a FSE image, which may complicate interpretation of the contrast.

Since a Brazil twin represents a change of hand of the quartz structure across the boundary, but no change in crystal structure, the lattice symmetry is the same on either side of the boundary. Therefore, there is no difference in the EBSD patterns across the boundary and Brazil twins are invisible both in FSE images and in EBSD maps (see also Olesen and Schmidt, 1990).

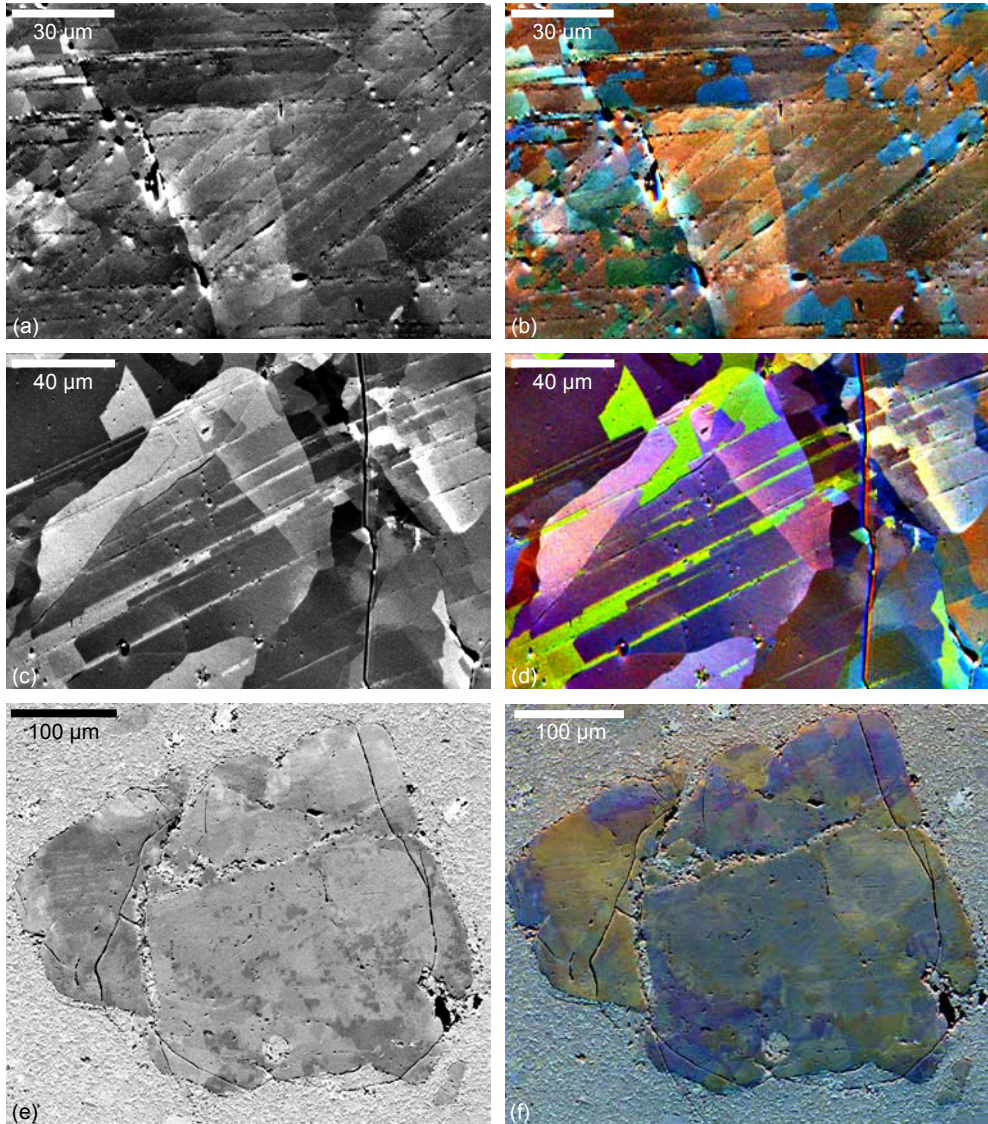


Figure 5.6 Greyscale and composite colour FSE images of shocked quartz grains with healed PDFs from **a** Popigai, imaged with the Bruker ARGUS™ detector. The image was acquired using the three detectors, but without colour-coding, resulting in a high contrast greyscale image. **b** Popigai (same area as **a**), imaged with the Bruker Argus detector using three detectors for RGB colour-coded imaging. **c** Ries, imaged with the Bruker ARGUSTM detector using the three detectors, but without colour-coding, resulting in a high contrast greyscale image. **d** Ries (same area as **c**), imaged with the Bruker Argus detector using three detectors for RGB colour-coded imaging. **e** Popigai, imaged with the Nordlys camera using two detectors. **f** Popigai, imaged with the Nordlys camera using two detectors, but composed of three images (red channel: WD 9.5 mm, tilt 68°; green channel: WD 15 mm, tilt 68°; blue channel: WD 15 mm, tilt 70°). Especially in **b** and **d**, Dauphiné twins are visualised very clearly as areas of contrasting colours (twins are blue and lime green in **b** and **d** respectively).

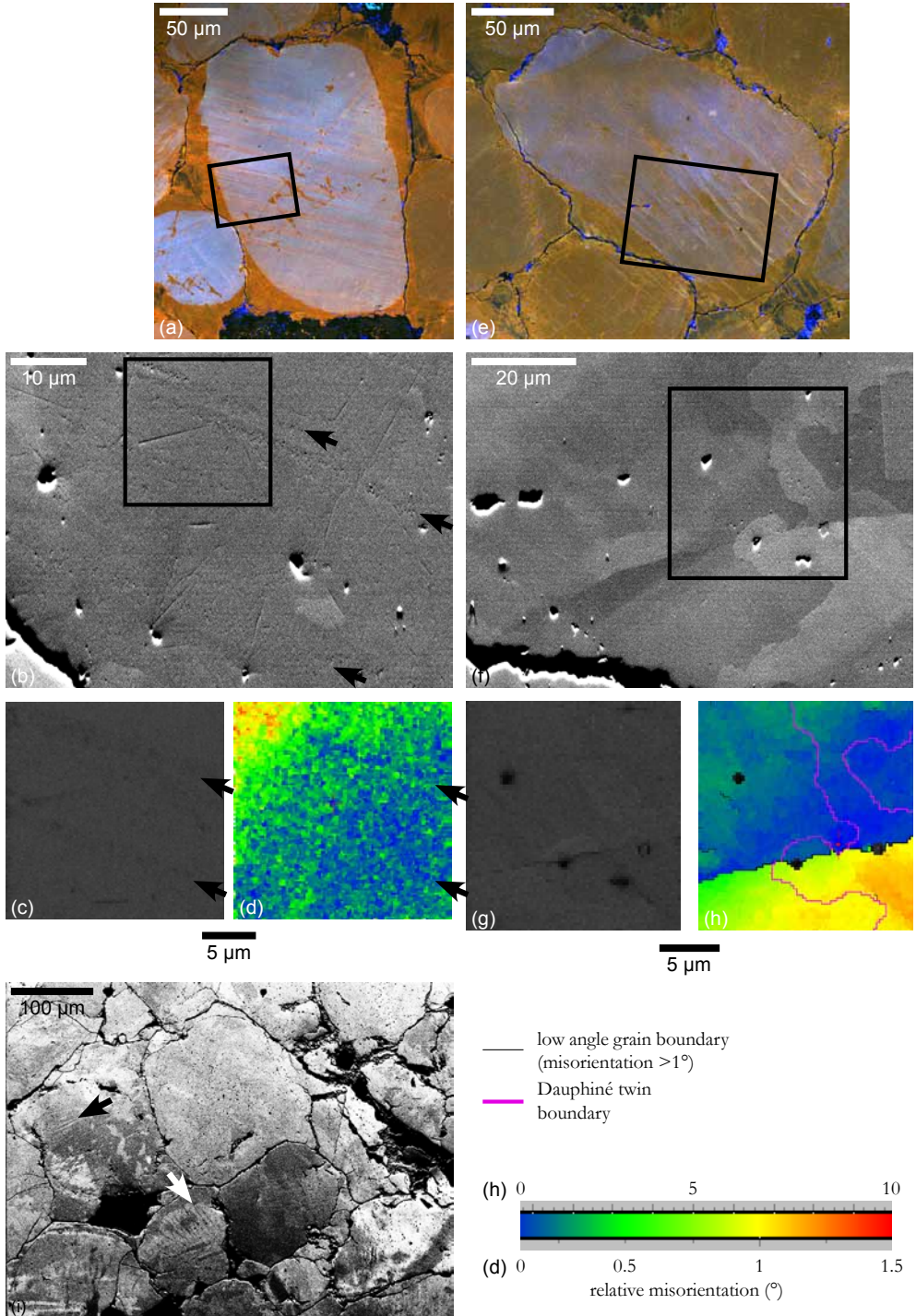
5.4.1.2 PDFs in pattern quality maps

Thick enough amorphous PDFs show up in pattern quality maps because, for amorphous material, no bands are present in EBSD patterns. Sometimes weak patterns are observed from amorphous PDFs, which could indicate that a small degree of crystal order is present in the material, either because the material has not lost all of its structure during amorphisation or because of incipient recrystallisation. More likely, however, is that the interaction volume of the electron beam with the sample is too large to only sample the PDF and therefore part of the neighbouring crystalline quartz contributes to the signal. Typical spatial resolution for EBSD in Al is 20-30 nm in the direction perpendicular to the beam and ~ 100 nm in the direction parallel to the beam (Humphreys and Brough, 1999; Humphreys et al., 1999). In quartz, the interaction volume of the beam with the sample is much larger than in metals, which decreases the spatial resolution. Monte Carlo simulations using Casino v2.42 software (Drouin et al., 2007; Drouin et al., 2001) indicate that an electron beam with an energy of 5-10 kV penetrates to a maximum depth of ~ 0.3 -1 μm . Therefore it is unlikely that thin amorphous PDFs are sampled by the electron beam without a contribution from the surrounding crystalline quartz, especially when the PDF is at an angle $< 90^\circ$ to the sample surface. Furthermore, thin amorphous PDFs might be invisible in pattern quality maps if the spatial resolution of the map is not high enough: if the step size is too large, thin features might not be sampled. Healed PDFs are very thin planes of high defect density and the spatial resolution of EBSD measurements is not high enough to detect them. In the rare cases healed PDFs do appear in pattern quality maps, this is probably due to an exceptionally high density of defects and fluid inclusions along the PDF plane.

5.4.2 Dauphiné twins

Most of the Dauphiné twins that are observed in the studied quartz grains have straight boundaries, often parallel to PDFs. The same is observed in TEM (see figure 4.2b and c in chapter 4). These observations indicate that the twins are most likely shock-related and associated with PDFs. Two explanations for the presence of Dauphiné twins in shocked quartz exist: they could be related to stresses during impact (Chen et al., 2011; Wenk et al., 2011; Wenk et al., 2005), or they could be the result of the back-transformation to α -quartz during cooling of β -quartz (Trepmann and Spray, 2005). Dauphiné twins formed during the transformation

Figure 5.7 CL, FSE images and EBSD maps of quartz grains with tectonic deformation lamellae from the Flinders Ranges in Australia. a Composite colour SEM-CL image. The black box shows location of higher magnification image in b. b Higher magnification of the same grain as in a, FSE image. Deformation lamellae (black arrows) can just be recognised as broad lines of fluid inclusions. c Pattern quality map (step size 0.2 μm) of the area in the black box in c. Elongated areas of slightly weaker diffraction patterns, that are due to the trails of fluid inclusions, indicate the position of the deformation lamellae (black arrows). d Relative misorientation map (maximum deviation 1.5°, relative to red cross; step size 0.2 μm) of the same area. The decorated deformation lamellae (black arrows) have very low misorientations. e Composite colour SEM-CL image of a second grain. The black box shows the location of the higher magnification image in f. f Higher magnification of the same grain as in e, FSE image. The deformation lamellae that are visible in the CL image in e cannot be recognised, but subgrains and Dauphiné twins are visible. g Pattern quality map (step size 0.5 μm) of the black boxed area in f. h Relative misorientation map of the same area (maximum deviation 10°, relative to red crosses; step size 0.5 μm). Dauphiné twins are shown by pink lines, no tectonic deformation lamellae can be recognised. The orientation of the Dauphiné twins seem unrelated to the deformation lamellae in the CL image in e. i Low magnification FSE image in which tectonic deformation lamellae (arrows) can be recognised as elongated domains with a different orientation than the rest of the grain.



from β - to α -quartz commonly have very irregularly shaped boundaries (Frondel, 1945). Stress-induced Dauphiné twins on the other hand can have crystallographically determined, straight boundaries and can be square or triangle-shaped (Zinserling and Schubnikow, 1933). Zinserling and Shubnikow (1933) studied mechanically induced Dauphiné twins at room temperature and near 573°C. Their experiments resulted in twins with remarkably straight boundaries and geometries that are similar to those reported in shocked quartz grains. In the higher temperature experiment, the twinning penetrates deeper into the crystal and the twin surface is larger than at the same pressures at room temperature, but the shape of the twins remains similar. Wenk et al. (2007) reported that (non-shock related) mechanical Dauphiné twins are generated by differential stresses of ~ 100 MPa at temperatures of 300–400°C. Therefore, if shock related Dauphiné twins are stress-induced, they must be (relatively) low shock pressure features, similar to the pressure range in which mechanical Brazil twins and planar fractures form.

To explain the relation between shock-related Dauphiné twins and PDFs, two scenarios can be discussed. If the twins are formed by the transformation of β - to α -quartz during cooling, it follows that the PDFs must have formed first and might have induced, or localised, the twinning (Trepmann and Spray, 2005). However, the geometry and crystallographic orientation of mechanically induced twins observed by Zinserling and Schubnikow (1933) provides an alternative model. If Dauphiné twins form as a result of stress at relatively low shock pressure, they could form before or at the same time as PDFs.

Both in experiments and in naturally deformed rocks it has been observed that mechanical Dauphiné twins form in quartz under high stress. The twinning process results in a preferred orientation of the $\{r\}$ and $\{z\}$ planes (e.g. Menegon et al., 2011; Tullis, 1970; Tullis and Tullis, 1972; Wenk et al., 2011; Wenk et al., 2006; Wenk et al., 2007; Wenk et al., 2005). In quartz, the direction of maximum compliance, or softest direction, is orthogonal to the positive rhombohedral plane $\{r\}$ and the direction of minimal compliance, or stiffest direction, is orthogonal to the negative rhombohedral plane $\{z\}$. No Dauphiné twinning occurs if the $\{r\}$ rhombs are already perpendicular to the direction of compressive stress (Menegon et al., 2011). However, in quartz crystals with the $\{z\}$ plane orthogonal to the compression direction, Dauphiné twinning allows the softest direction to align parallel to the maximum compressive stress, and thereby the $\{r\}$ plane to align orthogonal to the compression direction. The twinning process therefore reduces the stiffness of the crystal (i.e. twinning makes the grain more easily elastically deformable). Furthermore, deformation can be localised as a result of Dauphiné twin formation, because r twins yield plastically at lower stresses than z twins (Menegon et al., 2011).

Due to the change from softest to stiffest rhomb between two Dauphiné twin orientations, the boundary plane will form an elastic discontinuity in the crystal. This might locally intensify the stress during shock, as shock waves are strongly influenced by interfaces and heterogeneities in a material, which can cause reflection and reverberation of the waves. It is also possible that phase transformations nucleate heterogeneously on discontinuities in the crystal, such as Dauphiné twin boundaries. We therefore propose that mechanical Dauphiné twinning might play an important role in the onset of PDF formation. Dauphiné twin boundaries could form a preferential nucleation plane for amorphisation and PDF development, as a result of the heterogeneous elastic properties across twin boundaries, which results in heterogeneous nucleation of the amorphous phase. This hypothesis is particularly relevant in the lower regions of shock pressure conditions. As mechanical Dauphiné twins form relatively easily (they have been reported as a result of differential stress of ~ 100 MPa at 300–400°C (Wenk et al., 2007)),

twins might form at the onset of shock compression, with twin boundaries acting as weaker planes during continued shock loading, on which amorphous PDFs can nucleate preferentially. However, it should be noted that the most common PDF orientations in $\{10\bar{1}n\}$ are mostly not frequently reported Dauphiné twin boundary plane orientations. Growth Dauphiné twins can occur on any plane and although no systematic study of mechanical Dauphiné twin planes is reported in the literature, these are most likely to be m $\{10\bar{1}0\}$ or c (0001) planes (Lloyd, 2004; Zinslerling and Schubnikow, 1933). Our hypothesis would imply that under very high strain rates, other orientations may occur.

If mechanical Dauphiné twinning plays a role in PDF formation, the orientation of a quartz grain with respect to the shock pressure direction can be expected to influence the number of PDFs in a grain, or possibly the pressure at which PDFs start to occur. In grains that are in an orientation to the shock wave direction that is favourable for Dauphiné twinning (i.e. the z rhombs perpendicular to the shock wave direction), more PDFs can be expected to form, or start forming at lower pressures. In grains that with the r rhomb perpendicular to the shock wave direction, no Dauphiné twinning will occur. In the absence of possibly weaker Dauphiné twin planes, nucleation of PDFs might be more difficult and occur less frequently or at higher pressure. This would be quite straightforward to test in oriented shock experiments in the lower pressure range (~5-10 GPa).

Obviously, the above model for the relation between shock-induced Dauphiné twins and rhombohedral PDFs can only be valid for quartz grains that are in the α -configuration at the time of impact (Dauphiné twins cannot form in β -quartz) and that have not been heated to above the α - β transition temperature. In grains that have been in the β -state at any point during the impact process, any Dauphiné twins present must be the result of β - to α -quartz back-transformation during cooling, with the straight boundaries being a result of the presence of PDFs, or of a 'shape memory' of the material (the twins were present in the grain before passing through the α - β transition) which has been suggested to exist in quartz (Wenk et al., 2009; Wenk et al., 2006; Wenk et al., 2007). Furthermore, if this model for preferential amorphisation and PDF formation at Dauphiné twin boundaries is correct, the same might happen at shock-induced Brazil twin boundaries. Observations on quartz grains experimentally shocked at a range of (low) peak pressures and with the grains at different orientations to the shock direction (i.e. the r and the z planes perpendicular to the shock direction) would be required to test this hypothesis.

Although most Dauphiné twins in our samples have straight boundaries parallel to PDFs, some are more irregularly shaped. Given the extreme pressure and temperature conditions prevailing during and after an impact event, it seems plausible that not one, but both proposed formation systems, stress and β - to α -quartz transformation, can be responsible for twin formation. Regardless of their origin, most Dauphiné twins in shocked quartz grains have a very specific shape and are closely associated with PDFs. This characteristic geometry might be used as an additional indication to support the impact origin of planar microstructures in quartz. However, the presence of Dauphiné twins alone should never be interpreted as shock evidence. Pre-existing twins could be present in quartz grains and post-shock deformation and metamorphic events unrelated to the impact can easily induce additional Dauphiné twin formation (note for example the presence of Dauphiné twins in the tectonically deformed grain in figure 5.7h) (e.g. Lloyd, 2000; Menegon et al., 2011). Distinguishing different generations of twins might not always be straightforward or even possible.

5.4.3 Tectonic deformation lamellae vs. PDFs

EBSD mapping and FSE imaging provide sufficient criteria for the distinction of PDFs from tectonic deformation lamellae in quartz, which are often misinterpreted as shock lamellae. PDFs are planes of differently structured material (amorphous PDFs) or high dislocation density (healed PDFs) and consequently, if they show any contrast, they are well-defined, straight features in FSE images. Tectonic deformation lamellae, on the other hand, consist of narrow regions of the crystal with a slightly different orientation and are generally wider and more irregular and can be slightly curved (figure 5.7i). If decorated, tectonic lamellae can be recognised as broad, irregular traces of fluid inclusions (figure 5.7b), but are not as narrow and straight as decorated PDFs. Often tectonic deformation lamellae do not exhibit any contrast at all in FSE images (figure 5.7f). In addition, amorphous PDFs are shown clearly in pattern quality maps as dark lines (weak or no EBSPs) in the lighter background of the crystalline host grain. For tectonic deformation lamellae, this is not the case. Furthermore, the presence of Dauphiné twins with unusually straight boundaries in close association with microlamellae is an indication for the shock origin of the planar features. In tectonically deformed quartz grains, Dauphiné twins are not parallel to planar microstructures (figure 5.7h).

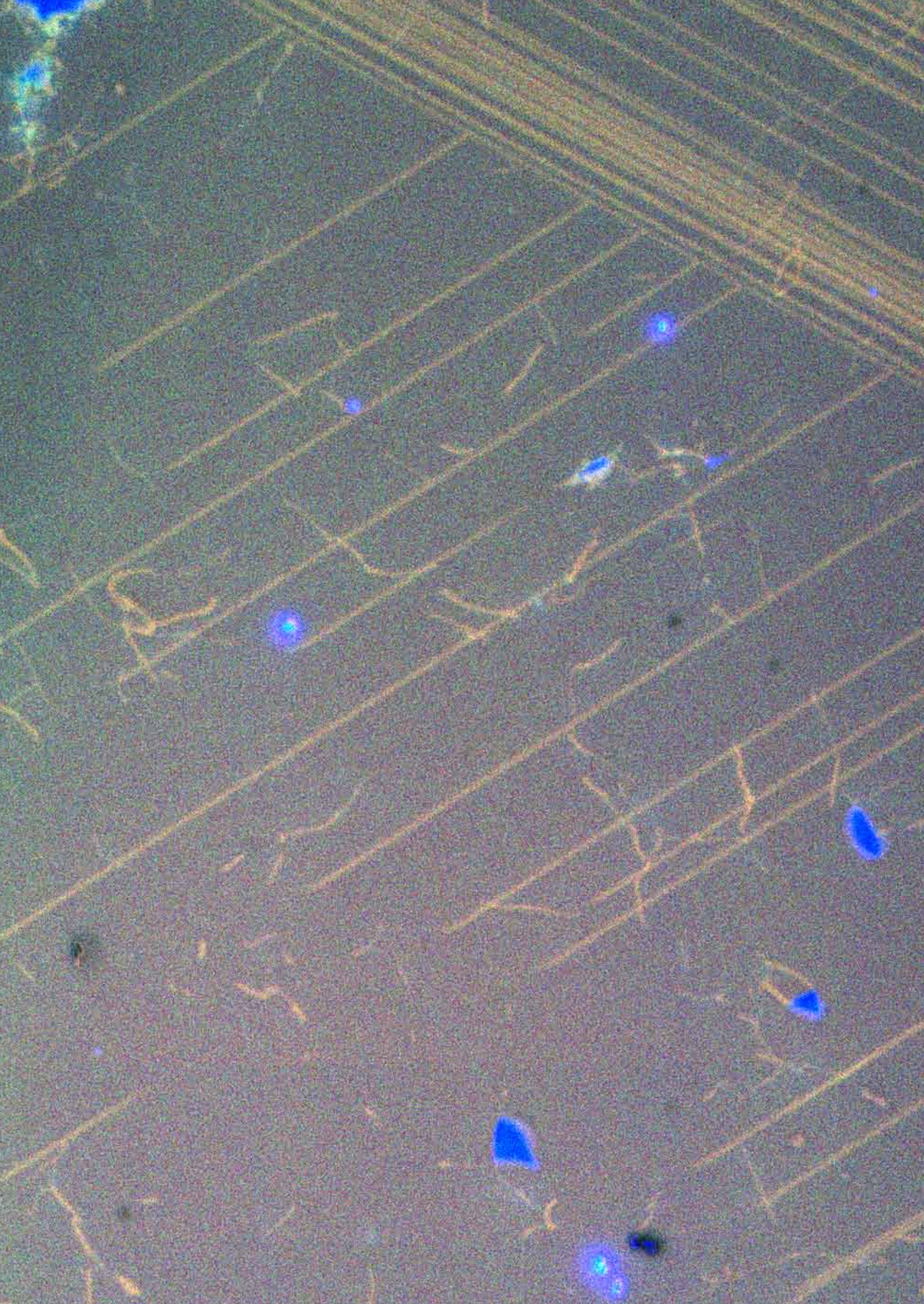
A more quantitative way in which EBSD can be useful in the study of PDFs in quartz is the combination of universal stage (U-stage) and EBSD orientation measurements. U-stage measurements of the 3D crystallographic orientation of PDFs are a widely used method to check the shock origin of planar microstructures in quartz (Ferrière et al., 2009; Stöffler and Langenhorst, 1994). However, a recent study (Voorn, 2010; Voorn et al., 2010) shows that it is possible to index the crystallographic orientation of tectonic deformation lamellae using a U-stage and get results that are very similar to those obtained from indexed PDFs. A combination of U-stage and EBSD orientation measurements, to obtain the full crystallographic orientation of studied grains (with EBSD) and the 3D orientation of the PDFs (in the U-stage), is a more reliable method to distinguish between tectonic deformation lamellae and PDFs. Even when only EBSD grain orientation measurements are available, the trace of the PDFs in FSE, SEM-CL or light microscopic images can be used to get a first approximation of their crystallographic orientation.

5.5 Conclusions

Amorphous and healed PDFs show different characteristics in FSE images and EBSD maps, but the distinction between the two types using these techniques is not as straightforward as in colour SEM-CL images or in TEM. The structure of the host quartz grain, on the other hand, can be characterised very well using FSE imaging and EBSD mapping. Mosaicism is detected quickly in FSE images, but is hard to quantify using EBSD, as the patterns from microcrystalline quartz were very weak. Furthermore, shock-related Dauphiné twins can be imaged in greyscale FSE images and confirmed in EBSD orientation maps. Colour FSE imaging is very useful in detecting Dauphiné twins as well and may be useful for identifying amorphous PDFs. The typical geometry of Dauphiné twins in close association with planar microstructures might be used as an extra indication for the shock origin of the lamellae. A new model is hypothesised for the preferential nucleation of PDFs along Dauphiné twin boundaries that formed mechanically at relatively low pressure in the early stages of shock.

FSE images and EBSD maps can be used to qualitatively distinguish between tectonic deformation lamellae and PDFs, while a more quantitative distinction is possible by combining EBSD measurements with 3D crystallographic orientations of planar microstructures obtained in a U-stage. In summary, FSE and EBSD techniques are very useful in studying shocked quartz and form a valuable additional technique for impact research.

Acknowledgements – Roald Tagle is thanked for kindly providing the Popigai samples and Rodger Hart for the Vredefort samples. Pim van Wamel has been of great help during sampling at the Ries crater, and Philippe Lambert at Rochechouart.



Chapter 6

Scanning electron microscope cathodoluminescence imaging of dislocations, subgrain boundaries and twin boundaries in quartz

M.F. Hamers, G.M. Pennock and M.R. Drury

The study of dislocations has been of great importance to determine deformation mechanisms in quartz and other geologically important minerals. Other relevant structures in both growth and deformation processes in quartz include Brazil and Dauphiné twinning. Dislocations and twin boundaries in quartz are most commonly imaged using a transmission electron microscope (TEM), because they cannot be observed using light microscopy. Here we show that red filtered cathodoluminescence imaging in a scanning electron microscope (SEM) is an additional method to visualise subgrain boundaries, Brazil and Dauphiné twin boundaries and some dislocations in quartz. Because standard petrographic thin sections can be studied in the SEM, the observed structures can be directly correlated to light microscopy studies. In contrast to TEM preparation methods, SEM techniques are non-destructive.

6.1 Introduction

Quartz is one of the main constituents of crustal rocks and its properties are therefore very relevant to crustal deformation. Both dislocations and (growth and mechanical) twinning in quartz have been extensively studied in the past half century (e.g. Comer, 1972; Frondel, 1945; McLaren and Phakey, 1965a; McLaren and Phakey, 1965b, 1969; McLaren et al., 1967; Sunagawa et al., 1990; Tullis, 1970; Tullis and Tullis, 1972; Van Goethem et al., 1977; Van Landuyt et al., 1985). In quartz, dislocations and Brazil and Dauphiné twin boundaries can only be directly observed using TEM or X-ray tomography of thick crystals, although by etching the surface of quartz, dislocations can also be made visible in a light microscope (Ball and White, 1977; Wegner and Christie, 1983). However, except TEM analysis, these techniques have a limited resolution. A disadvantage of the TEM is that TEM sample preparation methods are destructive and that TEM analysis can only be carried out on tiny samples, on the order of a few tens of microns in width and length. This makes it difficult to reliably estimate the density and distribution of heterogeneous microstructures in larger samples. Subgrain boundaries in quartz can be detected in a standard polarizing microscope, but TEM analysis is required for higher resolution imaging. As an alternative to TEM analysis, electron backscattered diffraction (EBSD) maps and forescattered electron (FSE) images, showing changes in crystal orientation, can be recorded in the SEM (e.g. Lloyd, 1987; Lloyd, 2004; Prior et al., 1999; Prior et al., 1996). EBSD is very useful to study subgrains and Dauphiné twins in quartz, but does not routinely show the presence of dislocations or Brazil twins (Olesen and Schmidt, 1990). Furthermore, EBSD mapping is very time consuming, plus the spatial resolution of EBSD maps in quartz is not as high as that of scanned images, especially in quartz, where beam damage restricts the step size to $>0.2 \mu\text{m}$.

In other materials, like diamond, silicon and gallium nitride, dislocations have been imaged using cathodoluminescence (e.g. Higgs et al., 1992; Lei et al., 2002; Pennycook et al., 1980; Sekiguchi and Sumino, 1996). In olivine, individual dislocations, dislocation walls and subgrain boundaries can be imaged in the SEM with a backscatter detector or in a standard petrographic microscope, after oxidation-induced iron decoration of the dislocations (Karato, 1987; Kohlstedt et al., 1976). This method provides a very useful way of studying the general presence and distribution of dislocations in olivine. Also electron channelling techniques can be used to image dislocations in semi-conductors (e.g. Wilkinson and Hirsch, 1997). Götze (2009) mentioned that the concentration of defects and dislocations in (sub)grain boundaries in quartz results in a high CL intensity.

In this paper, we describe a technique to image dislocations, subgrain boundaries and Brazil and Dauphiné twin boundaries in quartz with composite colour or red filtered cathodoluminescence in a scanning electron microscope (SEM-CL). The method is useful for getting an indication of the presence and distribution of dislocations, subgrains and twin boundaries and enables direct correlation to light microscopy. The techniques could therefore be very useful in microstructural studies of quartz-bearing rocks.

6.2 Materials and methods

Three different quartz samples were studied: a quartzite containing subgrains and Dauphiné twins from Cap de Creus, an undeformed single crystal of smoky quartz with Brazil twins and a

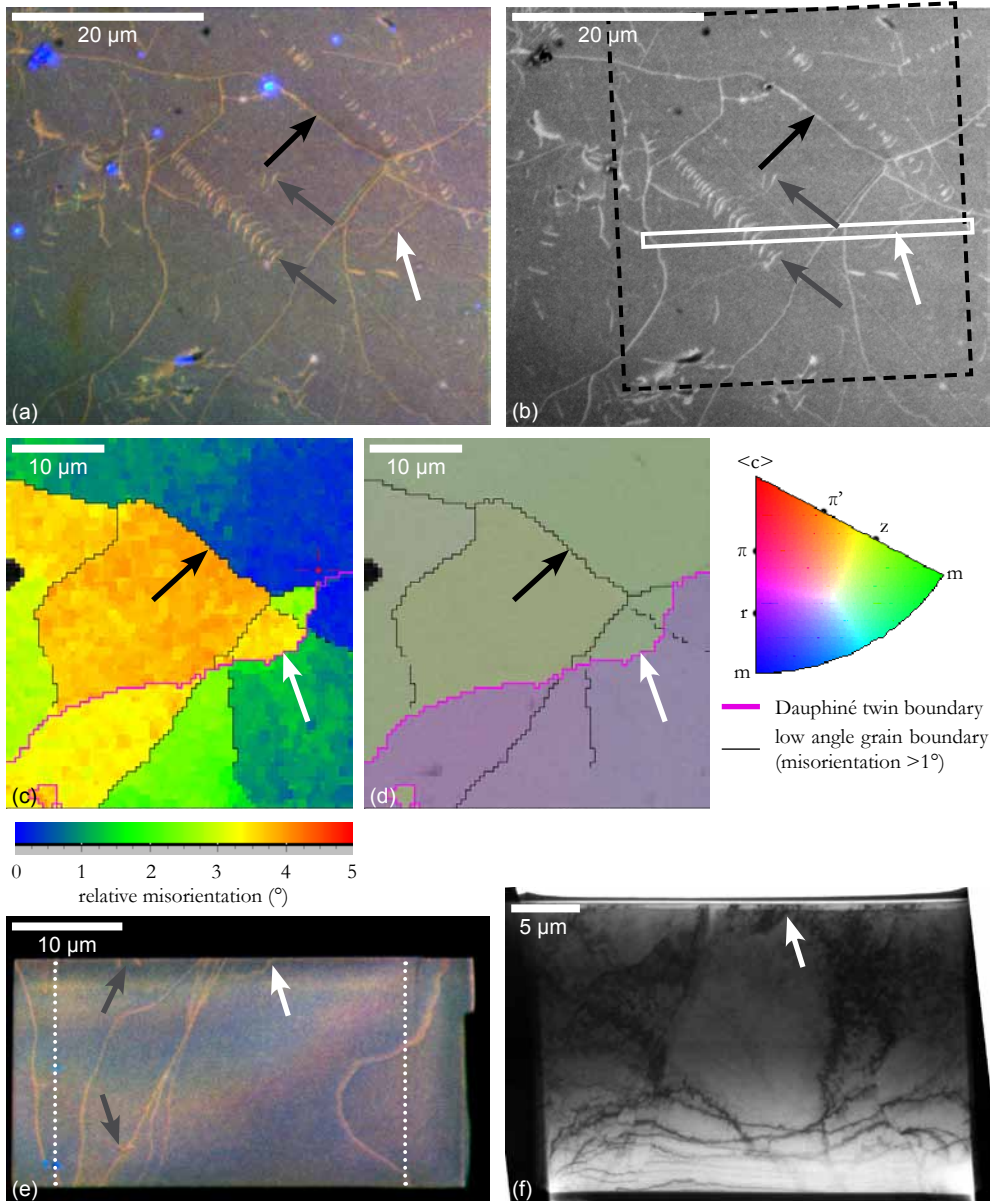


Figure 6.1 Deformed quartzite from Cap de Creus. Black arrows indicate subgrain boundaries; white arrows Dauphiné twins; grey arrows point out dislocation-like structures. **a** Composite colour SEM-CL image. **b** Red filtered SEM-CL image. White rectangle indicates location of TEM foil shown in **d** and **e**; black dashed rectangle shows location of EBSD map in **c**. **c** Processed relative texture map (maximum deviation 5°, relative to the red cross) of the area indicated in **b**, showing the slight misorientation across subgrain boundaries. **d** Processed pattern quality + inverse pole figure map of the same area as in **c**, showing subgrain and Dauphiné twin boundaries. **e** Composite colour SEM-CL image of the TEM section before thinning to the final thickness. Dotted lines indicate the width of the thinned part of the TEM foil. **f** TEM bright field image of the TEM foil.

shock deformed quartz grain from the 201 Ma Rochechouart impact structure in France, which contains healed shock lamellae (planar deformation features – PDFs) and Dauphiné twins. The Cap de Creus quartzite was sampled from the migmatite metamorphic zone. It is highly deformed and recrystallised with most grains showing well developed subgrains.

Samples were polished down to a 1 μm finish using standard polishing procedures with Al_2O_3 . A subsequent chemical mechanical polish was applied using colloidal silica (Syton) (Fynn and Powell, 1979) for 20-60 minutes, to obtain a surface of sufficiently high quality for FSE imaging and EBSD mapping. A thin layer of carbon coating was applied to the samples to reduce charging and drift problems.

SEM-CL images were recorded at room temperature in an FEI Nova Nanolab 600 dual beam SEM with focused ion beam (FIB) and a panchromatic Gatan PanaCL detector (Gatan UK, Oxford, UK) at the Electron Microscopy Utrecht lab (EMU), the Netherlands, using acceleration voltages of 5-10 kV and beam currents of 1.6-8.4 nA. Red, green and blue filters in the CL detector were used to record colour filtered images, which were combined into a colour composite RGB image. Because the contrast and brightness were adjusted individually

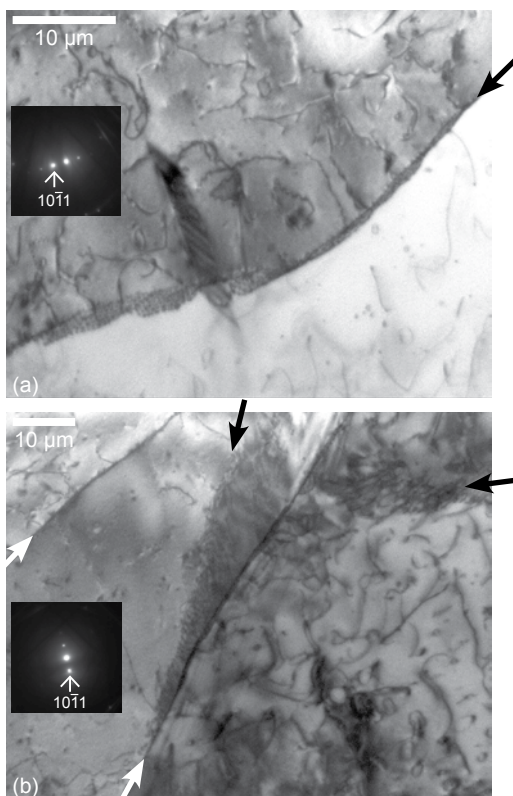


Figure 6.2 TEM bright field images at different tilt angles of the recrystallised Cap de Creus quartzite sample. **a** Subgrain boundary. **b** Subgrain boundaries (black arrows) and Dauphiné twin boundaries (white arrows). Both a and b show the high density of dislocations in the sample.

for each channel before combination into the RGB image, the CL colours in these images are not quantitative.

Fore-scattered electron (FSE) imaging and electron backscattered diffraction (EBSD) mapping were applied to the same area as imaged in CL for the Cap de Creus and Rochechouart samples. This was done at EMU using a Philips XL30 SFEG SEM with Nordlys camera. Acceleration voltages between 15-20 kV were used, with a nominal current of nA and a 50 μm aperture. Working distance was 20 mm with a sample tilt of 70°. Step sizes of 0.2 and 0.5 μm were used for mapping. Maps were processed by extrapolating single pixels with very different orientations to neighbouring pixels and replacing non-indexed points with one of the five nearest neighbours. Remaining zero solutions were copied manually from one of the nearest neighbouring pixels. An orientation averaging filter (Humphreys et al., 2001) (size 3x3, smoothing angle 5°) and artefact filter (critical angle 1°) were applied once.

TEM foils were also prepared in the FEI Nova Nanolab instrument, using the FIB for precise determination of the TEM sample location. For the Cap de Creus and smoky quartz samples, SEM-CL images were recorded on the thick TEM section before thinning down the foil to the final thickness of ~100-200 nm, to enable a direct correlation between CL and TEM images. TEM analysis was carried out on an FEI Tecnai 20 FEG instrument, also at EMU, operated at 200 kV, with a double tilt holder.

6.3 Results

6.3.1 Cap de Creus deformed quartzite

In figure 6.1a and b a composite colour SEM-CL image of the Cap de Creus sample and the red filtered image are shown respectively. Different microstructures can be traced as red luminescent features in the colour image (bright in the red filtered image). The EBSD maps in figures 6.1c and d identify the red luminescent lines as subgrain boundaries (black lines) and Dauphiné twin boundaries (pink line). In the SEM-CL images subgrain boundaries are more pronounced than Dauphiné twin boundaries. Also an overview of the TEM section from this grain in SEM-CL (figure 6.1e) and TEM bright field (figure 6.1f) images shows a direct correlation of subgrain and Dauphiné twin boundaries with red luminescent lines.

Also features with a dislocation-like geometry are present in the SEM-CL images, indicated with grey arrows in figure 6.1. Some look like free dislocations and others are similar to dislocation pile-ups (e.g. Whelan et al., 1957). The high dislocation density in this quartz is evident from the TEM bright field images in figure 6.2. Many more dislocations are observed in TEM images than in the SEM-CL images, so not all individual dislocations are detected in CL images. The CL image of the thick section (figure 6.1e) does not show any free dislocations, but part of the dislocation pile-up seems to be visible (grey arrow) in the top left of the section.

Dislocations, subgrains and twin boundaries all have the same colour within the same (colour) CL image.

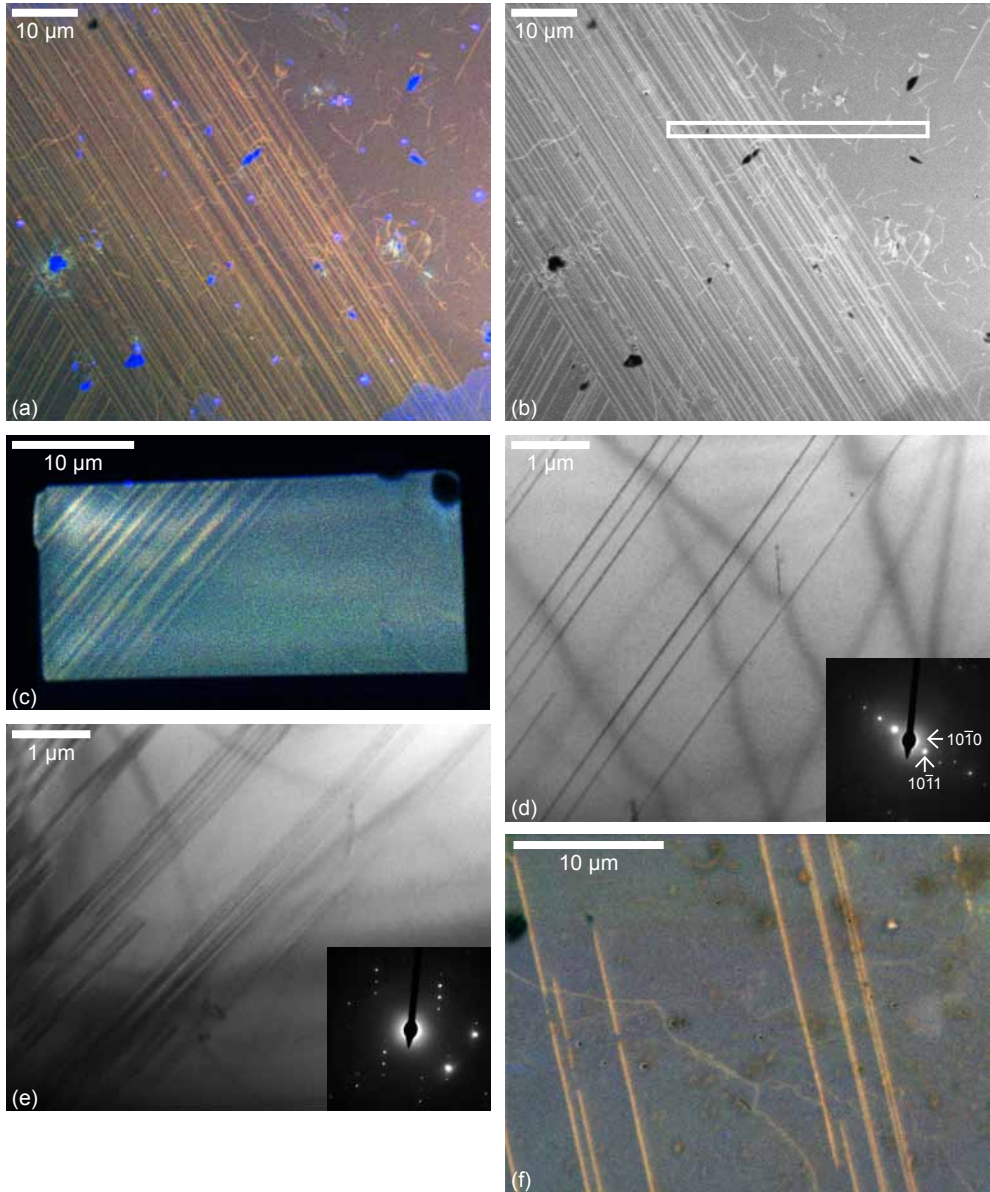


Figure 6.3 Smoky quartz single crystal. **a** Composite colour SEM-CL image showing Brazil twins as red luminescent lines. Blue luminescent spots and areas (e.g. in the bottom right corner) are remains of the polishing material on the sample surface. **b** Red filtered SEM-CL image. White rectangle indicates location of TEM foil shown in C and D. **c** Composite colour SEM-CL image of the TEM foil before thinning to the final thickness, showing Brazil twins as red luminescent lines. **d** TEM bright field image and corresponding selected area diffraction pattern (SADP), showing edge on Brazil twin boundary planes parallel to $\{1011\}$. **e** TEM bright field image and SADP of the same area as in d, but with the Brazil twin boundary planes in a tilted position. **f** Mechanical Brazil twins (straight red line oriented NNW-SSE) in a polished thin section of a quartzite from the Vredefort impact structure, South-Africa. Note that some thinner, more irregular red luminescent lines are observed, which are probably subgrain or Dauphiné twin boundaries.

6.3.2 Single crystal smoky quartz

SEM-CL and TEM images of a quartz single crystal with growth Brazil twins are shown in figure 6.3. The SEM-CL images (3a and 3b) show the twins as red luminescent straight lines in different orientations, which do not cross-cut. Also some features that look like free dislocations can be recognised in the CL images and they have the exact same colour as the twins, as is observed in the Cap de Creus sample (figure 6.1) for subgrain boundaries, Dauphiné twin boundaries and dislocations. The composite colour SEM-CL image of the TEM section before thinning (figure 6.3c) shows a direct correlation of the red luminescent lines with Brazil twin lamellae parallel to the $\{10\bar{1}1\}$ plane in TEM (figure 6.3d). As can be expected from an as-grown crystal, very few dislocations are present in the TEM section and none can be recognised in the CL image of the thick section. For comparison, an example of mechanical basal Brazil twins in a quartzite from the Vredefort impact structure in South-Africa is shown in figure 6.3f. These features show exactly the same CL behaviour as the growth Brazil twins in the smoky quartz.

6.3.3 Shocked quartz

Figure 6.4a shows the red filtered SEM-CL image of a shocked quartz grain with healed planar deformation features (PDFs) from the Rochechouart impact structure in France (see figure 2.4b in chapter 2 for the composite colour image). The bright (red) luminescent, straight lines indicated by black arrows are healed PDFs. PDFs are originally planes of amorphous silica, but after healing and recrystallisation of the amorphous material, they can be recognised as planes of high dislocation density (e.g. chapter 4; Goltrant et al., 1992; Trepmann and Spray, 2006). The PDFs in this grain therefore consist of planes of very high dislocation density.

Other bright (red) lines in the red filtered CL image correlate to Dauphiné twin boundaries, indicated in the EBSD map in figure 6.4c (white arrows). Similar to the subgrain boundaries in figure 6.1, the PDFs are more pronounced than the Dauphiné twin boundaries. The twins are also easily recognised in an FSE image (figure 6.4b).

6.4 Discussion

The correlated SEM-CL images, FSE images, EBSD maps and TEM analysis show that subgrain boundaries, twin boundaries and some dislocations in quartz appear in SEM-CL images as red luminescent features. Similar red luminescence has been observed previously in healed PDFs (see also figure 6.4), which consist of planes of high dislocation density, and in mechanical Brazil twins formed by a meteorite impact (see figure 6.3f and chapter 2). Dislocations, subgrain boundaries, healed PDFs and twin boundaries have the same CL colour within one image. Although the colours in the SEM-CL images are not quantitative, the same colour within one image should originate from an emission with the same dominant wavelength. It can therefore be assumed that the CL emission of dislocations (free, in subgrain boundaries or in healed PDFs) and twin boundaries has the same dominant peak in the red wavelength range of the spectrum. Unfortunately these features are too small-scale for CL spectroscopic measurements, which could quantify the wavelength of the CL emission and identify the defect centres or impurities responsible for the dominant peaks. However, by looking at emission peak ratios, in chapter 4 we measured a dominant 650 nm emission peak in red luminescent, healed PDFs

(i.e. planes of high dislocation density) from the Ries crater. The 650 nm emission has been confidently associated with the non-bridging oxygen hole centre (NBOHC) defect in the quartz crystal lattice (e.g. Götze et al., 2001; Stevens Kalceff, 2009 and references therein). This defect can form as a result of beam damage in quartz. In TEM, localised electron beam damage at dislocations, Brazil twin boundaries and, to a lesser extent, Dauphiné twin boundaries is a commonly observed phenomenon and continued beam damage finally results in complete (local) amorphisation (Carter and Kohlstedt, 1981; Cherns et al., 1980; Comer, 1972; McLaren and Phakey, 1965a; McLaren et al., 1970). Beam damage and associated production of NBOHC defects at dislocations were interpreted to be the main source of the red luminescence in healed PDFs (chapter 4). The same process can explain the red luminescence of dislocations, subgrain boundaries and twin boundaries.

6.4.1 Electron beam damage in quartz and the non-bridging oxygen hole centre defect

In both TEM and SEM the incident electron beam damages the sample lattice, inducing defects and disorder in the crystal structure and finally leading to local amorphisation. In general, the damage can occur by elastic or inelastic scattering. Elastic scattering causes knock-on damage: the direct transfer of kinetic energy displaces atoms or electrons (momentum transfer). This process depends on the energy of the incoming electrons. In quartz, >64 keV is required for the displacement of an O atom and > 197 keV for a Si atom (Pfeffer, 1985). Elastic damaging processes are therefore not relevant in the SEM, where the voltages used are normally no higher than ~30 keV. Inelastic scattering, on the other hand, probably depends on the current density delivered to the sample (Egerton et al., 2004) and may occur in quartz at beam energies exceeding ~5 keV (Stevens Kalceff, 2009 and references therein; Vigouroux et al., 1985). Inelastic scattering of the incoming electrons induces radiolysis, which is an electronic process in which atoms are excited by inelastic interactions of the electron beam with the sample. Subsequent non-radiative decay of electron irradiation-induced electron-hole pairs leads to the formation of stable defects. Radiolysis is thought to be the main process responsible for electron beam damage in quartz (e.g. Hobbs and Pascucci, 1980; Tsai and Griscom, 1991). Radiolytic dissociation of atomic bonds such as the Si-O bond can produce the NBOHC defect in quartz. The NBOHC is a hole trapped in the $2p\pi$ orbital (a valence band/orbital) of a non-bridging oxygen atom which is bonded to a silicon atom. This Si atom is bonded to three other oxygen atoms. The defect can be described as $O_3 \equiv Si-O\bullet$ where ‘ \bullet ’ represents a dangling bond (i.e. an unpaired electron) (Stevens Kalceff, 2009). Excitement of the defect and subsequent recombination of electrons in the non-bridging oxygen band-gap state with holes in the valence band edge produces the CL emission with 650 nm wavelength (Götze et al., 1999; Götze et al., 2001; Sigel and Marrone, 1981). The two main precursors for the NBOHC are $O_3 \equiv Si-O-Si \equiv O_3$, where electron irradiation breaks a Si-O bond, and $O_3 \equiv Si-OH$, where electron irradiation breaks the O-H bond (Stevens Kalceff, 2009). A CL emission around 630 nm with a quickly decreasing intensity is associated with the latter process, while the 650 nm red emission associated with dissociation of the Si-O bond initially increases and then stabilises (Götze et al., 2001; Stevens Kalceff, 2009). A third precursor might be $O_3 \equiv Si-O-M$, where M is an alkali ion and the O-M bond is dissociated by the electron beam, resulting in a 650 nm CL emission. However, this emission has a relatively low and also decreasing intensity (Stevens Kalceff, 2009). Furthermore, the peroxy linkage (Si-O-O-Si), an oxygen excess defect, may act as a precursor for the NBOHC defect with a 650 nm emission

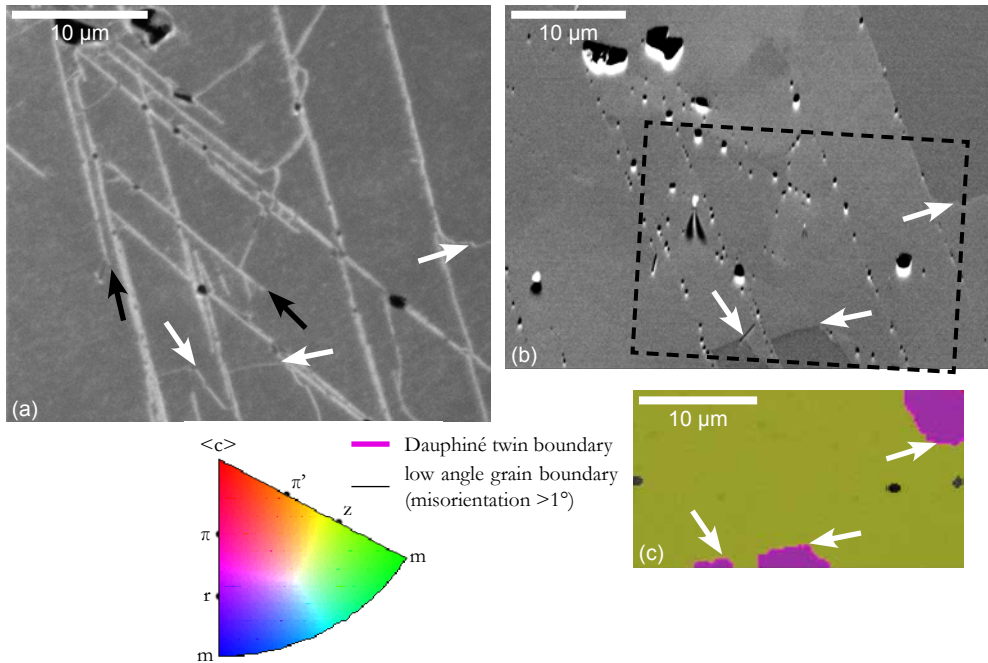


Figure 6.4 Shocked quartz grain from Rochechouart with healed planar deformation lamellae (PDFs) (black arrows) and Dauphiné twin boundaries (white arrows). **a** Red filtered SEM-CL image. **b** Forescattered electron image; black dashed rectangle shows the effective location of EBSD map in **c**. **c** Processed pattern quality + inverse pole figure map of the area indicated in **b**. Charging of the sample during mapping deflects the beam in the vertical direction, which effectively increases the step size in the y direction. The EBSD map is plotted with square pixels, so the microstructures shown in **c** are slightly shortened with respect to the area shown in **b**.

(Götze et al., 2001; Stevens Kalceff and Phillips, 1995; Stevens Kalceff et al., 2000). The 630 nm and 650 nm peaks cannot be distinguished in a CL spectrum and appear as one broad peak. In chapters 2 and 4 we observed increasing intensity of the red CL emission in healed PDFs and in chapter 4 we therefore interpreted preferential beam damage and production of NBOHC defects at the dislocations in the PDF plane as the main source of the red CL.

6.4.2 Dislocations and subgrain boundaries

It is likely that non-bridging oxygen atoms are already present in edge dislocations before electron irradiation, especially in dry samples. A pure edge (segment of a) dislocation consists of an extra half-plane in the crystal structure. The line of atoms at the end of the extra half-plane (the core of the dislocation) can have dangling bonds (non-bridging atoms). Depending on whether these are O or Si atoms, NBOHC defects might therefore be present in the line, resulting in a 650 nm emission under electron irradiation. The non-bridging Si bond, $O_3 \equiv Si \cdot$, is an oxygen vacancy defect known as an E' centre. No confirmed luminescence centre is associated with this defect (Stevens Kalceff, 2009). Also partial dislocations have dangling bonds (Trepied and Doukhan, 1978a). In hydrated quartz, the dislocation core will contain OH groups instead of, or in addition to, dangling bonds (e.g. Heggie, 1992; Trepied and Doukhan, 1978a). The O-H bond can be

dissociated by the electron beam to produce an NBOHC and might contribute to the red CL emission initially. Any excess oxygen present in the lattice might also diffuse to the dislocation core and attach to any dangling bonds, by forming a non-bridging oxygen attached to a Si atom, or a peroxy linkage (O-O) by attaching to a non-bridging oxygen, depending on which situation is energetically more favourable. In a pure screw (segment of a) dislocation, the only dangling bonds or OH groups will be at the sample surface, but most dislocations have a mixed character. Also at kinks and jogs in a dislocation line, dangling bonds or OH groups can be present (Heggie and Jones, 1986). Furthermore, the lattice around both edge and screw dislocations is locally distorted (Hull and Bacon, 2011). This could result in strained Si-O bonds, which are more easily dissociated by radiolysis than bonds in unstrained areas of the crystal and form a precursor for the NBOHC (Devine, 1990; Stevens Kalceff and Phillips, 1995), explaining the localised beam damage effect and increase in the local red CL emission.

The above discussion illustrates that a variety of precursor defects for the NBOHC can be present in dislocations cores and therefore in subgrain boundaries and healed PDFs consisting of dislocations. From our data, it is not possible to distinguish between the different precursors, but it is likely that the total emission observed in CL images is a combination of contributions from different defects.

In the TEM images in figure 6.2 many more dislocations are observed than in the CL images in figure 6.1. In the thick TEM section before thinning (figure 6.1e) no dislocations are observed at all, except maybe the dislocation pile-up in the top left of the section and one right below, more towards the bottom (grey arrows). Higher magnification TEM images (figure 6.2), however, show that the foil has a rather high dislocation density. Apparently only high concentrations of dislocations, such as subgrain boundaries and pile-ups, clearly show up in SEM-CL images. The features that look like individual dislocations in SEM-CL images (e.g. the grey arrow in the centre of figures 6.1a and b) might in fact be a group of dislocations that are very close together. The most obvious explanation for this is the much lower spatial resolution of SEM-CL images with respect to TEM images: TEM detects individual defects on the nanometre scale, while in SEM-CL, the electron beam penetrates the sample to a depth between ~ 0.3 - $1 \mu\text{m}$ (estimates based Monte Carlo simulations with beam energies of 5 and 10 kV, using Casino 2.42 software (Drouin et al., 2007; Drouin et al., 2001)). The CL emission is therefore a signal that averages the contribution of many dislocations and any other luminescent defects. Only high defect densities, such as subgrain boundaries and dislocation pile-ups, may give a signal that is significantly above the background. Furthermore, the orientation of the dislocations with respect to the sample surface in SEM could play a role, as in a dislocation at a high angle to the surface the whole dislocation is not sampled by the electron beam. In that case, the dislocation will only make up a small portion of the interaction volume and its CL emission is only a small contribution to the total CL emission of the interaction volume, which could render the red part of the emission weaker or invisible. In many deformed samples, the stress-induced dislocations will have the same orientation. It is therefore possible that, while in TEM the dislocations are more easily observed by changing the tilt and diffraction conditions, the surface imaged in the SEM, which is perpendicular to the TEM foil, might not be in a favourable position to sample enough of a dislocation for a significant CL emission. Another factor to consider could be variations in the local stress field around dislocations. For example, the stress concentration is higher near dislocations at the head of a pile-up, so more, or more strongly, strained bonds could be present that are easier to break than the bonds in areas of lower stress concentration. The lack of

dangling bonds or non-bridging defects in (segments of) screw dislocations and the high amount of them in edge (segments of) dislocations could also tend to make the CL intensity higher at edge than at screw (segments of) dislocations. However, radiolysis of strained Si-O bonds or OH groups at both types should render also screw dislocations visible after considerable exposure to the electron beam. Detailed TEM analysis and CL imaging of individual dislocations in a (S)TEM CL system could help clarifying which factors play a role in the CL emission at dislocations.

6.4.3 Twin boundaries

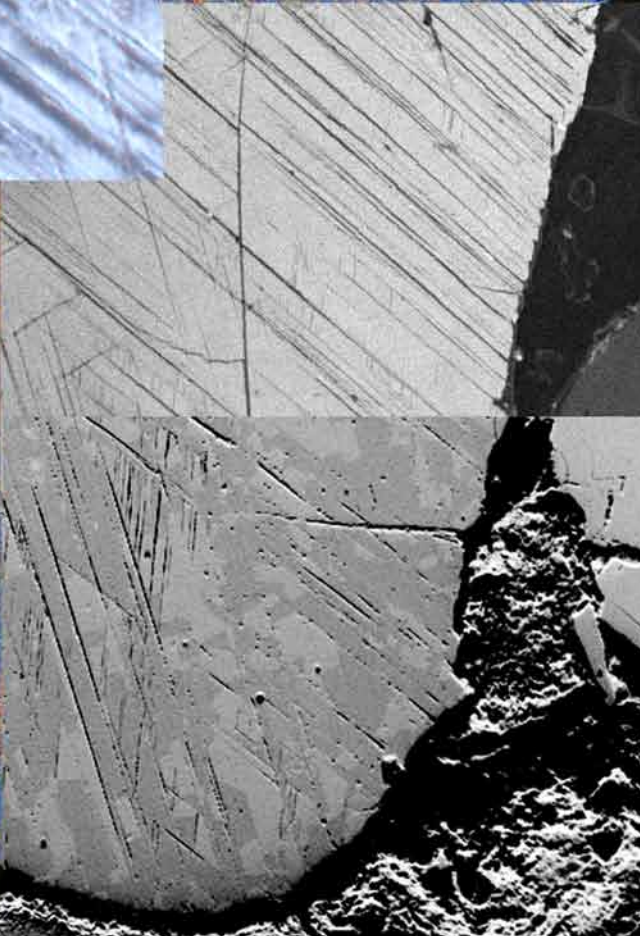
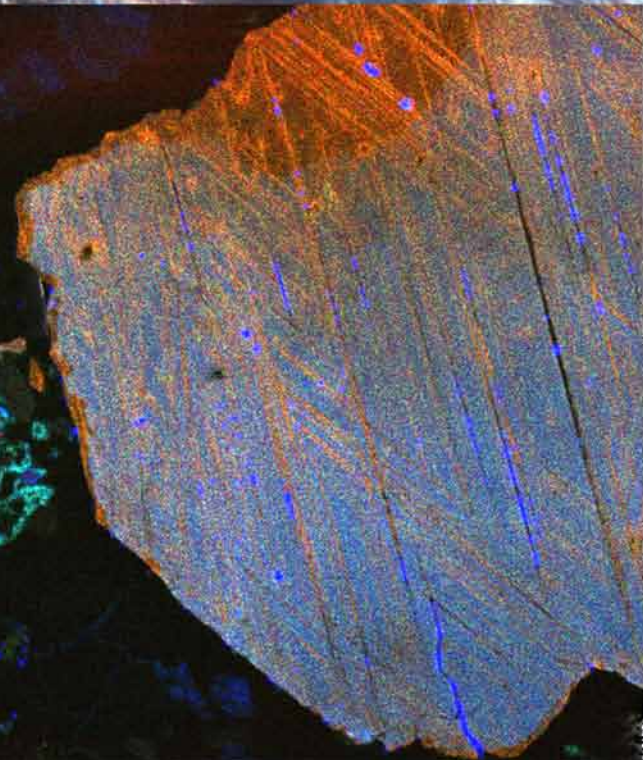
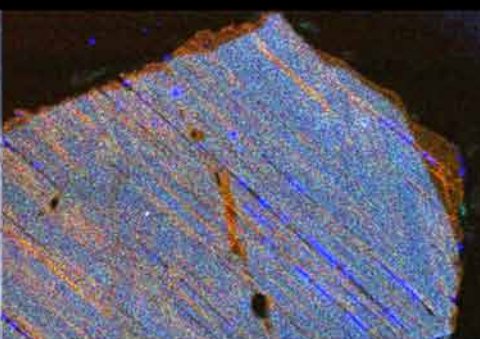
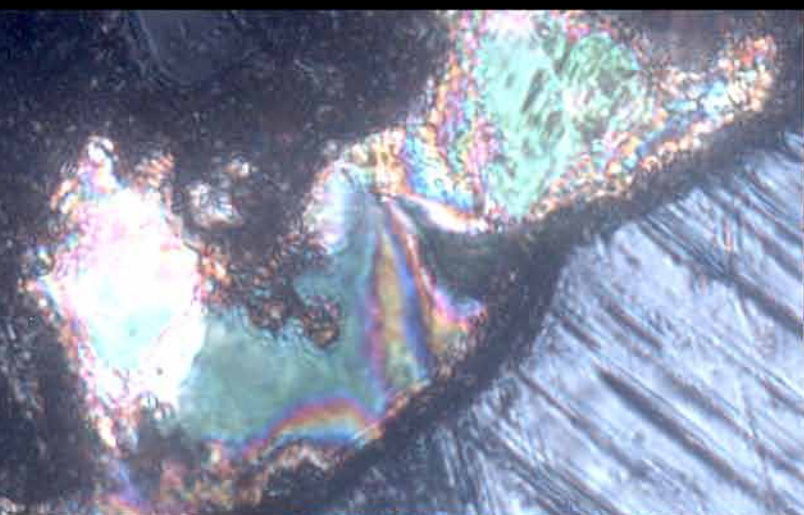
No atomic bonds need to be broken to form Dauphiné twins. Rather, a small rotation of the SiO₄ tetrahedra in the boundary, with only a slight change in bond angles across the boundary, is sufficient to produce a 180° rotation of the crystal structure (McLaren and Phakey, 1969; Van Goethem et al., 1977). Similarly, in Brazil twin boundaries no broken bonds should be present, but the configuration of the SiO₂ tetrahedra in the boundary is slightly distorted (McLaren and Phakey, 1966; Van Goethem et al., 1977). The crystal structure in the boundary region is therefore slightly distorted in both Dauphiné and Brazil twins, but it is the same in both growth and mechanical twins. In both mechanical and growth Brazil and Dauphiné boundaries, the bond angles in the boundary are slightly different with respect to the perfect SiO₂ crystal lattice. A change in bond angles changes the bond energy. In amorphous SiO₂, the Si-O-Si (intertetrahedral) bond angles vary between 120-180°, while in crystalline α -quartz these angles are less flexible and are ~144°. In amorphous silica, Si-O-Si bond angles <120° result in strained Si-O bonds (Devine, 1990), which form a precursor for the NBOHC defect. In crystalline silica, where there is less freedom in the Si-O-Si bridge angle, even a smaller distortion of the tetrahedral configuration may result in strained bonds. However, no strain contrast is observed from twin boundaries in TEM, but only fringe patterns occur due to structure factor or phase differences between the twinned parts of the crystal (McLaren and Phakey, 1969; McLaren et al., 1967; Trepied and Doukhan, 1978b; Van Goethem et al., 1977). This might be due to the planar character of the twin boundaries: the only strain is present in a very narrow region on the order of one Si-O bond length, but the lattice is not distorted even directly adjacent to the twin boundary. The localised concentration of strained Si-O bonds might be enough to produce the red CL emission. On the other hand, in the absence of significant strain in the lattice, concentration of impurities (alkali ions) or OH groups could also contribute significantly to the production of NBOHC defects. If these were the main source of the CL emission, the intensity of the emission can be expected to decrease with increasing irradiation time, in contrast to the CL emission associated with the NBOHC with Si-O bond precursor (Götze et al., 2001; Stevens Kalceff, 2009). However, this is not observed; on the contrary, the emission from the boundaries seems to increase in intensity or be stable during several scans of the same area. Similar to dislocations, the observed CL emission at twin boundaries might be a combination of initial red luminescence associated with OH groups and impurities, continued by dissociation of strained Si-O bonds due to the distorted tetrahedral structure in the boundary region. Additionally, peroxy linkages could play a role if they are present in a higher concentration in the twin boundaries than in the rest of the crystal.

It should be noted that, although Dauphiné twin boundaries seem to be slightly thinner and less pronounced than subgrain boundaries in SEM-CL images (e.g. figure 6.1), confident distinction of Dauphiné twin boundaries and subgrain boundaries is not possible in SEM-CL images. EBSD maps or TEM analysis are always required to quantify the orientation changes and determine

the nature of the boundary. Brazil twin boundaries, on the other hand, are easily distinguished from Dauphiné twin or subgrain boundaries by their characteristic straight line geometry. Some Brazil twin boundaries in CL images are thicker and brighter than others; these are probably not single twin planes, but groups of very closely spaced ones. Because of the relatively low spatial resolution of SEM-CL images compared to TEM bright field images, the individual structures might not always be discerned.

6.5 Conclusions

Correlated SEM-CL images, FSE images, EBSD maps and TEM analysis show that subgrain boundaries, twin boundaries and some dislocations in quartz can be imaged using composite colour or red filtered SEM-CL, and are red luminescent in these images. The red luminescence of dislocations and dislocation-related features, such as subgrain boundaries and healed PDFs, is probably related to NBOHC defects in the dislocation cores and localised electron beam damage. Strained Si-O bonds could play an important role in the production of the CL emission. It is likely that the same defect is responsible for the CL emission in Brazil and Dauphiné twin boundaries. Although SEM-CL imaging is not quantitative and other methods, such as EBSD and TEM analysis, are required to confirm the nature of the microstructures, the red luminescence allows a quick indication for the presence and spatial distribution of subgrain and twin boundaries in a quartz grain and can be a useful basis for measurements of subgrain size and twin density. The SEM-CL method can be applied to standard sized petrographic thin sections, but shows features that are invisible in light microscopy. This imaging technique can therefore be a useful addition to the microscopic investigation of quartz-bearing rock samples.



Chapter 7

An integrated scanning electron microscopy approach for shocked quartz

M.F. Hamers, G.M. Pennock and M.R. Drury

Shocked quartz is crucial evidence for meteorite impact craters or stratigraphic layers related to an impact, such as the global Cretaceous-Paleogene boundary impact layer. The often observed similarity in light microscopy of shock microstructures in quartz to tectonically formed micro-lamellae has led to many discussions and misinterpretations. Time-consuming, difficult and expensive transmission electron microscopy (TEM) analysis on tiny samples is often required to reliably prove the presence of shock lamellae in quartz. Here we show that the same type of information can be acquired using scanning electron microscopy (SEM). A combination of different SEM techniques not only enables the reliable identification of shock lamellae, but also provides a good general characterisation of shock microstructures in quartz. This integrated SEM approach is non-destructive and can be applied to standard sized petrographic thin sections, enabling a direct comparison to light microscopy.

Furthermore, the combined SEM and TEM observations can distinguish groups of shocked quartz grains, which have different, characteristic microstructures. These can be interpreted in terms of degree of healing in grains that have been shocked to moderate or high pressure. A TEM-scale blocky subgrain structure, described as mosaicism in earlier studies, is interpreted as a healed high shock pressure structure.

Table 7.1 Summary of observations of characteristic shock microstructures in SEM, using CL and FSE imaging and EBSD mapping, and in TEM, using imaging and diffraction techniques. In addition, the main advantages (green) and shortcomings (red) of the various methods are indicated.

	TEM		SEM-CL		FSE		EBSD	
Amorphous PDFs	Light in diffuse dark field images	Non-luminescent	Constant contrast	Dark in pattern quality map				
Healed PDFs	Planes of high dislocation density	Red luminescent	Variable contrast	Mostly invisible				
Brazil twins	Yes	Red luminescent	No	No				
Dauphiné twins	Yes	Red luminescent, confirmation by EBSD	Yes, with confirmation by EBSD	Clear				
High pressure phases	Yes	Indication	Qualitative (differences visible)	Yes				
Crystallographic orientation information	Qualitative (images) and quantitative (diffraction patterns)	No	Qualitative (differences visible)	Quantitative				
Crystal structure information (amorphous, crystalline, micro-crystalline)	Yes	No	Qualitative (differences visible)	Yes				
(dis)advantages of the technique	+ direct observations of defects and crystal structure/orientation	- no crystallographic information	+ crystallographic information, but only qualitative	+ quantitative crystallographic information				
	+ very high spatial and angular resolution	- limited spatial resolution	+ high spatial and angular resolution	- limited spatial and angular resolution (in quartz)				
	- destructive sample preparation	+ non-destructive	+ non-destructive	+ non-destructive				
	- very small samples	+ large samples	+ large samples	+ large samples				
- difficult, time-consuming technique and sample preparation	+ easy and quick	+ easy and quick	+ easy and quick	- relatively complicated technique				
- limited comparison with light microscopy	+ direct comparison with light microscopy	+ direct comparison with light microscopy	+ direct comparison with light microscopy	+ direct comparison with light microscopy				

7.1 Introduction

Ever since the Cretaceous–Paleogene mass extinction was linked to a major extraterrestrial event (Alvarez et al., 1980; Smit and Hertogen, 1980), meteorite impacts have received a lot of attention in the scientific and popular literature, especially in relation to other mass extinctions. An extraterrestrial cause has been proposed for the Permian–Triassic extinction (Basu et al., 2003; Becker et al., 2004; Retallack et al., 1998) and some preliminary impact evidence has been found near the Triassic–Jurassic boundary (Badjukov et al., 1987; Bice et al., 1992; Olsen et al., 2002; Simms, 2003). Planar deformation features (PDFs) in quartz are the most widely used evidence for the shock origin of a suspected geological structure or stratigraphic layer (French and Koeberl, 2010; Grieve et al., 1996; Stöffler and Langenhorst, 1994), but in an light microscope, PDFs are easily confused with tectonically formed (sub-) planar microstructures. This has led to various misinterpretations and discussions about supposed impact structures (Ernstson and Fiebag, 1992; Gorter and Glikson, 2012; Heidecker, 2012; Langenhorst and Deutsch, 1996; Langenhorst et al., 2005; Retallack et al., 1998). Until recently, only TEM observations could provide definitive evidence for the shock origin of planar microstructures in quartz, but advances in SEM techniques provide alternative methods (chapters 2, 4 and 5; Boggs et al., 2001). In this paper we show that a combination of cathodoluminescence (CL), forescatter electron (FSE) and electron backscatter diffraction (EBSD) techniques in the SEM forms a powerful integrated SEM approach to the study of shocked quartz that can fully characterise shock microstructures and therefore provides a complete alternative or addition to the existing TEM techniques.

7.1.1 Shock effects in quartz

Characteristic shock effects in quartz occur between peak shock pressures of about 7 and 35 GPa, ranging from brittle deformation to complete melting of the grain. At relatively low shock pressures (< 10 GPa) mechanical Brazil twins in the basal plane (0001) develop as a result of high shear stress. At higher pressures (10–35 GPa) PDFs form: thin amorphous lamellae with a crystallographically determined orientation, most frequently occurring parallel to $\{10\bar{1}3\}$, $\{10\bar{1}2\}$ and $\{1011\}$ (French and Koeberl, 2010; Grieve et al., 1996; Stöffler and Langenhorst, 1994). During post-shock high temperatures or metamorphic events amorphous PDFs recrystallise to planes of high dislocation density, still recognised in light microscopy by fluid inclusions that decorate the PDF plane. Above ~35 GPa quartz transforms to a dense amorphous phase (diaplectic glass) and at even higher pressures and temperatures melt glass (lechatelierite) forms. Other shock effects often observed in quartz are Dauphiné twins in close association with PDFs (chapter 5; Chen et al., 2011; Trepmann and Spray, 2005; Wenk et al., 2011; Wenk et al., 2005) and mosaicism (Dachille et al., 1968; Grieve et al., 1996; Huffman et al., 1993; Huffman and Reimold, 1996; Leroux and Doukhan, 1996; Stöffler and Langenhorst, 1994; Trepmann, 2008). Dauphiné twins could be mechanical (Chen et al., 2011; Wenk et al., 2011; Wenk et al., 2005) or they could form during back-transformation from β - to α -quartz of grains that have the β -configuration due to (local) high temperature (Trepmann and Spray, 2005). On the formation mechanism of mosaicism no consensus exists. In a light microscope, a mosaic structure is observed as a highly irregular, ‘mottled’ extinction under crossed polarisers (French and Koeberl, 2010; Grieve et al., 1996; Leroux and Doukhan, 1996; Stöffler and Langenhorst, 1994). On the TEM scale, submicroscopic crystalline domains (200 nm – 3 μ m) can be observed that are slightly misoriented (up to $\sim 20^\circ$) with respect to each other (e.g. Leroux and Doukhan, 1996; Trepmann,

Table 7.2 Location, rock type and microstructural characteristics of the three new TEM foils of shocked quartz grains used in this study.

Sample	Location	Rock type	CL emission of PDFs	PDF microstructure in TEM	Grain microstructure in TEM and FSE images
P2-1	Popigai (Russia)	Impact melt rock	no/red	not visible	microcrystalline
RI-47-1	Ries (Germany), Polsingen	Granite fragment with quartz vein, from impact melt rock	no/red	porous/not visible	microcrystalline
MRO-5-1	Rochechouart (France), Montoume	Impact melt rock	red	dislocations	microcrystalline

2008). In general, domain size decreases and misorientation increases with increasing peak shock pressure (Grieve et al., 1996; Stöffler and Langenhorst, 1994 and references therein; Trepmann, 2008), but no sound quantitative relation has been established. Mosaicism is furthermore detected in X-ray diffraction and in TEM diffraction patterns by elongation or streaking of the diffraction spots (asterism), which also allows for measurement of the degree of misorientation of the domains.

Stöffler and Langenhorst (1994) classify mosaicism as a relatively low shock phenomenon, starting to occur around 10 GPa and increasing in intensity until ~ 35 GPa. In shock experiments, mosaicism is observed in the light microscope in isolated grains from ~ 10 GPa and becomes pervasive between 10-20 GPa (Huffman et al., 1993; Huffman and Reimold, 1996; Reimold and Hörz, 1986a, b). Mosaicism is often observed in combination with PDFs in the same grain and is thought to represent the plastic response of quartz shocked at or above the Hugoniot elastic limit (HEL), distorting the lattice into misoriented microdomains, ranging in size between $>3 \mu\text{m}$ and $<200 \text{ nm}$ (decreasing with increasing pressure) (Huffman et al., 1993; Huffman and Reimold, 1996; Stöffler and Langenhorst, 1994). More recently mosaicism has been interpreted as the result of two intersecting sets of closely spaced PDFs, dividing the grain into small, slightly misoriented, crystalline domains surrounded by (initially) the amorphous material in the PDFs (Leroux and Doukhan, 1996; Trepmann, 2008). Trepmann (2008) furthermore suggests that mosaicism could represent a transitional state before a complete transformation into diaplectic glass of a grain with a high density of closely spaced amorphous PDFs. Since a high density and close spacing of PDFs indicate relatively high shock pressures (Ferrière et al., 2008; Langenhorst, 1994; Stöffler and Langenhorst, 1994), this model would imply that mosaicism is a high shock pressure phenomenon (most likely ~ 30 -35 GPa, just before the onset of diaplectic glass formation).

7.2 Techniques

7.2.1 Shocked quartz in the scanning electron microscope

Recently, several SEM methods have been explored as potential alternatives or additions to existing TEM techniques to identify PDFs and characterise shock structures in quartz (chapters 2, 4 and 5; Boggs et al., 2001). These SEM techniques include cathodoluminescence (CL) and forescattered electron (FSE) imaging and electron backscattered diffraction (EBSD) mapping. A summary of what TEM and SEM techniques show is given in table 7.1. The main advantages of the SEM methods are that they are non-destructive, as opposed to the preparation of TEM samples, and that standard sized petrographic thin sections can be studied, which allows a direct comparison to light microscopy. Sample preparation procedures are much quicker and easier than for TEM and especially SEM-CL and FSE imaging are much less time-consuming than TEM techniques. However, the spatial resolution of SEM techniques, in particular SEM-CL imaging, is limited compared to TEM.

Backscatter electron imaging (BSE) is not included in table 7.1, because the technique has not been studied in detail here. However, as BSE images show density contrast, they can be very useful to detect high pressure phases (denser and therefore brighter than crystalline quartz) and amorphous PDFs (lighter and therefore darker than crystalline quartz).

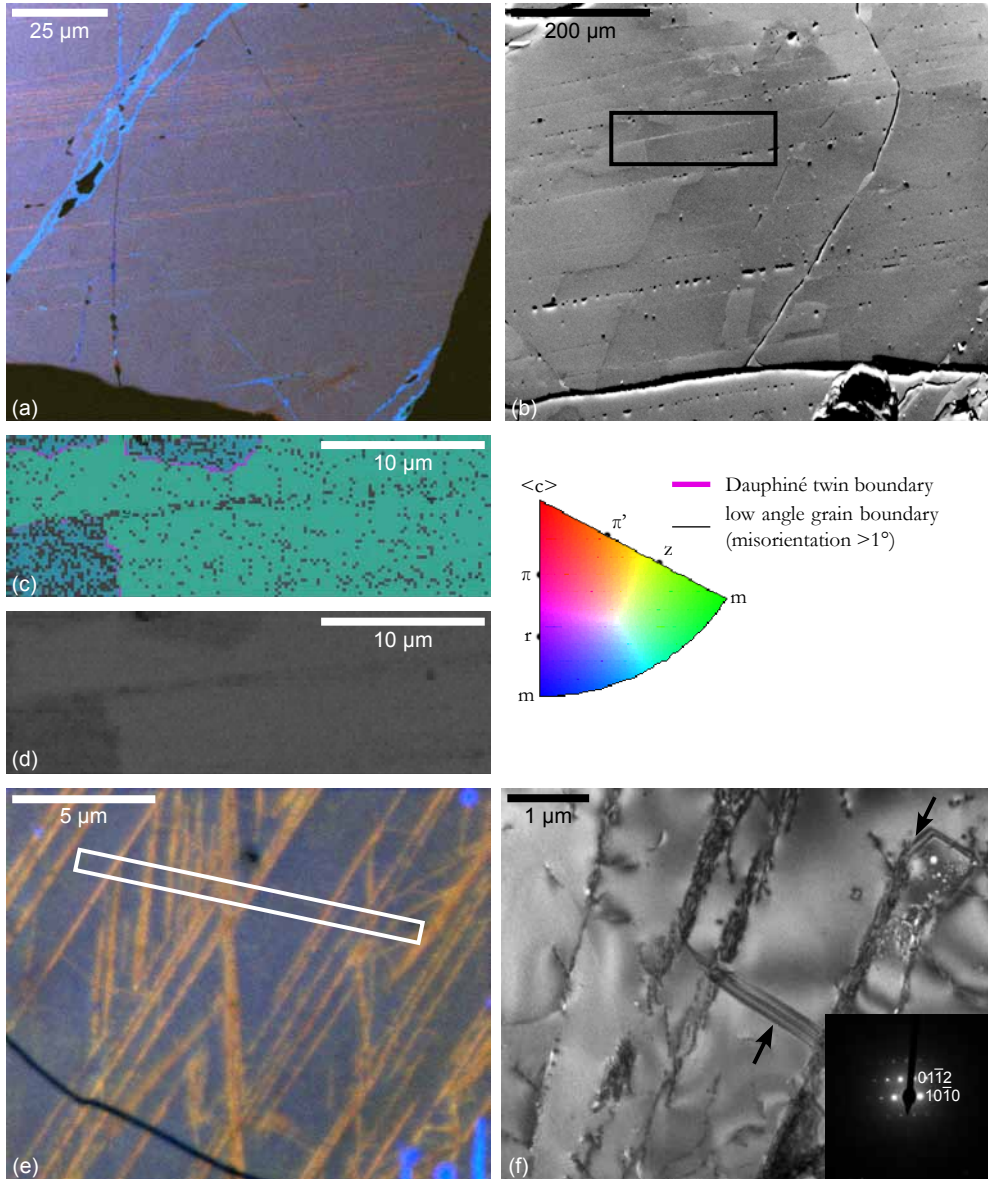


Figure 7.1 CL, FSE and EBSD images of grains in group A. **a** Composite colour CL image of a grain from the Popigai structure, with red luminescent PDFs. **b** FSE image of (a different area of) the same grain as in **a**. PDFs are partly invisible (but decorated by voids), and partly show contrast. The black box indicates the area of the EBSD maps in **c** and **d**. Angular to square domains of different contrast are Dauphiné twins, as shown by the EBSD map in **c**. **c** Pattern quality + inverse pole figure (PQ + IPF) map (step size 0.2 μm) of the black boxed area in **b**, showing the crystallographic orientation at each point with respect to the x-direction. The map shows the presence of Dauphiné twins with straight boundaries, partly parallel to PDFs. **d** Pattern quality map of the same area as **c**, showing the widest part of the PDF as a slightly darker line. The darker region in the lower left corner is a Dauphiné twin. **e** Composite colour SEM-CL image of a grain from the Rochechouart structure with red luminescent PDFs. The white rectangle shows the location of the TEM foil shown

7.2.1.1 SEM-CL imaging

Both greyscale and composite colour SEM-CL imaging are adequate techniques to distinguish between PDFs and tectonic deformation lamellae or other (sub)planar microstructures in quartz, such as healed fractures (chapter 2; Boggs et al., 2001). In addition, composite colour SEM-CL imaging at room temperature allows the distinction of amorphous (unaltered) PDFs from healed PDFs and basal Brazil twins: non-luminescent PDFs are amorphous, while healed PDFs and basal Brazil twins are red luminescent (chapter 4). The red luminescence is probably the effect of preferential beam damage at dislocations and twin boundaries. Rarely, individual dislocations can be recognised in SEM-CL images (e.g. figure 4.2d in chapter 4 in PDFs and in chapter 6 in non-shocked rocks). SEM-CL imaging appears to be the only technique that can image (undecorated) Brazil twins, as these are not visible in light microscopy, FSE images or EBSD maps. However, healed PDFs and Brazil twins cannot be distinguished on the basis of CL characteristics, because no information on crystallographic orientation is recorded in CL images. In both shocked and non-shocked quartz grains, red filtered or composite colour SEM-CL images show Dauphiné twin boundaries as bright or red lines, although subgrain boundaries in CL images look very similar to Dauphiné twin boundaries (see chapter 6). The distinction between subgrain and twin boundaries can be made based on additional EBSD analysis of the sample.

Furthermore, SEM-CL images can indicate the presence of potential high pressure phases (see chapter 4), but additional methods, such as TEM analysis or backscattered electron (BSE) imaging showing density contrast, are required for confirmation.

7.2.1.2 FSE imaging and EBSD mapping

Also in FSE images and EBSD maps, PDFs and tectonic deformation lamellae are easily distinguished (chapter 5). Amorphous and healed PDFs show different characteristics in FSE images and pattern quality maps: amorphous PDFs have a constant grey level throughout one FSE image, while healed PDFs show variable, more complex contrast. Because amorphous material gives no diffraction pattern, amorphous PDFs can be recognised in EBSD pattern quality maps as darker lines in a lighter matrix of crystalline quartz, providing the PDFs are wide enough to be resolved in an EBSD map. Healed PDFs are generally invisible in pattern quality maps, unless the PDF planes contain a high density of defects or fluid inclusions. Furthermore, FSE images and EBSD mapping provide information about the structure of the host quartz grain (see chapter 5). Dauphiné twins can be visualised in FSE images, with confirmation of the twinning relationship from EBSD. RGB colour-coded FSE imaging is particularly useful in detecting Dauphiné twins. A highly distorted crystal structure is recognised by weak EBSD patterns and microcrystalline domains are often visible in FSE images.

The three-dimensional crystallographic orientation of PDFs cannot be determined by EBSD measurements alone, but orientation estimates can be made based on the crystallographic orientation of the quartz grain measured by EBSD and the trace of PDFs in FSE images (see for example figure 7.2b). Furthermore, a combination of EBSD measurements and universal stage data obtained with a light microscope can provide the full crystallographic orientations of

in f. **f** TEM bright field image showing that the red luminescent PDFs are planes of high dislocation density (oriented NNE-SSW): they are healed PDFs. A Dauphiné twin boundary (black arrows) partly coinciding with the PDFs is also visible. The lack of streaked spots in the diffraction pattern (inset) shows the grain is a single crystal.

PDFs and the host quartz grain (Trepmann, 2008; Trepmann et al., 2005; Voorn, 2010; Voorn et al., 2010).

High pressure phases should be detected in FSE images as contrast variations due to crystallographic differences, although this was not tested. Crystalline high pressure polymorphs of quartz (coesite and stishovite) can in principle be identified by EBSD measurements, providing the crystals are large enough.

7.2.2 Samples

We show five examples of shocked quartz grains that were studied using composite colour SEM-CL imaging at room temperature, FSE imaging and EBSD mapping, and using TEM analysis for confirmation of the SEM results. This study is based on grains studied previously by SEM-CL (chapters 2 and 4), FSE imaging and EBSD (chapter 5), the TEM foils described in chapter 4 and three new TEM foils, which are listed in table 4.2. The quartz grains are from a range of different impact structures of different ages between 2.0 Ga and 3.6 Ma (see table 2.2 in chapter 2 and chapters 4 and 5). For a detailed description of the technical procedures, see chapters 2, 4 and 5.

7.3 Results

Shocked quartz grains can be grouped on the basis of characteristics that are observed in the SEM, using composite colour CL imaging, FSE imaging and EBSD mapping and in TEM, using bright field and diffuse dark field imaging and diffraction techniques (table 7.3). The microstructural characteristics of the grains in these groups are described below:

Group A grains: Single-crystal grains with only a few sets of red luminescent (healed) PDFs and Dauphiné twins with boundaries mostly parallel to PDFs (figure 7.1). PDFs can show contrast or be invisible in FSE images and are generally invisible in EBSD pattern quality maps. Dauphiné twins are observed in FSE images, but cannot be distinguished from other contrast changes (for example from subgrains) without quantification of the twin relation by EBSD measurements. In TEM bright field images, the PDFs consist of planes of high dislocation density and Dauphiné twin boundaries can be observed parallel to the PDFs.

Group B grains: Single-crystal grains with Dauphiné twins with boundaries mostly parallel to PDFs, but with both red (healed) and non-luminescent (amorphous) (parts of) PDFs (figure 7.2). Thick non-luminescent PDFs show a constant grey level in FSE images and can be seen as darker lines against a brighter crystalline matrix in EBSD pattern quality maps, because the

and the EBSD measurements). **c** Pattern quality map, showing thick amorphous PDFs as dark lines in a lighter matrix. Healed PDFs are not visible. **d** PQ +IPF map showing Dauphiné twin boundaries as pink lines. **e** TEM bright field image showing both amorphous PDFs (uniform grey) and healed PDFs (planes of high defect density). The diffraction pattern (inset) shows the grain is a single crystal and diffuse scattering confirms the presence of amorphous material. **f** FSE image of a grain from the El'gygytgyn crater with lighter and darker grey domains that show the geometry of shock-related Dauphiné twins (red arrows). PDFs are not visible in the FSE image, unless they are open. Dashed square shows the location of the image in **g**. **g** Composite colour SEM-CL image of the same grain as in **f**, showing non-luminescent (black arrow) and weakly red luminescent (white arrow) parts of PDFs. The location of the indicated PDFs is also shown in **f** with a black and a white arrow.

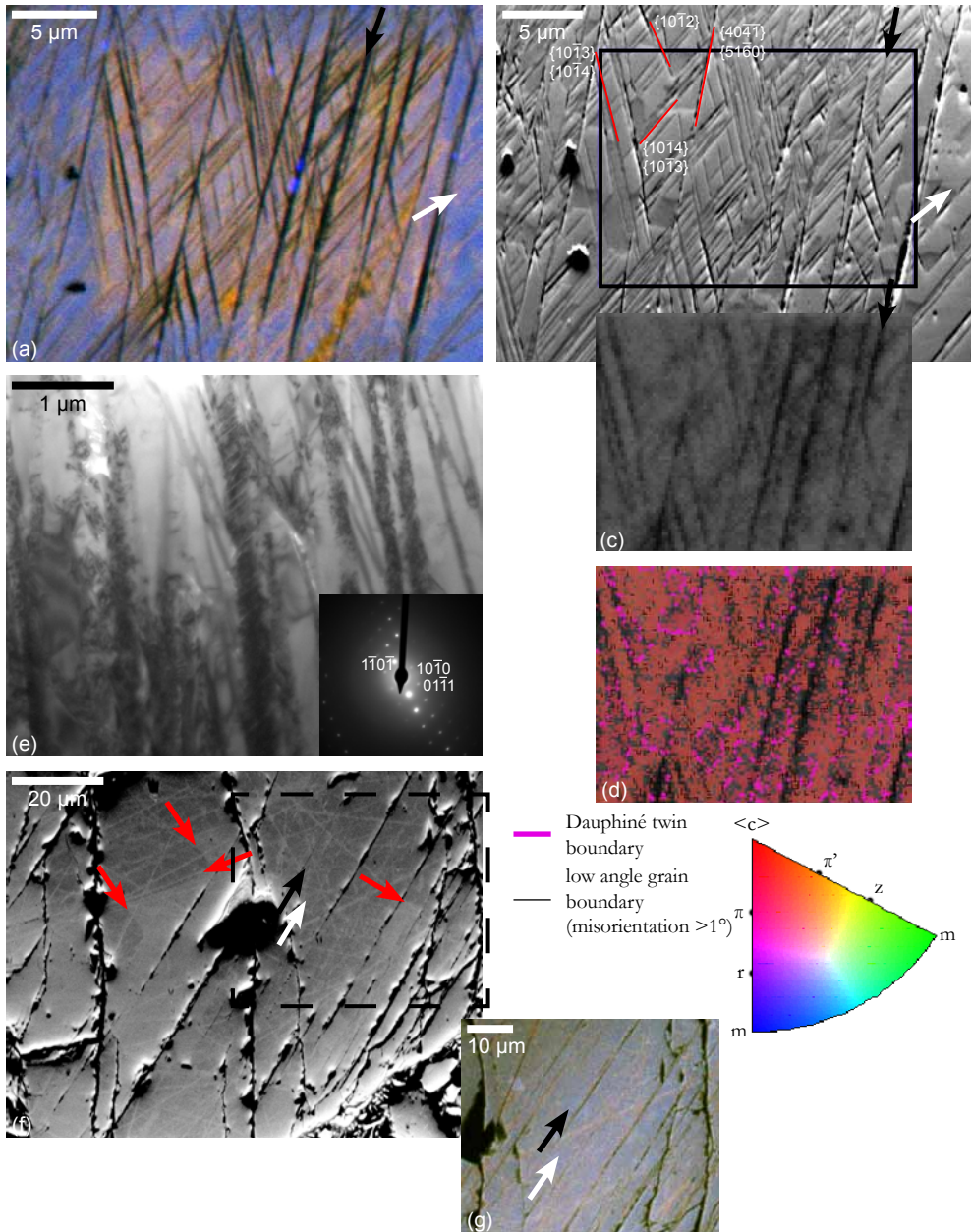


Figure 7.2 CL, FSE and EBSD images showing characteristic microstructures in grains in group B. **a** Composite colour CL image of a grain from the Ries crater, with red (white arrow) and non-luminescent (black arrow) PDFs. The redder rectangular area is the result of minor beam damage during EBSD mapping (shown in c and d). **b** FSE image of the same area is in a. Non-luminescent (amorphous) PDFs are clearly visible, while red (healed) PDFs can in most cases not be seen. The black box indicates the location of the EBSD maps shown below the FSE image. Dauphiné twins (see also d) can be recognised as lighter and darker domains in between the PDFs. Crystallographic planes that are consistent with the PDF orientations in this grain are indicated (based on trace analysis

amorphous material in the PDFs gives no bands in diffraction patterns. Red luminescent PDFs do not always show contrast in FSE images and are generally invisible in pattern quality maps. TEM again shows that the non-luminescent PDFs are amorphous, while the red luminescent PDFs contain a large number of defects. Some Dauphiné twin boundaries parallel to PDFs are also observed.

Group C grains: Microcrystalline grains with a very high density of closely spaced, crosscutting red luminescent (healed) PDFs (figure 7.3). These grains consist of microdomains that can be observed in FSE images. In TEM, the structure consists of blocky crystalline domains bounded by healed PDFs. Streaking of the outer diffraction spots shows the slight misorientation of the domains. This TEM structure was described previously as mosaicism (Leroux and Doukhan, 1996; Trepmann, 2008). TEM analysis suggests that the diffraction contrast that is observed between blocky crystalline domains in the grain in figure 7.3 is due to a Dauphiné twin relationship between some domains.

Group D grains: Microcrystalline grains with a very high density of thick, closely spaced, crosscutting red (healed) and non-luminescent (amorphous) (parts of) PDFs, with slight thickness variations and curvature (figure 7.4). Although CL images clearly show PDFs in this grain, the presence of PDFs is not as obvious in the corresponding FSE images of the same area. Instead, FSE shows sub-micrometer scale blocky domains of different grey level, with boundaries that define a trend parallel to the PDFs in the CL image. Some parts of PDFs are decorated by voids, which could be fluid inclusions or empty parts of PDFs due to differential polishing effects. EBSPs (electron backscatter diffraction patterns) from this grain are weak (often too weak to index). In a similar grain in the same thin section (figure 7.4e), PDFs can be seen in the pattern quality map as darker lines in a lighter matrix (figure 7.4f), but in most grains of this type, EBSPs are very weak and mapping provides very little information. TEM shows a microcrystalline grain structure, with slightly misoriented domains indicated by streaking of diffraction spots (figure 7.4b). Although it is not directly observed in the TEM images, some diffuse scattering in the diffraction pattern suggests the presence of amorphous material in the grain.

Group E grains: Almost completely amorphous grains with a very high density of wide, closely spaced, crosscutting non-luminescent (amorphous) PDFs, with slight thickness variations and curvature (figure 7.5). EBSPs from this grain are very weak and could not be automatically indexed by the EBSD software, indicating that the crystal structure of the grain is highly distorted and possibly nearly amorphous. TEM analysis confirms that a large portion of the grain consists of thick amorphous PDFs (bright in diffuse dark field images), but in between the amorphous lamellae, small crystalline domains remain. Streaking of the diffraction spots shows that the crystalline domains are slightly misoriented with respect to each other. Diffuse scattering in the diffraction pattern confirms the presence of amorphous material. Some of the grains in this group appear as (almost) diaplectic glass in light microscopy.

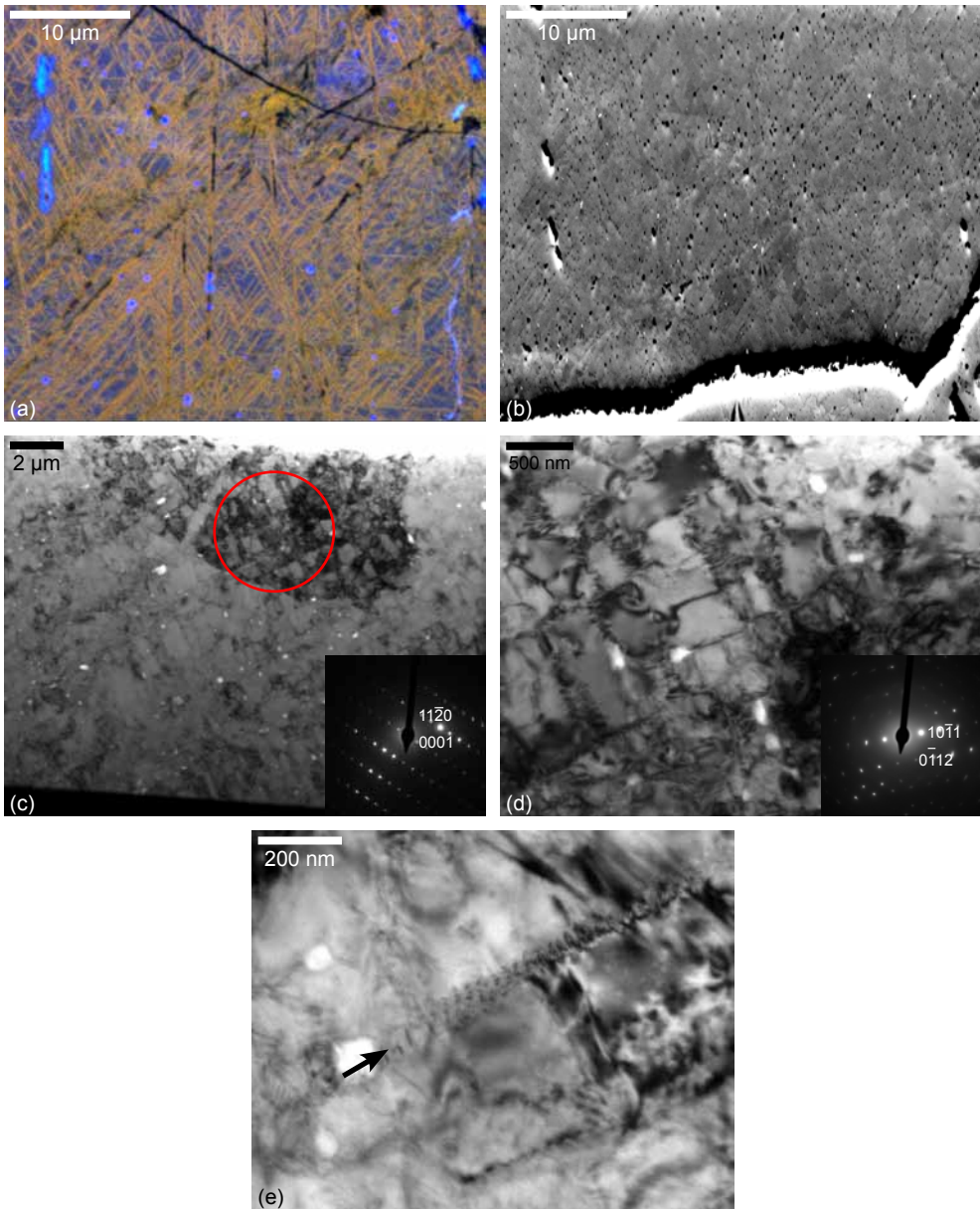


Figure 7.3 CL, FSE and EBSD images of grains in group C. **a** Composite colour CL image of a grain from the Rochechouart structure with a high density of cross-cutting red luminescent PDFs. **b** FSE image of the area immediately below the area shown in a. Small scale, sometimes blocky (white arrow) domains with varying contrast can be seen. **c** TEM bright field images of the same grain, showing that the grain consists of blocky microdomains bound by PDFs. Minor streaking of the outer diffraction spots (inset) indicates a slight misorientation between the blocky domains. The single diffraction pattern of the area indicated by the red circle suggests that the contrast differences between blocky domains are probably Dauphiné twins. **d, e** Higher magnification TEM bright field images show that the PDFs are healed and consist of arrays of dislocations (black arrow).

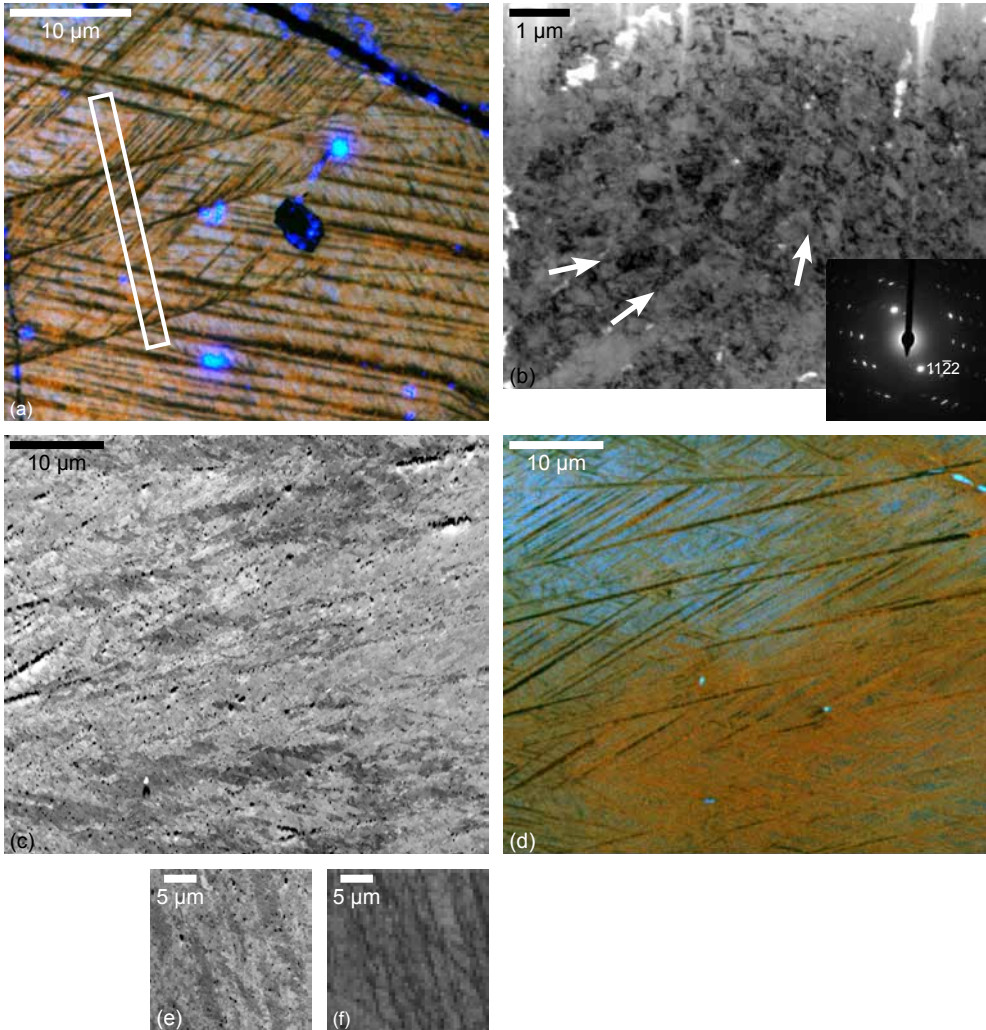


Figure 7.4 CL, FSE and EBSD images of grains in group D. **a** Composite colour CL image of a grain from the Ries crater, with both red and non-luminescent parts of PDFs. The white rectangle shows the location of the TEM foil shown in **b**. **b** TEM bright field image of the grain shown in **a**. The image reveals a microcrystalline grain structure with slightly misoriented domains (streaking of diffraction spots in inset), sometimes with a blocky shape. PDFs are very hard to see, but some directions are indicated by the white arrows. Some planes that correlate with PDFs in the CL image are porous in the TEM section (holes on the top left and on the edge of the image area on the left). Minor diffuse scattering in the diffraction pattern suggests the presence of some amorphous material, but this was not imaged. **c** FSE image of another grain from the same specimen, showing small scale blocky domains and domains following the orientations of the PDFs in **d**, but individual PDFs cannot be discerned, unless they are open or decorated with voids. **d** Composite colour CL image of the same area as in **c**, showing both red and non-luminescent parts of PDFs. Voids that are visible in **c** are also non-luminescent. **e** FSE image of a similar grain in the same sample as **c** and **d**, showing similar characteristics. **f** Pattern quality map of the area shown in **e**, with PDFs showing as dark lines in a lighter matrix, suggesting the presence of amorphous PDFs.

7.4 Discussion

7.4.1 SEM versus TEM

Table 7.1, which summarises the information that can be obtained from TEM and SEM, illustrates that a combination of SEM techniques can be sufficient for a full first characterisation of shock microstructures in quartz. The main reason for studying shocked quartz using TEM techniques is that defects and microstructures can be observed in sufficiently high detail to determine the origin of planar microstructures (i.e. shock or tectonic). Additionally, crystallographic orientations of PDFs can be measured in TEM, although statistically relevant orientation data sets for shock pressure estimates can only be obtained using a universal stage in a light microscope (Ferrière et al., 2009). However, the detailed discussions in chapters 2, 4 and 5 and the examples in the current study show that SEM techniques can be used to distinguish between tectonic deformation lamellae and PDFs, and furthermore to characterise PDFs in more detail. Amorphous and crystalline quartz show different characteristics in SEM-CL images as well as in FSE images and EBSD pattern quality maps. Colour SEM-CL images can be used to distinguish between amorphous and healed PDFs (chapter 4), determine the number of PDFs and PDF sets and furthermore provide shape and (apparent) thickness characteristics. FSE imaging and EBSD pattern quality maps can give a first indication of the substructure of PDFs (amorphous or healed) and are especially useful to characterise the microstructure of the grain, for example whether it is microcrystalline or single crystal in nature or whether Dauphiné twins are present in the grain (chapter 5). Dauphiné twins can be identified by EBSD and imaged with FSE, microcrystallinity in the host grain is detected in FSE images, and a highly disordered to near-amorphous crystal structure is apparent from very weak or no EBSPs and weak FSE contrast. Additionally, the crystallographic orientation measurements recorded in EBSD maps can be used to estimate PDF orientations, or to complement universal stage data (Trepmann, 2008; Trepmann et al., 2005; Voorn, 2010; Voorn et al., 2010). In summary, the combination of SEM techniques provides the same type of information as TEM, so that further TEM analysis is not required for the reliable identification of PDFs in quartz. However, direct study of defects in shocked grains is only possible in TEM, because the CL emission, FSE contrast and EBSD characteristics of PDFs are only an indirect reflection of the underlying defect structure. When detailed study of defect structures is required or to resolve the presence of very thin amorphous PDFs, the TEM remains unchallenged as the highest resolution instrument.

When applying SEM methods to (shocked) quartz, a well polished, clean sample surface is crucial, in particular for FSE imaging and EBSD mapping. Although a carbon coating is necessary in high vacuum SEM systems, the best results are obtained when the thickness of the carbon layer is restricted to the absolute minimum that is required to avoid charging problems. Normally a layer of a few nm thickness should be sufficient. Furthermore, when more than one SEM technique is applied to the same sample area in a quartz sample to obtain a one to one correlation, CL imaging should be the first step in the procedure. The CL emission of quartz is rather sensitive to beam damage and can change as a result of electron irradiation (see also discussions in chapters 4 and 6). The higher voltages and currents required for BSE and FSE imaging and EBSD mapping with respect to CL imaging will inevitably affect the CL emission in the area of interest.

7.4.2 Healing effects at moderate and high shock pressure

The combined microstructural observations on PDFs and host quartz, plus the number of PDF sets and PDF density, show that grains have different types of microstructures, which can be interpreted as consecutive stages in a process of healing and recrystallisation, for grains that have experienced moderate and high shock pressure. This trend of healing stages in grains shocked at moderate and high pressure is illustrated in figure 7.6.

The number of PDF sets and PDF density in a grain are accepted relative shock pressure indicators and increase with increasing peak shock pressure (Ferrière et al., 2008; Grieve et al., 1996). Quartz grains of a single crystal nature with a low number and density of PDFs are therefore interpreted as the result of (relatively) low shock pressure (top part of figure 7.6). Healing and recrystallisation of these grains leads to single crystal grains, usually with Dauphiné twins, with healed PDFs consisting of arrays of dislocations or planes of high defect density, with a red CL emission in SEM-CL images (figure 7.1, top right in figure 7.6). An intermediate stage would result in a structure such as observed in the grain in figure 7.2 (top centre in figure 7.6), with both amorphous and healed PDFs present in the same grain.

Highly shocked grains (lower part of figure 7.6), with a high density of cross-cutting, thick PDFs, recrystallise to a TEM-scale blocky subgrain structure, that is also visible in FSE images. Unaltered grains consist of a high density of amorphous PDFs, with crystalline domains in between that are slightly misoriented with respect to each other (figure 7.5, figure 7.6 bottom left). As a whole these grains are close to complete amorphisation (diaplectic glass). If post-shock annealing takes place, the amorphous PDFs recrystallise and the tiny microcrystalline domains between the amorphous material grow to a microcrystalline grain structure with partly healed and partly amorphous PDFs (figure 7.4, figure 7.6 bottom centre). Although no amorphous PDFs have been observed directly in the TEM sample shown in figure 7.4b, diffuse scattering in the diffraction pattern (which was taken in an area without visible damage by the ion beam during sample preparation) suggests that some amorphous material is present in the grain. Furthermore the holes observed in some of the PDFs near the top of the TEM section could indicate preferential milling (damage by the ion beam during sample preparation) of amorphous material in the PDFs, unless the PDFs were originally porous. With continuing recrystallisation of PDFs a blocky structure with small, slightly misoriented domains bound by planes of high dislocation density (in fact healed PDFs) develops (figure 7.3, figure 7.6 bottom right). This interpretation of the TEM-scale blocky subgrain structure as healed highly shocked grains is consistent with the theory put forward by Trepmann (2008), who stated that the structure might be ‘...the result of crystallization of the amorphous phase present along a high density of rhombohedral PDFs during post-shock annealing’. Because grains shocked to high pressures may be heated to above the α - β transition temperature during or after shock, Dauphiné twin relations can be expected in these grains. However, their identification is challenging because the crystal structure in highly shocked grains is microcrystalline and disordered. Orientation measurements by EBSD are often not possible in these grains, because they produce weak EBSD patterns. However, TEM analysis suggests that the orientations of some blocky crystalline domains in the grain in figure 7.3 are indeed related by a Dauphiné twin relationship.

An estimation of the transition pressure from “moderate” to “high” shock microstructures in this model is not straightforward. Methods for shock barometry involving the number of PDF sets and their orientations are usually applied to whole thin sections instead of single grains, and

the methods were developed in light microscopy studies (Grieve et al., 1996). In SEM images, often a higher number of PDF orientations and more individual PDFs are observed than in light microscopy (see for example chapter 2). If we assume that standard shock barometry methods can be extrapolated to SEM observations on single grains, a rough estimate of the pressure range for moderate and high pressure microstructures can be made.

The group of microstructures that is interpreted as the result of moderate pressure (single crystals with Dauphiné twins) can be formed from ~ 10 GPa, when PDFs start to develop (Goltrant et al., 1992; Grieve et al., 1996; Stöffler and Langenhorst, 1994), but may occur over a range of pressures. In the grain shown in figure 7.2a-e and the top centre of figure 7.6, for example, the PDFs are very closely spaced and pervasive throughout the grain. Four different PDF orientations are present, which fit $\{10\bar{1}2\}$, $\{10\bar{1}3\}$, $\{10\bar{1}4\}$ and $\{40\bar{4}1\}$ orientations, indicating a shock pressure ~ 20 -25 GPa (Grieve et al., 1996). PDFs in grains that are interpreted to heal to the blocky subgrain structure (microcrystalline crystals with misorientations) are

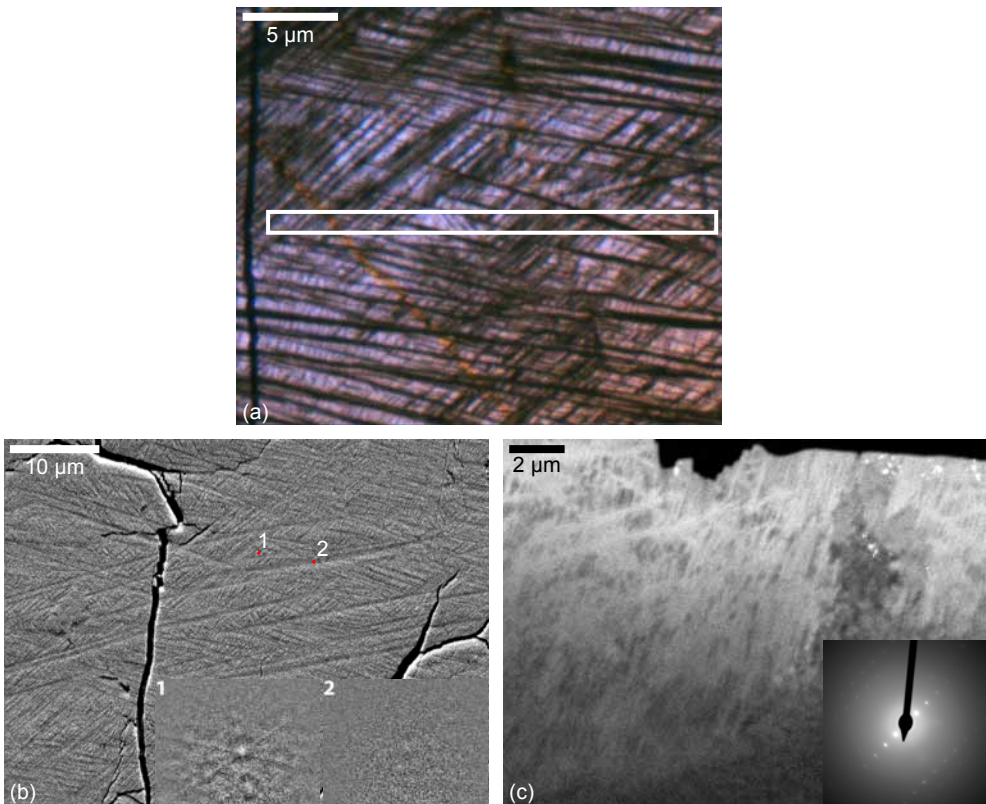


Figure 7.5 CL, FSE and EBSD images of grains in group E. **a** Composite colour CL image of a grain from the Ries crater with non-luminescent PDFs. The white rectangle shows the location of the TEM foil shown in **c**. **b** FSE image of the same grain as in **a**. Insets show EBSDs from quartz in between PDFs (1) and a wide PDF (2). EBSDs are too weak for mapping, but the insets show that no pattern comes from the PDF and only a very weak pattern from the host grain. **c** TEM diffuse dark field images, showing that PDFs are brighter than the remaining material in between. The diffraction pattern in the inset shows very strong diffuse scattering, confirming the amorphous nature of a large portion of the grain.

thicker and more irregular, with some thickness variations (unless they are healed, figure 7.3 and lower right in figure 7.6). These are PDF characteristics that were observed in experiments at pressures exceeding 25 GPa (Langenhorst, 1994). In these grains, a higher number of sets is often present (at least seven in the grain shown in figure 7.5 and the lower left of figure 7.6). Furthermore the grains in which these PDFs occur can be almost isotropic in light microscopy, indicating they are close to diaplectic glass, which forms around ~ 35 GPa (Grieve et al., 1996). These grains are therefore probably shocked to pressures between 25-35 GPa. Therefore, in our interpretation, the “moderate” pressure range is ~ 10 -25 GPa and “high” pressure is between 25-35 GPa. Especially in the moderate pressure range, more detailed pressure estimations can be made based on number of PDF sets and PDF orientations (Ferrière et al., 2008; Grieve et al., 1996; Holm et al., 2011; Hörz, 1968; Robertson, 1975). Of course, (pre-)shock temperatures may influence the pressure ranges at which these microstructures form (e.g. Langenhorst, 1994; Langenhorst and Deutsch, 1994).

If the interpretation of microstructures in terms of healing of grains shocked to moderate and high pressure is correct, one would expect to find a low density of thin, amorphous (non-luminescent) PDFs, probably with Dauphiné twins, in unaltered quartz grains shocked to low or moderate pressures. However, these grains are not observed in our sample set, even in a recent crater like El'gygytyn (3.6 Ma – figures 7.2e and f). All PDFs in our samples appear to have experienced some post-shock alteration. Exclusively non-luminescent PDFs are only observed in highly shocked grains – the grains with a very high density of thick, irregular, amorphous PDFs such as the one shown in figure 7.5. As was discussed in chapter 4, this could mean that the thin amorphous PDFs that form at moderate shock pressures are not non-luminescent, or that they heal more quickly than the thicker amorphous PDFs and are therefore not observed in our set of natural samples. SEM-CL imaging and TEM analysis on quartz shocked experimentally in the lower pressure range of PDF formation could fill the gap in the observations in this study and test our interpretation.

7.4.3 Mosaicism

The TEM-scale blocky subgrain structure observed in the grain in figure 7.3 has been described as mosaic in previous studies (e.g. figure 6 in Leroux and Doukhan, 1996; figure 4 in Trepmann, 2008). Trepmann (2008) explicitly interprets the structure as a healed high density of cross-cutting PDFs. While Leroux and Doukhan (1996) see mosaicism as a brittle process (shattering of the crystal), they also propose that the TEM-scale mosaic structure they observe in quartz from the Manson impact structure might be the result of intersecting sets of PDFs, which divide the quartz into small domains. In their view, localised strain in the amorphous PDFs might enable slight rotation and misorientation of the individual domains, which seems contradictory to formation of the structure by shattering. Leroux and Doukhan (1996) furthermore observe more mosaic grains at higher shock pressure: in the Manson drill core they found grains with some mosaicism and a high PDF density at 51m depth (estimated shock pressure 25-35 GPa), changing to almost only mosaicism at 77m depth (estimated shock pressure 35-45 GPa).

The microstructures observed in our samples are consistent with formation of the blocky subgrain structure by crystallisation of a high density of amorphous PDFs. A large number of cross-cutting PDF would divide the grain in small crystalline blocks, with amorphous material around them. Misorientation of the blocks may be accommodated by volume changes during

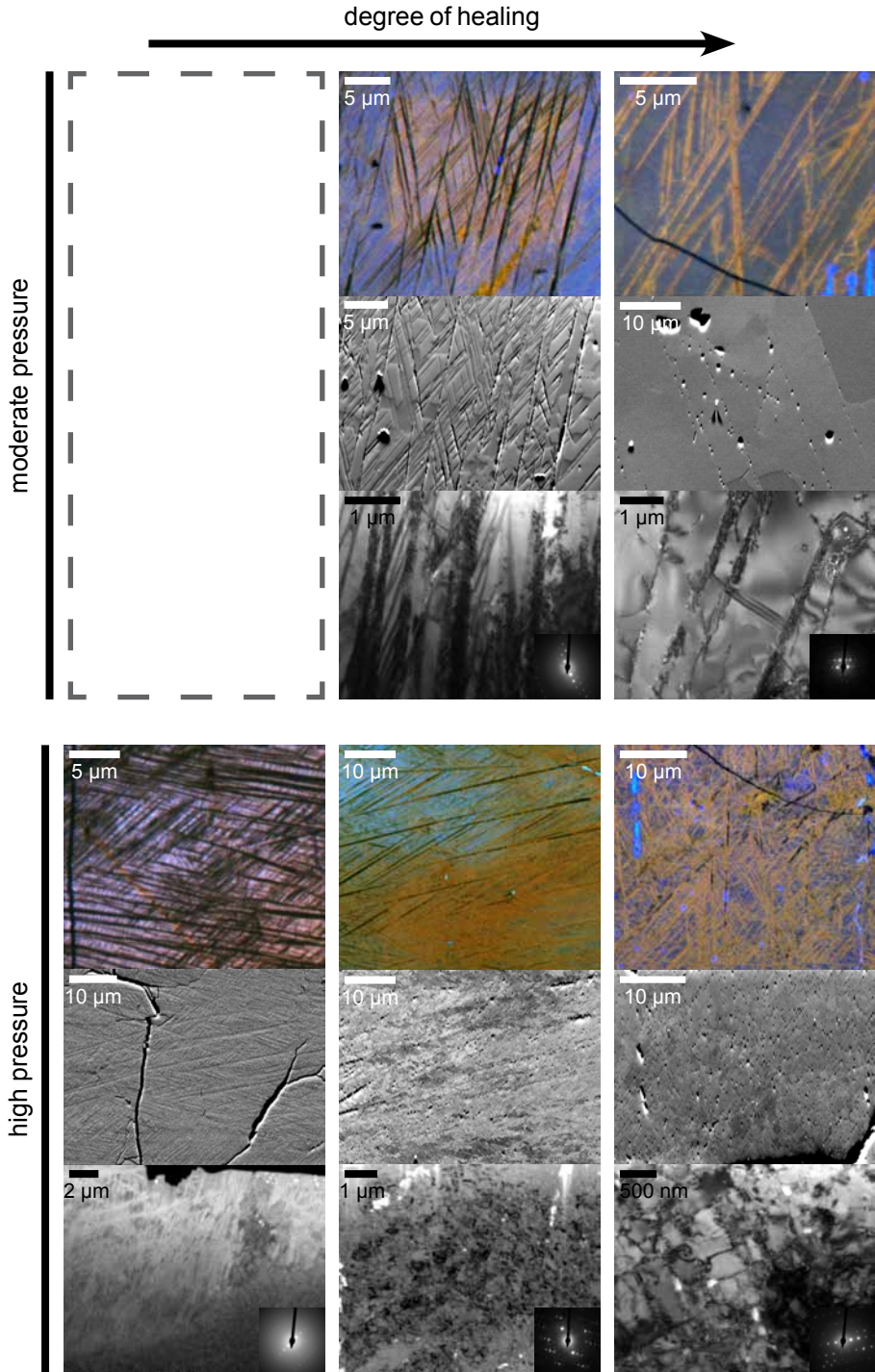


Figure 7.6 Schematic representation of the healing trend in moderately and highly shocked quartz grains, based on the interpretation of representative microstructures shown in figures 7.1-7.5.

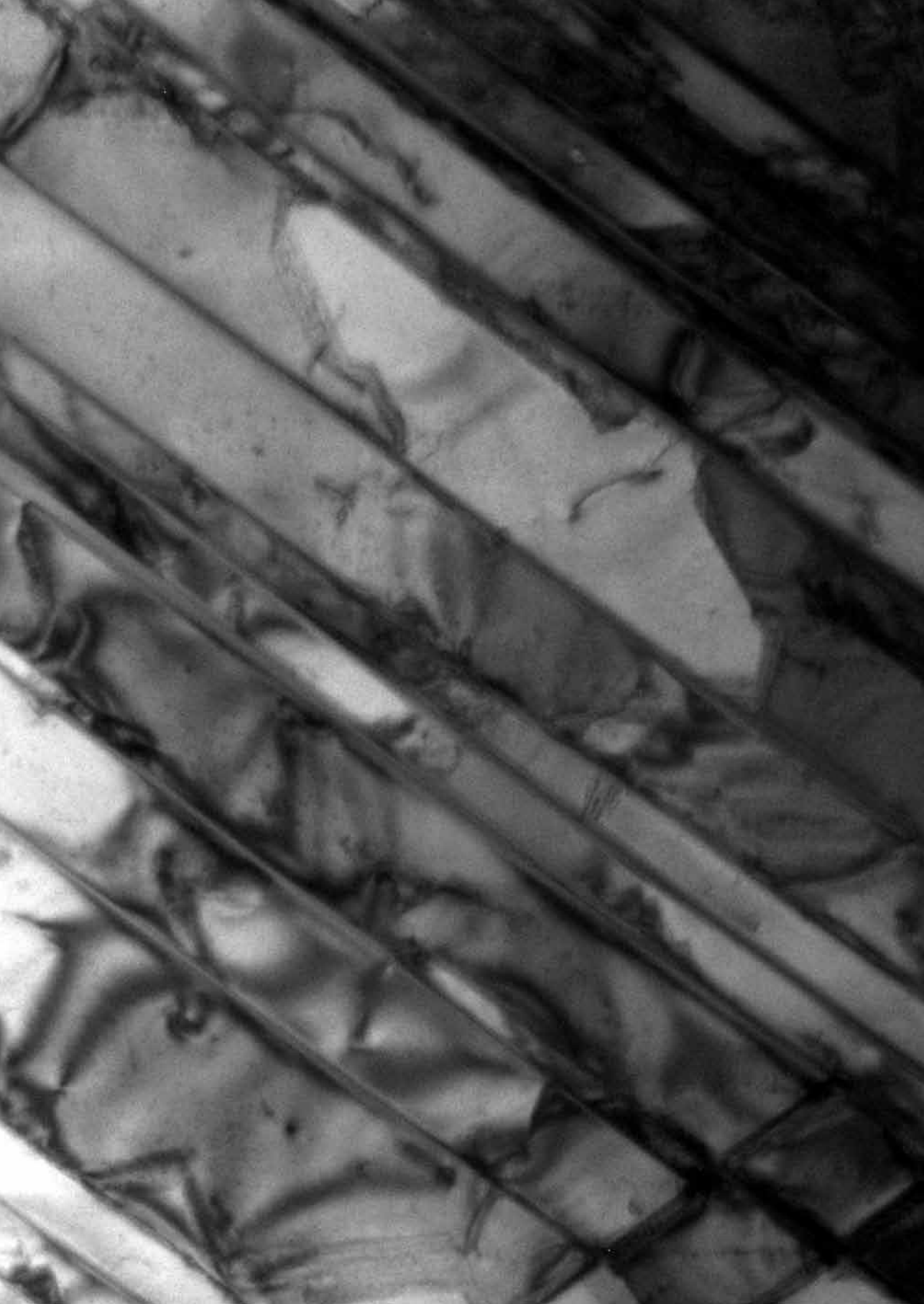
compression and release, which allow a certain amount of freedom for relative movement of the crystalline domains surrounded by the amorphous PDFs. Depending on the compressibility of the amorphous phase, also some internal strain (lattice bending or rotation) might occur in the individual blocks. Subsequent crystallisation of the amorphous PDFs during post-shock high temperatures or metamorphic events will lead to the microcrystalline or blocky subgrain structure observed in this paper and by Leroux and Doukhan (1996) and Trepmann (2008). As Trepmann (2008) suggested, this interpretation implies that the blocky subgrain structure observed at the TEM-scale and in FSE images can be seen as an indication for high shock pressure, probably $>25\text{-}30$ GPa, just before the onset pressure for diaplectic glass formation.

In earlier light microscopy and X-ray diffraction studies, mosaicism was interpreted as a plastic response of quartz, shocked at or above the Hugoniot elastic limit (HEL), which distorts the lattice into misoriented microdomains (Huffman et al., 1993; Huffman and Reimold, 1996; Stöffler and Langenhorst, 1994). This structure is observed at low shock pressures and also in grains without PDFs, in both natural and experimentally shocked samples (e.g. Huffman and Reimold, 1996). The mosaic structure observed in low pressure samples cannot form as described above, by crystallisation of cross-cutting, amorphous PDFs. We therefore suggest that mosaicism on the scale of the light microscope and the TEM-scale blocky subgrain structure observed in our samples and in Leroux and Doukhan (1996) or Trepmann (2008) are microstructures that form by different mechanisms, but result in similar characteristics, especially in diffraction patterns. Mosaicism occurs as a primary shock microstructure at moderate pressures from $\sim 10\text{-}25$ GPa (Huffman and Reimold, 1996), while the blocky subgrain structure forms as a healed microstructure in grains shocked to higher pressures, exceeding ~ 25 GPa, as proposed by Trepmann (2008).

7.5 Conclusions

TEM observations on (potentially) shocked quartz grains are usually carried out with the aim of confirming the shock origin of planar microstructures, to determine the substructure of PDFs (i.e. amorphous vs. healed), the microstructure of the grain and in some cases PDF orientation. These microstructures can all be assessed in the SEM, and on much larger samples. Without any doubt the TEM provides a lot more detailed observations that can be of great value, but the SEM is a valuable addition and alternative to existing techniques for identifying and characterising shocked quartz. This is illustrated by the combined CL, FSE and EBSD observations in this paper, that show moderately and highly shocked quartz grains at different stages of healing, and indicate that TEM-scale mosaicism is healed high pressure microstructure.

Acknowledgements – Uwe Reimold and Jörg Fritz are thanked for kindly providing the experimentally shocked samples, Uwe Reimold and Uli Raschke for the El'gygytgyn sample, Roald Tagle for the Popigai samples and Rodger Hart for the Vredefort samples. Pim van Wamel has been of great help during sampling at the Ries crater, and Philippe Lambert at Rochechouart.



Chapter 8

Afterthoughts – mechanical twinning and the formation of planar deformation features in quartz

Shocked quartz is of crucial importance for the reliable identification of terrestrial meteorite impact structures and impact related stratigraphic levels. Extensive studies of shock microstructures in quartz have shown a wide range of effects, including planar deformation features (PDFs), planar fractures and mechanical Brazil twins in the basal plane. Also Dauphiné twins have been observed in shocked quartz grains with PDFs, but no consensus exists on their formation mechanism. In general, shock effects occurring in quartz in the lower shock pressure range between ~5-10 GPa, in the transition from brittle deformation to phase transformations, are less well-characterised than high pressure effects.

In this chapter, preliminary analysis of a quartzite sample that was experimentally shocked to 8 GPa presents direct evidence for mechanical Dauphiné twinning. PDFs are observed in SEM and TEM analysis, but not in a light microscope. These PDFs are amorphous lamellae with unusual geometry and spacing compared to conventional PDFs. We suggest that these anomalous PDFs may have developed on non-basal, mechanical Brazil twin planes and that PDF formation in the low shock pressure regime is closely related to mechanical twinning.

8.1 Introduction

Of all minerals exhibiting shock metamorphic effects, quartz is most extensively studied. Because quartz is one of the main constituents of the Earth's crust and because it is resistant to weathering and therefore stable over geological time spans, it is widely used as a shock indicator in both impact structures and ejecta layers. A wide range of microscopic shock effects can occur in quartz. At relatively low shock pressures (< 10 GPa) mechanical Brazil twins in the basal plane (0001) form as a result of high shear stress (Carter, 1965; Goltrant et al., 1991; McLaren et al., 1967) and planar fractures form in the basal plane and in low-index rational planes. At higher pressures (10-35 GPa) PDFs form: thin amorphous lamellae with a crystallographically determined orientation, most frequently occurring parallel to $\{10\bar{1}3\}$, $\{10\bar{1}2\}$ and $\{10\bar{1}1\}$. Above ~ 35 GPa quartz transforms to an amorphous phase (diaplectic glass) and at even higher pressures and temperatures melt glass (lechatelierite) forms (French and Koeberl, 2010; Grieve et al., 1996 and references therein; Stöffler and Langenhorst, 1994). Another frequently observed shock effect reported in recent studies is the presence of Dauphiné twins that are closely related to PDFs (chapter 5; Chen et al., 2011; Trepmann and Spray, 2005; Wenk et al., 2011; Wenk et al., 2005). For impact-related Dauphiné twins, both a mechanical origin (Chen et al., 2011; Wenk et al., 2011; Wenk et al., 2005) and formation during back-transformation from β - to α -quartz (Trepmann and Spray, 2005) have been proposed. In chapter 5 a model was discussed in which mechanical Dauphiné twinning plays an important role in the onset of PDF formation. It was also suggested that a similar relationship might exist between shock-induced mechanical Brazil twins and PDFs.

Although shock effects in quartz have been extensively studied in the last decades, the lower pressure range and the transition from brittle to plastic deformation and phase transformations have remained relatively underexposed. In the context of distinction between shock-related and tectonic deformation, the low pressure regime, where shock and tectonics overlap and might form similar microstructures, this is an important range to study. Here, in order to specify the relationship between mechanical twinning and PDF formation in quartz and test the hypothesis that they are closely related, we analyse microstructures in a quartzite shocked experimentally at relatively low pressure (8 GPa). The results and discussion in this chapter are very preliminary and speculative, but show the potential for further research in the lower shock pressure regime.

8.1.1 Mechanical twinning in shocked quartz

8.1.1.1 Brazil twins

Mechanical Brazil twins in the basal plane of quartz are a well-known microstructure in naturally shocked quartz. These twins form under high deviatoric stress exceeding ~ 2 GPa and are produced by basal $\langle a \rangle$ shear (McLaren et al., 1967). Twin planes are therefore normally bound by twin dislocations. Trepied and Doukhan (1978) argued that also in $\{10\bar{1}1\}$, which is a common orientation for growth Brazil twins, Brazil twins can form mechanically by successive $a/2$ shears in adjacent $\{10\bar{1}1\}$ planes.

Brazil twins are not visible in thin section in a light microscope, unless they are decorated by voids or fluid inclusions, but are detected in transmission electron microscopy and can be imaged using cathodoluminescence in the scanning electron microscope (SEM-CL) (see chapters 2, 4 and 6).

8.1.1.2 Dauphiné twins

Mechanical Dauphiné twinning does not accommodate any deformation or change the crystal lattice across the boundary, but reverses positive and negative a-axes and changes the stiffness of the twinned region, making the mineral more easily elastically deformable. Dauphiné twinning aligns the positive r $\{10\bar{1}1\}$ planes perpendicular to the direction of highest compressive stress, resulting in a preferred orientation of the positive and negative rhombohedra (Menegon et al., 2011; Tullis and Tullis, 1972; Wenk et al., 2005).

Dauphiné twin boundaries are not bound by twin dislocations and can, theoretically, occur on any plane (Trepied and Doukhan, 1978). However, in practice, mechanical Dauphiné twin boundaries seem to be confined to the basal c (0001) and prism m $\{10\bar{1}0\}$ planes (Lloyd, 2004; Zinserling and Schubnikow, 1933), although no systematic evaluation of orientations of mechanical Dauphiné twin boundaries is reported in the literature.

Like Brazil twins, Dauphiné twins are not visible in light microscopy, because the twinning process does not affect the optical axis in quartz (the c -direction). However, the twins can be observed in the SEM (in high quality, high magnification CL images (see chapter 6), in forescatter electron images and in electron backscatter diffraction maps) and in TEM.

8.2 Material and methods

The sample used in this study is an experimentally shocked (8 GPa) Hospital Hill quartzite. Experimental details are presented in the original studies by Reimold and Hörz (1986a, b). In these studies, only extensional fractures, but no PDFs were previously reported in this sample. This is as expected at a shock pressure of 8 GPa, as only mechanical basal Brazil twins and fractures form at pressures below 7-10 GPa (Stöffler and Langenhorst, 1994).

In the current study, we used composite colour scanning electron microscopy cathodoluminescence (SEM-CL) imaging on a polished thin section and transmission electron microscopy (TEM) analysis of a foil prepared from the thin section in an SEM with focussed ion beam. A detailed description of the techniques can be found in chapter 4.

One grain ('grain 1') in the polished thin section was first imaged using composite colour SEM-CL and secondary electrons (SE). Subsequently a TEM foil, 100-200 nm thick, was prepared from this grain using a focused ion beam for precise location of the TEM sample. Before thinning down to the final thickness, the thick TEM foil was imaged using SEM-CL and SE. The thick foil was \sim 2-2.5 μ m thick (top-bottom).

A second grain ('grain 2') was studied in composite colour SEM-CL and SE images of the polished thin section.

8.3 Results

8.3.1 Cathodoluminescence and secondary electron imaging

Grain 1 shows one penetrative set of closely spaced, thin, red luminescent PDFs, trending NW-SE in figure 8.1a. Because the thin section was old and the adhesive fragile, the sample was not re-

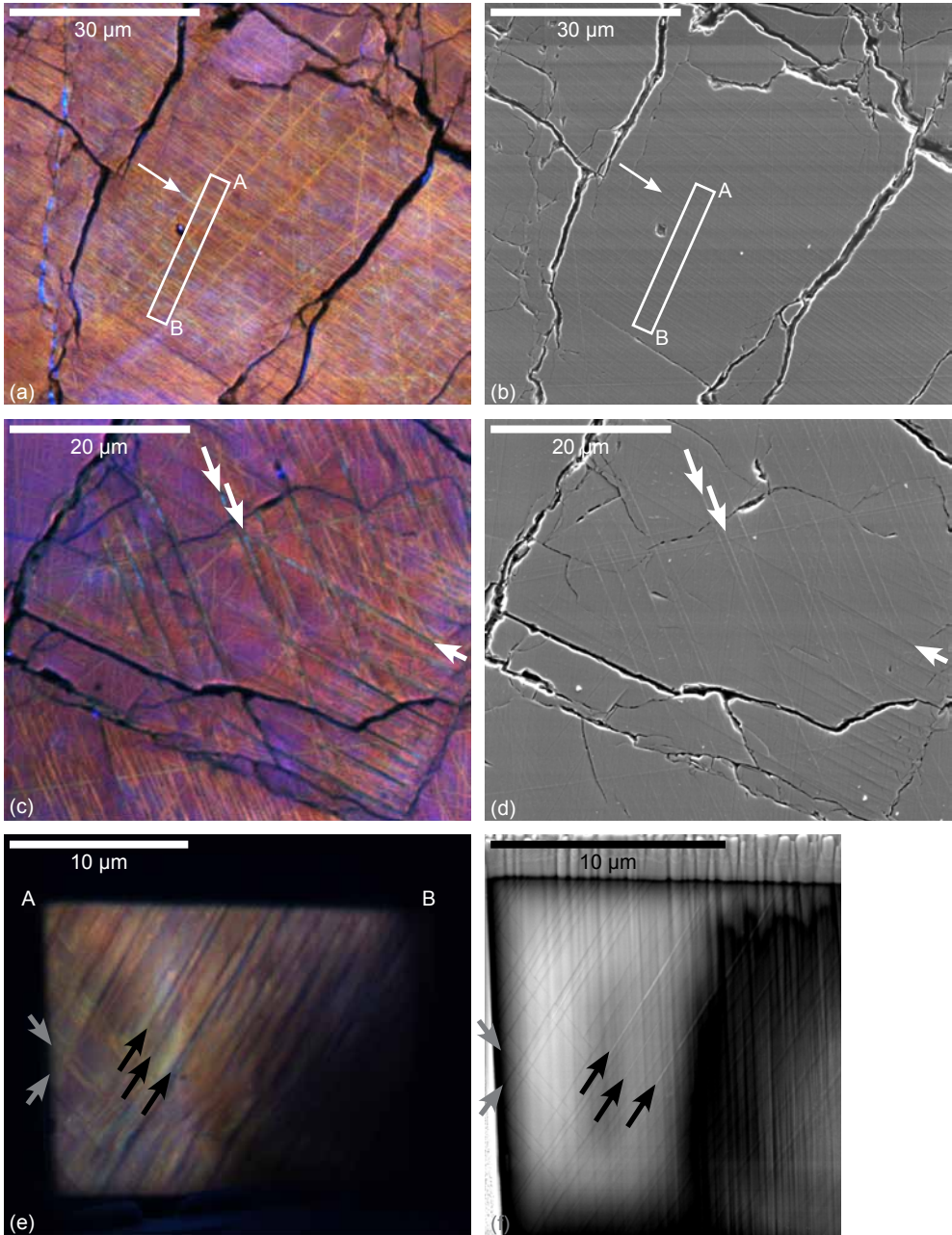


Figure 8.1 Composite colour SEM-CL and SE images of two quartz grains in the experimentally shocked sample. **a** Composite colour SEM-CL image of grain 1, showing one prominent, penetrative set of closely spaced, narrow, red luminescent PDFs. Some parts of PDFs are bright blue luminescent. Red luminescent lines in random orientations are polishing scratches. The white rectangle shows the location of the FIB-prepared TEM foil. A and B are indicated for relation of the orientation of the TEM foil to this image. **b** SE image of the same area as in **a**. PDFs (and some polishing scratches) are observed as thin lines of different contrast, that is probably mainly topography-related, but might

polished for SEM analysis, which is evident in the many polishing scratches that can be recognised in both CL and SE images (figures 8.1a-d). Although polishing scratches are often also red luminescent, they are in most cases easily distinguished from PDFs by their random orientation and non-parallel nature. Some small segments of PDFs are not red, but bright blue luminescent. The PDFs show weak contrast in the SE image in figure 8.1b; mostly they are slightly lighter than the rest of the grain, but also darker contrast can be observed. It is not evident whether the contrast is mostly a topography effect or also contains a density component. Especially the blue luminescent parts of PDFs appear light. This is more clearly observed in grain 2 (figures 8.1c and d).

In grain 2, two sets of PDFs are present (figures 8.1c and d). Some PDFs are red luminescent, but some parts of PDFs are non-luminescent or bright blue luminescent. The non-luminescent parts are wider than the narrow red luminescent PDFs. The blue and non-luminescent parts of the PDFs are clearly visible in the SE image in figure 8.1d. Again, especially the blue luminescent parts are brighter in the SE image, but the non-luminescent parts can be slightly darker than the surrounding quartz. In the lower left corner of the image is a part of the grain in which only red luminescent PDFs are present. These red PDFs show no, or only very weak, contrast in the SE image.

SEM-CL and SE images were recorded of the thick TEM foil of grain 1 before thinning to the final thickness of $\sim 100\text{-}200$ nm (figures 8.1e and f). The bright blue luminescence that is locally observed in the polished thin section is not present in the CL images of the thick foil. Many PDFs are red luminescent, but some are non-luminescent. An SE image of the thick foil is shown in figure 8.1f. Vertical lines are due to curtaining: an irregular milling effect that can occur when using a focussed ion beam at high current. The lighter and darker parts of the surface are probably a charging effect. In the SE image of the thick foil most PDFs are very narrow (max. 10s of nm) and straight and darker than the surrounding material. Some wider PDFs are brighter than the host grain (arrows in figure 8.1f). These correspond to thicker, non-luminescent PDFs in the CL image in figure 8.1e. The CL and especially SE images of the thick foil reveal the presence of a second set of PDFs (grey arrows in figures 8.1e and f), that is invisible in the SEM images of the polished thin section in figures 8.1 a and b. The second set of PDFs is oriented at an (apparent) angle of 74° to the main set. This second set is not as well developed as the first and is only present in part of the TEM foil.

also have a density component. Especially the bright blue luminescent parts are slightly brighter (white arrows in a and b). **c** Composite colour SEM-CL image of grain 2, showing two sets of PDFs, which are mostly red luminescent, but also contain non-luminescent or bright blue luminescent parts. **d** SE image of the same area as in c. PDFs in most regions in the grain show contrast in SE, except the red luminescent PDFs in the lower left corner of the image. Bright blue luminescent parts of PDFs are brighter than the surrounding quartz in the SE image (white arrows in the top centre) and also non-luminescent parts of PDFs are clearly visible (white arrow on the right hand side). **e** Composite colour SEM-CL images of the thick TEM foil. Two sets of PDFs are observed (grey arrows). Some are red luminescent, but also slightly thicker, non-luminescent PDFs occur (black arrows). A and B indicate the orientation of the TEM foil with respect to the polished thin section and correspond to A and B in figures 8.1a and b. **f** SE image of the thick TEM section with increased contrast, showing the two sets of PDFs (grey arrows). Most PDFs are slightly darker, but several are brighter than the rest of the grain (black arrows), suggesting a higher density. Vertical lines are curtaining, an effect of milling at high currents.

8.3.2 TEM

In TEM images of the foil cut from grain 1, both sets of PDFs observed in the SEM images of the thick TEM foil are clearly visible (figure 8.2a). The PDFs in the main set often occur in closely spaced pairs (figures 8.2c and 8.3a). The thickness of the PDFs ranges between ~ 10 - 30 nm, but is fairly constant in each individual PDF. In diffuse dark field images (figure 8.2a) the PDFs are brighter than the surrounding quartz, indicating the presence of amorphous material in the PDFs. No change in contrast (and hence no change in crystal orientation) is apparent on either side of the PDFs in the crystalline host grain. Also in TEM images, the second set of PDFs is observed (white arrows in figure 8.2a).

A subgrain boundary is present near the centre of the TEM foil, oriented N-S with a curve at the bottom (figures 8.2b and c). The PDFs cut through the subgrain boundary without detectable offset.

Dauphiné twins are present between the PDFs, indicated by single diffraction patterns recorded in areas showing different diffraction contrasts (figures 8.3b-f). The Dauphiné twins have boundaries that are often parallel in different parts of the grain and with large portions of their boundaries coinciding with PDFs. For two segments of twin boundary between PDFs, orientations could be estimated (figures 8.3c and d), which fit with $\{10\bar{1}0\}$ and possibly $\{2\bar{2}01\}$.

Some of the PDFs do not continue across the TEM foil, but apparently end in the middle of relatively undisturbed crystal. On closer inspection, the end of a lamella usually seems to be closely related to contrast features suggesting the presence of a dislocation or a Dauphiné twin boundary (e.g. figures 8.3a and e, white dashed arrows).

8.3.3 Crystallographic orientation of the PDFs

Combined information from geometrical relationships between the CL and TEM images, the orientation of the TEM section in the grain, and TEM orientation analysis indicates that the main set of PDFs has a $\{\bar{1}2\bar{1}2\}$ orientation, with the second set parallel to r $\{10\bar{1}1\}$.

As mentioned above, the second set of PDFs is not visible in the CL image of the polished thin section. This may be explained by the orientations of the PDFs. The second PDF set, that is only visible in the TEM section, is observed to continue close to the top of the thick section (figure 8.1f), which is the surface of the polished thin section. TEM diffraction patterns at different tilts (not shown) indicate that for this grain the basal plane is perpendicular to the surface of the polished thin section and one of the $\{11\bar{2}0\}$ planes is parallel to the surface of the polished thin section. In this orientation the traces of the $\{10\bar{1}1\}$ and $\{\bar{1}2\bar{1}2\}$ are parallel.

8.4 Discussion

8.4.1 Dauphiné twins

TEM analysis shows that many small Dauphiné twins are present in the grain, closely related to the PDFs: large portions of the twin boundaries are parallel to the PDFs and the twin boundaries do not cross PDFs. The close association of the Dauphiné twins with the PDFs suggests that the twins were formed by the shock event. Because the sample has been shocked to a peak

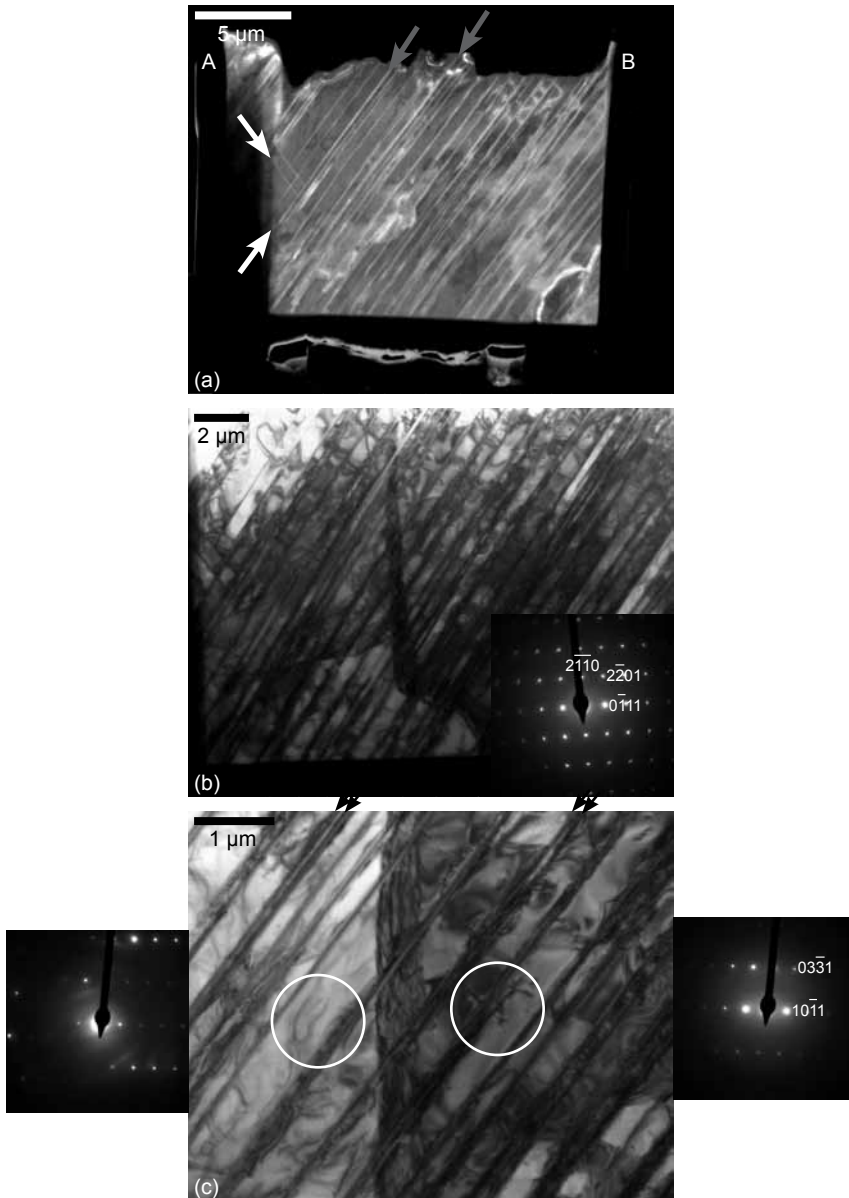


Figure 8.2 TEM images of the thin TEM foil. **a** Diffuse dark field image, showing the PDFs as thin bright lines in a darker matrix, indicating that the PDFs are amorphous. White arrows indicate the two orientations A and B correspond to A end B in figure 8.1a and b. **b** Bright field image showing the penetrative character and close spacing of the PDFs and the presence of a subgrain boundary in the centre of the foil (vertical). **c** Bright field image at high magnification showing the subgrain boundary in more detail. Diffraction patterns left and right of the subgrain boundary show the slight orientation difference across the boundary. PDFs cross the boundary without noticeable offset. Black arrows indicate closely spaced pairs of PDFs.

shock pressure of only 8 GPa at room temperature, it is highly unlikely that the shock or post-shock temperature has exceeded the α - β transition temperature (573°C at ambient pressure and increasing with increasing pressure) at any stage. Shock and post-shock temperatures in quartzite shocked to 8 GPa are on the order of 100°C and stay far below 500°C (e.g. figure 4 in Stöffler, 1972; figure 6 in Stöffler and Langenhorst, 1994). The twins can therefore not have formed during back transformation from β - to α -quartz and must be mechanical. This interpretation is supported by the observation that short segments of the Dauphiné twin boundaries in the crystal between the PDFs are straight and often parallel in different parts of the TEM section. This suggests that the orientation of the boundaries is crystallographically determined.

No amorphous material was detected on Dauphiné twin boundaries, so the hypothesis that amorphous PDFs might preferentially form on Dauphiné twin boundaries, which was proposed in chapter 5, cannot be confirmed.

8.4.2 Red luminescent amorphous PDFs

The PDFs in grain 1 are brighter than the surrounding quartz in TEM DDF images, indicating they are amorphous. In the composite colour SEM-CL images in figure 8.1a the same features are red luminescent. In chapter 4 we showed that non-luminescent PDFs are amorphous, while healed PDFs and basal Brazil twins are red luminescent. The correlation between the FIB-prepared TEM foil and composite colour SEM-CL images of grain 1 in the current chapter clearly shows that thin amorphous PDFs formed at low shock pressure can be red luminescent. This possibility was briefly discussed in chapter 4, but no such PDFs were observed in that study. The observation of red luminescent amorphous PDFs suggests that in samples shocked to lower pressure, the SEM-CL imaging method can only be used to identify PDFs, but it is not a reliable technique to distinguish between thin amorphous PDFs and healed PDFs or Brazil twins. However, it should be noted that the PDFs studied in chapter 4 were all visible in light microscopy, while the thin amorphous PDFs in grain 1 in this chapter are not and can only be observed in SEM and TEM images. Therefore, for PDFs that are visible in a light microscope and especially in highly shocked grains, such as those shown in figure 4.1 in chapter 4, SEM-CL imaging is still a useful distinction technique. For low shock samples, additional TEM analysis might be required to confirm the amorphous nature of PDFs, although the presence of inclusions decorating PDF planes is a strong indication of a healed structure.

The blue luminescence in parts of the PDFs (figures 8.1a and c) indicates the presence of a different phase. This might be a high pressure phase, as in chapter 4, blue luminescence was observed in a high density phase (possibly stishovite) within amorphous PDFs. However, no evidence for the presence of stishovite or another crystalline high pressure phase was found in the sample studied in this chapter during TEM analysis and the bright blue luminescence was also not observed in the thick TEM foil. No definitive interpretation of the blue luminescent phase can be provided from these data.

The SE images of the polished thin section and the thick foil indicate the potential presence of a higher density (brighter) phase in several PDFs. In TEM diffuse dark field images of the thin foil, these PDFs correspond to the broadest and apparently slightly brighter amorphous PDFs (three PDFs are indicated in figure 8.1f, of which the two clearest examples are indicated by grey arrows in figure 8.2a). These PDFs are non-luminescent in the CL images of the thick section (figure 8.1e, black arrows). This suggests a transition between red luminescent, very

narrow amorphous PDFs to thicker, non-luminescent amorphous PDFs, such as observed in the previous chapters.

From this preliminary study it is unclear what causes the difference between red and non-luminescent amorphous PDFs. As the sample studied in this chapter has been shocked to relatively low pressure, it is possible that the structure in these PDFs is less disordered than in PDFs in more highly shocked grains. The PDFs in this grain are so thin that they are not visible in a light microscope, which shows that not much damaged material is present. Temperature might also play a role, as grains shocked to higher pressures have inevitably experienced higher temperatures than low shock samples. The local presence of thicker, non-luminescent parts of PDFs, such as in grain 2 and in the thick TEM foil of grain 1, might reflect locally increased shock pressure and/or temperature.

No quantification of the red CL emission of the PDFs in this grain is available, but it is likely that it is related to the nonbridging oxygen hole centre (NBOHC) defect that is generally responsible for the red CL emission with peak at 650 nm in both crystalline and amorphous SiO₂ (e.g. Götze et al., 2001; Stevens Kalceff, 2009; Stevens Kalceff and Phillips, 1995; Stevens Kalceff et al., 2000). The NBOHC defect can be related to strained Si-O bonds, OH groups, alkali ions and peroxy linkages (Si-O-O-Si) and can form by radiolytic dissociation of these precursors under electron beam irradiation (Stevens Kalceff and Phillips, 1995).

8.4.3 Brazil twins?

Although the microstructures observed in grain 1 are clearly amorphous PDFs, they show unusual and interesting characteristics. The PDFs are extremely narrow (~10-30 nm) and are not visible in a light microscope. The structures are very straight and penetrative through most of the grain. Furthermore, TEM images showing the PDFs edge on (e.g. figures 8.2c and 8.3a) reveal that they often occur in closely spaced pairs. Similar structures have been reported in two previous studies (Cordier et al., 1993; Gratz et al., 1988).

In quartz crystals deformed using a diamond anvil cell, Cordier et al. (1993) observed straight, very narrow (~10 nm) lamellae parallel to low index planes, some with the same orientation as observed in our sample, $\{\bar{1}212\}$. The lamellae described by Cordier et al. occurred at low pressure, probably <5 GPa, and, when tilted, show an irregular fringe pattern. Several hypotheses for the origin of these lamellae were put forward, including cleavage, twinning and very narrow amorphous lamellae, but the structures could not be fully explained.

In shock loading experiments on previously deformed single quartz crystals, Gratz et al. (1988) reported observing thin (~5 nm) amorphous lamellae parallel to the basal plane of quartz in crystals shocked to a peak pressure of 12 GPa. These lamellae occurred in very closely spaced arrays that were usually connected to fractures.

Based on the geometrical and shape characteristics of the low shock PDFs observed in this and the two previous studies, we suggest that these features may originally have been Brazil twins, but have transformed to amorphous lamellae due to preferential shock amorphisation in the Brazil twin boundary plane. The contrast at the tip of some PDFs suggesting the presence of a dislocation is consistent with this interpretation. Composite colour SEM-CL images (figure 8.4) of the grain studied here, mechanical Brazil twins in quartz from the Vredefort structure and growth Brazil twins in the single crystal studied in chapter 6 further illustrate the similarities

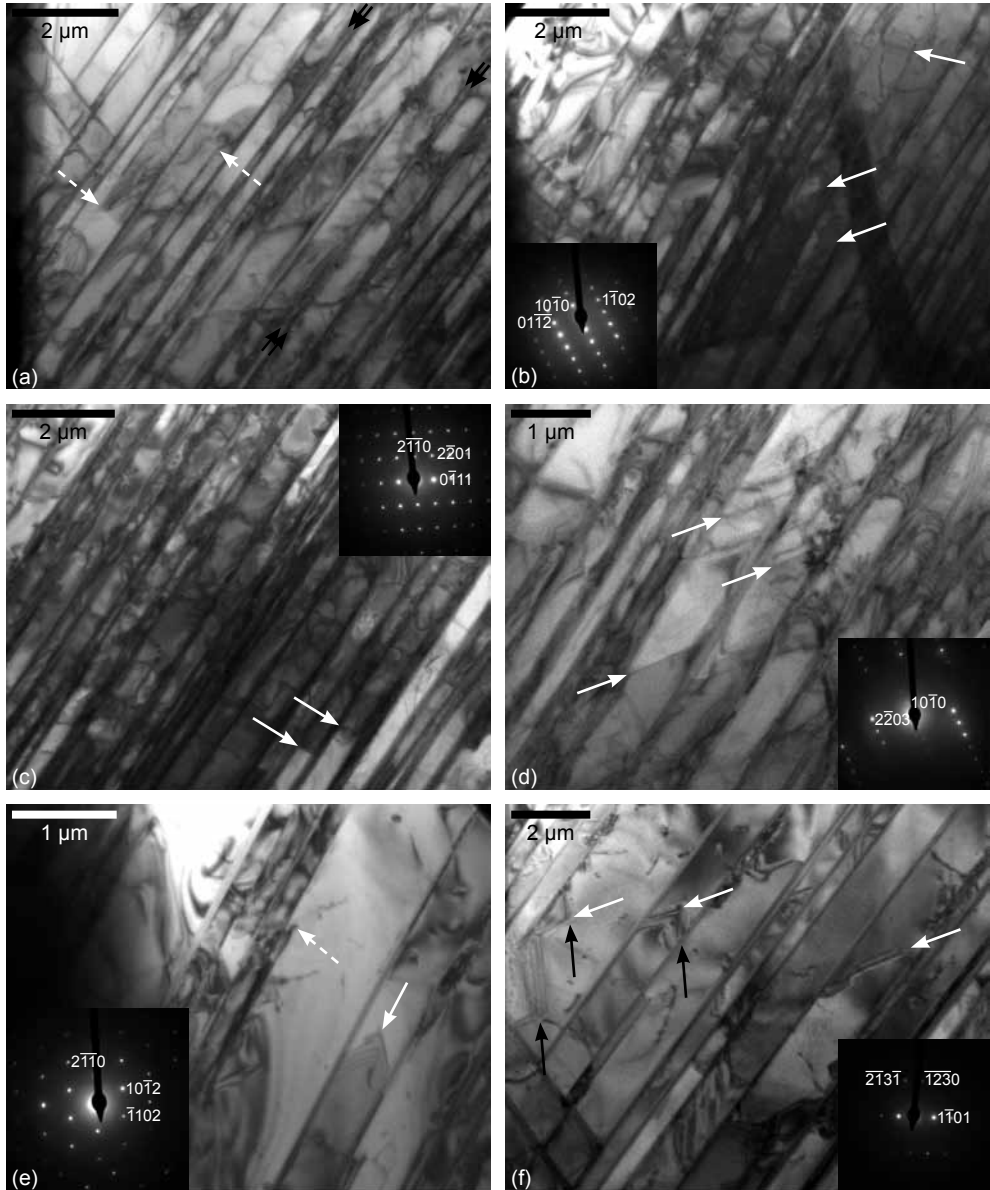


Figure 8.3 TEM bright field images of the thin TEM foil. **a** The PDFs often occur in closely spaced pairs (black arrows). Some PDFs end in the middle of the grain, with contrast suggesting the presence of a dislocation or Dauphiné twin boundary (dashed white arrows). **b** White arrows left of the subgrain boundary indicate parallel domains of different contrast, which show a single diffraction pattern, indicating the domains are probably Dauphiné twins consistent with a $\{10\bar{1}0\}$ orientation. The white arrow right of the subgrain boundary indicates a Dauphiné twin boundary in a different orientation. **c**, **d** Different parts of the TEM foil with Dauphiné twin boundaries in different orientations, consistent with $\{2\bar{2}01\}$ in **c** and with $\{10\bar{1}0\}$ in **d**. **e** A Dauphiné twin boundary with an angular geometry (white arrow) and a PDF ending in a dislocation (dashed white arrow). **f** Dauphiné twin boundaries in different parts of the TEM foil have (apparently) parallel boundaries (white and black arrows indicate two apparently corresponding orientations). From images at other tilts the orientations indicated by black arrows are consistent with a $\{10\bar{1}0\}$ orientation.

between the PDFs in this chapter and Brazil twins. Furthermore, closely spaced pairs such as occurring in the PDFs in grain 1 are also frequently observed in mechanical Brazil twins (figures 8.2c and 8.3a; for Brazil twins the pairs are nicely illustrated in for example figure 5b in Goltrant et al. (1992)).

Assuming that this hypothesis is correct, the precursor Brazil twins cannot have been growth twins, because TEM images show that the PDFs cross a subgrain boundary (figures 8.2b and c), which must be the result of deformation after growth of the crystal. Furthermore, because the features are so pervasive in the whole sample and CL imaging shows the red luminescent features are present throughout the sample and not only in this grain, they must have formed during the shock experiment. Brazil twins, whether mechanical or growth in nature, are not observed in SE images. The features in this grain do appear in high contrast SE images, because they are amorphous. However, in grain 2, red luminescent PDFs were observed that do not show any contrast in the corresponding SE image, while in other parts of the grain they do (figure 8.1c and d). The characteristics of red PDFs that are invisible in SE are consistent with Brazil twins, on which no transformation to amorphous material has occurred.

The crystallographic orientation of the PDFs, however, is not basal, as is usually observed in shock induced mechanical Brazil twins. The main PDF set has a $\{\bar{1}2\bar{1}2\}$ orientation, while the second set, which is only observed in the TEM section, is parallel to $\{10\bar{1}1\}$. Both are known PDF orientations, with $\{10\bar{1}1\}$ more frequently observed than $\{\bar{1}2\bar{1}2\}$. The precursor twins would thus be shock induced mechanical Brazil twins, non-basal, but in $\{\bar{1}2\bar{1}2\}$ and $\{10\bar{1}1\}$. Although mechanical Brazil twins in an orientation other than basal are not reported from deformation experiments, Trépiéd and Doukhan (1978) argued that also Brazil twins parallel to $\{10\bar{1}1\}$ can be mechanical, formed by successive $a/2$ shears in adjacent $\{10\bar{1}1\}$ planes. Further analysis of the potential for mechanical Brazil twin formation on the $\{\bar{1}2\bar{1}2\}$ plane will be needed to test our hypothesis.

Trépiéd and Doukhan (1978) state that the formation of mechanical Brazil twins in $\{10\bar{1}1\}$ requires higher energy than the formation of basal Brazil twins. Mechanical Brazil twins in $\{10\bar{1}1\}$ might therefore form at higher pressures than basal Brazil twins, which can be produced in static high pressure experiments at shear stresses exceeding ~ 2 GPa (McLaren et al., 1967). In shocked quartz, basal Brazil twins observed in grains with no or few rhombohedral PDFs and are thought to form at peak shock pressures < 5 - 10 GPa (Grieve et al., 1996; Trepmann, 2008). Alternatively, the orientation of specific planes with respect to the direction of the shock wave might play a role in determining the orientation of mechanical Brazil twins.

8.4.4 Twins and PDF formation

The straight and possibly crystallographically determined boundaries of the Dauphiné twins are consistent with a mechanical origin. The longest Dauphiné twin boundaries coinciding with the planar features in the grain and the observation that Dauphiné twins do not cross PDFs suggest formation after the PDFs. Although mechanical Dauphiné twins are known to occur in quartz deformed at low shear stress (Wenk et al., 2006; Wenk et al., 2007), the Dauphiné twins in this grain must have formed at shear stresses above those required for mechanical Brazil twin formation, if the PDFs formed on Brazil twin planes.

The low shock pressure range just before the onset of PDF formation at ~ 10 GPa represents the transition from the brittle regime to the regime of plastic deformation and phase transformations. In other materials (e.g. alumina, Al_2O_3) this pressure regime is observed to be dominated by twinning processes. In alumina, a transition from fracture-dominated to twin-dominated deformation across the Hugoniot elastic limit (HEL) in shocked alumina is observed and twinning accommodates the change from intergranular fracturing to intragranular cleavage, with cleavage developing on the twin boundary planes during pressure release (Chen et al., 2006). In deformation processes under normal crustal conditions, brittle failure can be preceded by slight plastic deformation, with fractures initiated at slip planes in which dislocation movement occurs (Christie et al., 1964). In models of screw dislocation movement in body-centred cubic iron, twins were observed nucleating from dislocations, at stresses and strain rates so high that dislocation movement was not quick enough to accommodate deformation (Marian et al., 2004).

We suggest that in the low shock pressure regime, mechanical twinning could be the dominant deformation process in quartz. The stress and strain rates during shock are too high for dislocation movement to play a significant role. Therefore twinning might initially accommodate deformation, with the twin boundaries acting as heterogeneities in the crystal lattice that accommodate further deformation in highly localised zones. Under continued shock loading, twinning is not sufficient to accommodate the high strain and the relatively weak twin boundary planes may collapse and become amorphous. As was discussed in chapter 5, Dauphiné twinning makes a crystal more easily elastically deformable and the boundaries form an elastic discontinuity in the quartz structure. In Brazil twin boundaries, there is a structural irregularity to accommodate the change from left-handed to right-handed quartz, which could act as a heterogeneous plane on which amorphous PDFs form more easily.

Although not present in the grains studied in this chapter, formation of planar fractures (PFs) on Brazil twin boundaries might also be considered. Planar fractures usually form in a (0001) or $\{10\bar{1}1\}$ orientation, but also $\{11\bar{2}2\}$ is observed (Trepmann, 2008). In a similar process to cleavage formation under shock loading in alumina on twin boundary planes (Chen et al., 2006), planar fractures could form during pressure release on Brazil twin boundaries in (0001) , $\{10\bar{1}1\}$ and possibly $\{11\bar{2}2\}$. A similar model was proposed for tectonic cleavage in quartz by Flörke et al. (1981), who observed cleavage in quartz parallel to Brazil twins. These cleavage planes were interpreted as release fractures on Brazil twin planes, induced by small tectonically induced thermal shocks in combination with hydrolytic weakening.

8.4.5 Questions and finding the answers

In order to confirm or disqualify the hypothesis for PDF and planar fracture formation at twin boundaries in the lower shock pressure regime, many questions need to be answered. The most important condition for this model to work is the formation of mechanical Brazil twins parallel to $\{1\bar{2}12\}$. This is the first problem that should be worked out, as without the possibility of Brazil twin boundaries in this orientation, the model becomes very implausible. Japan twins (e.g. Momma et al., 2009) do have their twin plane in $\{11\bar{2}2\}$, but have a distinctive twin operation (an 84° tilt of the *c*-axis) that should be recognised in TEM analysis. Furthermore, Japan twins are only observed as (rare) growth twins.

Also mechanical Dauphiné twins deserve more attention. We did not observe amorphisation along Dauphiné twins in grain 1, so the model that was proposed in chapter 5 of PDFs nucleating

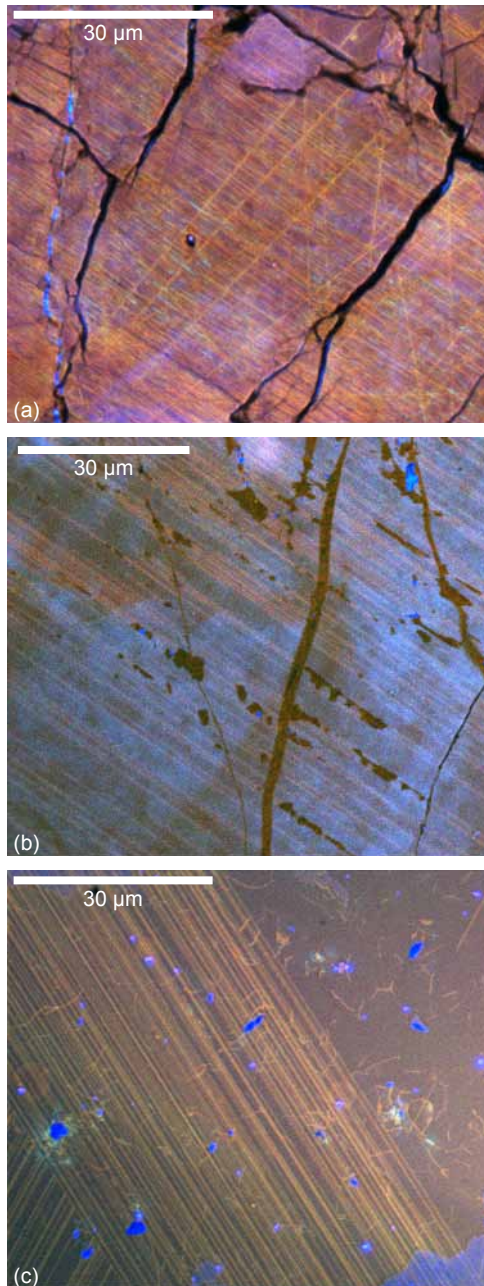


Figure 8.4 Composite colour SEM-CL images of **a** the PDFs in grain 1, **b** mechanical Brazil twins in quartzite from the Vredefort impact structure in South-Africa and **c** growth Brazil twins in a single quartz crystal that was also studied in chapter 6. Comparison of these three images shows the striking similarities of the PDFs in the experimentally shocked sample to Brazil twins.

in Dauphiné twin boundaries could not be confirmed. However, small Dauphiné twin domains between the thin amorphous PDFs, with boundaries parallel in different parts of the TEM foil (figures 8.3b, c and d), have a geometry that is very similar to the commonly observed geometry of some PDF sets that are observed between and bound by other PDF sets (e.g. in the top left part of figure 4.2a in chapter 4).

PDF formation along Dauphiné twin boundaries would imply formation in a pseudo-hexagonal crystal structure, so PDFs parallel to both positive and negative crystal forms would be expected to occur. This is normally not observed in α -quartz (e.g. Trepmann and Spray, 2005). Whether the elastic discontinuity across a Dauphiné twin boundary is enough to localise deformation and nucleate a PDF, or whether Dauphiné twinning rather facilitates deformation by softening the crystal cannot be determined from the data currently available. It seems challenging, but if mechanical Dauphiné twins and those related to β - to α -quartz transformation show distinctive characteristics, the presence of either (or both) could provide a lot of information on shock conditions and indicate whether the temperature in the target rocks has been above the α - β transition. Furthermore, it would be useful to know if mechanical Dauphiné twins have strictly crystallographically determined boundaries, if so, in which orientations, and whether these are pressure dependent and might correlate to frequently occurring PDF orientations.

To account for all PDFs having a mechanical twin boundary as a precursor, twins would have to form in all PDF orientations, but the most frequent PDF planes – $\{10\bar{1}3\}$ and $\{10\bar{1}2\}$ – are not known twin planes, Brazil or Dauphiné. The hypothesis proposed in this chapter might therefore be an additional mechanism for PDF formation at low pressure, rather than an alternative for the model proposed by Goltrant et al. (1992), in which PDFs form as a result of instabilities in the shear modulus of certain planes at higher pressures (>10 GPa). Different mechanisms might operate to form amorphous planes at low pressure than at high pressure – the different character of amorphous PDFs formed at low and at high pressure supports this idea.

An interesting aspect of shock microstructures forming in the low shock pressure regime is whether these features can be used as shock indicators or not. They might be indistinguishable from microstructures formed during high stress and strain rate tectonic deformation and seismogenic faulting (e.g. cataclases and pseudotachylites). One of the two previous reports of similar planar features to the ones described in this chapter (Cordier et al., 1993) were from high stress and strain rate experiments in a diamond anvil cell, which were, although similar in geometry, not shock experiments.

8.5 Conclusions

Although the results in this chapter are preliminary and the discussion therefore remains rather speculative, the role of mechanical twinning in shock deformation of quartz seems to be more important than previously assumed. The presence of Dauphiné twins in close relation to PDFs in a quartzite shocked experimentally to 8 GPa that has not been above the α - β transition temperature shows that the twins are mechanical. The strikingly similar geometry of narrow (10–30 nm), amorphous, red luminescent PDFs and Brazil twins suggest that the PDFs might have been preceded by twin boundaries. The PDFs may be interpreted as mechanical Brazil twins in $\{10\bar{1}1\}$ and $\{1\bar{2}12\}$ orientations, along which preferential amorphisation has occurred. If this

hypothesis can be confirmed, preferential amorphisation along twin boundaries could form an additional or alternative model for PDF formation in quartz, especially at low shock pressures.

Acknowledgements – Uwe Reimold is kindly thanked for letting us use his sample for this study.



Chapter 9

Main conclusions and suggestions for further research

9.1 Main conclusions

The most important conclusion of the research presented in this thesis is that a combination of different SEM techniques is sufficient to identify PDFs in quartz and provides a preliminary characterisation of shock microstructures. Because a direct correlation can be made between SEM and light microscopy observations, SEM techniques bridge the gap between light microscopy observations on large samples and highly detailed TEM analysis of the sub-micron scale defects in shock microstructures. In more detail:

- Greyscale and composite colour SEM-CL imaging, FSE imaging and EBSD mapping provide reliable criteria for the distinction between PDFs and non-shock related (sub-) planar microstructures in quartz, in particular tectonic deformation lamellae.
- Composite colour SEM-CL imaging shows that in general, non-luminescent PDFs are amorphous, while healed PDFs and basal Brazil twins are red luminescent.
- The red luminescent emission in healed PDFs is related to a high density of dislocations in the PDF plane and has a dominant emission peak around 650 nm.
- Subgrain boundaries, Dauphiné and Brazil twin boundaries and some dislocations are also red luminescent, with probably also a dominant peak at 650 nm, and can be imaged in composite colour or red filtered SEM-CL images.
- The 650 nm emission peak is related to the non-bridging oxygen hole centre defect, which in the studied microstructures is probably related to the presence of non-bridging O atoms, strained Si-O bonds and OH groups, and is most likely the result of localised electron beam damage at subgrain and twin boundaries and at dislocations.
- FSE imaging and EBSD mapping can be used to identify PDFs and give an indication of their structural state (amorphous vs. healed); provided they are thick enough, amorphous PDFs do not give EBSD patterns and are observed in pattern quality maps as darker lines in a lighter matrix. In FSE images, amorphous PDFs have the same grey level throughout an image, while healed PDFs show variable and more complex contrast.
- FSE imaging and EBSD mapping allow a quick and easy characterisation of grain structure: a microcrystalline grain structure is detected in FSE images and Dauphiné twins

can be imaged with FSE and confirmed with EBSD measurements. Colour-coded FSE images are particularly useful for imaging Dauphiné twins.

- Combined SEM and TEM observations on shocked quartz grains show combinations of microstructures that can be related to different stages of healing in grains shocked to moderate and high pressure and suggest that mechanical twinning in the low shock pressure regime may play a more important role in PDF development than previously assumed.

9.2 Suggestions for further research

9.2.1 Other minerals

The application of SEM techniques to shocked quartz grains in the current study can easily be extended to other minerals. Zircon and monazite are minerals that show microscopic shock effects and are stable over very long time periods. These minerals can therefore be very useful for identifying ancient and severely altered impact structures. Detailed knowledge of the shock effects influencing the structure and properties of these minerals could also be important in dating studies of impact rocks, which can be carried out on both zircon and monazite. A significant number of studies on zircon exists already (Cavosie et al., 2010; Cintrón et al., 2011; Deutsch and Schärer, 1990; Leroux et al., 1999; Moser et al., 2011; Timms and Reddy, 2009; Timms et al., 2011; Wittmann et al., 2006) and preliminary study of monazite is promising (Van Zalinge, 2012; Van Zalinge et al., 2012).

Also feldspars can be of interest, because like quartz, feldspar is a major constituent of the Earth's crust and exhibits a range of microscopic shock effects at different pressures (e.g. Ferrière and Osinski, 2012; French and Koeberl, 2010). TEM study of feldspar is often hindered by rapid beam damage (Lee, 2010), so SEM techniques may provide an easier method for observing shock microstructures in this mineral. Furthermore, feldspars generally show a higher CL intensity than quartz, facilitating the application of CL imaging methods.

9.2.2 Further study of quartz

9.2.2.1 Shocked quartz at the Permian-Triassic and Triassic-Jurassic boundaries and disputed impact structures

Although the evidence for impact at geological boundaries defined by a major mass extinction, other than the Cretaceous-Palaeogene (K-Pg) boundary (see chapter 3), seems to be rather weak, an extraterrestrial event has also been proposed as the cause of the end-Permian mass extinction (Basu et al., 2003; Becker et al., 2004; Retallack et al., 1998) and some preliminary impact evidence has been found near the Triassic-Jurassic boundary (Badjukov et al., 1987; Bice et al., 1992; Olsen et al., 2002; Simms, 2003). It would be straightforward to check reports of shocked quartz from the appropriate stratigraphic levels using the sample preparation procedures employed in chapter 3 and the SEM techniques described in the other chapters.

Recently proposed impact structures for which the presence of shocked quartz is reported, but has not been confirmed by reliable methods are another obvious subject of future SEM study. In this context, particularly the Maniitsoq structure in Greenland (Garde et al., 2012) may

be of interest. If confirmed as an impact structure, Maniitsoq would be a rare example of an ancient, large impact structure that has affected deeper crustal and possibly even mantle rocks, which are under rather different pressure and temperature conditions at the time of impact than upper crustal rocks. The higher pre-impact pressures and temperatures might affect the shock microstructures that form in different minerals, as proposed by Garde et al. (2012).

9.2.2.2 High pressure polymorphs

Chapter 4 showed that composite colour SEM-CL images can give an indication for the presence of high pressure phases in shocked quartz grains. CL imaging therefore potentially provides a very useful, quick method to detect small amounts of high pressure phases. Systematic study of the CL emission and crystal structure of these phases may define the reliability and potential of this technique. Detection of high pressure polymorphs using EBSD was not attempted in the current study, but should be relatively straightforward, providing the high pressure phases are present in large enough crystals.

9.2.2.3 Shock effects in the low shock pressure range and the role of mechanical twinning

An interesting issue emerging from this thesis is the role of mechanical twinning in quartz in the lower pressure regimes of the impact process. Is mechanical twinning related to the development of PDFs? In chapters 5 and 8 we suggested that both mechanical Brazil and Dauphiné twins might act as nucleation planes for the amorphous phase in PDFs. Oriented shock experiments at different peak shock pressures in the low to moderate pressure range (~5-15 GPa) could provide samples in which the development of mechanical twins and PDFs can be studied in detail, using electron microscopy techniques.

References

- Adams, B.L., Wright, S.I. and Kunze, K., 1993. Orientation Imaging - the Emergence of a New Microscopy. *Metallurgical Transactions a - Physical Metallurgy and Materials Science*, 24(4): 819-831.
- Alexopoulos, J.S., Grieve, R.A.F. and Robertson, P.B., 1988. Microscopic lamellar deformation features in quartz: Discriminative characteristics of shock-generated varieties. *Geology*, 16(9): 796-799.
- Alvarez, L.W., Alvarez, W., Asaro, F. and Michel, H.V., 1980. Extraterrestrial Cause for the Cretaceous-Tertiary Extinction. *Science*, 208(4448): 1095-1108.
- Badjukov, D.D., Lobitzer, H. and Nazarov, M.A., 1987. Quartz grains with planar features in the Triassic-Jurassic boundary sediments from Northern Limestone Alps, Austria. Abstracts of the Lunar and Planetary Science Conference, 18: 38.
- Ball, A. and White, S., 1977. An etching technique for revealing dislocation structures in deformed quartz grains. *Tectonophysics*, 37(4): T9-T14.
- Barringer, D.M., 1906. Coon Mountain and its Crater. *Proceedings of the Academy of Natural Science of Philadelphia*, 57: 861-886.
- Basu, A.R., Petaev, M.I., Poreda, R.J., Jacobsen, S.B. and Becker, L., 2003. Chondritic meteorite fragments associated with the Permian-Triassic boundary in Antarctica. *Science*, 302(5649): 1388-1392.
- Becker, L. et al., 2004. Bedout: A possible end-Permian impact crater offshore of Northwestern Australia. *Science*, 304(5676): 1469-1476.
- Bernet, M. and Bassett, K., 2005. Provenance analysis by single-quartz-grain SEM-CL/optical microscopy: *Journal of Sedimentary Research*, 75: 492-500.
- Bice, D.M., Newton, C.R., McCauley, S., Reiners, P.W. and McRoberts, C.A., 1992. Shocked Quartz at the Triassic-Jurassic Boundary in Italy. *Science*, 255(5043): 443-446.
- Blenkinsop, T.G. and Drury, M.R., 1988. Stress estimates and fault history from quartz microstructures. *Journal of Structural Geology*, 10(7): 673-684.
- Boggs, S., Krinsley, D.H., Goles, G.G., Seyedolali, A. and Dypvik, H., 2001. Identification of shocked quartz by scanning cathodoluminescence imaging. *Meteoritics & Planetary Science*, 36(6): 783-791.
- Boggs, S., Jr., Kwon, Y.-I., Goles, G.G., Rusk, B.G., Krinsley, D. and Seyedolali, A., 2002. Is quartz cathodoluminescence color a reliable provenance tool? A quantitative examination: *Journal of Sedimentary Research* 72: 408-415.
- Böhm, A., 1883. Ueber die Gesteine des Wechsels: *Zeitschrift für Kristallographie, Mineralogie und Petrographie* 5: 197-214.
- Bohor, B.F., Modreski, P.J. and Foord, E.E., 1987. Shocked Quartz in the Cretaceous-Tertiary Boundary Clays: Evidence for a Global Distribution. *Science*, 236(4802): 705-709.
- Bottomley, R., Grieve, R., York, D. and Masaitis, V., 1997. The age of the Popigai impact event and its relation to events at the Eocene/Oligocene boundary. *Nature*, 388(6640): 365-368.
- Brinkhuis, H. and Smit, J. (Editors), 1996a. The Geulhemmerberg Cretaceous/Tertiary boundary section (Maastrichtian type area, SE Netherlands). *Geologie en Mijnbouw special issue*, 75. Kluwer, Dordrecht, 101-293 pp.
- Brinkhuis, H. and Smit, J., 1996b. The Geulhemmerberg Cretaceous/Tertiary boundary section (Maastrichtian type area, SE Netherlands); an introduction. *Geologie en Mijnbouw*, 75: 101-106.
- Buchner, E., Seyfried, H. and van den Bogaard, P., 2003. Ar-40/Ar-39 laser probe age determination confirms the Ries impact crater as the source of glass particles in Graupensand sediments (Grimmelfingen Formation, North Alpine Foreland Basin). *International Journal of Earth Sciences*, 92(1): 1-6.

References

- Buhl, E., Poelchau, M.H., Dresen, G. and Kenkmann, T., 2013. Deformation of dry and wet sandstone targets during hypervelocity impact experiments, as revealed from the MEMIN Program. *Meteoritics & Planetary Science*: no-no.
- Canup, R.M., 2004. Simulations of a late lunar-forming impact. *Icarus*, 168(2): 433-456.
- Carlisle, D.B. and Braman, D.R., 1991. Nanometer-Size Diamonds in the Cretaceous Tertiary Boundary Clay of Alberta. *Nature*, 352(6337): 708-709.
- Carter, C.B. and Kohlstedt, D.L., 1981. Electron irradiation damage in natural quartz grains. *Physics and Chemistry of Minerals*, 7(3): 110-116.
- Carter, N.L., 1965. Basal quartz deformation lamellae; a criterion for recognition of impactites. *American Journal of Science*, 263(9): 786-806.
- Cavosie, A.J., Quintero, R.R., Radovan, H.A. and Moser, D.E., 2010. A record of ancient cataclysm in modern sand: Shock microstructures in detrital minerals from the Vaal River, Vredefort Dome, South Africa. *Geological Society of America Bulletin*, 122(11-12): 1968-1980.
- Chao, E.C.T., Fahey, J.J. and Littler, J., 1961. Coesite from Wabar Crater, near Al Hadida, Arabia. *Science*, 133(3456): 882-883.
- Chao, E.C.T., Fahey, J.J., Littler, J. and Milton, D.J., 1962. Stishovite, SiO₂, a Very High Pressure New Mineral from Meteor Crater, Arizona. *J. Geophys. Res.*, 67(1): 419-421.
- Chao, E.C.T., Shoemaker, E.M. and Madsen, B.M., 1960. First Natural Occurrence of Coesite. *Science*, 132(3421): 220-222.
- Chen, K., Kunz, M., Tamura, N. and Wenk, H.-R., 2011. Evidence for high stress in quartz from the impact site of Vredefort, South Africa. *European Journal of Mineralogy*, 23: 169-178.
- Chen, M.W., McCauley, J.W., Dandekar, D.P. and Bourne, N.K., 2006. Dynamic plasticity and failure of high-purity alumina under shock loading. *Nat Mater*, 5(8): 614-618.
- Cherns, D., Hutchison, J.L., Jenkins, M.L., Hirsch, P.B. and White, S., 1980. Electron irradiation induced vitrification at dislocations in quartz. *Nature*, 287(5780): 314-316.
- Chopin, C., 1984. Coesite and pure pyrope in high-grade blueschists of the Western Alps: a first record and some consequences. *Contributions to Mineralogy and Petrology*, 86(2): 107-118.
- Christie, J.M. and Ardell, A.J., 1974. Substructures of Deformation Lamellae in Quartz. *Geology* 2: 405-408.
- Christie, J.M., Heard, H.C. and LaMori, P.N., 1964. Experimental deformation of quartz single crystals at 27 to 30 kilobars confining pressure and 24 degrees C. *American Journal of Science*, 262(1): 26-55.
- Christie, J.M. and Raleigh, C.B., 1959. The origin of deformation lamellae in quartz. *American Journal of Science* 257: 385-407.
- Cintrón, N.O. et al., 2011. In Situ U-Th-Pb Geochronology of Detrital Shocked Monazite in Pleistocene Fluvial Deposits Along the Vaal River, South Africa. *Lunar and Planetary Institute Science Conference Abstracts*, 42: 2253.
- Cloete, M., Hart, R.J., Schmid, H.K., Drury, M., Demanet, C.M. and Sankar, K.V., 1999. Characterization of magnetite particles in shocked quartz by means of electron- and magnetic force microscopy: Vredefort, South Africa. *Contributions to Mineralogy and Petrology* 137: 232-245.
- Comer, J.J., 1972. Electron microscope study of dauphiné microtwins formed in synthetic quartz. *Journal of Crystal Growth*, 15(3): 179-187.
- Cordier, P., Doukhan, J.C. and Peyronneau, J., 1993. Structural transformations of quartz and berlinite AlPO₄ at high pressure and room temperature: a transmission electron microscopy study. *Physics and Chemistry of Minerals*, 20(3): 176-189.
- Cordier, P. and Gratz, A.J., 1995. TEM study of shock metamorphism in quartz from the Sedan nuclear test site. *Earth and Planetary Science Letters* 129: 163-170.
- Cordier, P., Vrána, S. and Doukhan, J.C., 1994. Shock metamorphism in quartz at Sevetin and Susice (Bohemia)? A TEM investigation. *Meteoritics*, 29(1): 98-99.
- Dachille, F., Gigl, P. and Simons, P.Y., 1968. Experimental and analytical studies of crystalline damage useful for the recognition of impact structures. In: B.M. French and N.M. Short (Editors), *Shock metamorphism of natural materials*. Mono Book Corp., Baltimore, pp. 644.
- Day, A., 1993. *Developments in the EBSD techniques and their application to grain imaging*, University of Bristol, Bristol, 155 pp.

- Day, A.P. and Quedstedt, T.E., 1999. A comparison of grain imaging and measurement using horizontal orientation and colour orientation contrast imaging, electron backscatter pattern and optical methods. *Journal of Microscopy*, 195(3): 186-196.
- Deenen, M.H.L. et al., 2010. A new chronology for the end-Triassic mass extinction. *Earth and Planetary Science Letters*, 291(1-4): 113-125.
- Deutsch, A. and Schärer, U., 1990. Isotope systematics and shock-wave metamorphism: I. U-Pb in zircon, titanite and monazite, shocked experimentally up to 59 GPa. *Geochimica et Cosmochimica Acta*, 54(12): 3427-3434.
- Devine, R.A.B., 1990. Radiation damage and the role of structure in amorphous SiO₂. *Nuclear Instruments and Methods in Physics Research Section B: Beam Interactions with Materials and Atoms*, 46(1-4): 244-251.
- Dingley, D.J. and Randle, V., 1992. Microtexture determination by electron back-scatter diffraction. *Journal of Materials Science*, 27(17): 4545-4566.
- Drouin, D. et al., 2007. CASINO V2.42—A Fast and Easy-to-use Modeling Tool for Scanning Electron Microscopy and Microanalysis Users. *Scanning*, 29(3): 92-101.
- Drouin, D. et al., 2001. monte CARlo SIMulation of electroN trajectory in sOLids, Sherbrooke, Quebec, Canada.
- Drury, M.R., 1993. Deformation lamellae in metals and minerals. In: J.N. Boland and J.D. Fitz Gerald (Editors), *Defects and Processes in the Solid State: Geoscience Applications*. Elsevier Science Publishers B. V., Amsterdam, pp. 195-212.
- Earth Impact Database, <http://www.passc.net/EarthImpactDatabase/index.html>.
- Ebert, M., Hecht, L., Deutsch, A. and Kenkmann, T., 2013. Chemical modification of projectile residues and target material in a MEMIN cratering experiment. *Meteoritics & Planetary Science*, 48(1): 134-149.
- Egerton, R.F., Li, P. and Malac, M., 2004. Radiation damage in the TEM and SEM. *Micron*, 35(6): 399-409.
- Engelhardt, W.v. and Bertsch, W., 1969. Shock induced planar deformation structures in quartz from the Ries crater, Germany. *Contributions to Mineralogy and Petrology*, 20: 203-234.
- Ernstson, K. and Fiebag, J., 1992. The Azuara impact structure (Spain) - new insights from geophysical and geological investigations. *Geologische Rundschau*, 81(2): 403-427.
- Ernstson, K., Hammann, W., Fiebag, J. and Graup, G., 1985. Evidence of an impact origin for the Azuara structure (Spain). *Earth and Planetary Science Letters*, 74(4): 361-370.
- Everhart, T.E. and Thornley, R.F.M., 1960. Wide-band detector for micro-microampere low-energy electron currents. *Journal of Scientific Instruments*, 37(7): 246.
- Ferrière, L., Koeberl, C., Ivanov, B.A. and Reimold, W.U., 2008. Shock Metamorphism of Bosumtwi Impact Crater Rocks, Shock Attenuation, and Uplift Formation. *Science*, 322(5908): 1678-1681.
- Ferrière, L., Koeberl, C., Libowitzky, E., Reimold, W.U., Greshake, A., and Brandstätter, F., 2010. Ballen quartz and cristobalite in impactites: New investigations. *Geological Society of America Special Papers*, 465: 609-618.
- Ferrière, L., Koeberl, C. and Reimold, W.U., 2009a. Characterisation of ballen quartz and cristobalite in impact breccias: new observations and constraints on ballen formation. *European Journal of Mineralogy*, 21(1): 203-217.
- Ferrière, L., Morrow, J.R., Amgaa, T. and Koeberl, C., 2009b. Systematic study of universal-stage measurements of planar deformation features in shocked quartz: Implications for statistical significance and representation of results. *Meteoritics & Planetary Science*, 44(6): 925-940.
- Ferrière, L. and Osinski, G.R., 2012. Shock Metamorphism, Impact Cratering. John Wiley & Sons, Ltd, pp. 106-124.
- Field, D.P., Merriman, C.C., Allain-Bonasso, N. and Wagner, F., 2012. Quantification of dislocation structure heterogeneity in deformed polycrystals by EBSD. *Modelling and Simulation in Materials Science and Engineering*, 20(2): 024007.
- Fitting, H.-J., Barfels, T., Trukhin, A.N. and Schmidt, B., 2001. Cathodoluminescence of crystalline and amorphous SiO₂ and GeO₂. *Journal of Non-Crystalline Solids*, 279: 51-59.
- Flörke, O.W., Mielke, H.G., Weichert, J. and Kulke, H., 1981. Quartz with rhombohedral cleavage from Madagascar. *American Mineralogist*, 66(5-6): 596-600.
- French, B.M., 1998. Traces of Catastrophe: A Handbook of Shock-Metamorphic Effects in Terrestrial Meteorite Impact Structures. LPI Contribution, 954. Lunar and Planetary Institute, Houston, 120 pp.
- French, B.M., Cordua, W.S. and Plescia, J.B., 2004. The Rock Elm meteorite impact structure, Wisconsin: Geology and shock-metamorphic effects in quartz. *Geological Society of America Bulletin*, 116(1-2): 200-218.

References

- French, B.M. and Koeberl, C., 2010. The convincing identification of terrestrial meteorite impact structures: What works, what doesn't, and why. *Earth-Science Reviews*, 98(1-2): 123-170.
- French, B.M. and Short, N.M., 1968. Shock metamorphism of natural materials. Mono Book Corp., Baltimore, MD, 644 pp.
- Fritz, J., Wünnemann, K., Reimold, W.U., Meyer, C. and Hornemann, U., 2011. Shock experiments on quartz targets pre-cooled to 77 K. *International Journal of Impact Engineering*, 38(6): 440-445.
- Fron del, C., 1945. Secondary Dauphiné twinning in quartz. *American Mineralogist*, 30(5-6): 447-460.
- Fron del, C., 1962. System of Mineralogy: Silica Minerals. Dana's system of mineralogy. J. Wiley & Sons.
- Fynn, G.W. and Powell, W.J.A., 1979. The Cutting and Polishing of Electro-Optic Materials. Wiley.
- Garde, A.A., McDonald, I., Dyck, B. and Keulen, N., 2012. Searching for giant, ancient impact structures on Earth: The Mesoarchaean Maniitsoq structure, West Greenland. *Earth and Planetary Science Letters*, 337-338: 197-210.
- Glikson, A., 2004. Comment on "Bedout: A Possible End-Permian Impact Crater Offshore of Northwestern Australia". *Science*, 306(5696): 613b.
- Goltrant, O., Cordier, P. and Doukhan, J.-C., 1991. Planar deformation features in shocked quartz; a transmission electron microscopy investigation. *Earth and Planetary Science Letters*, 106(1-4): 103-115.
- Goltrant, O., Leroux, H., Doukhan, J.-C. and Cordier, P., 1992. Formation mechanisms of planar deformation features in naturally shocked quartz. *Physics of the Earth and Planetary Interiors*, 74(3-4): 219-240.
- Gortler, J.D. and Glikson, A.Y., 2012. Talundilly, Western Queensland, Australia: geophysical and petrological evidence for an 84 km-large impact structure and an Early Cretaceous impact cluster. *Australian Journal of Earth Sciences*, 59(1): 51-73.
- Götte, T., 2009. Petrological modifications in continental target rocks from terrestrial impact structures: evidence from cathodoluminescence. In: A. Gucsik (Editor), *Cathodoluminescence and its application in the planetary sciences*. Springer, Berlin, pp. 45-60.
- Götze, J., 2009. Chemistry, textures and physical properties of quartz geological interpretation and technical application. *Mineralogical Magazine*, 73: 645-671.
- Götze, J. and Kempe, U., 2008. A comparison of optical microscope- and scanning electron microscope-based cathodoluminescence (CL) imaging and spectroscopy applied to geosciences: *Mineralogical Magazine* 72: 909-924.
- Götze, J., Plötze, M., Fuchs, H. and Habermann, D., 1999. Defect structure and luminescence behaviour of agate - results of electron paramagnetic resonance (EPR) and cathodoluminescence (CL) studies. *Mineralogical Magazine*, 63(2): 149-149.
- Götze, J., Plötze, M. and Habermann, D., 2001. Origin, spectral characteristics and practical applications of the cathodoluminescence (CL) of quartz – a review. *Mineralogy and Petrology*, 71(3): 225-250.
- Gratz, A.J., Fisler, D.K. and Bohor, B.F., 1996. Distinguishing shocked from tectonically deformed quartz by the use of the SEM and chemical etching. *Earth and Planetary Science Letters*, 142(3-4): 513-521.
- Gratz, A.J., Nellis, W.J., Christie, J.M., Brocius, W., Swegle, J., and Cordier, P., 1992. Shock metamorphism of quartz with initial temperatures -170 to + 1000° C. *Physics and Chemistry of Minerals*, 19(5): 267-288.
- Gratz, A.J., Tyburczy, J., Christie, J., Ahrens, T. and Pongratz, P., 1988. Shock Metamorphism of Deformed Quartz. *Physics and Chemistry of Minerals*, 16(3): 221-233.
- Grieve, R.A.F., Coderre, J.M., Robertson, P.B. and Alexopoulos, J., 1990. Microscopic planar deformation features in quartz of the Vredefort structure: Anomalous but still suggestive of an impact origin: *Tectonophysics* 171: 185-200.
- Grieve, R.A.F., Langenhorst, F. and Stöffler, D., 1996. Shock metamorphism of quartz in nature and experiment: II. Significance in geoscience. *Meteoritics & Planetary Science*, 31(1): 6-35.
- Grieve, R.A.F. and Theriault, A.M., 1995. Planar Deformation Features in Quartz: Target Effects: Abstracts of the Lunar and Planetary Science Conference 26: 515-516.
- Griscom, D.L., 1985. Defect structure of glasses: Some outstanding questions in regard to vitreous silica. *Journal of Non-Crystalline Solids*, 73(1-3): 51-77.
- Gucsik, A., Koeberl, C., Brandstatter, F., Libowitzky, E. and Reimold W.U., 2003. Scanning electron microscopy, cathodoluminescence, and Raman spectroscopy of experimentally shock-metamorphosed quartzite: *Meteoritics & Planetary Science* 38: 1187-1197.

- Güldemeister, N., Wünnemann, K., Durr, N. and Hiermaier, S., 2013. Propagation of impact-induced shock waves in porous sandstone using mesoscale modeling. *Meteoritics & Planetary Science*, 48(1): 115-133.
- Haddad, S.C., Worden, R.H., Prior, D.J. and Smalley, P.C., 2006. Quartz Cement in the Fontainebleau Sandstone, Paris Basin, France: Crystallography and Implications for Mechanisms of Cement Growth. *Journal of Sedimentary Research*, 76(2): 244-256.
- Hartogh, P. et al., 2011. Ocean-like water in the Jupiter-family comet 103P/Hartley 2. *Nature*, 478(7368): 218-220.
- Heggie, M. and Jones, R., 1986. Models of hydrolytic weakening in quartz. *Philosophical Magazine A*, 53(5): L65-L70.
- Heggie, M.I., 1992. A molecular water pump in quartz dislocations. *Nature*, 355(6358): 337-339.
- Heidecker, E.J., 2012. Discussion of Gorter & Glikson: Talundilly, Western Queensland, Australia: geophysical and petrological evidence for a 84 km-large structure and an Early Cretaceous impact cluster. *Australian Journal of Earth Sciences*, 59(7): 1083-1083.
- Higgs, V., Lightowlers, E.C., Tajbakhsh, S. and Wright, P.J., 1992. Cathodoluminescence imaging and spectroscopy of dislocations in Si and Si_{1-x}Gex alloys. *Applied Physics Letters*, 61(9): 1087-1089.
- Hildebrand, A.R. et al., 1991. Chicxulub Crater: A possible Cretaceous/Tertiary boundary impact crater on the Yucatan Peninsula, Mexico. *Geology*, 19(9): 867-871.
- Hobbs, L., W. and Pascucci, M., R., 1980. Radiolysis and defect structure in electron-irradiated α -quartz. *J. Phys. Colloques*, 41(C6): C6-237-C6-242.
- Holm, S., Alwmark, C., Alvarez, W. and Schmitz, B., 2011. Shock barometry of the Siljan impact structure, Sweden. *Meteoritics & Planetary Science*: no-no.
- Hörz, F., 1968. Statistical measurements of deformation structures and refractive indices in experimentally shock loaded quartz. In: B.M. French and N.M. Short (Editors), *Shock metamorphism of natural materials*. Mono book corp., Baltimore, pp. 644.
- Huffman, A.R., Brown, J.M., Carter, N.L. and Reimold, W.U., 1993. The Microstructural Response of Quartz and Feldspar Under Shock Loading at Variable Temperatures. *J. Geophys. Res.*, 98(B12): 22171-22197.
- Huffman, A.R. and Reimold, W.U., 1996. Experimental constraints on shock-induced microstructures in naturally deformed silicates. *Tectonophysics*, 256(1-4): 165-217.
- Hull, D. and Bacon, D.J., 2011. *Introduction to Dislocations*. Elsevier, 272 pp.
- Humphreys, F.J., Bate, P.S. and Hurley, P.J., 2001. Orientation averaging of electron backscattered diffraction data. *Journal of Microscopy*, 201(1): 50-58.
- Humphreys, F.J. and Brough, I., 1999. High resolution electron backscatter diffraction with a field emission gun scanning electron microscope. *Journal of Microscopy*, 195(1): 6-9.
- Humphreys, F.J., Huang, Y., Brough, I. and Harris, C., 1999. Electron backscatter diffraction of grain and subgrain structures — resolution considerations. *Journal of Microscopy*, 195(3): 212-216.
- Izett, G.A., 1990. The Cretaceous/Tertiary boundary interval, Raton Basin, Colorado and New Mexico, and its content of shock-metamorphosed minerals; evidence relevant to the K/T boundary impact-extinction theory. *Geological Society of America Special Papers*, 249: 1-100.
- Jourdan, F. and Reimold, W.U.(Editors), 2012., *Elements*, pp. 84.
- Kamo, S.L., Reimold, W.U., Krogh, T.E. and Colliston, W.P., 1996. A 2.023 Ga age for the Vredefort impact event and a first report of shock metamorphosed zircons in pseudotachylitic breccias and Granophyre. *Earth and Planetary Science Letters*, 144(3-4): 369-387.
- Karato, S., 1987. Scanning electron microscope observation of dislocations in olivine. *Physics and Chemistry of Minerals*, 14(3): 245-248.
- Kayama, M., Nishido, H., Endo, Y., Sekine, T., Gucsik, A. and Ninagawa, K., 2010. Estimation of shock pressure on quartz and alkali feldspar from Ries crater using cathodoluminescence spectroscopy, 73d Annual Meeting of the Meteoritical Society: New York, USA, abstract 5192.
- Kempe, U., Götze, J., Dandar, S. and Habermann, D., 1999. Magmatic and metasomatic processes during formation of the Nb-Zr-REE deposits Khaldzan Buregte and Tsakhir (Mongolian Altai): Indications from a combined CL-SEM study. *Mineralogical Magazine*, 63(2): 165-165.
- Kenkmann, T. et al., 2011. Impact cratering in sandstone: The MEMIN pilot study on the effect of pore water. *Meteoritics & Planetary Science*, 46(6): 890-902.

References

- Kieffer, S.W., 1971. Shock Metamorphism of the Coconino Sandstone at Meteor Crater, Arizona. *J. Geophys. Res.*, 76(23): 5449-5473.
- Kieffer, S.W., Phahey, P.P. and Christie, J.M., 1976. Shock processes in porous quartzite: Transmission electron microscope observations and theory. *Contributions to Mineralogy and Petrology*, 59(1): 41-93.
- Koch, P.S. and Christie, J.M., 1981. Spacing of deformation lamellae as a palaeopiezometer. *Transactions of the American Geophysical Union* 62: 1030.
- Kohlstedt, D.L., Goetze, C., Durham, W.B. and Sande, J.V., 1976. New Technique for Decorating Dislocations in Olivine. *Science*, 191(4231): 1045-1046.
- Kowitz, A., Schmitt, R.T., Uwe Reimold, W. and Hornemann, U., 2013. The first MEMIN shock recovery experiments at low shock pressure (5–12.5 GPa) with dry, porous sandstone. *Meteoritics & Planetary Science*, 48(1): 99-114.
- Landtwing, M.R. and Pettke, T., 2005. Relationships between SEM-cathodoluminescence response and trace-element composition of hydrothermal vein quartz: *American Mineralogist* 90: 122-131.
- Langenhorst, F., 1994. Shock Experiments on Pre-Heated Alpha-Quartz and Beta-Quartz: II. X-Ray and TEM Investigations. *Earth and Planetary Science Letters*, 128(3-4): 683-698.
- Langenhorst, F. and Deutsch, A., 1994. Shock Experiments on Pre-Heated Alpha-Quartz and Beta-Quartz: I. Optical and Density Data. *Earth and Planetary Science Letters*, 125(1-4): 407-420.
- Langenhorst, F. and Deutsch, A., 1996. The Azuara and Rubielos Structures, Spain: Twin Impact Craters or Alpine Thrust Systems? TEM Investigations on Deformed Quartz Disprove Shock Origin. *Lunar and Planetary Science*, 27: 725-726.
- Langenhorst, F. and Deutsch, A., 2012. Shock metamorphism of minerals. *Elements*, 8(1): 31-36.
- Langenhorst, F., Kyte, F.T. and Retallack, G.J., 2005. Reexamination of Quartz Grains from the Permian-Triassic Boundary Section at Graphite Peak, Antarctica. *Lunar and Planetary Science Conference Abstracts*, 36: 2358.
- Lee, M.R., 2010. Transmission electron microscopy (TEM) of Earth and planetary materials: A review. *Mineralogical Magazine*, 74(1): 1-27.
- Lei, H. et al., 2002. Raman and cathodoluminescence study of dislocations in GaN. *Journal of Applied Physics*, 92(11): 6666-6670.
- Leroux, H. and Doukhan, J.-C., 1993. Dynamic deformation of quartz in the landslide of Koefels, Austria. *Eur J Mineral*, 5(5): 893-902.
- Leroux, H. and Doukhan, J.-C., 1996. A transmission electron microscope study of shocked quartz from the Manson impact structure. *Geological Society of America Special Papers*, 302: 267-274.
- Leroux, H., Reimold, W.U. and Doukhan, J.C., 1994. A TEM investigation of shock metamorphism in quartz from the Vredefort Dome, South-Africa. *Tectonophysics*, 230(3-4): 223-239.
- Leroux, H., Reimold, W.U., Koeberl, C., Hornemann, U. and Doukhan, J.C., 1999. Experimental shock deformation in zircon: a transmission electron microscopic study. *Earth and Planetary Science Letters*, 169(3&4): 291-301.
- Liu, L., Zhang, J., Green Ii, H.W., Jin, Z. and Bozhilov, K.N., 2007. Evidence of former stishovite in metamorphosed sediments, implying subduction to >350 km. *Earth and Planetary Science Letters*, 263(3-4): 180-191.
- Lloyd, G.E., 1987. Atomic number and crystallographic contrast images with the SEM: a review of backscattered electron techniques. *Mineralogical Magazine*, 51(359): 3-19.
- Lloyd, G.E., 1994. An appreciation of the SEM electron channeling technique for microstructural analysis of geological materials. In: H.J. Bunge, S. Siegesmunde, W. Skrotzki and K. Weber (Editors), *Textures of geological materials*. DGM Informationsgesellschaft Verlag, Oberursel, pp. 109–126.
- Lloyd, G.E., 2000. Grain boundary contact effects during faulting of quartzite: an SEM/EBSD analysis. *Journal of Structural Geology*, 22(11&12): 1675-1693.
- Lloyd, G.E., 2004. Microstructural evolution in a mylonitic quartz simple shear zone: the significant roles of dauphine twinning and misorientation. *Geological Society, London, Special Publications*, 224(1): 39-61.
- Luo, S.-N., Ahrens, T.J. and Asimow, P.D., 2003. Polymorphism, superheating, and amorphization of silica upon shock wave loading and release. *J. Geophys. Res.*, 108(B9): 2421.
- Lyons, J.B., Officer, C.B., Borella, P.E. and Lahodinsky, R., 1993. Planar lamellar substructures in quartz: *Earth and Planetary Science Letters* 119: 431-440.

- Marian, J., Cai, W. and Bulatov, V.V., 2004. Dynamic transitions from smooth to rough to twinning in dislocation motion. *Nat Mater*, 3(3): 158-163.
- Marshall, D.J., 1988. Cathodoluminescence of geological materials. Unwin Hyman, Boston, 146 pp.
- Martin, B., Flörke, O.W., Kainka, E. and Wirth, R., 1996. Electron irradiation damage in quartz, SiO₂. *Physics and Chemistry of Minerals*, 23(7): 409-417.
- McLaren, A. and Phakey, P.P., 1965a. A transmission electron microscope study of amethyst and citrine. *Australian Journal of Physics*, 18: 135-141.
- McLaren, A.C. and Phakey, P.P., 1965b. Dislocations in Quartz Observed by Transmission Electron Microscopy. *Journal of Applied Physics*, 36(10): 3244-3246.
- McLaren, A.C. and Phakey, P.P., 1966. Electron Microscope Study of Brazil Twin Boundaries in Amethyst Quartz. *physica status solidi (b)*, 13(2): 413-422.
- McLaren, A.C. and Phakey, P.P., 1969. Diffraction Contrast from Dauphiné Twin Boundaries in Quartz. *physica status solidi (b)*, 31(2): 723-737.
- McLaren, A.C., Retchford, J.A., Griggs, D.T. and Christie, J.M., 1967. Transmission Electron Microscope Study of Brazil Twins and Dislocations Experimentally Produced in Natural Quartz. *physica status solidi (b)*, 19(2): 631-644.
- McLaren, A.C., Turner, R.G., Boland, J.N. and Hobbs, B.E., 1970. Dislocation structure of the deformation lamellae in synthetic quartz; a study by electron and optical microscopy. *Contributions to Mineralogy and Petrology*, 29(2): 104-115.
- Menegon, L., Piazzolo, S. and Pennacchioni, G., 2011. The effect of Dauphiné twinning on plastic strain in quartz. *Contributions to Mineralogy and Petrology*, 161(4): 635-652.
- Meyer, C. et al., 2011. Shock experiments in support of the Lithopanspermia theory: The influence of host rock composition, temperature, and shock pressure on the survival rate of endolithic and epilithic microorganisms. *Meteoritics & Planetary Science*, 46(5): 701-718.
- Momma, K., Nagase, T., Kudoh, Y. and Kuribayashi, T., 2009. Computational simulations of the structure of Japan twin boundaries in quartz. *European Journal of Mineralogy*, 21(2): 373-383.
- Montanari, A. and Koeberl, C., 2000. *Impact Stratigraphy: The Italian Record*. Lecture Notes in Earth Sciences, 93. Springer.
- Morgan, J. et al., 2006. Analyses of shocked quartz at the global K-P boundary indicate an origin from a single, high-angle, oblique impact at Chicxulub. *Earth and Planetary Science Letters*, 251(3-4): 264-279.
- Moser, D.E. et al., 2011. New zircon shock phenomena and their use for dating and reconstruction of large impact structures revealed by electron nanobeam (EBSD, CL, EDS) and isotopic UPb and (UTh)/He analysis of the Vredefort dome. *Canadian Journal of Earth Sciences*, 48(2): 117-139.
- Müller, W.F., 1969. Elektronenmikroskopischer Nachweis amorpher Bereiche in stoßwellenbeanspruchtem Quarz. *Naturwissenschaften*, 56(5): 279-279.
- Nesse, W.D., 2004. *Introduction to optical mineralogy*: Oxford, Oxford University Press, 348 p.
- Okumura, T., Gucsik, A., Nishido, H., Ninagawa, K. and Toyoda S., 2009. Raman and cathodoluminescence spectroscopical microcharacterization of planar deformation features in shocked quartz from Ries impact crater (Germany). *Geological Society of America Annual Meeting*, Volume 41, No. 7: Portland, Oregon, USA, p. 308.
- Olesen, N.Ø. and Schmidt, N.-H., 1990. The SEM/ECP technique applied on twinned quartz crystals. *Geological Society, London, Special Publications*, 54(1): 369-373.
- Olsen, P.E. et al., 2002. Ascent of dinosaurs linked to an iridium anomaly at the Triassic-Jurassic boundary. *Science*, 296(5571): 1305-1307.
- Osinski, G.R., 2007. Impact metamorphism of CaCO₃-bearing sandstones at the Houghton structure, Canada. *Meteoritics & Planetary Science*, 42(11): 1945-1960.
- Osinski, G.R. and Pierazzo, E., 2013. *Impact cratering: processes and products*. Blackwell Publishing Ltd., 316 pp.
- Pennock, G.M., Drury, M.R., Peach, C.J. and Spiers, C.J., 2006. The influence of water on deformation microstructures and textures in synthetic NaCl measured using EBSD. *Journal of Structural Geology*, 28(4): 588-601.
- Pennock, G.M., Drury, M.R., Trimby, P.W. and Spiers, C.J., 2002. Misorientation distributions in hot deformed NaCl using electron backscattered diffraction. *Journal of Microscopy*, 205(3): 285-294.

References

- Pennycook, S.J., Brown, L.M. and Craven, A.J., 1980. Observation of cathodoluminescence at single dislocations by STEM. *Philosophical Magazine A*, 41(4): 589-600.
- Perny, B., Eberhardt, P., Ramseyer, K., Mullis, J. and Pankrath, R., 1992. Microdistribution of Al, Li, and Na in alpha quartz; possible causes and correlation with short-lived cathodoluminescence. *American Mineralogist*, 77(5-6): 534-544.
- Pfeffer, R.L., 1985. Damage center formation in SiO₂ thin films by fast electron irradiation. *Journal of Applied Physics*, 57(12): 5176-5180.
- Poelchau, M.H. and Kenkmann, T., 2011. Feather features: A low-shock-pressure indicator in quartz. *Journal of Geophysical Research*, 116(B2): B02201.
- Prior, D.J. et al., 1999. The application of electron backscatter diffraction and orientation contrast imaging in the SEM to textural problems in rocks. *American Mineralogist*, 84(11-12): 1741-1759.
- Prior, D.J., Trimby, P.W., Weber, U.D. and Dingley, D.J., 1996. Orientation contrast imaging of microstructures in rocks using forescatter detectors in the scanning electron microscope. *Mineral Mag*, 60(6): 859-869.
- Ramseyer, K., Aldahan, A.A., Collini, B. and Landström, O., 1992. Petrological modifications in granitic rocks from the Siljan impact structure: evidence from cathodoluminescence. *Tectonophysics*, 216(1-2): 195-204.
- Ramseyer, K. and Mullis, J., 1990. Factors influencing the short-lived blue cathodoluminescence of alpha-quartz. *American Mineralogist*, 75(7-8): 791-800.
- Ramseyer, K. and Mullis, J., 2000. Geologic application of cathodoluminescence in silicates. In: M. Pagel, V. Barbin, P. Blanc and D. Ohnenstetter (Editors), *Cathodoluminescence in Geosciences*. Springer, Berlin, pp. 177-191.
- Reimer, L. and Hawkes, P.W., 1998. *Scanning Electron Microscopy: Physics of Image Formation and Microanalysis*. Springer.
- Reimold, W.U. and Hörz, F., 1986a. Experimental shock metamorphism of Witwatersrand quartzite, *Geocongress '86*, Johannesburg, South-Africa, pp. 53-57.
- Reimold, W.U. and Hörz, F., 1986b. Textures of experimentally shocked (5.1 - 35.5 GPa) Witwatersrand quartzite, *Lunar and Planetary Science XVII*. Lunar and Planetary Institute, Houston, pp. 703-704.
- Reimold, W.U., Raschke, U. and Schmitt, R.T., 2012. Petrography of the impact breccias of the ICDP drill core from El'gygytgyn, Russia. *Meteoritics & Planetary Science*, 47(S1): 5119.
- Retallack, G.J. et al., 1998. Search for evidence of impact at the Permian-Triassic boundary in Antarctica and Australia. *Geology*, 26(11): 979-982.
- Robertson, P.B., 1975. Zones of shock metamorphism at the Charlevoix impact structure, Quebec. *Geological Society of America Bulletin*, 86(12): 1630-1638.
- Roep, T.B. and Smit, J., 1996. Sedimentological aspects of the K/T boundary at Geulhemmerberg, Zuid Limburg, the Netherlands. *Geologie en Mijnbouw*, 75: 119-131.
- Rusk, B.G. and Reed, M., 2002. Scanning electron microscope-cathodoluminescence analysis of quartz reveals complex growth histories in veins from the Butte porphyry copper deposit, Montana: *Geology*: 727-730.
- Rusk, B.G., Reed, M.H., Dilles J.H. and Kent, A.J.R., 2006. Intensity of quartz cathodoluminescence and trace-element content in quartz from the porphyry copper deposit at Butte, Montana: *American Mineralogist* 91: 1300-1300.
- Schmieder, M., Buchner, E., Schwarz, W.H., Trieloff, M. and Lambert, P., 2010. A Rhaetian ⁴⁰Ar/³⁹Ar age for the Rochechouart impact structure (France) and implications for the latest Triassic sedimentary record. *Meteoritics & Planetary Science*: no-no.
- Schwartz, A.J., Kumar, M., Adams, B.L. and Field, D.P. (Editors), 2000. *Electron Backscatter Diffraction in Materials Science*. Springer, 403 pp.
- Schwarzer, R.A., Field, D.P., Adams, B.L., Kumar, M. and Schwartz, A.J., 2009. Present State of Electron Backscatter Diffraction and Prospective Developments. *Electron Backscatter Diffraction in Materials Science*. Springer US, pp. 1-20.
- Sekiguchi, T. and Sumino, K., 1996. Cathodoluminescence study on dislocations in silicon. *Journal of Applied Physics*, 79(6): 3253-3260.
- Seyedolali, A., Krinsley, D.H., Boggs, S., Ohara, P.F., Dypvik, H. and Goles, G.G., 1997. Provenance interpretation of quartz by scanning electron microscope-cathodoluminescence fabric analysis: *Geology* 25: 787-790.
- Shoemaker, E.M. and Chao, E.C.T., 1961. New evidence for the impact origin of the Ries Basin, Bavaria, Germany. *Journal of Geophysical Research*, 66(10): 3371-3378.

- Sigel, G.H. and Marrone, M.J., 1981. Photoluminescence in as-drawn and irradiated silica optical fibers: an assessment of the role of non-bridging oxygen defect centers. *Journal of Non-Crystalline Solids*, 45(2): 235-247.
- Simms, M.J., 2003. Uniquely extensive seismite from the latest Triassic of the United Kingdom: Evidence for bolide impact? *Geology*, 31(6): 557-560.
- Smit, J. and Brinkhuis, H., 1996. The Geulhemmerberg Cretaceous/Tertiary boundary section (Maastrichtian type area, SE Netherlands); summary of results and a scenario of events. *Geologie en Mijnbouw*, 75: 283-293.
- Smit, J. and Hertogen, J., 1980. An extraterrestrial event at the Cretaceous-Tertiary boundary. *Nature*, 285(5762): 198-200.
- Smit, J. and Kyte, F.T., 1984. Siderophile-rich magnetic spheroids from the Cretaceous-Tertiary Boundary in Umbria, Italy. *Nature*, 310(5976): 403-405.
- Smit, J. and Rocchia, R., 1996. Neutron activation analysis of trace elements in the Geulhemmerberg Cretaceous/Tertiary boundary section, SE Netherlands. *Geologie en Mijnbouw*, 75: 269-274.
- Smith, D.C., 1984. Coesite in clinopyroxene in the Caledonides and its implications for geodynamics. *Nature*, 310(5979): 641-644.
- Stähle, V., Altherr, R., Koch, M. and Nasdala, L., 2008. Shock-induced growth and metastability of stishovite and coesite in lithic clasts from suevite of the Ries impact crater (Germany). *Contributions to Mineralogy and Petrology*, 155(4): 457-472.
- Stevens Kalceff, M.A., 2009. Cathodoluminescence microcharacterization of point defects in α -quartz. *Mineral Mag*, 73(4): 585-605.
- Stevens Kalceff, M.A. and Phillips, M.R., 1995a. Cathodoluminescence microcharacterization of the defect structure of quartz. *Physical Review B*, 52(5): 3122.
- Stevens Kalceff, M.A. and Phillips, M.R., 1995b. Electron irradiation induced outgrowths from quartz. *Journal of Applied Physics*, 77(8): 4125-4127.
- Stevens Kalceff, M.A., Phillips, M.R., Moon, A.R. and Kalceff, W., 2000. Cathodoluminescence microcharacterisation of silicon dioxide polymorphs. In: M. Pagel, V. Barbin, P. Blanc and D. Ohnenstetter (Editors), *Cathodoluminescence in Geosciences*. Springer, Berlin, pp. 193-224.
- Stöffler, D., 1972. Deformation and transformation of rock-forming minerals by natural and experimental shock processes: I. Behavior of minerals under shock compression. *Fortschritte der Mineralogie*, 49: 50-113.
- Stöffler, D. and Grieve, R.A.F., 2007. Impactites. In: D. Fettes and J. Desmons (Editors), *Metamorphic Rocks: A Classification and Glossary of Terms, Recommendations of the International Union of Geological Sciences*. Cambridge University Press, Cambridge, UK, pp. 82-92, 111-125 and 126-242.
- Stöffler, D. and Langenhorst, F., 1994. Shock Metamorphism of Quartz in Nature and Experiment: I. Basic Observation and Theory. *Meteoritics*, 29(2): 155-181.
- Stolper, E.M. and Ahrens, T.J., 1987. On the nature of pressure-induced coordination changes in silicate melts and glasses. *Geophys. Res. Lett.*, 14(12): 1231-1233.
- Sunagawa, I., Taijing, L. and Balitsky, V.S., 1990. Generation of Brazil and Dauphiné twins in synthetic amethysts. *Physics and Chemistry of Minerals*, 17(4): 320-325.
- Surenian, R., 1988. Scanning electron microscope study of shock features in pumice and gneiss from köfels (Tyrol, Austria). *Geol. Paläont. Mitt. Innsbruck*, 15: 135-143.
- Timms, N.E. and Reddy, S.M., 2009. Response of cathodoluminescence to crystal-plastic deformation in zircon. *Chemical Geology*, 261(1-2): 12-24.
- Timms, N.E. et al., 2011. Resolution of impact-related microstructures in lunar zircon: A shock-deformation mechanism map. *Meteoritics & Planetary Science*, 47(1): 120-141.
- Trepied, L. and Doukhan, J.C., 1978a. Dissociated 'a' dislocations in quartz. *Journal of Materials Science*, 13(3): 492-498.
- Trepied, L. and Doukhan, J.C., 1978b. Some precisions on the Brazil twins in quartz. *physica status solidi (a)*, 50(1): K37-K41.
- Trepmann, C.A., 2008. Shock effects in quartz: Compression versus shear deformation - An example from the Rochechouart impact structure, France. *Earth and Planetary Science Letters*, 267(1-2): 322-332.
- Trepmann, C.A., Gotte, T. and Spray, J.G., 2005. Impact-related Ca-metasomatism in crystalline target-rocks from the Charlevoix structure, Quebec, Canada. *Canadian Mineralogist*, 43(2): 553-567.

References

- Treppmann, C.A. and Spray, J.G., 2005. Planar microstructures and Dauphiné twins in shocked quartz from the Charlevoix impact structure, Canada. In: T. Kenkmann, F. Hörz and A. Deutsch (Editors), *Large Meteorite Impacts III*. Geological Society of America Special Paper, pp. 315-328.
- Treppmann, C.A. and Spray, J.G., 2006. Shock-induced crystal-plastic deformation and post-shock annealing of quartz: microstructural evidence from crystalline target rocks of the Charlevoix impact structure, Canada. *European Journal of Mineralogy*, 18(2): 161-173.
- Trukhin, A.N., Jansons, J.L., Dyuzheva, T.I., Lityagina, L.M. and Bendeliani, N.A., 2003. Luminescence of different modifications of crystalline silicon dioxide: Stishovite and coesite. *Solid State Communications*, 127(6): 415-418.
- Trukhin, A.N., Jansons, J.L. and Truhins, K., 2004. Luminescence of silica glass containing aluminum oxide: *Journal of Non-Crystalline Solids* 347: 80-86.
- Tsai, T.E. and Griscom, D.L., 1991. Experimental evidence for excitonic mechanism of defect generation in high-purity silica. *Physical Review Letters*, 67(18): 2517-2520.
- Tschauner, O., Luo, S.-N., Asimow, P.D. and Ahrens, T.J., 2006. Recovery of stishovite-structure at ambient conditions out of shock-generated amorphous silica. *American Mineralogist*, 91(11-12): 1857-1862.
- Tullis, J., 1970. Quartz: Preferred Orientation in Rocks Produced by Dauphiné Twinning. *Science*, 168(3937): 1342-1344.
- Tullis, J. and Tullis, T., 1972. Preferred orientation of quartz produced by mechanical Dauphiné twinning: Thermodynamics and axial experiments. In: H.C. Heard, I.Y. Borg, N.L. Carter and C.B. Raleigh (Editors), *Flow and Fracture of Rocks*. Geophysical Monograph Series. AGU, Washington, D.C., pp. 67-82.
- Twiss, R.J., 1974. Structure and Significance of Planar Deformation Features in Synthetic Quartz. *Geology*, 2(7): 329-332.
- Van Goethem, L., Van Landuyt, J. and Amelinckx, S., 1977. The $\alpha \rightarrow \beta$ transition in amethyst quartz as studied by electron microscopy and diffraction. The interaction of dauphiné with Brazil twins. *physica status solidi (a)*, 41(1): 129-137.
- Van Landuyt, J., Van Tendeloo, G., Amelinckx, S. and Walker, M.B., 1985. Interpretation of Dauphiné-twin-domain configurations resulting from the alpha - beta phase transition in quartz and aluminum phosphate. *Physical Review B*, 31(5): 2986.
- Van Zalinge, M.E., 2012. The Guarda structure, NE-Portugal: a meteorite impact crater or not? MSc. Thesis, Utrecht University, Utrecht, 83 pp.
- Van Zalinge, M.E., Hamers, M.F. and Drury, M.R., 2012. The Guarda structure (Portugal): impact structure or not? Microstructural studies of quartz, zircon and monazite. *Meteoritics and Planetary Science Supplement*, 75: 5045.
- Vernooij, M.G.C. and Langenhorst, F., 2005. Experimental reproduction of tectonic deformation lamellae in quartz and comparison to shock-induced planar deformation features: *Meteoritics & Planetary Science* 40: 1353-1361.
- Vigouroux, J.P., Duraud, J.P., Le Moel, A., Le Gressus, C. and Griscom, D.L., 1985. Electron trapping in amorphous SiO₂ studied by charge buildup under electron bombardment. *Journal of Applied Physics*, 57(12): 5139-5144.
- Voorn, M.H., 2010. A new way to confirm meteorite impact produced planar features in quartz: combining Universal Stage and Electron Backscatter Diffraction techniques. MSc Thesis, Utrecht University, Utrecht.
- Voorn, M.H., Hamers, M.F. and Drury, M.R., 2010. Comparison of orientation measurements of planar deformation features and tectonic deformation lamellae in quartz. *Meteoritics & Planetary Science*, 45: A209-A209.
- Vrána, S., 1987. The Ševětín astrobleme, southern Bohemia, Czechoslovakia. *Geologische Rundschau*, 76(2): 505-528.
- Walderhaug, O. and Rykkje, J., 2000. Some examples of the effect of crystallographic orientation on the cathodoluminescence colors of quartz: *Journal of Sedimentary Research* 70: 545-548.
- Wegner, M.W. and Christie, J.M., 1983. Chemical etching of deformation sub-structures in quartz. *Physics and Chemistry of Minerals*, 9(2): 67-78.
- Wenk, H.-R. et al., 2009. Dauphiné twinning and texture memory in polycrystalline quartz. Part 3: texture memory during phase transformation. *Physics and Chemistry of Minerals*, 36(10): 567-583.
- Wenk, H.-R., Janssen, C., Kenkmann, T. and Dresen, G., 2011. Mechanical twinning in quartz: Shock experiments, impact, pseudotachylites and fault breccias. *Tectonophysics*, 510(1-2): 69-79.
- Wenk, H.-R. et al., 2006. Dauphiné twinning and texture memory in polycrystalline quartz. Part 1: Experimental deformation of novaculite. *Physics and Chemistry of Minerals*, 33(10): 667-676.

- Wenk, H.R., Bortolotti, M., Barton, N., Oliver, E. and Brown, D., 2007. Dauphine twinning and texture memory in polycrystalline quartz. Part 2: In situ neutron diffraction compression experiments. *Physics and Chemistry of Minerals*, 34(9): 599-607.
- Wenk, H.R., Lonardelli, I., Vogel, S.C. and Tullis, J., 2005. Dauphiné twinning as evidence for an impact origin of preferred orientation in quartzite: An example from Vredefort, South Africa. *Geology*, 33(4): 273-276.
- Werner, C., 1904. Das Ries in der Schwäbisch Fränkischer Alb. *Blätter des Schwäbischen Albvereins*.
- Whelan, M.J., Hirsch, P.B., Horne, R.W. and Bollmann, W., 1957. Dislocations and Stacking Faults in Stainless Steel. *Proceedings of the Royal Society of London. Series A, Mathematical and Physical Sciences*, 240(1223): 524-538.
- White, S.H., 1973. Deformation lamellae in naturally deformed quartz. *Nature Physical Science*, 245: 26-28.
- Wilkinson, A.J. and Hirsch, P.B., 1997. Electron diffraction based techniques in scanning electron microscopy of bulk materials. *Micron*, 28(4): 279-308.
- Williams, D.B. and Carter, C.B., 2009. *Transmission Electron Microscopy: A Textbook for Materials Science*. Springer.
- Williams, G.E. and Gostin, V.A., 2005. Acraman-Bunyeroo impact event (Ediacaran), South Australia, and environmental consequences: twenty-five years on: *Australian Journal of Earth Sciences: An International Geoscience Journal of the Geological Society of Australia* 52: 607 - 620.
- Wirth, R., 2004. Focused Ion Beam (FIB): A novel technology for advanced application of micro- and nanoanalysis in geosciences and applied mineralogy. *European Journal of Mineralogy*, 16: 863-876.
- Wirth, R., 2009. Focused Ion Beam (FIB) combined with SEM and TEM: Advanced analytical tools for studies of chemical composition, microstructure and crystal structure in geomaterials on a nanometre scale. *Chemical Geology*, 261(3-4): 217-229.
- Wirth, R., Vollmer, C., Brenker, F., Matsyuk, S. and Kaminsky, F., 2007. Inclusions of nanocrystalline hydrous aluminium silicate "Phase Egg" in superdeep diamonds from Juina (Mato Grosso State, Brazil). *Earth and Planetary Science Letters*, 259(3-4): 384-399.
- Wittmann, A., Kenkmann, T., Schmitt, R.T. and Stöffler, D., 2006. Shock-metamorphosed zircon in terrestrial impact craters. *Meteoritics & Planetary Science*, 41(3): 433-454.
- Wright, S.I. and Nowell, M.M., 2006. EBSD Image Quality Mapping. *Microscopy and Microanalysis*, 12(01): 72-84.
- Yamamoto, M., Ficken, K., Baas, M., Bosch, H.J. and de Leeuw, J.W., 1996. Molecular palaeontology of the earliest Danian at Geulhemmerberg (the Netherlands). *Geologie en Mijnbouw*, 75: 255-267.
- Zinkernagel, U., 1978. Cathodoluminescence of quartz and its application to sandstone petrology: *Contributions to Sedimentary Geology* 8: 1-69.
- Zinserling, K. and Schubnikow, A., 1933. Über die Plastizität des Quarzes. *Zeitschrift für Kristallographie*, 85: 454-461.

Publications

Published

Hamers, M.F., and Drury, M.R., 2011, Scanning electron microscope-cathodoluminescence (SEM-CL) imaging of planar deformation features and tectonic deformation lamellae in quartz: *Meteoritics & Planetary Science*, 46, 1814-1831.

In preparation

Hamers, M.F., Drury, M.R., and Smit, J., No evidence for shocked quartz at the Cretaceous-Palaeogene boundary in the Geulhemmerberg section, south-east Netherlands.

Hamers, M.F., Pennock, G.M., Herwegh, M., and Drury, M.R., Distinction of amorphous and healed planar deformation features in shocked quartz using composite colour scanning electron microscope cathodoluminescence imaging.

Hamers, M.F., Pennock, G.M., Palasse, L.N., and Drury, M.R., Characterisation of shock microstructures in quartz by foreshattered electron imaging and electron backscattered diffraction.

Hamers, M.F., Pennock, G.M., and Drury, M.R., Scanning electron microscopy cathodoluminescence imaging of dislocations, subgrain boundaries and twin boundaries in quartz.

Hamers, M.F., Pennock, G.M., and Drury, M.R., An integrated scanning electron microscopy approach for shocked quartz.

Curriculum Vitae



Maartje Hamers was born as the second of three sisters in Amsterdam on December 5, 1981. Her parents soon moved the family to the quieter village of Uitgeest, where she lived until her graduation from the Murrnellius Gymnasium in nearby Alkmaar in 2000. She then spent a year studying Italian in Florence and Spanish in Salamanca, but moved to Utrecht in 2001 to study Earth Sciences. In 2005, her BSc thesis on CO₂ sequestration in hydrocarbon reservoirs was supervised by Prof. Chris Spiers at the High Pressure and Temperature laboratory. With a palaeomagnetic fieldwork in the Donbas basin (eastern Ukraine) and resulting MSc thesis titled 'A new late Palaeozoic apparent polar wander path for Baltica', supervised by (then future) Dr Maud Meijers, Dr Douwe van Hinsbergen and Prof. Cor Langereis at the Palaeomagnetic Laboratory 'Fort Hoofddijk', she completed her MSc in 2007. Some months of working in a book store and at TNO Earth, Environmental and Life Sciences funded a four-month road trip through Eastern Europe, the Balkans and Turkey. Upon returning to the Netherlands she decided that after the slowly drifting continents of her MSc thesis, it was time for a spectacular increase in speed to supersonic: meteorite impacts. From December 2008 to early 2013 she studied shock microstructures in quartz using electron microscopy at Utrecht University in the Structural Geology and Tectonics group under supervision of Prof. Martyn Drury and Dr Gill Pennock. The results of this research are presented in this PhD thesis. In between field trips and microscopy sessions, some time was reserved for two years of photography studies, also in Utrecht.

Dankwoord

Het is zover: het einde! Vier jaar lang de aandacht richten op één onderwerp in zoveel mogelijk detail is niet altijd makkelijk, laat staan leuk. Hoe spectaculair meteorietinslagen ook klinken, na de zoveelste microscoopsessie tot in de avonduren met als klap op de vuurpijl een gecrashte microscoop of een mislukt preparaat is er niet veel meer aan. Maar zo tegen het einde vallen een hoop puzzelstukken op hun plek. Het verhaal begint vorm te krijgen en opeens is er bijna een boek! Met een verzameling tekst en plaatjes voor je die de belichaming zijn van ruim vier jaar werk komt er uiteindelijk toch maar één conclusie: misschien was het toch de moeite waard. Uiteraard zijn er veel mensen die op de één of andere manier hebben bijgedragen aan de goede afloop van dit onderzoek en die daarvoor mijn eeuwige dank verdienen.

Ten eerste zijn dat natuurlijk mijn begeleiders, **Martyn Drury** en **Gill Pennock**. Martyn, you could really find a whole new world (or should I say paper) in a grain of sand, even at times when I was sure there was absolutely nothing whatsoever that could possibly be of any interest to anyone. Thanks for setting up the project, for always being so positive and for letting me do things my own way. Gill, you are the EBSD Master. Thanks for pointing out all the ‘ants’ I did not always want to see; taking care of them really improved the thesis. Thank you both so much for sacrificing every single free minute between Christmas and February to read countless versions of my thesis chapters. And it might not be impossible that your vegetable garden provided the vitamins vital to my and Wolter’s survival in the past four years!

Then I would like to thank the members of the dissertation committee for reviewing the thesis and sharing their expertise: **Patrick Cordier**, **Alex Deutsch**, **Geoff Lloyd**, **Uwe Reimold** and **Claudia Trepmann**. I have also benefitted greatly from discussions with both Alex Deutsch and Uwe Reimold at conferences and during a visit to the Natural History Museum in Berlin. Uwe, your generosity in providing samples has made many results in this thesis possible.

Zonder één van de architecten van de KT-inslagtheorie, **Jan Smit**, was dit onderzoek een stuk moeizamer van de grond gekomen. Jan, jouw onuitputtelijke voorraad monsters van elke denkbare grenssectie ter wereld lijkt het hele concept van veldwerk bijna overbodig te maken. Dank voor al je hulp, ideeën, monsters en introductie in de wondere wereld van de KT-grens. Ik heb veel plezier beleefd aan de veldtripjes in Spanje, Italië en niet te vergeten de ondergrondse gangen van de Geulhemmerberg.

Pim van Wamel wil ik hartelijk bedanken voor zijn hulp met het veldwerk naar de Rieskrater. Dit heeft de basis gelegd voor veel resultaten in dit proefschrift. Een vruchtbare expeditie, met veel gezellige momenten, goed eten en Duits bier.

The quantification of the CL signal of red PDFs in chapter 4 would not have been possible

without **Marco Herwegh** at the University of Bern in Switzerland. Thank you for letting me use the SEM in Bern and helping to solve the problems involved in measuring such small structures. **Philip**, dank voor de gezelligheid tijdens en na het SEM-werk in Bern.

The endless enthusiasm and energy of **Laurie Palasse** at Bruker Berlin have been incredible. Laurie, your beautiful colour FSE images are worthy of a place on the wall of any art gallery.

Roald Tagle, Rodger Hart, Ulli Raschke and **Jörg Fritz** kindly provided me with samples from Popigai, Vredefort, El'gygytyn and shock experiments respectively. Thank you!

Zonder een leuke vakgroep is er natuurlijk geen lol te beleven aan wetenschap. Dank daarom aan iedereen in en rond Structurele Geologie de afgelopen jaren. Naast Martyn en Gill ook **Reinoud** voor een indrukwekkende stroom professorale en geologische wijsheden en nog steeds inspirerende colleges en veldcursussen. Op **Herman** kon ik altijd rekenen, niet in de laatste plaats voor een altijd positieve, eigenwijze en licht anarchistische kijk op de wereld. **Auke**, ook van jou heb ik een hoop geleerd over microscopie, wetenschap en de wereld in het algemeen. Without 'de hipste Fransman ooit' **Côme** the first three years would have been a lot more boring! Thanks for your invariably smiling face, countless coffee breaks and going kapot in Kafé België. I hope you and Maud have a great time in the US. **Annelies**, de andere 'extraterrestrial lady' (Vissers, 2011), 'Pink Lady' (Levebvre, 2010) en tot voor kort kamergenootje: zonder jouw TEM-expertise en -lessen was dit proefschrift nu nog steeds niet klaar geweest. Dank je! De bezoeken van onze geadopteerde Delftse groepsgeenoot **Wouter** werden altijd zeer gewaardeerd. Ik vond het gezellig je in de eerste periode van mijn onderzoek als part-time kamergenoot te hebben. **Cong**, it was great to have you in our group for a year and I enjoyed discussing the peculiarities of both our countries. Good to have you back for another visit. The recent arrival of **Olli** and **Maartje** has brought new life to the group, so thank you and welcome to Utrecht! **Magda**, jij staat altijd klaar en er is niets dat je niet kan regelen. Heel veel dank voor alles. **Kalijn**, al hoor je dan stiekem misschien bij een andere vakgroep, ik ben blij dat je de laatste maanden mijn kamergenootje was en dat je hier de afgelopen jaren ook nog rondzwierf. Fijn dat je een goede plek hebt gevonden.

Ook buiten de vakgroep zijn veel mensen belangrijk geweest de afgelopen jaren. Bij de microscopen in het Kruyt zijn dat **Matthijs** (aka the FIB-SEM wizard), **Hans** en **Chris**. Alledrie stonden ze altijd met een grote grijns klaar om vakkundig hulp te bieden en in te grijpen bij een domme actie van mijn kant of pure onwil van één van de microscopen. In het Kruyt valt altijd wat te lachen, en flauwe grappen zijn nu eenmaal de beste grappen. Mannen, bedankt!

Diep in de krochten van het Aardwetenschappengebouw is het **HPT-lab** verstoep. Onze gezamenlijke seminars, borrels en de jaarlijkse barbecue zijn altijd een welkome onderbreking van het werk geweest. Vooral **Anne, Bart, André, Jon, Sander, Sabine, Tim** en **Elisenda** wil ik bedanken voor alle biertjes, koffie, pizza, leuke momenten en klaagzangen op het PhD-leven. Thanks also to the **Petrology group**, who are always in for lunch! **Inge**, dank voor je carrière-advies en wie weet kom ik je in de toekomst interviewen (als je toch Marsmannetjes vindt?).

Elk onderzoek valt of staat met goede technische ondersteuning. **Otto Stiekema** heeft ontelbaar veel slijpplaatjes voor me gemaakt en liet me altijd mijn gang gaan als ik zelf iets wilde polijsten. **Tilly Bouten** stond altijd klaar om die slijpplaatjes te coaten en heeft me de eerste introductie op de SEM gegeven. **Peter van Krieken** bood altijd direct hulp bij de lichtmicroscopie en monsterpreparatie. Ook **Roel van Elsas** van de VU mag in dit rijtje niet ontbreken: hij heeft

me laten zien hoe mineraalscheiding werkt en het werk gedaan voor een groot aantal monsters.

De beste herinneringen aan de afgelopen jaren komen misschien wel van het begeleiden van studenten. Als eerste **Maarten**, die bijna prehistorische apparatuur uit het stof haalde en zo'n grondige masterscriptie inleverde dat hij er haast op zou kunnen promoveren. **Marit**, ons veldwerk in Portugal was bij vlagen hilarisch en ondanks het schrijnende gebrek aan Portugese kraters heb je een dijk van een afstudeerscriptie geschreven. De maanden stage bij TNO met Mariëlle waarbij je nog een keer met mij naar de SEM kwam waren een leuke bonus. Allebei heel veel succes met jullie eigen promotie.

De onvermoeibare Aliaga-crew van 2009 en 2010 wil ik bedanken voor de leukste weken van de afgelopen vier jaar: **Frits, Herman, Wout, Joris, Lennart, Jochem, Sander, Roderic, Chris, Desiree** en natuurlijk **Renske**, met wie ik ook na het veldwerk nog veel lol heb gehad. In 2011 ruilde ik Aliaga voor de Pyreneeën en heb daar twee minstens zo aangename weken gehad met **Reinoud, Martyn, Bart** en **Anne**. Alle **bachelorstudenten** uit Aliaga, de practica van Deformatie&Metamorfose en de Pyreneeën: ik zal jullie niet stuk voor stuk noemen, maar jullie waren natuurlijk allemaal geweldig!

Dan mijn geo-vrienden, met wie ik al sinds het begin van de studie bijna twaalf (!) jaar geleden een haat-liefdeverhouding met stenen, goede en zeker ook veel slechte gesprekken en grappen en eigenlijk bijna alles deel. **Mariël**, de afgelopen jaren hebben veel onvergetelijke momenten opgeleverd in Nederland en Genève. De barbecue aan het meer, kaasfondues, flessen champagne, dansjes met de rode kater en Oud&Nieuw-huiskamerdisco's hebben zeker bijgedragen aan onze wetenschappelijke doorbraken! Dank dat je mijn paranimf bent. **Henk**, dank dat je Henk bent! We komen nog veel vaker op bezoek in Aberdeen en welke uithoek jullie hierna weer uitzoeken (lekker genieten). **Mariëlle**, jij zat altijd dichtbij. Ik zal onze lunches in de altijd sfeervolle TNO-kantine missen. Ook die met jou **Len**! Ook **Mijke&Victor** (komende winter ga ik écht weer mee de sneeuw in!), **Nicole, Julia, Happie, Jurgen, Thomas** en **Youri** had ik niet kunnen missen de afgelopen jaren.

Desiree, ook jij bedankt dat je paranimf wil zijn. Onze onderzoeken liepen bijna synchroon en nu promoveren we bijna tegelijk (oké jij wint). Fijn dat we deze periode konden delen op de uni (schilfertruffels en de scheldende koffieautomaat!) en daarbuiten. In dat laatste had natuurlijk ook **Willem** een belangrijk aandeel. Heel veel succes in Noorwegen!

Grote hoeveelheden herrie, modder, bier en poffertjes bij concerten en festivals met **Billy&Leo(+Lesley!)** en aanhang zorgden altijd voor zeer welkome afleiding (en vaak minder welkome katers). Allemaal, en ook al mijn andere vrienden, dank.

Papa, mama, Leonoor en **Sofie**, bij jullie kan ik altijd terecht voor afleiding, relativering en gewoon thuis zijn. Niets is waardevoller dan dat (en is het nu afgelopen met die impactgrappen!?). **Joke** en **Evert-Jan**, jullie zijn mijn tweede thuis.

Lieve **Wolter**, met jou is alles leuker. Ik ben terug!

